

VIRTUAL ANALOG MODELING OF AUDIO CIRCUITRY  
USING WAVE DIGITAL FILTERS

A DISSERTATION  
SUBMITTED TO THE DEPARTMENT OF MUSIC  
AND THE COMMITTEE ON GRADUATE STUDIES  
OF STANFORD UNIVERSITY  
IN PARTIAL FULFILLMENT OF THE REQUIREMENTS  
FOR THE DEGREE OF  
DOCTOR OF PHILOSOPHY

Kurt James Werner  
December 2016

© 2016 by Kurt James Werner. All Rights Reserved.  
Re-distributed by Stanford University under license with the author.

This dissertation is online at: <http://purl.stanford.edu/jy057cz8322>

I certify that I have read this dissertation and that, in my opinion, it is fully adequate in scope and quality as a dissertation for the degree of Doctor of Philosophy.

**Julius Smith, III, Primary Adviser**

I certify that I have read this dissertation and that, in my opinion, it is fully adequate in scope and quality as a dissertation for the degree of Doctor of Philosophy.

**Jonathan Abel**

I certify that I have read this dissertation and that, in my opinion, it is fully adequate in scope and quality as a dissertation for the degree of Doctor of Philosophy.

**Jonathan Berger**

Approved for the Stanford University Committee on Graduate Studies.

**Patricia J. Gumpert, Vice Provost for Graduate Education**

*This signature page was generated electronically upon submission of this dissertation in electronic format. An original signed hard copy of the signature page is on file in University Archives.*



# Abstract

The Wave Digital Filter (WDF) approach to discretizing electronic circuits has generated substantial interest in the Virtual Analog research community, which is attracted to the potential for systematic and modular simulation of vintage electronic musical instruments (e.g., synthesizers, drum machines) and audio effects (e.g., guitar amplifiers, distortion pedals). Unfortunately, traditional WDF techniques falter at the complexity of typical audio circuits, which contain complicated (non-series/parallel) topologies and multiple nonlinear devices (e.g., diodes, transistors, triodes). In this dissertation, I review classical WDF techniques and propose novel ways of systematically modeling circuits with complicated topologies and multiple nonlinearities. Throughout, the classic Bass Drum circuit from the Roland TR-808 serves as a motivating example and each of the four chapters contains a case study simulating a different one of its subcircuits.

The first two chapters consider linear reference circuits. After deriving the standard WDF building blocks and demonstrating their use in a simulation of the TR-808 Bass Drum's output filter, I explain their substantial limitations in the context of modeling analog audio circuitry. To overcome these limitations, I introduce a novel Modified-Nodal-Analysis-based approach to creating WDFs from circuits with complicated (non-series/parallel) topologies and show it in action on several versions of the Bass Drum's central circuit (the Bridged-T Resonator).

The next two chapters consider nonlinear reference circuits. I review the standard WDF technique for handling reference circuits with a single one-port nonlinear device, exemplified by a model of the TR-808 Bass Drum's Pulse Shaper subcircuit. In order to overcome the limitation to a single nonlinearity, I propose a novel approach that accommodates multiple nonlinearities and apply it towards a simulation of the full nonlinear version of the Bass Drum's Bridged-T Resonator.

Together, these four case studies form a complete model of the TR-808 Bass Drum that almost exactly matches the behavior of the real circuit, demonstrating the utility of the classical WDF techniques combined with my proposed methods. Beyond this case study, the proposed methods enable the simulation of a huge class of audio circuitry that was previously beyond the scope of WDF modeling.



# Acknowledgments

This work would not have been possible without the help of my colleagues, friends, and family at CCRMA and beyond. Although in some sense a dissertation is a lonely endeavor, I've had the pleasure to work alongside quite a few collaborators. Vaibhav Nangia and I spent long hours parsing the basics of Wave Digital Filter theory together and the main findings of this dissertation grew out of our struggles. In 2015–2016 I had the opportunity to work with a group of Wave Digital Filter researchers at CCRMA: Michael Olsen, Ross Dunkel, and Maximilian Rest. Their relentless enthusiasm and support was key in developing some of the secondary findings of this work. Thanks to Michael for his time and expertise in incorporating iterative methods into my approach to Wave Digital Filter modeling; without this my structural insights for tackling larger circuits would be useless in practice. Thanks to Ross for his perfectionism and insistence on thinking big. His Fender Bassman preamp model is still the most complicated extant Wave Digital Filter model of an audio circuit, and that work gave me the confidence to finally tackle the TR-808 Bass Drum circuit. Thanks to Max for his attention to detail and belief in the value of my work; his efforts in his master's thesis to translate my largely theoretical work into a practical real-time code framework are much appreciated. A fruitful collaboration with Alberto Bernardini and Augusto Sarti from the Politecnico di Milano is specifically reflected in the section on solving diode clipper nonlinearities with the Lambert  $W$  function, but goes well beyond that material. Outside the realm of Wave Digital Filters, thanks to Chet Gney and Mayank Sanganeria for their friendship and for the opportunity to collaborate on wah pedal and circuit-bent FM synthesizer modeling, respectively. Finally, thank you to François Germain. As the other half of my Ph.D. cohort, François has been with me from the beginning in my research, offering detailed and insightful criticism, pushing me to do my best work and strive for mathematical rigor, and offering invaluable conceptual, editorial, and emotional support. François' willingness to spend the time and energy to dig deep into any topic, and his skill and intelligence to actually understand them all, is rare, profound, sometimes frightening, and valuable beyond measure.

CCRMA is a wonderful and welcoming community. To name only a few of the friends and colleagues who've made CCRMA a great place for me, thanks to Myles Borins, Marina Bosi, Tim O'Brien, Maddie Brown, Lauchlan Casey, Alex Chechile, John Chowning, Gina Collechia, Chris Carlson, Luke Dahl, Emily Gruber, John Granzow, Woody Herman, Jennifer Hsu, Kai-Chieh Huang,

Madeline Huberth, Doug James, Jay Kadis, Blair Kaneshiro, Hyung-Suk Kim, Sasha Leitman, Sara Martín, Hunter McCurry, Romain Michon, Irán Román, Bruno Ruviaro, Spencer Salazar, Lauri Savioja, Kitty Shi, and Nathan Volman. Specifically, thanks to Dave Kerr, Fernando Lopez-Lezcano, Carr Wilkerson, Elliot Kermit-Canfield, Eoin Callery, Jorge Herrera, Rob Hamilton, Chryssie Nanou, Christopher Jette, Matt Wright, Martin Krämer, Nette Worthy, and Debbie Barney for their proactive support. Outside of CCRMA, I must thank professor Gregory Kovacs from the Electrical Engineering department for offering me a desk early in my graduate career, in an era before CCRMA Ph.D. candidates had their own space.

Beyond the friends and colleagues who have enriched my experience at CCRMA so much, the Alice Wilbur Chapman Fund supported me financially and enabled my research for these five years.

I've benefited greatly from the guidance, patience, kindness, and expertise of the CCRMA faculty. First, I want to thank Dave Berners. In my first year, his lectures on filter theory, discretization, and Virtual Analog modeling introduced me to the field. Later on, his introduction to the classical circuit simulation frameworks was an essential part of fitting the moving pieces of my key findings together. Ge Wang's ability to match energy and positivity with a keen critical apparatus is an inspiration to me and an important part of the culture at CCRMA. Thank you to Takako Fujioka for your efforts in checking up on me and offering timely personal and professional advice. Chris Chafe was a great source of encouragement and his work as director of CCRMA is a huge part of what makes the place such a great interdisciplinary institute.

I owe a huge debt of gratitude to my dissertation committee. They gave me both the freedom to develop my own research agenda and the support to carry it out. In discussions on circuit bending to Bach to MP3 artifacts and beyond, Jonathan Berger's perspective has always kept me focused on wider applications, on the bigger picture, on the deeper story. Jonathan Abel's willingness to join me in filling whiteboard after whiteboard in search of answers is always a thrill, and always enlightening. From Jonathan I learned that there is great value in deep knowledge of the wider literature, and there is also great value in understanding things from first principles. My adviser Julius Smith introduced me to Wave Digital Filters and more broadly, to research. Julius' combination of encyclopedic knowledge, formal rigor, and intuition inspires me daily. Julius, for believing in me before my research had yielded any results, for your constant encouragement, for advocating for me after the results started piling up, and for bouncing innumerable opportunities my way, thank you.

A million thanks to my partner Melissa Kagen for being the best, for being a shining and brilliant scholarly example and a terrifying refining furnace of editorial help, for her understanding during stressful times, and for keeping me sane in the world outside of lumped systems and their discretization.

Finally, thanks most of all to my parents Kim and Craig Werner for a lifetime of love and support.

# Contents

<b>Abstract</b>	<b>v</b>
<b>Acknowledgments</b>	<b>vii</b>
<b>Introduction</b>	<b>1</b>
Summary of the Dissertation . . . . .	2
Literature Review . . . . .	4
Black Box Modeling . . . . .	4
White Box Modeling . . . . .	4
TR-808 Rhythm Composer . . . . .	9
<b>1 Linear Wave Digital Filters</b>	<b>15</b>
1.1 Preliminaries . . . . .	16
1.1.1 Port Definition . . . . .	16
1.1.2 Realizability . . . . .	17
1.1.3 Connection Tree . . . . .	17
1.1.4 Wave Variable Definitions . . . . .	18
1.2 Algebraic One-Ports . . . . .	21
1.2.1 Resistor . . . . .	21
1.2.2 Ideal Voltage Source . . . . .	22
1.2.3 Ideal Current Source . . . . .	24
1.2.4 Resistive Voltage Source . . . . .	25
1.2.5 Resistive Current Source . . . . .	27
1.2.6 Short Circuit . . . . .	28
1.2.7 Open Circuit . . . . .	29
1.2.8 Switch . . . . .	30
1.2.9 Singular Network Elements . . . . .	31
1.3 Reactive One-Ports . . . . .	33
1.3.1 Capacitor . . . . .	33
1.3.2 Inductor . . . . .	41

1.3.3	Choosing a Discretization Method . . . . .	46
1.4	Two-Ports . . . . .	47
1.4.1	Simple Two-Port Connections . . . . .	48
1.4.2	Two-Port Series/Parallel Adaptors Containing Sources . . . . .	51
1.4.3	Ideal Transformer . . . . .	54
1.4.4	Controlled Sources . . . . .	56
1.4.5	Ideal Converters . . . . .	61
1.4.6	Unit Element and QUARLs . . . . .	64
1.4.7	Gyrator . . . . .	65
1.4.8	Changes of Variables . . . . .	67
1.4.9	Nullor . . . . .	69
1.4.10	Two-Ports Based on $y$ , $z$ , $h$ , and $g$ Parameters . . . . .	70
1.5	Three-Ports . . . . .	74
1.5.1	Three-Port Parallel Adaptor . . . . .	74
1.5.2	Three-Port Series Adaptor . . . . .	76
1.5.3	Three-Port Circulator . . . . .	77
1.6	$N$ -Ports . . . . .	78
1.6.1	$N$ -Port Parallel Adaptors . . . . .	78
1.6.2	$N$ -Port Series Adaptors . . . . .	79
1.6.3	$N$ -Port Circulator . . . . .	80
1.6.4	$\mathcal{R}$ -Type . . . . .	81
1.7	Case Study: TR-808 Output Filter . . . . .	81
1.8	Review . . . . .	89
<b>2</b>	<b>Topological Advances for Wave Digital Filters</b>	<b>91</b>
2.1	Previous Work . . . . .	92
2.1.1	Martens and Meerkötter . . . . .	92
2.1.2	Special Adaptors . . . . .	92
2.1.3	Circuits Involving Operational Amplifiers . . . . .	94
2.1.4	Methods Involving Global Iteration or “Dynamic Adaptation” . . . . .	97
2.1.5	SPQR Tree . . . . .	98
2.2	Proposed method . . . . .	101
2.2.1	Thévenin Adaptors . . . . .	102
2.2.2	Modified Nodal Analysis . . . . .	103
2.2.3	Stamping . . . . .	104
2.2.4	Adaptation . . . . .	106
2.3	Resolving Multiple Linear Nonadaptable Elements . . . . .	106
2.3.1	Configure Structure Using Replacement Graphs . . . . .	107

2.3.2	Resolve Root . . . . .	107
2.3.3	Example Application . . . . .	109
2.4	Case Studies . . . . .	111
2.4.1	Passive Bridged-T Filter . . . . .	111
2.4.2	Bridged-T Resonator . . . . .	116
2.4.3	Bridged-T Resonator With Feedback . . . . .	121
2.5	Conclusion . . . . .	127
<b>3</b>	<b>One-Port Nonlinearities in Wave Digital Filters</b>	<b>129</b>
3.1	Diode Modeling . . . . .	129
3.2	Previous Work . . . . .	131
3.2.1	Connection Tree . . . . .	131
3.2.2	Piecewise Linear Models . . . . .	132
3.2.3	Iterative Schemes . . . . .	136
3.2.4	Analytic Solutions . . . . .	137
3.2.5	Consolidated One-Port Combinations . . . . .	138
3.2.6	Simplified Multiports . . . . .	140
3.3	Case Study . . . . .	140
3.4	Review . . . . .	145
<b>4</b>	<b>Advances to Wave Digital Filters With Multiple Nonlinearities</b>	<b>147</b>
4.1	Nonlinear Devices . . . . .	147
4.1.1	Transistor Modeling . . . . .	148
4.1.2	Triode Modeling . . . . .	152
4.2	Previous Work . . . . .	153
4.2.1	Fictitious Delays and Cross-Control Models . . . . .	154
4.2.2	Iteration . . . . .	155
4.2.3	Linearization and Simplified Models . . . . .	155
4.2.4	Evaluation of Previous Work . . . . .	156
4.3	Proposed Method . . . . .	157
4.3.1	Grouping Nonlinearities . . . . .	158
4.3.2	Mathematical Structure . . . . .	159
4.3.3	Resolving Implicit Relationships . . . . .	162
4.3.4	Deriving System Matrices . . . . .	164
4.4	Case Studies . . . . .	165
4.4.1	Envelope Generator . . . . .	165
4.4.2	Nonlinear Bridged-T Resonator With Feedback . . . . .	171
4.5	Conclusion . . . . .	179

<b>Conclusion</b>	<b>181</b>
TR-808 Bass Drum Simulation . . . . .	181
Tone Control Study . . . . .	182
Pulse Amplitude Study . . . . .	182
Decay Control Study . . . . .	186
Variation Study . . . . .	188
Summary of Contributions . . . . .	188
Chapter 1 Contributions . . . . .	189
Chapter 2 Contributions . . . . .	190
Chapter 3 Contributions . . . . .	190
Chapter 4 Contributions . . . . .	191
Final Comments . . . . .	192
<b>A Derivation of the Extended <math>y</math>-Parameter Model</b>	<b>195</b>
A.1 Extended $y$ -Parameter Model . . . . .	195
A.2 Linearize Transistor . . . . .	196
A.3 DC Solution . . . . .	201
A.4 Completed Model . . . . .	204
<b>B Derivation of the Output Filter Simplified Model</b>	<b>205</b>
<b>C Tom/Conga equivalent Resistance Calculation</b>	<b>209</b>
C.1 Derivation of Passive Bridged-T Filter Transfer Function . . . . .	211
C.2 Derivation of Bridged-T Resonator Properties . . . . .	213
<b>Bibliography</b>	<b>219</b>

## List of Tables

1.1 TR-808 Bass Drum and Extended Two-Port $y$ -Parameter Component Values. . . . .	83
2.1 Some Modified Nodal Analysis Element Stamps. . . . .	105
2.2 Bridged-T Resonator Values for Various TR-808 Voices. . . . .	112
2.3 TR-808 Bass Drum, Bridged-T Resonator With Feedback. . . . .	122

3.1	Pulse Shaper Component Values. . . . .	141
4.1	Envelope Generator Component Names and Values. . . . .	167
4.2	Nonlinear Bridged-T Resonator Component Names and Values. . . . .	171
A.1	Sequence of Newton Iterations. . . . .	203
B.1	Summary of Simplified Model Transfer Functions. . . . .	207
C.1	Bridged-T Resonator Values for Toms and Congas. . . . .	211

# List of Figures

I	Roland TR-808 Rhythm Composer. . . . .	10
II	TR-808 Bass Drum Schematic. . . . .	11
III	TR-808 Bass Drum Circuit Separated into Parts. . . . .	13
1.1	Kirchhoff- and Wave-Domain Representations of a Generic One-Port. . . . .	17
1.2	Kirchhoff- and Wave-Domain Representations of a Resistor One-Port. . . . .	21
1.3	Kirchhoff- and Wave-Domain Representations of an Ideal Voltage Source. . . . .	23
1.4	Battery Symbol and Port Definition. . . . .	24
1.5	Kirchhoff- and Wave-Domain Representations of an Ideal Current Source. . . . .	24
1.6	Kirchhoff- and Wave-Domain Representations of a Resistive Voltage Source. . . .	26
1.7	Kirchhoff- and Wave-Domain Representations of a Resistive Current Source. . . .	27
1.8	Kirchhoff- and Wave-Domain Representations of an Ideal Short Circuit One-Port.	29
1.9	Kirchhoff- and Wave-Domain Representations of an Ideal Open Circuit One-Port.	30
1.10	Kirchhoff- and Wave-Domain Representations of an Ideal Switch One-Port. . . . .	31
1.11	Kirchhoff- and Wave-Domain Representations of a Nullator One-Port. . . . .	31
1.12	Kirchhoff- and Wave-Domain Representations of a Norator One-Port. . . . .	32
1.13	Mappings From the $s$ to $z$ Planes, Including BLT, BE, and $\alpha$ Transforms. . . . .	34
1.14	Kirchhoff- and Wave-Domain Representations of a Capacitor (BLT). . . . .	35
1.15	Wave-Domain Representations of a Capacitor (Warped BLT). . . . .	36
1.16	Wave-Domain Representations of a Capacitor (BE). . . . .	38
1.17	Wave-Domain Representations of a Capacitor ( $\alpha$ Transform). . . . .	39
1.18	Wave-Domain Representations of a Capacitor (Möbius transform). . . . .	40

1.19	Kirchhoff- and Wave-Domain Representations of a Inductor One-Port (BLT) . . . . .	42
1.20	Wave-Domain Representations of an Inductor (Warped BLT). . . . .	43
1.21	Wave-Domain Representations of an Inductor (BE). . . . .	44
1.22	Wave-Domain Representations of an Inductor ( $\alpha$ Transform). . . . .	45
1.23	Wave-Domain Representations of an Inductor (Möbius Transform). . . . .	46
1.24	Kirchhoff- and Wave-Domain Representations of a Two-Port Parallel Connection.	49
1.25	K- and W-Domain Representations of a Two-Port Series Connection (Inverter). .	50
1.26	K- and W-domain Representations of Two-Port Parallel + Ideal Current Source.	52
1.27	Current and Voltage Source Identities. . . . .	52
1.28	K- and W-domain Representations of Two-Port Series + Ideal Voltage Source. .	53
1.29	Kirchhoff- and Wave-Domain Representations of a Two-Port Transformer. . . . .	55
1.30	Kirchhoff- and Wave-Domain Representations of a Two-Port Active Transformer.	56
1.31	Kirchhoff- and Wave-Domain Representations of a VCVS. . . . .	57
1.32	Kirchhoff- and Wave-Domain Representations of a VCCS. . . . .	58
1.33	Kirchhoff- and Wave-Domain Representations of a CCVS. . . . .	59
1.34	Kirchhoff- and Wave-Domain Representations of a CCCS. . . . .	60
1.35	K- and W-Domain Representations of an Ideal Voltage Converter Two-Port. . . .	62
1.36	K- and W-Domain Representations of an Ideal Current Converter Two-Port. . . .	63
1.37	K- and W-Domain Representations of an Ideal Power Converter Two-Port. . . .	64
1.38	Kirchhoff- and Wave-Domain Representations of a Two-Port Gyrator. . . . .	65
1.39	Kirchhoff- and Wave-Domain Representations of a Two-Port Active Gyrator. . . .	67
1.40	Kirchhoff- and Wave-Domain Representations of a Two-Port Dualizer. . . . .	68
1.41	Kirchhoff- and Wave-Domain Representations of a Two-Port Nullor. . . . .	69
1.42	Four Types of Operational Amplifiers and Their Ideal Equivalents Using a Nullor.	69
1.43	NPN Bipolar Junction Transistor and its Idealized Nullor Equivalent. . . . .	70
1.44	$y$ -Parameter Amplifier. . . . .	71
1.45	$z$ -Parameter Amplifier. . . . .	72
1.46	$h$ -Parameter Amplifier. . . . .	73
1.47	$g$ -Parameter Amplifier. . . . .	74
1.48	Kirchhoff- and Wave-Domain Representations of Three-Port Parallel Connection. .	75
1.49	Kirchhoff- and Wave-Domain Representations of Three-Port Series Connection. .	76
1.50	Kirchhoff- and Wave-Domain Representations of Three-Port Circulator. . . . .	77
1.51	Decomposing Parallel Connections into Three-Port Parallel Connections. . . . .	79
1.52	Decomposing Series Connections into Three-Port Series Connections. . . . .	80
1.53	Decomposing Circulators into Three-Port Circulators. . . . .	81
1.54	TR-808 Bass Drum Output Filter. . . . .	82
1.55	Overall Magnitude Response for Simplified TR-808 Bass Drum Output Filter. .	84

1.56	TR-808 Bass Drum Output Filter, Rearranged to Highlight Topology. . . . .	86
1.57	TR-808 Bass Drum Output Filter, Wave Digital Filter Structure. . . . .	86
1.58	Connection Tree for TR-808 Bass Drum. . . . .	87
1.59	Overall Magnitude Response for TR-808 Bass Drum Output Filter. . . . .	88
2.1	Lattice Section, Bridged-T Section, and Twin-T Section. . . . .	93
2.2	Brune/Type-C Section and Brune Equivalent. . . . .	93
2.3	Jaumann Section and Type-D Section. . . . .	94
2.4	Type-E Section and Richards Equivalent. . . . .	94
2.5	Op-amp Differential Amplifier Topology and Equivalent Circuit. . . . .	95
2.6	Op-Amp-Based Filters Which can be Framed as Differential Amplifiers. . . . .	96
2.7	Op-Amp-Based Filters Which can't be Framed as Differential Amplifiers. . . . .	97
2.8	Deriving a WDF Adaptor Structure for the Fender Bassman Tone Stack. . . . .	99
2.9	Deriving a WDF Adaptor Structure for the Tube Screamer Tone/Volume Stage. .	100
2.10	Instantaneous Thévenin Port Equivalents. . . . .	102
2.11	Framework Signal Flow Graphs, Derived and Resolved. . . . .	108
2.12	Overview of Modeling Approach to Hammond Organ Vibrato/Chorus Circuit. .	110
2.13	Passive Bridged-T Circuit. . . . .	111
2.14	Passive Bridged-T Filter, WDF. . . . .	112
2.15	Connection Tree for Passive Bridged-T Filter. . . . .	113
2.16	Bridged-T Filter, Thévenin Equivalents Attached. . . . .	113
2.17	Forming MNA matrix $\mathbf{X}$ . . . . .	114
2.18	Various Passive Bridged-T Filter Magnitude Responses. . . . .	115
2.19	Bridged-T Resonator Schematic, Nullor- and Controlled-Source-Based Models. .	116
2.20	Idealized (Nullor-Based) Bridged-T Resonator Circuit, WDF. . . . .	117
2.21	Connection Tree for Idealized (Nullor-Based) Bridged-T Resonator Circuit. . . .	117
2.22	Idealized (Nullor-Based) Bridged-T Resonator, Thévenin Equivalents Attached. .	118
2.23	Forming MNA matrix $\mathbf{X}$ . . . . .	118
2.24	Various Bridged-T Resonator Magnitude Responses. . . . .	120
2.25	Non-Ideal (Controlled-Source-Based) Bridged-T Resonator Circuit, WDF. . . . .	121
2.26	Connection Tree for Non-Ideal (Controlled-Source-Based) Bridged-T Resonator. .	121
2.27	Bridged-T Resonator with Feedback Schematic. . . . .	122
2.28	Bridged-T Resonator with Feedback, Idealized (Nullor-Based) Model. . . . .	123
2.29	Nullor-Based Bridged-T Resonator Circuit with Feedback Stage, WDF. . . . .	124
2.30	Connection Tree for Nullor-Based Bridged-T Resonator Circuit with Feedback. .	124
2.31	Bridged-T Resonator with Feedback, Non-Ideal (Controlled-Source-Based) Model.	125
2.32	Controlled-Source-Based Bridged-T Resonator Circuit with Feedback, WDF. . . .	126
2.33	Connection Tree for Controlled-Source-Based Bridged-T Resonator w/ Feedback. .	127

3.1	A Diode. . . . .	130
3.2	Diode Kirchhoff-Domain $v-i$ Characteristic, and Log-Scaled Version. . . . .	130
3.3	Example Connection Tree with Single Nonlinearity. . . . .	132
3.4	Ideal Diode and Piecewise-Linear Active Resistor (“Chua’s diode”). . . . .	133
3.5	Chua’s Circuit, Wave Digital Filter. . . . .	134
3.6	Chua’s Circuit Connection Tree. . . . .	134
3.7	Piecewise Linear Kirchhoff- and Wave-Domain Characteristics ( $R = 1$ ). . . . .	135
3.8	Diode Pair and Two Orientation-Dependent Simplified Versions. . . . .	136
3.9	Diode Pair Kirchhoff- and Wave-Domain Characteristics ( $R = 1$ ). . . . .	137
3.10	Generalized Diode Clippers and Two Orientation-Dependent Simplified Versions. .	139
3.11	Pulse Shaper Schematic, Rearranged to Highlight Topology, and WDF. . . . .	141
3.12	Connection Tree for Pulse Shaper Circuit. . . . .	142
3.13	Time Domain Response of Pulse Shaper in Response to Input Pulses (Zoom In). .	143
3.14	Time Domain Response of the Pulse Shaper in Response to Input Pulses. . . . .	144
4.1	NPN BJT, Terminals and Ports. . . . .	148
4.2	Different Equivalent Circuit Models of NPN BJTs. . . . .	150
4.3	PNP BJT, Terminals and Ports. . . . .	151
4.4	Triode, Terminals and Ports. . . . .	152
4.5	Deriving a WDF Adaptor Structure for the Big Muff Pi Clipping Stage. . . . .	159
4.6	Proposed Method Signal Flow Graphs. . . . .	161
4.7	Envelope Generator Schematic, Rearranged to Highlight Topology, and WDF. . .	166
4.8	Envelope Generator Connection Tree. . . . .	168
4.9	Definition of Port Variables of Nonlinearities and Circuit for MNA. . . . .	169
4.10	Time Domain Response of the Envelope Generator to Different Pulse Amplitudes.	170
4.11	Nonlinear Bridged-T Resonator with Feedback Schematic and Nullor Realization.	172
4.12	Nonlinear Bridged-T Resonator Rearranged to Highlight Topology, and WDF. . .	174
4.13	Nonlinear Bridged-T Resonator with Feedback Connection Tree. . . . .	175
4.14	Definition of Port Variables of Nonlinearities and Circuit for MNA. . . . .	176
4.15	Time Domain Response of Nonlinear Bridged-T Resonator at Six Decay Settings.	177
4.16	Time Domain Response of Nonlinear Bridged-T Resonator, Attack Detail. . . . .	178
4.17	Circuits Which Have Been Modeled Using the Proposed Method. . . . .	180
I	Comparing Wave Digital Filter and SPICE for a Family of Tone Settings. . . . .	183
II	Comparing Wave Digital Filter and SPICE for a Family of Pulse Amplitudes. . . .	184
III	Comparing WDF/SPICE for a Family of Input Amplitudes, Detail on Attack. . .	185
IV	Normalizing Wave Digital Filter Simulations of Figure III by Pulse Amplitude. .	186
V	Comparing Wave Digital Filter and SPICE for a Family of Decay Settings. . . . .	187

VI	Demonstrating Amplitude and Timbre Variation on Repeated Notes. . . . .	188
A.1	Extended $y$ -Parameter Equivalent Circuit. . . . .	196
A.2	Splitting Resistances on Extended $y$ -Parameter Equivalent Circuit. . . . .	196
A.3	Diode and Linear Companion Model. . . . .	197
A.4	Diode Linearization. Values rounded to four significant figures. . . . .	198
A.5	NPN Transistor, Equivalent Circuit, and Linear Companion Model. . . . .	199
A.6	Emitter-Follower Two-Port and Linearized Companion Model. . . . .	199
A.7	TR-808 Bass Drum Output Filter at DC. Values Rounded to Six Decimal Places.	202
B.1	TR-808 Bass Drum Tone, Level, and Output Buffer Simplified Model. . . . .	205
B.2	TR-808 Bass Drum Tone, Level, and Output Buffer Equivalent Circuit. . . . .	206
B.3	Simplified TR-808 Bass Drum Tone, Level, and Output Buffer Responses. . . . .	207
C.1	$R_1$ Branch Linearization. . . . .	209
C.2	Tom/Conga $R_1$ Resistance as a Function of Knob Position $x \in [0, 1]$ . . . . .	211
C.3	Passive Bridged-T Filter with Nodes Labeled. . . . .	212
C.4	Bridged-T Resonator Model (Ideal, Nullor-Based) with Nodes Labeled. . . . .	213
C.5	Circuit-Theoretic Nullator and Norator Equivalences. . . . .	215



# Introduction

Musicians like vintage stuff: classic guitar tube amplifiers, dusty analog synthesizers, crunchy distortion pedals employing rare and faulty Japanese germanium diodes manufactured for only a few months in the 1970s. I exaggerate only slightly. After all, what guitarist wouldn't want at least the option to dial in the tone of their heroes; which synthesist wouldn't want access to the Moog synthesizer tones of Wendy Carlos and Keith Emerson? Outside the realm of electronics, which violinist wouldn't like to take a Stradivarius for a spin? The sounds of the past and the instruments through which they were created are a central part of our musical heritage. To address sustained demand for increasingly rare, expensive, and inaccessible audio circuitry, manufacturers and researchers have developed sophisticated techniques for mimicking vintage devices. As a research field and marketing buzzword, this trend is known as Virtual Analog. Engineers working in Virtual Analog use a variety of systematic and ad hoc techniques to model vintage devices.

Although most commercial and research effort is aimed at preserving classic synthesizer and guitar tones, I'm concerned rather with the preservation of a more niche musical tradition: *circuit bending* [1]. Circuit bending is the practice of modifying musical circuitry in both experimental and systematic ways, with the goal of unlocking new sounds which have never been heard before. Reed Ghazala initiated the practice in the 1960s as an affordable way of experimenting with audio synthesis. Today circuit bending is an important part of musical and artistic practice, although the pantheon of affordable consumer electronics (Casio keyboards, Texas Instruments Speak & Spell, etc.) which form a foundational text for the movement are becoming quite rare themselves.

Unlike, for example, modeling one particular guitar distortion or one particular classic synthesizer's square wave tone, the prospect of Virtual Analog modeling of circuit bending is extremely hampered by a proliferation of possibilities in these circuits. After all, a circuit bender may reach into an instrument with their soldering iron to add, remove, modify, and supplement electronic components; to add new controls usually in the form of switches, potentiometers, and conductive body contacts; to add or remove entire sections of the circuit; or to introduce surprising feedback paths which the designer never dreamed of. A distortion pedal may have one or two controls, an analog synthesizer may have a pulse-width control, but for a circuit-bent instrument, the possibilities are endless. Perhaps the central irony of attempting to model circuit-bent instruments is that although

the practice doesn't require any special theoretical knowledge for practitioners, effectively modeling a circuit-bent instrument is far more complex than modeling an instrument whose design is fixed. My early attempts at modeling three voices (the Bass Drum [2], Cymbal [3], and Cowbell [4]) from the classic TR-808 drum machine convinced me that using ad hoc techniques to model circuit-bent instruments would be prohibitively difficult to generalize.

In my view, the best prospect for modeling circuit-bent instruments is deep modeling of the physics of the devices on the level of individual electrical components and their interconnections. Fortunately, the well-known but somewhat esoteric *Wave Digital Filter* [5] formalism which was originated by Alfred Fettweis in the early 1970s is built on exactly these principles, and indeed Virtual Analog researchers have recently begun applying it to modeling audio circuitry [6]. Unfortunately, Wave Digital Filter theory was not originally intended for modeling audio circuits. Hence, electrical devices which are common in audio circuits like operational amplifiers, common circuit design paradigms involving complicated topologies and feedback, and the common case of circuits involving more than one nonlinear devices are not handled in general, or sometimes at all, by the classical theory. Take away all audio circuits involving operational amplifiers, all audio circuits involving feedback, all audio circuits involving more than one diode or even a single transistor, and there aren't very many circuits left. So, in the field of Virtual Analog, the elegant, accurate, and robust Wave Digital Filter approach has very limited applicability and has remained a bit of a curiosity.

## Summary of the Dissertation

This dissertation collects my work on extending the Wave Digital Filter formalism far enough that it may handle audio circuits in the general case, with no theoretical limitation on the use of electrical devices that are common in audio, the number or type of nonlinearities, or ways in which these components are connected. In addition to laying the groundwork for Wave Digital Filter modeling of circuit-bent electronic musical instruments, this also enables Wave Digital Filter modeling of standard audio circuitry like guitar amplifier circuits, filters, oscillators, and distortion pedals. Much of the work is concerned with reviewing classical theory and introducing novel techniques which enable modeling of complicated topologies and multiple nonlinear elements. However each Chapter also devotes some space to modeling one part of the Roland TR-808 Bass Drum circuit, demonstrating the modeling techniques covered in that Chapter. At the end, they are combined to form a complete Virtual Analog model.

Here in the Introduction, we will first review previous and related work in the Virtual Analog context. Following that, an introduction to the TR-808 Rhythm Composer is given, with a focus on its Bass Drum circuit which is the subject of the case studies in each of the four Chapters. The first two Chapters consider linear circuits, and the last two focus on nonlinear circuits.

In Chapter 1, the basics of Wave Digital Filter modeling of linear circuits are reviewed. A parametric wave definition which encompasses the classical voltage, power, and current waves is proposed, and wave domain models for common and uncommon linear electronic devices and standard series and parallel connections are derived. These methods enable Wave Digital Filter modeling of linear circuits with simple circuit topologies. A case study on the Output Filter from the TR-808 Bass Drum shows these techniques in action.

In Chapter 2, the issue of complicated topologies is introduced. Many audio circuits have complicated topologies that cannot be decomposed into series and parallel connections and may contain absorbed multiport linear elements like nullors and controlled sources. We review previous work on this topic and introduce two novel techniques. The first handles arbitrarily complex circuit topologies in a Wave Digital Filter and the second leverages the first to handle multiple linear non-adaptable elements collected at the root of a Wave Digital Filter simulation. These methods enable Wave Digital Filter modeling of linear circuits with complicated topologies and absorbed multiport elements. A case study on a family of different simplified versions of the Bridged-T Resonator from the TR-808 Bass Drum show how these techniques can be applied.

In Chapter 3, the basics of Wave Digital Filter modeling of nonlinear circuits are reviewed. These methods cover one-port nonlinearities only, including the case where multiple nonlinearities can be consolidated into a single one-port (e.g., diode clippers). A case study on the Pulse Shaper from the TR-808 Bass Drum shows these techniques in action.

In Chapter 4, the most complicated and general class of circuits is considered: a circuit which may have any topology and which may involve any number of nonlinear circuit elements. After reviewing the various approaches to modeling circuits in this category, we propose a novel techniques to handle multiple nonlinearities collected at the root of a Wave Digital Filter simulation. By providing systematic techniques for setting up a block diagram of the simulation of any circuit, deriving the behavior of any block in the block diagram, and ensuring the blocks can be connected together, these techniques make the Wave Digital Filter formalism very widely applicable and enable, in theory, Wave Digital Filter simulation of any standard audio circuit. Case studies on the Envelope Generator and full Nonlinear Bridged-T Resonator from the TR-808 Bass Drum demonstrate the systematic application of these techniques.

In a Conclusion, all of the case studies are put together to form a full Virtual Analog simulation of the TR-808 Bass Drum Circuit and final comments on the approach are given. Three Appendixes cover the derivation of the extended  $y$ -parameter model used in the Chapter 1 case study (Appendix A), the derivation of a simplified model of the TR-808 Bass Drum's Output Filter (Appendix B), and the calculation of the equivalent resistance of the diode clipper branch in the TR-808 Tom and Conga circuits, linearized at dc (Appendix C).

## Literature Review

Virtual Analog modeling is concerned with preserving the sound of electronic musical instruments as well as historical musical practice [6, 7, 8, 9, 10, 11]. This field has generated substantial commercial activity, beginning with the Nord Lead in 1994 [12]. At the same time, it poses substantial research challenges. Many classic electronic musical instruments are quite complex and nonlinear, and modeling them is difficult task. Indeed, nonlinear aspects of audio circuitry such as triodes [13, 14] are often identified as the most important aspect of a device’s sound.

Here we’ll briefly review the background literature on Virtual Analog modeling. Specifically, we’ll review “black box” modeling approaches which mimic the behavior of an analog system without necessarily exploiting any knowledge about the actual structure of the system and “white box” modeling approaches which exploit knowledge of a circuit’s structure and its physics to create a digital model.

### Black Box Modeling

Black box approaches model a system without exploiting knowledge about its underlying physical structure. This can be particularly useful if a circuit’s schematic is not known or is considered too complex to be tractable or for classes of problems with a similar structure, e.g., Virtual Analog oscillator design or modeling distortion effects. For each case, it is essential to develop a relevant signal processing algorithm parameterized by meaningful parameters that can be estimated through input/output measurements [15]. In some cases these algorithms resemble existing mathematical frameworks like a Volterra system [16, 17] or Wiener and Hammerstein system [18, 19]. In other cases, custom generalized signal processing algorithms may be developed to fit the class of systems [20, 21, 22]. Black box techniques are also common in modeling guitar amplifiers [23, 24], loudspeakers [25], distortion circuits [19], and musical filter [18]. For linear systems, this problem reduces to the classic problem of transfer function or impulse response measurement.

Virtual Analog research is also concerned with efficient, accurate digital synthesis of analog waveforms. Although classic synthesizers indeed used circuitry to generate these waveforms, this research thread focuses more on the behavior of the oscillators than the physical system that produced them. This research area is quite mature [26, 27, 28, 29, 30, 31, 32, 33, 34, 35, 36, 37, 38, 39, 40, 41] and developed in parallel with, and with the same motivation as, the physical modeling literature on circuits.

### White Box Modeling

White box approaches use knowledge of a circuit’s structure to derive digital models. This is a useful approach when a circuit’s schematic is known, which is often the case with classic audio circuits and is certainly the case when a circuit is being designed from scratch. The simplest

white box approach builds on digital filter theory and models linear circuits by discretizing their continuous-time transfer functions directly. In this approach, a continuous-time transfer function is discretized (usually using the Bilinear Transform) and factored into biquadratic filters to avoid numerical sensitivity issues [42, 43, 44, 45]. In Virtual Analog this has been applied successfully to, e.g., modeling linear filters from the SP-12 Drum Machine [46] and the Fender Bassman tone stack [47]. Although these derivations are done assuming linear time-invariance, alterations to the basic approach aim at accommodating time-varying filters [45]. In these cases, complicated coefficient update may be simplified using, e.g., common sub-factor extraction [48].

If a circuit is simple, it is often easy to derive its transfer function by hand using basic analysis tools from electrical engineering such as loop analysis, mesh analysis, or node analysis. If a circuit is more complicated, it may be helpful to write out a signal flow graph of its constituent equations and solve the transfer function using Mason’s gain rule [49, 50, 51, 4]. For the most complicated circuits, it will be necessary to make recourse to one of the classical systematic circuit formulations like Nodal Analysis, Modified Nodal Analysis, or Tableau Analysis [52].

For Virtual Analog modeling of complicated and nonlinear circuits, several systematic modeling paradigms have been proposed. The most prominent is nonlinear State-Space Modeling. Another approach called Port Hamiltonian systems is based on state-space modeling of energy flow within a system. A final approach which is the subject of this dissertation is Wave Digital Filter modeling.

### State-Space Modeling

In the Virtual Analog community, one family of white box modeling approaches builds on the *state space* formalism from control engineering. Early sound synthesis work which leveraged state space modeling aimed at reconciling physical modeling and signal modeling, and focused on applications to wind instruments [53]. The specific formulation proposed by Borin *et al.* [54, 55], which accommodates memoryless nonlinearities, launched interest in state space circuit modeling in Virtual Analog. This formulation is a vector generalization of Smith’s approach to solving the reed-bore interaction in Digital Waveguides [56]. In the approach of Borin *et al.*, the state-space model is discretized and the resulting implicit loop through the nonlinearities is solved using table lookup or iterative solutions like Newton–Raphson iteration. Rather than circuits, Borin *et al.* actually targeted *acoustic* systems; they gave as examples case studies on hammer–string interaction in piano simulation and reed–bore interaction in a woodwind model. However, they did also model a Chua’s circuit. Their approach is known as the *K Method* and has led to a family of techniques targeted to circuit simulation [57, 58]. Two flavors of iterative solutions are proposed in the literature, one based on current iteration (the “classical” K Method) and one on voltage iteration (the “modified” or “VK Method”) [57, 7]. The K Method has been used to model audio circuits like guitar bright switches, diode clippers, and common emitter and common cathode amplifiers [59, 57, 58].

To use the K Method to discretize a circuit, it is required to find the set of Ordinary Differential

Equations (ODE) that describe the circuit. This can be tedious to do by hand, so the *Nodal K Method* (NK Method) was developed to systematize the derivation of the circuit ODE in the form required for the K-method [57]. The NK Method works by populating a continuous-time nonlinear state space system, discretizing that system, and using the K Method to resolve the implicit part of the system. The discrete time system will have different properties depending on which discretization method is used for the discretization [60].

There are some circuits which have a non-invertible conductance matrix when modeled with the NK approach, meaning that the NK Method fails for those circuits on a structural level. To handle these cases, the *Discrete K Method* (DK Method) was proposed [58]. The DK Method discretizes reactances at the start, forming their linear companion models before populating a state-space system. Linear companion models will always have some conductance, which guarantees an invertible conductance matrix. An extension to the NK Method allows the inclusion of operational amplifiers [61]. The NK Method has been used to model, e.g., a treble booster guitar pedal (Electro-Harmonix Screaming Bird) [62].

After discretization, the standard state-space equations require keeping track of not only the current inputs to the circuit but also the previous inputs, increasing the memory requirements of the simulation. In [63], Dempwolf *et al.* propose a *canonicalized* state space approach which transforms the state-space system by defining a new set of state variables and rearranging the equations so that the new state update equation only depends on the current input vector (see also [64, pp. 189–200]), showing applications to Fender Tone Stack type AA763 and Marshall JCM900 Preamp. A drawback of this approach is that it does not include the automatic derivation of system matrices as in the standard Nodal DK Method [65]. This canonicalization approach is used in [66] to simulate an analog guitar compressor pedal (the MXR DynaComp), where an approach to including a simplified model of an operational transconductance amplifier is also presented; another compressor (the UREI 1176LN) is simulated in [67].

A related approach to canonicalization is given in [68], which also extends the nodal DK method to efficiently handle variable circuit elements (e.g., potentiometer). Here, canonicalization is done on an element-by-element basis rather than on the global state space matrices. This approach to handling variable circuit elements is used in [69], which deals with the simulation of a Fender-style guitar preamplifier using the Dempwolf model [70]. There, Macak *et al.* introduce further refinements to potentiometer modeling (the introduction of “virtual constant resistors”) which ensures that certain matrices which must be inverted are kept full rank.

The method of [68] has been used to simulate an analog phaser (the MXR Phase 90) [71] and a bucket-brigade-based analog flanger circuit (the Electro-Harmonix Deluxe Electric Mistress) [72]. The method of [63] was used in [73] to model the Boss SD-1 Super Overdrive distortion pedal, where Holters *et al.* also introduced a behavioral extension to deal with op-amp clipping.

Recent work by Holmes and van Walstijn [74] studied in detail specifics of the nonlinear solver

in state space systems of the form proposed in [68]. Applications to simulation and parameter optimization of a treble booster circuit (the Dallas Rangemaster Treble Booster) are shown in [75].

The NK Method has some inherent limitations. First, every node in the circuit must be connected. Second, there may not be any nodes which are only connected to nonlinearities. Finally, nonlinearities must always be represented as voltage-controlled current sources [76]. To overcome these limitations, Holters and Zölzer propose a *Generalized* modeling paradigm [76]. This enables, e.g., the incorporation of behavioral soft-clipping operational amplifier models [76] of the form proposed in [61] and complex nonlinear transformer models like the Jiles–Atherton model [77, 78]. Improved table lookup methods based on  $kd$  trees have been proposed to improve solution of the implicit nonlinear relationship within this framework [79].

### **Port Hamiltonian Modeling**

The Port Hamiltonian approach to Virtual Analog modeling is an emerging technique which is based on state-space modeling of energy flow within a multi-physics system [80], discretized using a discrete gradient [81]. In the Virtual Analog context, Falaize *et al.* have used this approach to model a Crybaby wah pedal [82], loudspeakers [83, 84, 85], different parts of a Rhodes piano [80], diode clippers, and transistor amplifiers [86].

### **Wave Digital Filters**

Alfred Fettweis developed the Wave Digital Filter concept in the early 1970s [87, 88] as a way of designing special digital filters with the same structure as certain analog prototypes (or “reference filters”). These structures rendered the behavior of those analog reference filters robust against electrical component variation. Digital filters designed according to Wave Digital Filter principles and based on these reference filters use wave variables as their signal variables [89] and enjoy excellent tolerance characteristics. Their frequency responses are insensitive to coefficient truncation and roundoff accumulation (especially compared to, for instance, a direct-form realization of their continuous-time transfer functions) [87, 88].<sup>1</sup> These properties come from the fact that Wave Digital Filters are derived by *local* discretization of circuit elements and their connections [91], a process which (when implemented properly) strictly ensures that the energetic properties of the analog reference circuit are replicated in the Wave Digital Filter [92].

Some of the most important early work on Wave Digital Filters focused on developing the basic concept [87, 88], investigating their pseudo-passivity and energetic properties [92], and bringing the concept of a Wave Digital Filter “adaptor” to maturity through the introduction of reflection-free ports [91]. The first 16 years of Wave Digital Filter developments are reviewed in Fettweis’s landmark 1986 article, “Wave Digital Filters: Theory and Practice” [5], which remains a central

---

<sup>1</sup>A Wave Digital Filter-like approach has also been used in the synthesis of active analog filters called “wave active filters” [90].

resource for Wave Digital Filters today. Wave Digital Filter research has gone far beyond the design of digital filters based on analog reference circuits. One research trend is concerned with using a multidimensional generalization of the Wave Digital Filter concept for the solution of Partial Differential Equations [93, 94]. For the purpose of this dissertation, we'll only consider the case of lumped circuits described by Ordinary Differential Equations.

The Wave Digital Filter approach was recognized in the music technology field as early as 1987 [95], where Julius Smith recognized their connection to his Digital Waveguide Modeling approach [96, 97]. Although Wave Digital Filters were originally designed as a way to design digital filters with good properties, based on known topologies and design procedures for analog reference circuits, research interest in them has pivoted towards their use in emulation of musical lumped systems [98, 99, 100, 101, 102]. Lumped systems involve only time derivatives (no spatial derivatives) and are characterized by dual variable pairs known generally as across/through or effort/flow pairs. In the electrical context these variables are voltage / current; in the mechanical rectilinear context these variables are force and velocity. Examples of other types of systems that can be modeled as lumped systems include mechanical rotational systems, acoustical [103] or fluid dynamic systems [104]. Equivalences among these domains can be drawn using two different kinds of analogies: the “conventional”/“impedance” analogy [104, 97], or the “Firestone”<sup>2</sup>/“mobility”/“admittance” analogy [108]. Firestone vigorously condemns the conventional analogy,<sup>3</sup> largely based on the fact that it does not preserve the system's topology. Since the early 1990s, Wave Digital Filters have been used in the modeling of many lumped mechanical systems [98], including piano hammers [109, 110, 111, 112, 6], reeds [113, 94], brass mouthpieces [114], and woodwind tone-holes [115, 116, 117]. In many of these cases, Wave Digital Filter models of the lumped part of the system (e.g., reed or hammer) were interfaced [118, 112, 119, 120] with Digital Waveguide models of the distributed part of the system (e.g., string or tube). This relates strongly to the two-port method of Lawson *et al.* [121, 122, 123, 124].

Wave Digital Filter concepts are covered in some textbooks, e.g. [124, 125, 126, 97]. However, the techniques presented in these texts do not solve the problems faced by the Virtual Analog algorithm designer. Most of the literature is focused on linear reference circuits whose topology can be decomposed entirely into series and parallel connection. Work coming out of electrical engineering tends to cover the traditional Wave Digital Filter development [5], which is focused on linear reference circuits with ladder [127] or lattice topologies [128]; this parallels the focus on ladder structures in classical network theory [129]. Work from the physical modeling literature [97] focuses on mechanical rectilinear systems including loudspeakers [130], where reference circuits are derived via an equivalent circuit transformation from a mechanical system [104] and thus their topologies tend to be restricted to series and parallel connections. Electrical analogies for lumped systems are

---

<sup>2</sup>Although this convention is commonly known as the “Firestone analogy,” it appears to have been discovered independently [105] by Darrieus [106] and Hähnle [107].

<sup>3</sup>“The author nominates for oblivion the conventional left-handed mechanical-electrical analogy.” [108]

also used in loudspeaker design [131]. When modeling distributed mechanical systems in the *Digital Waveguide* context [97], it is common to consider the nonlinearities (e.g., a nonlinearity at the bridge of a guitar and a nonlinearity at the nut of the guitar) to be decoupled by a propagation delay [132]; hence multiple coupled nonlinearities are not considered a pressing issue.

Recently, interest in Wave Digital Filters has been extended to the complicated case of modeling nonlinear audio circuits [6]. The unique issues that arise in modeling nonlinear audio circuits using Wave Digital Filters have generated a large body of research. A review of linear Wave Digital Filter principles is given in Chapter 1. A review of advanced topological aspects of Wave Digital Filters is given in Chapter 2. A review of the literature on Wave Digital Filters with one nonlinearity is given in Chapter 3. Finally, a review of the literature on multiple nonlinearities is given in Chapter 4. Extending these techniques so that they may be rendered applicable to a very general class of audio circuits is the subject of this dissertation.

While emphasizing that the Wave Digital Filter approach should be valid for any lumped system which can be represented as an electrical circuit, we restrict our focus exclusively to electrical circuits in the remainder of the dissertation.

## TR-808 Bass Rhythm Composer

The Roland TR-808 Rhythm Composer is a very popular analog drum machine released in 1980. A picture of a TR-808 is shown in Figure I. Today its sound is ubiquitous and it has been used on more hit records than any other drum machine [133]. However, only 12,000 units were ever produced (between 1980–1983) [134].

Throughout this dissertation, we'll use the Bass Drum circuit from the Roland TR-808 Rhythm Composer as a motivating example. The complexity of the TR-808's circuitry poses a new challenge to the Virtual Analog field; considering it from a circuit modeling standpoint puts pressure on the field to generate new research. Indeed, the case study in each chapter will focus on one subcircuit of the TR-808's bass drum circuit, applying the theoretical material of that chapter to creating a Wave Digital Filter model of that subcircuit and culminating in a model of the entire bass drum.

The schematic for the TR-808 Bass Drum is shown in Figure II [135]. This remarkable and versatile circuit is activated by passing short (1 ms wide) pulses with amplitudes between 4–14 V in to the circuit at  $v_{in}$ . This pulse is shaped by one subcircuit and delivered to a resonant bandpass filter. At the same time the center frequency of that bandpass filter is modulated by an envelope generator which was also activated by the input pulse. The output of the ringing bandpass filter is further filtered to control its spectral content. This description only covers a basic and idealized concepts of the circuit's operation; in fact secondary effects are also at play and account for the classic and difficult to imitate sound of the TR-808 Bass Drum. The circuit is parameterized by the input pulse amplitude and user-controllable tone, decay, and level knobs.



Figure I: Roland TR-808 Rhythm Composer.

The produced sound is, to a very rough approximation, a decaying  $\approx 50$  Hz sinusoid. This closely matches measured fundamental frequency of concert bass drums that were available at the time of the TR-808's design [136, pp. 271–273]. It was also known at the time that a concert bass drum's timbre could be modeled using decaying sinusoids of different amplitudes, frequencies, and decay rates—Fletcher and Basset reported that 435 such decaying sinusoids were necessary to accurately model a recorded bass drum timbre [137]. The fact that the TR-808 Bass Drum can achieve a convincing bass drum sound using only a single decaying sinusoid, implemented not with a digital computer but as an analog circuit, gives us a glimpse at the skill and sensitivity of the the TR-808 circuit's designers.

In this work, we will decompose the TR-808 Bass Drum into four sub-circuits. This division, which is based on circuit-theoretic equivalences as well as mild simplifying assumptions, is shown in Figure III. These four subcircuits are the Pulse Shaper, the Envelope Generator, the Nonlinear Bridged-T Resonator, and the Output Filter. Making the assumption of ideal voltage sources and ideal operational amplifiers, the division of the Pulse Shaper from the Envelope Generator and the division of the Bridged-T Resonator from the Output Filter are justified by exact circuit-theoretic equivalences. These also happen to parallel a conceptual division of the circuit into subcircuits with

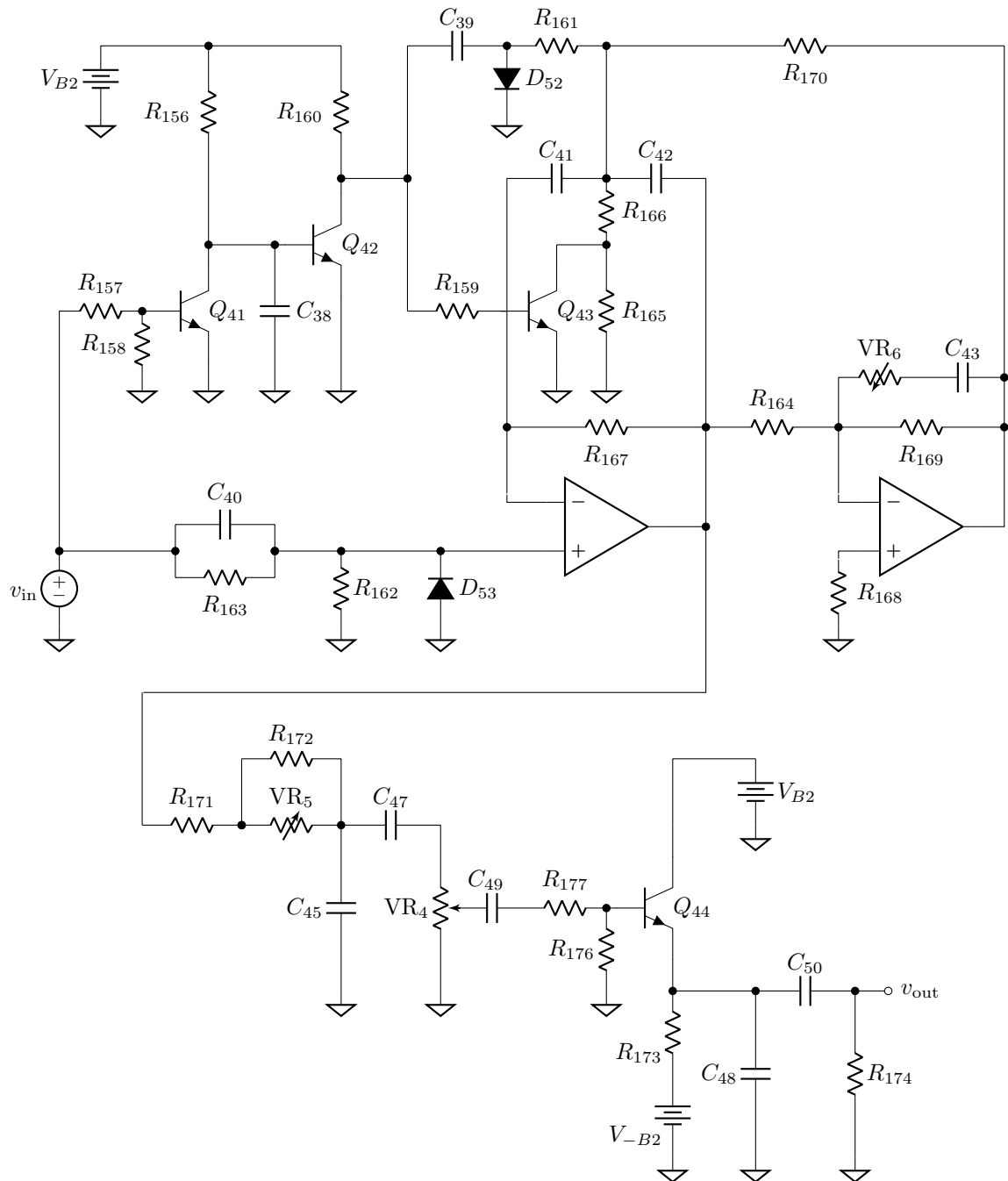


Figure II: TR-808 Bass Drum Schematic.

individual functions, as reflected in the device's service notes [135]. The division of the Envelope Generator and the Bridged-T Resonator is a mild simplifying assumption which does not alter the dynamics of the circuit significantly but greatly eases our modeling effort.

In the following four Chapters each of these subcircuits will be modeled using classical and proposed Wave Digital Filter approaches. In Chapter 1, a linearized version of the Output Filter will be modeled as an example of classical linear Wave Digital Filter techniques. In Chapter 2, a family of simplified versions of the Bridged-T Resonator will be modeled to demonstrate the novel topological techniques proposed in that Chapter. In Chapter 3, the Pulse Shaper will be modeled as an example of classical one-port nonlinear Wave Digital Filter techniques. In Chapter 4 the Envelope Generator and full Nonlinear Bridged-T Resonator are modeled, demonstrating the application of the proposed techniques for modeling circuits with multiple nonlinearities. Finally in the Conclusion all four subcircuits will be recombined into a complete Wave Digital Filter model. At this time we will look closer at a few aspects of the TR-808 Bass Drum's sound.

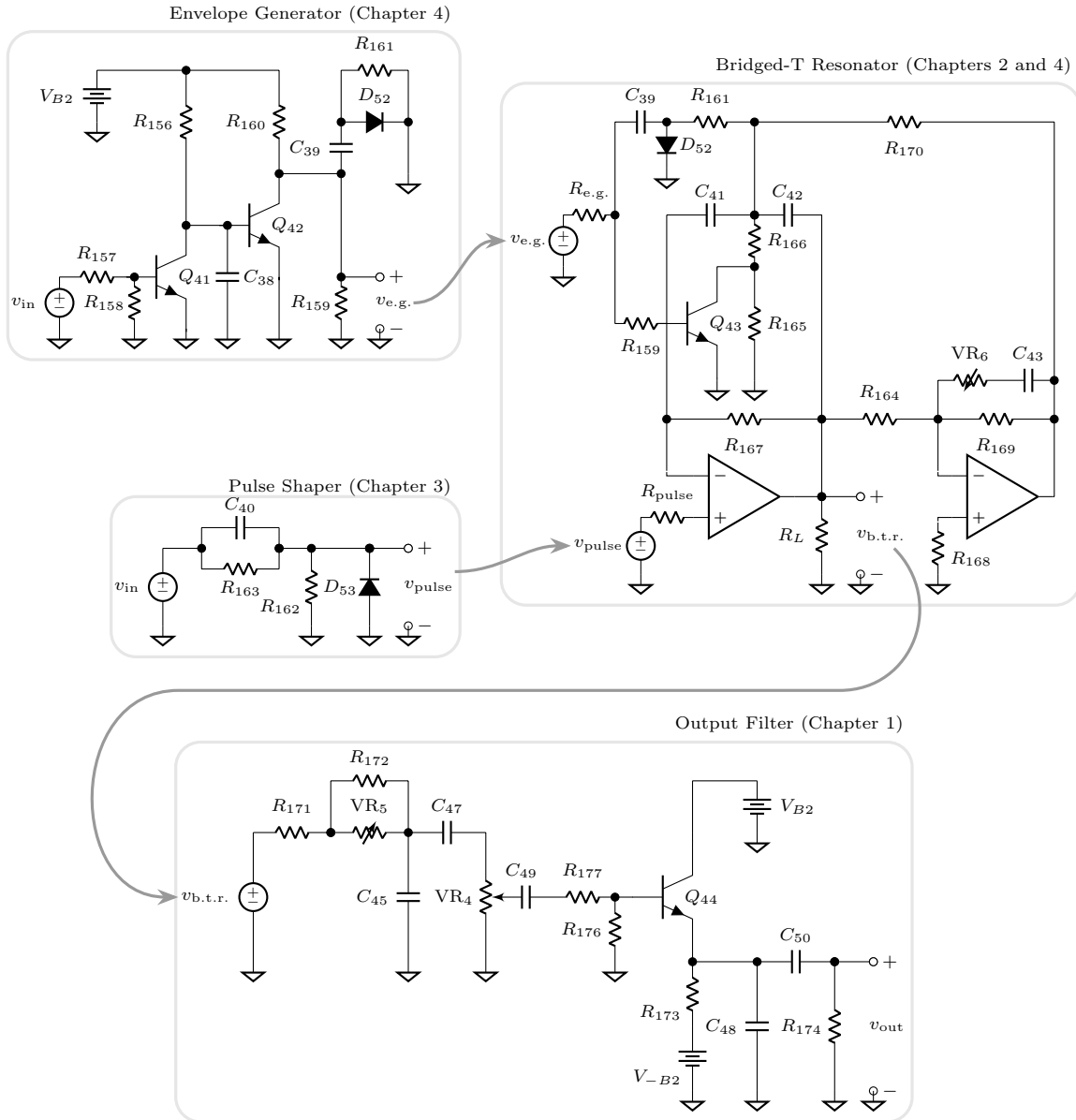


Figure III: TR-808 Bass Drum Circuit Separated into Parts.



# Chapter 1

## Linear Wave Digital Filters

In this chapter we will consider linear electrical circuits and the basics of Wave Digital Filter modeling. This comprises a tutorial review of linear Wave Digital Filter theory from the perspective of Virtual Analog circuit modeling, as well as some new contributions and a real-world case study on the Roland TR-808 Bass Drum's Output Filter.

The electrical elements we cover will run the gamut from standard to purely theoretical. Some of these elements (e.g., resistors, capacitors, inductors, transformers) are of importance to the Virtual Analog designer because they occur in standard audio circuits. Some are idealized but may reasonably stand in for parts of audio circuits—e.g., an ideal voltage source may represent the input to an audio circuit or a battery, ideal controlled sources may represent connections between subcircuits or amplifier two-ports, or a nullor may represent an operational amplifier in a negative feedback configuration, although the real-world circuits are not so idealized. Some are purely theoretical, although they serve an important role in filter design and/or theoretical purpose in managing aspects of a Wave Digital Filter design. These include ideal voltage/current/power converters, gyrators, dualizers, and circulators. Although these are not real circuit elements (or at least not ones that are used regularly in audio circuits), they are an important part of analog filter *design* and we will consider them for completeness.

We will focus on handling all of the standard one-, two-, and three-port linear electrical elements and their interconnection topologies rather than on the *computational cost* of doing so. The computational efficiency of Wave Digital Filters is a major advantage of the approach, but we will not dwell on it in this dissertation. Information on efficient realization of voltage-wave Wave Digital Filter adaptors is easily found in the literature [87, 91, 102].

The structure of this chapter is as follows. We'll begin with some preliminaries on ports in network theory, and realizability in digital structures (§1.1). These set up an overview and introduction to the Wave Digital Filter approach, after which we define the wave variables used in

Wave Digital Filter theory, including a new parametric wave definition. Following these preliminaries, we'll develop the basic building blocks of Wave Digital Filter theory, beginning with algebraic one-ports (§1.2): resistors, sources, open/short circuits, etc. After this, we'll develop Wave Digital Filter models of reactive one-ports (§1.3): capacitors and inductors. There we'll go beyond the standard Bilinear Transform approach to reactance discretization and put a special emphasis on alternative discretization methods, including Warped Bilinear Transform, Backward Euler, the  $\alpha$  Transform, and the Möbius Transform. Following this we'll develop Wave Digital Filter models of two-ports (§1.4), including basic topological connections (series/parallel), two-port electrical devices (transformers, gyrators, etc.), abstractions of more complicated two-port amplifiers ( $y$ -,  $z$ -,  $h$ -, and  $g$ -parameter models, ideal converters, nullors), and more abstract two-ports like dualizers. Building up to three-ports (§1.5), we'll derive the foundational topological connections of Wave Digital Filter theory, the three-port series and parallel adaptors, and the three-port circulator. Finally rules for realizing  $N$ -port series and parallel adaptors and circulators from combinations of three-ports are reviewed (§1.6). Having derived the standard WDF building blocks, we conclude the chapter by demonstrating their use in a simulation of the TR-808 Bass Drum's Output Filter (§1.7) and reviewing the capabilities and limitations of the presented techniques (§1.8).

## 1.1 Preliminaries

In this section we'll review background material which forms the basis of Wave Digital Filter theory, including ports (§1.1.1), realizability of digital structures (§1.1.2), and the Connection Tree concept (§1.1.3) which allows the order of calculations in a Wave Digital Filter structure to be systematized. Following that we'll introduce wave variables (§1.1.4), the signal variables in the Wave Digital Filter context.

### 1.1.1 Port Definition

Many electrical elements can be characterized by the behavior at their ports. Ports are characterized by two terminals (one which is designated positive and one which is designated negative), a port voltage across these terminals, and a port current through these terminals [129]. The port voltage is defined as the voltage drop from the positive terminal to the negative terminal. The port current is defined as the current into the positive terminal or equivalently the current out of the negative terminal.

A one-port is shown in the Kirchhoff domain in Figure 1.1a and in the wave domain in Figure 1.1b. In the Kirchhoff domain, the port is characterized by its port voltage  $v_0$  and its port current  $i_0$ . In the wave domain it is characterized by an incident wave  $a_0$  and a reflected wave  $b_0$ , as well as a port resistance  $R_0$  which parameterizes these waves.

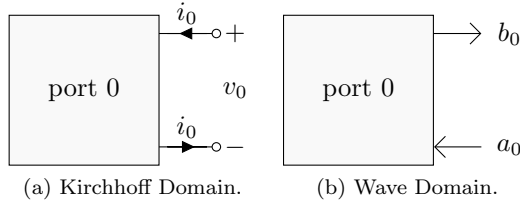


Figure 1.1: Kirchhoff- and Wave-Domain Representations of a Generic One-Port.

### 1.1.2 Realizability

For a digital filter structure to be “realizable” means that its computation can be structured explicitly into a series of adds, multiplies, reads and writes to delay registers, etc. Formal criteria defining realizability are given in the literature [138, 139, 5], but for our purposes realizability only means that there are no delay-free directed loops (or, “delay-free loops”) in the structure. A delay-free loop is a signal flow path that forms a loop without passing through any delays.

### 1.1.3 Connection Tree

Typically, Wave Digital Filter structures are organized into tree structures. To ensure that these structures are realizable, we must identify and remove every delay-free loop in the structure. This is a daunting task, but luckily it has been systematized by the *Binary Connection Tree* (BCT) concept [6, 140, 132]. In this work, in recognition of adaptors with more than two downward-facing ports in a tree structure, we will always speak more broadly of (not necessarily binary) *Connection Trees* [141].

The Connection Tree concept involves designating one element of the tree as its root, and then letting the rest of the structure organize itself into a tree below the root. In these trees we have three types of elements: the aforementioned *root* which has no upward facing ports and one or more downward-facing port, *adaptors* which have one upward facing port and one or more downward facing ports, and *leaves* which have one upward-facing port. We notice that any delay-free loop in this computational structure can be seen as originating in an upward-facing port, following some path down the tree, connecting back to the same upward-facing port, and then closing the loop.

From this we conclude that breaking the delay-free loop at each upward-facing port in the Wave Digital Filter structure will suffice to ensure a realizable structure. Breaking this delay-free loop is called “adapting” the port, and is a central precept of Wave Digital Filter theory. We will find that some ports can be adapted and some cannot. The task of modeling a reference circuit as a Wave Digital Filter is simplest when the circuit happens to contain at most one non-adaptable element. Of course we can not count on this property holding in general, and the presence of multiple nonadaptable elements is a major source of problems in applying Wave Digital Filter theory to Virtual Analog modeling. Resolving this issue in the linear and nonlinear case will be a major focus

later in this dissertation, in Chapters 2 and 4.

### 1.1.4 Wave Variable Definitions

In the two previous sections, we established that a good way to structure calculations in a digital simulation was to first decompose a circuit into a tree structure and then ensure that there can be no delay-free directed loops in the structure by ensuring that there can be no delay-free directed paths at the upward-facing port of each block in the simulation. However so far we have provided no way to satisfy this second criteria.

The Wave Digital Filter approach to avoiding delay-free directed paths at the upward-facing port of each block involves the introduction of *wave variables*. In the Wave Digital Filter literature, it is common to emphasize a physical interpretation of these wave variables. Indeed, the physical interpretation can help with developing an intuition about the scattering equations that parameterize the parts of a wave digital structure, provide a link to microwave engineering, and it also meshes philosophically with the energetic interpretation of Wave Digital Filters that helps to guarantee stability. However, this dissertation will emphasize an interpretation of the wave variable transformation as an arbitrary linear transformation.

In Wave Digital Filters, the use of voltage waves is common, although power and current waves are used as well [142]. We'll first define voltage, power, and current waves, then introduce a parametric wave definition that encompasses all these definitions. A discussion of alternative wave definitions follows.

#### Voltage Waves

At a port 0 characterized by port voltage  $v_0$  and port current  $i_0$ , the incident and reflected voltage waves  $a_0$  and  $b_0$  are defined by linear combinations of  $v_0$  and  $i_0$  that are parameterized by a free parameter  $R_0$  called port resistance<sup>1</sup>

$$\begin{aligned} a_0 &= v_0 + R_0 i_0 \\ b_0 &= v_0 - R_0 i_0. \end{aligned} \tag{1.1}$$

An important property of wave variable definitions is that they are invertible. Consider (1.1) written in matrix form

$$\begin{bmatrix} a_0 \\ b_0 \end{bmatrix} = \begin{bmatrix} 1 & R_0 \\ 1 & -R_0 \end{bmatrix} \begin{bmatrix} v_0 \\ i_0 \end{bmatrix}. \tag{1.2}$$

---

<sup>1</sup>In this section and elsewhere, we'll usually drop both continuous ( $t$ ) and discrete ( $n$ ) time indices for compactness, except when talking about reactances or time-varying signals.

The determinant of matrix  $\begin{bmatrix} 1 & R_0 \\ 1 & -R_0 \end{bmatrix}$  is  $-2R_0$ . Hence, the wave variable definition is only invertible if  $R_0 \neq 0$ .<sup>2</sup> Assuming  $R_0 \neq 0$  holds, the inverse of the voltage wave definition is

$$\begin{aligned} v_0 &= \frac{1}{2}a_0 + \frac{1}{2}b_0 \\ i_0 &= \frac{1}{2R_0}a_0 - \frac{1}{2R_0}b_0. \end{aligned} \quad (1.3)$$

In fact, inverse definitions are what we will substitute into Kirchhoff-domain equations as the first step of deriving their behavior in the wave domain.

Finally, the voltage wave definition and its inverse for a collection of ports with port voltages  $\mathbf{v}$ , port currents  $\mathbf{i}$ , incident waves  $\mathbf{a}$ , reflected waves  $\mathbf{b}$ , and a diagonal matrix of port resistances  $\mathbf{R}$  are written in matrix form as

$$\begin{array}{ccc} \mathbf{a} = \mathbf{v} + \mathbf{R}\mathbf{i} & \longleftrightarrow & \mathbf{v} = \frac{1}{2}\mathbf{a} + \frac{1}{2}\mathbf{b} \\ \mathbf{b} = \mathbf{v} - \mathbf{R}\mathbf{i} & & \mathbf{i} = \frac{1}{2}\mathbf{R}^{-1}\mathbf{a} - \frac{1}{2}\mathbf{R}^{-1}\mathbf{b} \end{array}. \quad (1.4)$$

## Power Waves

The use of power waves in Wave Digital Filters is also common. At a port 0, the power wave definition and its inverse are

$$\begin{array}{ccc} a_0 = R_0^{-1/2}v_0 + R_0^{1/2}i_0 & \longleftrightarrow & v_0 = \frac{R_0^{1/2}}{2}a_0 + \frac{R_0^{1/2}}{2}b_0 \\ b_0 = R_0^{-1/2}v_0 - R_0^{1/2}i_0 & & i_0 = \frac{R_0^{-1/2}}{2}a_0 - \frac{R_0^{-1/2}}{2}b_0 \end{array}. \quad (1.5)$$

The power wave definition and its inverse for a collection of ports are written in matrix form as

$$\begin{array}{ccc} \mathbf{a} = \mathbf{R}^{-1/2}\mathbf{v} + \mathbf{R}^{1/2}\mathbf{i} & \longleftrightarrow & \mathbf{v} = \frac{1}{2}\mathbf{R}^{1/2}\mathbf{a} + \frac{1}{2}\mathbf{R}^{1/2}\mathbf{b} \\ \mathbf{b} = \mathbf{R}^{-1/2}\mathbf{v} - \mathbf{R}^{1/2}\mathbf{i} & & \mathbf{i} = \frac{1}{2}\mathbf{R}^{-1/2}\mathbf{a} - \frac{1}{2}\mathbf{R}^{-1/2}\mathbf{b} \end{array}. \quad (1.6)$$

Power waves are preferred for time-varying reference circuits and structures involving nonlinear reactances [94].

---

<sup>2</sup>It is also common to require that  $R_0$  is positive rather than negative. The requirement that  $R_0$  is positive simplifies bookkeeping of energy metrics in the Wave Digital Filter, and will also follow as a consequence of adaptation rules, when all the elements in the wave digital filter are positive.

## Current Waves

The use of Current waves in Wave Digital Filters is less common, although they are still occasionally used. At a port 0, the current wave definition and its inverse are

$$\begin{aligned} a_0 &= R_0^{-1}v_0 + i_0 & v_0 &= \frac{R_0}{2}a_0 + \frac{R_0}{2}b_0 \\ b_0 &= R_0^{-1}v_0 - i_0 & i_0 &= \frac{1}{2}a_0 - \frac{1}{2}b_0 \end{aligned} \quad (1.7)$$

The current wave definition and its inverse for a collection of ports are written in matrix form as

$$\begin{aligned} \mathbf{a} &= \mathbf{R}^{-1}\mathbf{v} + \mathbf{i} & \mathbf{v} &= \frac{1}{2}\mathbf{Ra} + \frac{1}{2}\mathbf{Rb} \\ \mathbf{b} &= \mathbf{R}^{-1}\mathbf{v} - \mathbf{i} & \mathbf{i} &= \frac{1}{2}\mathbf{a} - \frac{1}{2}\mathbf{b} \end{aligned} \quad (1.8)$$

Current waves are the dual of voltage waves [142].

## Parametric Wave Definition

The previous voltage, power, and current wave definitions can all be considered specific instances of a more general wave definition that is parameterized by a parameter  $\rho$

$$\begin{aligned} a_0 &= R_0^{\rho-1}v_0 + R_0^\rho i_0 & v_0 &= \frac{1}{2}R_0^{1-\rho}a_0 + \frac{1}{2}R_0^{1-\rho}b_0 \\ b_0 &= R_0^{\rho-1}v_0 - R_0^\rho i_0 & i_0 &= \frac{1}{2}R_0^{-\rho}a_0 - \frac{1}{2}R_0^{-\rho}b_0 \end{aligned}, \quad (1.9)$$

where  $\rho$  defines the wave type. Standard wave definitions correspond to

$$\rho = \begin{cases} 1 & \text{for voltage waves} \\ 1/2 & \text{for power waves} \\ 0 & \text{for current waves} \end{cases}, \quad (1.10)$$

although other values of  $\rho$  are valid as well.

This parametric wave definition and its inverse for a collection of ports are written in matrix form as

$$\begin{aligned} \mathbf{a} &= \mathbf{R}^{\rho-1}\mathbf{v} + \mathbf{R}^\rho \mathbf{i} & \mathbf{v} &= \frac{1}{2}\mathbf{R}^{1-\rho}\mathbf{a} + \frac{1}{2}\mathbf{R}^{1-\rho}\mathbf{b} \\ \mathbf{b} &= \mathbf{R}^{\rho-1}\mathbf{v} - \mathbf{R}^\rho \mathbf{i} & \mathbf{i} &= \frac{1}{2}\mathbf{R}^{-\rho}\mathbf{a} - \frac{1}{2}\mathbf{R}^{-\rho}\mathbf{b} \end{aligned}. \quad (1.11)$$

### Alternate Wave Definitions

Alternative wave definitions are sometimes used. A voltage wave formulation which differs by a factor of 1/2 is favored by Karjalainen [102] and Smith [97], and is identical to the variable definition used in digital waveguide modeling [143]. A version where one wave is not parameterized by port resistance was proposed in the 1970s [144, 121]. A fully generalized definition is proposed by Lawson [123] [124, pp. 61–63].

In this dissertation we will only consider the standard voltage wave definition and the parametric wave definition.

## 1.2 Algebraic One-Ports

One-port devices are the simplest electronic devices, whose behavior is defined as the relationship between voltage and current at a single port. For each of these one-port devices, a wave-domain equation is derived by substituting a wave definition into its Kirchhoff-domain  $v-i$  relationship and solving for the reflected wave  $b$ .

### 1.2.1 Resistor

The behavior of a resistor is defined by Ohm's law, which instantaneously relates port voltage  $v_0$  to port current  $i_0$  by the resistor's resistance  $R$

$$v_0 = R i_0. \quad (1.12)$$

The symbol and port definition for a resistor, adapted and unadapted Wave Digital Filter symbols, and adapted and unadapted Wave Digital Filter signal-flow diagrams are shown in Figure 1.2.

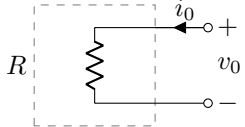
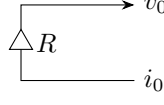
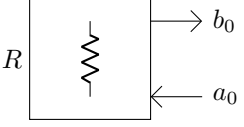
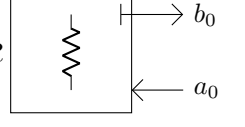
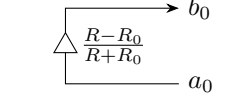
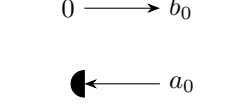
symbol	Kirchhoff domain	Wave Domain	
	unadapted	adapted ( $R_0 = R$ )	
 	 		

Figure 1.2: Kirchhoff- and Wave-Domain Representations of a Resistor One-Port.

Plugging the parametric wave definition (1.9) into the Kirchhoff-domain resistor equation (1.12)

$$\frac{1}{2}R_0^{1-\rho}a_0 + \frac{1}{2}R_0^{1-\rho}b_0 = \frac{1}{2}R R_0^{-\rho}a_0 - \frac{1}{2}R R_0^{-\rho}b_0 \quad (1.13)$$

and solving for the reflected wave  $b_0$  yields the unadapted continuous-time wave-domain equation

$$b_0 = \frac{R - R_0}{R + R_0}a_0. \quad (1.14)$$

Since there are no derivatives in (1.14), this is also valid in discrete time. The unadapted wave-domain equation (1.14) is suitable for use at the root of a Wave Digital Filter connection tree. On the other hand, it contains a delay-free directed path from its input  $a_0$  to its output  $b_0$  so it is *not* yet suitable for use as a leaf in the connection tree.

To adapt the Wave Digital Filter resistor, hence rendering it suitable for inclusion in a Wave Digital Filter connection tree, we exploit the free port resistance parameter  $R_0$  that we introduced when we plugged in the parametric wave variable definition. By setting  $R_0 = R$ , the coefficient  $\frac{R - R_0}{R + R_0}$  is set to 0, yielding the adapted wave-domain resistor equation

$$b_0 = 0. \quad (1.15)$$

In Wave Digital Filter notation, the resistor's reflected wave is shown as a “wave source” that always produces  $b_0 = 0$  and its incident wave is shown as a “wave sink” that just “throws out” whatever wave is incident upon it.

Under the physical interpretation of wave variables, the unadapted wave-domain equation for the resistor (1.14) simply expresses the scattering at an impedance mismatch, which is parameterized by an “impedance step over impedance sum” scattering coefficient. Under this interpretation, adapting the Wave Digital Filter resistor by setting  $R_0 = R$  can be seen as an impedance matching operation. Matched impedances don't produce reflections, hence  $b = 0$ , and if no further impedance mismatch is seen, an incident wave will just keep travelling and never return (hence the incident wave sink).

Notice that the parametric wave factor  $\rho$  appears in neither of the unadapted resistor equation (1.14), nor the adaptation criteria  $R_0 = R$ , nor the adapted resistor equation (1.15). That means that the same Wave Digital Filter resistor model is valid for voltage, power, and current waves.

### 1.2.2 Ideal Voltage Source

An ideal voltage source produces a voltage  $e(t)$  across its port

$$v_0(t) = e(t) \quad (1.16)$$

while drawing or sourcing as much port current as is necessary to produce this voltage. The symbol and port definition for an ideal voltage source, the unadapted Wave Digital Filter symbol, and the unadapted Wave Digital Filter signal-flow diagram are shown in Figure 1.3.

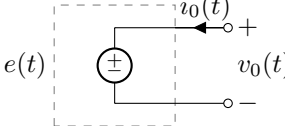
	Kirchhoff domain	Wave Domain	
symbol		unadapted	adapted
signal	 $e(t)$	 $e(t)$	N/A
	$e(t) \longrightarrow v_0(t)$	$e[n] \xrightarrow{2R_0^{\rho-1}} b_0[n]$ $\Delta -1$ $a_0[n]$	N/A

Figure 1.3: Kirchhoff- and Wave-Domain Representations of an Ideal Voltage Source One-Port.

Plugging the parametric wave definition (1.9) into the Kirchhoff-domain ideal voltage source equation (1.16)

$$\frac{1}{2}R_0^{1-\rho}a_0(t) + \frac{1}{2}R_0^{1-\rho}b_0(t) = e(t) \quad (1.17)$$

and solving for the reflected wave  $b_0(t)$  yields the unadapted continuous-time wave-domain equation

$$b_0(t) = 2R_0^{\rho-1}e(t) - a_0(t). \quad (1.18)$$

The discrete-time version is formed by replacing  $t$  with  $n$

$$b_0[n] = 2R_0^{\rho-1}e[n] - a_0[n]. \quad (1.19)$$

The unadapted wave-domain equation (1.19) is suitable for use at the root of a Wave Digital Filter connection tree, but is not for use as a leaf in the connection tree on account of the delay-free directed path from its input  $a_0[n]$  to its output  $b_0[n]$ . Unlike the case of the resistor, the ideal voltage source's wave domain equation does not depend on the port resistance and hence it cannot be adapted.

In Wave Digital Filter notation, the ideal voltage source's value  $e[n]$  is again shown as a “wave source.”

Notice that unlike the resistor, the parametric wave factor  $\rho$  does appear in the unadapted ideal voltage source equation (1.19). This means that the Wave Digital Filter model of an unadapted

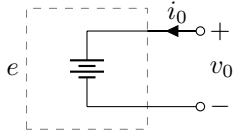


Figure 1.4: Battery Symbol and Port Definition.

ideal voltage source is different for voltage, power, and current waves

$$\underbrace{b_0[n] = 2e[n] - a_0[n]}_{\text{voltage waves}} \quad \underbrace{b_0[n] = 2\sqrt{R_0} e[n] - a_0[n]}_{\text{power waves}} \quad \underbrace{b_0[n] = 2R_0 e[n] - a_0[n]}_{\text{current waves}} . \quad (1.20)$$

Batteries are idealized as non-time-varying ideal voltage sources, as shown in Figure 1.4.

### 1.2.3 Ideal Current Source

An ideal current source produces a current  $j(t)$  through its port

$$i_0(t) = -j(t) \quad (1.21)$$

while developing as much port voltage as is necessary to produce this current. Here we've chosen the polarity that respects the duality between Thévenin and Norton circuits; be aware that the port polarity is sometimes defined in the opposite way [145, p. 46]. The symbol and port definition for an ideal current source, unadapted Wave Digital Filter symbol, and unadapted Wave Digital Filter signal-flow diagram are shown in Figure 1.5.

	Kirchhoff domain	Wave Domain	
symbol		unadapted	adapted
			N/A
signal	$j(t) \xrightarrow{-1} i_0(t)$	$j[n] \xrightarrow{2R_0^P} b_0[n]$	N/A

Figure 1.5: Kirchhoff- and Wave-Domain Representations of an Ideal Current Source One-Port.

Plugging the parametric wave definition (1.9) into the Kirchhoff-domain ideal current source

equation (1.21)

$$\frac{1}{2}R_0^{-\rho}a_0(t) - \frac{1}{2}R_0^{-\rho}b_0(t) = -j_0(t) \quad (1.22)$$

and solving for the reflected wave  $b_0(t)$  yields the unadapted continuous-time wave-domain equation

$$b_0(t) = 2R_0^\rho j(t) + a_0(t). \quad (1.23)$$

Again the discrete-time version is formed by replacing  $t$  with  $n$

$$b_0[n] = 2R_0^\rho j[n] + a_0[n]. \quad (1.24)$$

The unadapted wave-domain equation (1.24) is suitable for use at the root of a Wave Digital Filter connection tree, but is not for use as a leaf in the connection tree on account of the delay-free directed path from its input  $a_0[n]$  to its output  $b_0[n]$ . As with the ideal voltage source, the ideal current source's wave domain equation does not depend on the port resistance and hence it cannot be adapted.

In Wave Digital Filter notation, the ideal current source's value  $j[n]$  is again shown as a “wave source.”

As with the ideal voltage source, the parametric wave factor  $\rho$  does appear in the unadapted ideal current source equation (1.24). This means that the Wave Digital Filter model of an unadapted ideal current source is different for voltage, power, and current waves

$$\underbrace{b_0[n] = 2R_0 j[n] + a_0[n]}_{\text{voltage waves}} \quad \underbrace{b_0[n] = 2\sqrt{R_0} j[n] + a_0[n]}_{\text{power waves}} \quad \underbrace{b_0[n] = 2j[n] + a_0[n]}_{\text{current waves}}. \quad (1.25)$$

#### 1.2.4 Resistive Voltage Source

In §1.2.2 we derived the discrete, wave-domain equation for an ideal voltage source and found that it cannot be adapted. Hence, although it is suitable for use at the root of a Wave Digital Filter tree, it is unsuitable for inclusion as a leaf in a standard Wave Digital Filter tree. Since there may, in general, be more than one non-adaptable electrical element in a reference circuit and only one of them can be the root in a standard Wave Digital Filter, the nonadaptable ideal voltage can cause a problem.

This problem does not arise for resistive voltage sources. A resistive voltage source comprises a resistor  $R$  in series with an ideal voltage source  $e(t)$ . Using Kirchhoff's voltage law, this arrangement is described by

$$v_0(t) - e(t) = R i_0(t). \quad (1.26)$$

The symbol and port definition for a resistive voltage source, adapted and unadapted Wave Digital Filter symbols, and adapted and unadapted Wave Digital Filter signal-flow diagrams are shown in

Figure 1.6.

	Kirchhoff domain	Wave Domain	
symbol		unadapted	adapted ( $R_0 = R$ )
	$e(t)$	$e(t)$	$e(t)$
	$e(t) \rightarrow +$ $\oplus$ $R$ $i_0(t) \downarrow$	$e[n] \xrightarrow{\frac{2R_0^\rho}{R+R_0}} +$ $\oplus$ $a_0[n]$	$e[n] \xrightarrow{R^{\rho-1}}$

Figure 1.6: Kirchhoff- and Wave-Domain Representations of a Resistive Voltage Source One-Port.

Plugging the parametric wave definition (1.9) into the Kirchhoff-domain ideal current source equation (1.26)

$$\frac{1}{2}R_0^{1-\rho}a_0(t) + \frac{1}{2}R_0^{1-\rho}b_0(t) - e(t) = \frac{1}{2}R R_0^{-\rho}a_0(t) + \frac{1}{2}R R_0^{-\rho}b_0(t) \quad (1.27)$$

and solving for the reflected wave  $b_0(t)$  yields the unadapted continuous-time wave-domain equation

$$b_0(t) = \frac{R - R_0}{R + R_0}a_0(t) + \frac{2R_0^\rho}{R + R_0}e(t). \quad (1.28)$$

Again the discrete-time version is formed by replacing  $t$  with  $n$

$$b_0[n] = \frac{R - R_0}{R + R_0}a_0[n] + \frac{2R_0^\rho}{R + R_0}e[n]. \quad (1.29)$$

The unadapted wave-domain equation (1.29) is suitable for use at the root of a Wave Digital Filter connection tree, but is not for use as a leaf in the connection tree on account of the delay-free directed path from its input  $a_0[n]$  to its output  $b_0[n]$ .

To adapt the resistive voltage source, we exploit the free port resistance parameter  $R_0$ . By setting  $R_0 = R$  (just as we did for the resistor), the coefficient  $\frac{R - R_0}{R + R_0}$  is set to 0, yielding the adapted wave-domain resistive voltage source equation

$$b_0[n] = R^{\rho-1}e[n]. \quad (1.30)$$

Again, since the factor  $\rho$  appears in (1.30), the behavior depends on the wave definition.

If, in the reference circuit, the ideal voltage source is already in series with a resistor, we can

(and should) combine the ideal voltage source and the resistor into a resistive voltage source without any loss of accuracy. If the ideal voltage source is not in series with a resistor, we can introduce a small fictitious resistor in series with the ideal voltage source. This changes the behavior of the electrical circuit, but if the resistor is small, it won't change by much. Also, no real-world voltage source is actually ideal since they have a limited ability to supply current. So arguably, even when a schematic contains an ideal voltage source, the actual reference circuit should have a series resistance. Ideally, this resistance value would be measured, predicted from first principles, or estimated by a rule of thumb. In practice, it is usually fine to just pick a small resistance like  $1\Omega$ ; it is also worth mentioning that since resistors dissipate energy this is an incrementally passive modification.

### 1.2.5 Resistive Current Source

In §1.2.3 we derived the discrete, wave-domain equation for an ideal current source and found that it cannot be adapted. As with the voltage source, we now consider a resistive current source.

A resistive current source comprises a resistor  $R$  in parallel with an ideal current source  $j(t)$ . Using Kirchhoff's current law, this arrangement is described by

$$j(t) + i_0(t) = v_0(t)/R. \quad (1.31)$$

The symbol and port definition for a resistive current source, adapted and unadapted Wave Digital Filter symbols, and adapted and unadapted Wave Digital Filter signal-flow diagrams are shown in Figure 1.7.

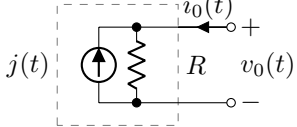
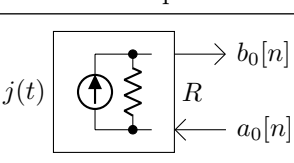
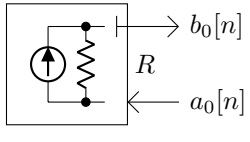
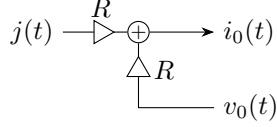
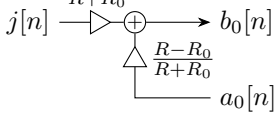
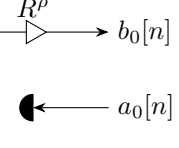
symbol	Kirchhoff domain	Wave Domain	
		unadapted	adapted ( $R_0 = R$ )
			
			

Figure 1.7: Kirchhoff- and Wave-Domain Representations of a Resistive Current Source One-Port.

Plugging the parametric wave definition (1.9) into the Kirchhoff-domain resistive current source

equation (1.31)

$$j(t) + \frac{1}{2}R_0^{-\rho}a_0(t) - \frac{1}{2}R_0^{-\rho}b_0(t) = \frac{1}{2}\frac{R_0^{1-\rho}}{R}a_0(t) + \frac{1}{2}\frac{R_0^{1-\rho}}{R}b_0(t) \quad (1.32)$$

and solving for the reflected wave  $b_0(t)$  yields the unadapted continuous-time wave-domain equation

$$b_0(t) = \frac{R - R_0}{R + R_0}a_0(t) + \frac{2RR_0^\rho}{R + R_0}j(t). \quad (1.33)$$

Again the discrete-time version is formed by replacing  $t$  with  $n$

$$b_0[n] = \frac{R - R_0}{R + R_0}a_0[n] + \frac{2RR_0^\rho}{R + R_0}j[n]. \quad (1.34)$$

The unadapted wave-domain equation (1.34) is suitable for use at the root of a Wave Digital Filter connection tree, but is not for use as a leaf in the connection tree on account of the delay-free directed path from its input  $a_0[n]$  to its output  $b_0[n]$ .

To adapt the resistive current source, we exploit the free port resistance parameter  $R_0$ . By setting  $R_0 = R$  (just as we did for the resistor), the coefficient  $\frac{R - R_0}{R + R_0}$  is set to 0, yielding the adapted wave-domain resistive current source equation

$$b_0[n] = 2R^\rho j[n]. \quad (1.35)$$

Again, since the factor  $\rho$  appears in (1.35), the behavior depends on the wave definition.

### 1.2.6 Short Circuit

An ideal short circuit has zero port voltage

$$v_0 = 0 \quad (1.36)$$

while at the same time allowing an arbitrary amount of port current to flow. The symbol and port definition for an ideal short circuit, unadapted Wave Digital Filter symbol, and unadapted Wave Digital Filter signal-flow diagram are shown in Figure 1.8.

Plugging the parametric wave definition (1.9) into the Kirchhoff-domain short circuit equation (1.36)

$$\frac{1}{2}R_0^{1-\rho}a_0 + \frac{1}{2}R_0^{1-\rho}b_0 = 0 \quad (1.37)$$

and solving for the reflected wave  $b_0$  yields the unadapted continuous-time wave-domain equation

$$b_0 = -a_0. \quad (1.38)$$

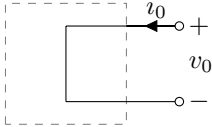
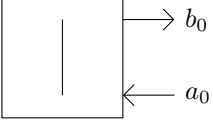
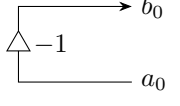
symbol	Kirchhoff domain	Wave Domain	
		unadapted	adapted
 $0 \longrightarrow v_0$	 $b_0$ $a_0$	$b_0$	N/A
	 $b_0$ $a_0$	$b_0$	N/A

Figure 1.8: Kirchhoff- and Wave-Domain Representations of an Ideal Short Circuit One-Port.

The unadapted wave-domain equation (1.38) is suitable for use at the root of a Wave Digital Filter connection tree, but is not for use as a leaf in the connection tree on account of the delay-free directed path from its input  $a_0$  to its output  $b_0$ . As with the ideal voltage and current sources, the short's wave domain equation does not depend on the port resistance and hence it cannot be adapted.

The unadapted short (1.38) is identical to an ideal voltage source (1.19) with  $e = 0$  or an ideal resistor (1.14) with zero electrical resistance

$$b_0 = -a_0 = \left[ 2R_0^{\rho-1}e - a_0 \right]_{e=0} = \left[ \frac{R - R_0}{R + R_0} a_0 \right]_{R=0}. \quad (1.39)$$

### 1.2.7 Open Circuit

An ideal open circuit has zero port current

$$i_0 = 0 \quad (1.40)$$

while placing no restrictions on port voltage. The symbol and port definition for an ideal open circuit, unadapted Wave Digital Filter symbol, and unadapted Wave Digital Filter signal-flow diagram are shown in Figure 1.9.

Plugging the parametric wave definition (1.9) into the Kirchhoff-domain short circuit equation (1.40)

$$\frac{1}{2}R_0^{-\rho}a_0 - \frac{1}{2}R_0^{-\rho}b_0 = 0 \quad (1.41)$$

and solving for the reflected wave  $b(t)$  yields the unadapted continuous-time wave-domain equation

$$b_0 = a_0. \quad (1.42)$$

The unadapted wave-domain equation (1.42) is suitable for use at the root of a Wave Digital Filter

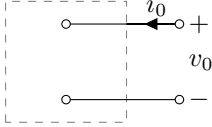
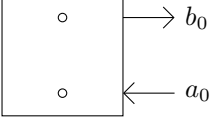
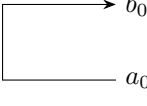
	Kirchhoff domain	Wave Domain	
symbol		unadapted	adapted
signal			N/A
	0 $\longrightarrow$ $i_0$		N/A

Figure 1.9: Kirchhoff- and Wave-Domain Representations of an Ideal Open Circuit One-Port.

connection tree, but is not for use as a leaf in the connection tree on account of the delay-free directed path from its input  $a_0$  to its output  $b_0$ . As with the short, the open circuit’s wave domain equation does not depend on the port resistance and hence it cannot be adapted.

The unadapted open circuit (1.42) is identical to an ideal resistor (1.14) with infinite electrical resistance

$$b_0 = a_0 = \lim_{R \rightarrow \infty} \frac{R - R_0}{R + R_0} a_0. \quad (1.43)$$

### 1.2.8 Switch

The short circuit and open circuit one-ports can be considered the two different settings of an ideal single-pole, single-throw switch. From that perspective, the two one-ports are unified into a single wave-domain equation where  $\lambda$  accounts for whether the switch is closed or open

$$b_0[n] = \lambda a_0[n], \text{ where } \lambda = \begin{cases} -1 & \text{closed switch} \\ +1 & \text{open switch} \end{cases} \quad (1.44)$$

Switches are an important part of analog audio circuits, where they are used to control settings, e.g., in a “bright switch/filter” [59, 7]. The symbol and port definition for a switch, unadapted Wave Digital Filter symbols, and unadapted Wave Digital Filter signal-flow diagram are shown in Figure 1.10.

An open circuit may be approximated as a resistance that is significantly larger than the other resistances in the circuit and a closed circuit may be approximated by a resistance that is significantly smaller than the other resistances in the circuit. Vladimirescu recommends a ratio of  $R_{\text{off}}/R_{\text{on}} \leq 10^{12}$  [146, pp. 65–68].

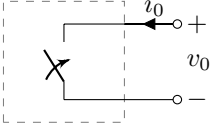
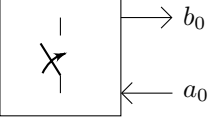
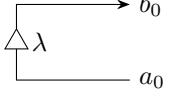
symbol	Kirchhoff domain	Wave Domain	
		unadapted	adapted
 closed: $0 \longrightarrow v_0$ open: $0 \longrightarrow i_0$			N/A
			N/A

Figure 1.10: Kirchhoff- and Wave-Domain Representations of an Ideal Switch One-Port.

### 1.2.9 Singular Network Elements

We close our discussion of one-port algebraic devices by considering a class of special one-port network elements: the “nullator” and “norator.” These theoretical network elements are singular [147] and sometimes called “degenerate” [148, p. 53].

#### Nullator

The *nullator* is a theoretical idealized network element that is characterized by zero port voltage and zero port current

$$v_0 = 0 \quad (1.45)$$

$$i_0 = 0. \quad (1.46)$$

The symbol and port definition for a nullator is shown in Figure 1.11.

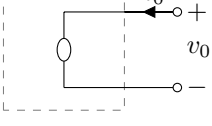
symbol	Kirchhoff domain	Wave Domain	
		unadapted	adapted
 $0 \longrightarrow v_0$ $0 \longrightarrow i_0$		N/A	N/A
		N/A	N/A

Figure 1.11: Kirchhoff- and Wave-Domain Representations of a Nullator One-Port.

A unique facet of this network element is that from the standpoint of voltage, the nullator looks

like a short circuit, and from the standpoint of current, the nullator looks like an open circuit. Even theoretically, nullators cannot appear by themselves in a circuit—each one must be accompanied by another theoretical one-port device called a *norator* [147, 148].

In fact if we try to plug the parametric wave definition (1.9) into the nullator equations (1.45)–(1.46), we end up with the following two restrictions

$$a_0 = 0 \quad (1.47)$$

$$b_0 = 0. \quad (1.48)$$

Since it is not possible in the Wave Digital Filter context to put a restriction on the input wave to a port, but only to chose an output wave based on the input wave, this can be considered an overconstrained definition and thus is not suitable for inclusion in a Wave Digital Filter tree as is.

### Norator

The *norator* is a theoretical idealized network element that is characterized by no restrictions on either port voltage or port current. The symbol and port definition for a norator is shown in Figure 1.2.

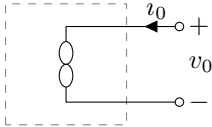
	Kirchhoff domain	Wave Domain	
		unadapted	adapted
symbol		N/A	N/A
signal	N/A	N/A	N/A

Figure 1.12: Kirchhoff- and Wave-Domain Representations of a Norator One-Port.

A unique facet of this network element is that from the standpoint of voltage, the nullator looks like an open circuit, and from the standpoint of current, the nullator looks like a short circuit. Even theoretically, norators cannot appear by themselves in a circuit—each one must be accompanied a nullator [147, 148].

Since the norator don't put any restrictions on the voltage or current of the port, they also put no restrictions on the reflected wave from the port. Since in the Wave Digital Filter context we mus chose an output wave based on the input wave, this can be considered an underconstrained definition and thus is not suitable for inclusion in a Wave Digital Filter tree as is.

## 1.3 Reactive One-Ports

So far, all the Wave Digital Filter one-ports that we have treated have been algebraic / memoryless. That is, their Kirchhoff-domain equations relate instantaneously a voltage, a current, and potentially an input. In deriving wave-domain equations, we have so far ended up with an instantaneous and linear relationship between an incident wave  $a$ , a reflected wave  $b$ , and potentially an input ( $e$  or  $j$ ). In this section, we'll derive wave-domain equations for two *reactive* one-port elements: the capacitor (§1.3.1) and the inductor (§1.3.2). Reactive elements have a continuous-time derivative in their constitutive equations which must be approximated in discrete time by discretization.

Typically, Wave Digital Filters use the trapezoidal rule for integration to approximate these derivatives [5]. Thinking on the Laplace plane, the trapezoidal rule is identical to the Bilinear Transform, a conformal mapping from the  $s$  to  $z$  planes. In control engineering, the trapezoidal rule is also known as “Tustin’s method” [149]. Here, we’ll discuss alternative discretization strategies, including the Warped Bilinear Transform,  $\alpha$  transform and the Möbius transform, which contains the  $\alpha$  transform, forward Euler, backward Euler, and the warped and unwarped Bilinear Transforms as special cases.<sup>3</sup>

Here, we start with a continuous-time equation in the Kirchhoff domain, execute a change of variables to the wave domain, use the Laplace transform to write the constituent equation in terms of the Laplace differentiation operator  $s$ , discretize the Laplace expression using the Bilinear Transform of another  $s \rightarrow z$  mapping, and use the inverse  $z$ -transform to find a discrete-time, wave-domain difference equation which can be adapted as with the algebraic one-ports.

### 1.3.1 Capacitor

The behavior of a linear capacitor with capacitance  $C$  is modeled by the differential equation

$$C \frac{dv_0(t)}{dt} = i_0(t) \quad (1.49)$$

which relates the time derivative of port voltage  $\frac{dv_0(t)}{dt}$  to port current  $i_0(t)$  by the capacitance  $C$ .

In the Laplace domain, this relationship is

$$CsV_0(s) = I_0(s). \quad (1.50)$$

Plugging the parametric wave definition (1.9) into the Kirchhoff-domain capacitor equation (1.50)

$$\frac{1}{2}CR_0^{1-\rho}sA_0(s) + \frac{1}{2}CR_0^{1-\rho}sB_0(s) = \frac{1}{2}R_0^{-\rho}A_0(s) - \frac{1}{2}R_0^{-\rho}B_0(s) \quad (1.51)$$

---

<sup>3</sup>A completely different approach based on Runge–Kutta discretization has also been explored in the Wave Digital Filter context [150, 151, 152], but will not be considered further here since it profoundly alters the global simulation structure.

and solving for the reflected wave  $B_0(s)$  yields the Laplace- and wave-domain transfer function

$$H_0(s) = \frac{B_0(s)}{A_0(s)} = \frac{1 - R_0 C s}{1 + R_0 C s}. \quad (1.52)$$

### Bilinear Transform

Creating a discrete-time equation from (1.52) is not as simple as it is for the algebraic one-ports. To do so, we must choose a strategy for forming a  $z$ -plane transfer function  $H_0(z^{-1}) = B_0(z^{-1})/A_0(z^{-1})$  that approximates (1.52) and then implement  $H_0(z^{-1})$  as a difference equation using delays, multipliers, and adders. A standard way of approaching this is to use a mapping from the  $s$ -plane to the  $z$ -plane

$$H_0(z^{-1}) = H_0(s)|_{s=f(z^{-1})} \quad (1.53)$$

that corresponds to a numerical integration technique.

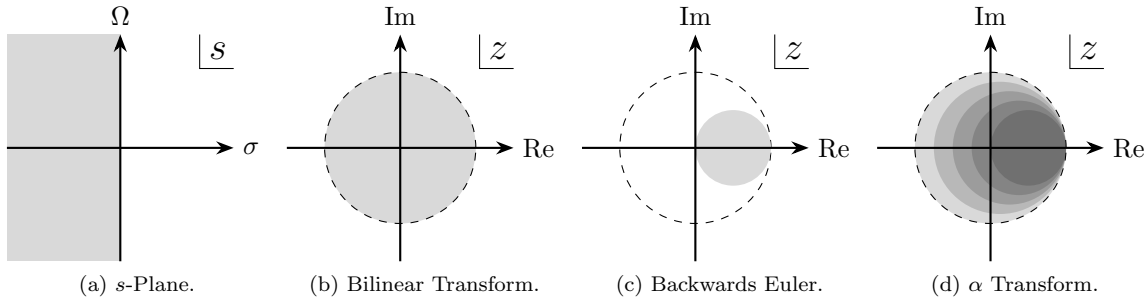


Figure 1.13: Mappings from the  $s$  to  $z$  Planes, Including the Bilinear Transform, Backwards Euler, and the  $\alpha$  Transform. On the  $z$  planes, the unit circle is shown as a dotted circle. For the  $\alpha$  Transform, a family of transforms  $\alpha \in [0.00, 0.25, 0.5, 0.75, 1.00]$  is shown.

The typical choice of mapping for a Wave Digital Filter reactance is the Bilinear Transform. The Bilinear Transform (BLT) forms  $H(z^{-1})$  each  $s$  in some  $H(s)$  by a function of  $z^{-1}$

$$s = f_{\text{BLT}}(z^{-1}) = \frac{2}{T} \frac{1 - z^{-1}}{1 + z^{-1}}. \quad (1.54)$$

Sometimes it is useful to look at the mapping in terms of  $z$  rather than  $z^{-1}$

$$s = \frac{2}{T} \frac{z - 1}{z + 1}. \quad (1.55)$$

The Bilinear Transform maps the  $j\Omega$  axis from the  $s$  plane exactly to the unit circle on the  $z$  plane, except for a well-known frequency warping. This warping is a consequence of the compression of the  $s$ -plane frequency range  $\Omega \in [-\infty, +\infty]$  to the  $z$ -plane frequency range  $\omega \in [-\pi, +\pi]$ . This

warping is described by

$$\omega = \frac{2}{T} \tan^{-1} \left( \Omega \frac{T}{2} \right). \quad (1.56)$$

As a conformal mapping, the BLT maps dc on the  $s$  plane ( $s = 0$ ) to  $z = 1$  on the  $z$  plane and the extended  $s$ -plane point  $s \rightarrow \infty$  to the Nyquist location  $z = -1$  on the  $z$  plane. The mapping of dc can be easily visualized by considering the numerator zero of (1.55) and the mapping of  $s = \infty$  to Nyquist can be easily visualize by considering the denominator pole of (1.55). At the same time, the entire left-half plane on the  $s$ -plane is mapped to the inside of the unit circle on the  $z$  plane, as shown in Figures 1.13a–1.13b. The Bilinear Transform is identical to the trapezoidal rule for integration. Hence the trapezoidal rule reaches the highest order of consistency (consistent with order two) possible for A-stable<sup>4</sup> linear multi-step methods, a criteria known as the “first Dahlquist barrier” [153].

symbol	Kirchhoff domain	Wave Domain	
		unadapted	adapted ( $R_0 = \frac{T}{2C}$ )
$C$			
$I_0(s)$			
$V_0(s)$			

Figure 1.14: Kirchhoff- and Wave-Domain Representations of a Capacitor, Discretized Using the Bilinear Transform.

Applying the BLT to the continuous-time, wave-domain capacitor equation (1.52) and collecting terms

$$H_0(z^{-1}) = \frac{B_0(z^{-1})}{A_0(z^{-1})} = \frac{(T - 2R_0C) + (T + 2R_0C)z^{-1}}{(T + 2R_0C) + (T - 2R_0C)z^{-1}} \quad (1.57)$$

then taking the inverse  $z$ -transform and solving for the reflected wave  $b_0[n]$  yields the unadapted discrete-time wave-domain equation

$$b_0[n] = -\frac{T - 2R_0C}{T + 2R_0C} b_0[n - 1] + \frac{T - 2R_0C}{T + 2R_0C} a_0[n] + a_0[n - 1]. \quad (1.58)$$

The unadapted wave-domain equation (1.58) is suitable for use at the root of a Wave Digital Filter connection tree. It can be adapted by setting  $R_0 = \frac{T}{2C}$ , which sets the coefficients  $-\frac{T - 2R_0C}{T + 2R_0C}$  and

<sup>4</sup>not to be confused with “astable”

$\frac{T-2R_0C}{T+2R_0C}$  to zero and yields the adapted wave-domain capacitor equation

$$b_0[n] = a_0[n - 1]. \quad (1.59)$$

Interestingly, the adapted Wave Digital Filter capacitor is simply a unit delay when it is discretized using the Trapezoidal Rule / BLT.

The symbol and port definition for a capacitor, adapted and unadapted Wave Digital Filter symbols, and adapted and unadapted Wave Digital Filter signal-flow diagrams for the Bilinear Transform discretization are shown in Figure 1.14.

### Warped Bilinear Transform

A well-known variation on the Bilinear Transform is the *Warped* Bilinear Transform, which alters the Bilinear Transform  $s \rightarrow z$  transformation to

$$s = f_{WBBLT}(z^{-1}) = \frac{2}{T'} \frac{1 - z^{-1}}{1 + z^{-1}}. \quad (1.60)$$

where  $T'$  is the only term that is changed from the standard Bilinear Transform definition.  $T'$  can be chosen so that exactly one continuous time frequency  $\Omega_0 \in ]0, \pi[$  is mapped perfectly from the analog domain to the digital domain, according to

$$T' = 2\tan(\Omega_0 T/2) / \Omega_0. \quad (1.61)$$

The Warped Bilinear Transform is not discussed commonly in the Wave Digital Filter context; an example of its application is modeling the Hammond organ vibrato/chorus circuit [154].

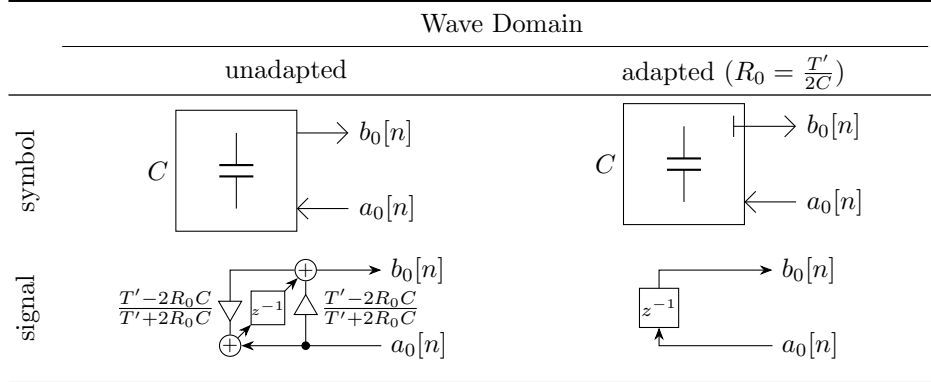


Figure 1.15: Wave-Domain Representations of a Capacitor, Discretized Using the *Warped* Bilinear Transform.

The derivation of the wave-domain  $z$ -plane transfer function of an unadapted capacitor is identical

to the unwarped case, except that  $T$  is replaced by  $T'$

$$H_0(z^{-1}) = \frac{B_0(z^{-1})}{A_0(z^{-1})} = \frac{(T' - 2R_0C) + (T' + 2R_0C)z^{-1}}{(T' + 2R_0C) + (T' - 2R_0C)z^{-1}}. \quad (1.62)$$

Again this results in a difference equation

$$b_0[n] = -\frac{T' - 2R_0C}{T' + 2R_0C} b_0[n-1] + \frac{T' - 2R_0C}{T' + 2R_0C} a_0[n] + a_0[n-1] \quad (1.63)$$

which is now adapted by  $R_0 = \frac{T'}{2C}$ , yielding the adapted difference equation

$$b_0[n] = a_0[n-1]. \quad (1.64)$$

Interestingly, the only difference between a wave-domain capacitor discretized with the standard Bilinear Transform and the Warped Bilinear Transform is the port resistance; in both cases the capacitor itself ends up as a simple delay.

The adapted and unadapted Wave Digital Filter symbols and adapted and unadapted Wave Digital Filter signal-flow diagrams for the capacitor discretized using the Warped Bilinear Transform are shown in Figure 1.15.

### Backward Euler

Another standard discretization rule is Backwards Euler. Backwards Euler can be represented as an  $s \rightarrow z$  mapping

$$s = f_{\text{BE}}(z^{-1}) = \frac{1 - z^{-1}}{T}. \quad (1.65)$$

Although the Wave Digital Filter approach is usually associated with the Bilinear Transform, there is nothing preventing us from using Backwards Euler to discretize reactive elements. In fact it will sometimes be preferable to the Trapezoidal Rule, as we will see in the case study of Chapter 3.

As a conformal mapping, Backward Euler maps dc on the  $s$  plane  $z = 1$  and  $s \rightarrow \infty$  to the point  $z = 0$ . This is shown in Figure 1.13c. The mapping of dc can again be seen by looking at the transform numerator zero; since there is no explicit denominator pole, the mapping of  $s \rightarrow \infty$  to  $z = 0$  is due to the non-strictly-proper nature of the transform.

Applying Backwards Euler discretization to the continuous-time, wave-domain capacitor equation (1.52) and collecting terms

$$H_0(z^{-1}) = \frac{B_0(z^{-1})}{A_0(z^{-1})} = \frac{(T - R_0C) + (R_0C)z^{-1}}{(T + R_0C) + (R_0C)z^{-1}} \quad (1.66)$$

then taking the inverse  $z$ -transform and solving for the reflected wave  $b_0[n]$  yields the unadapted

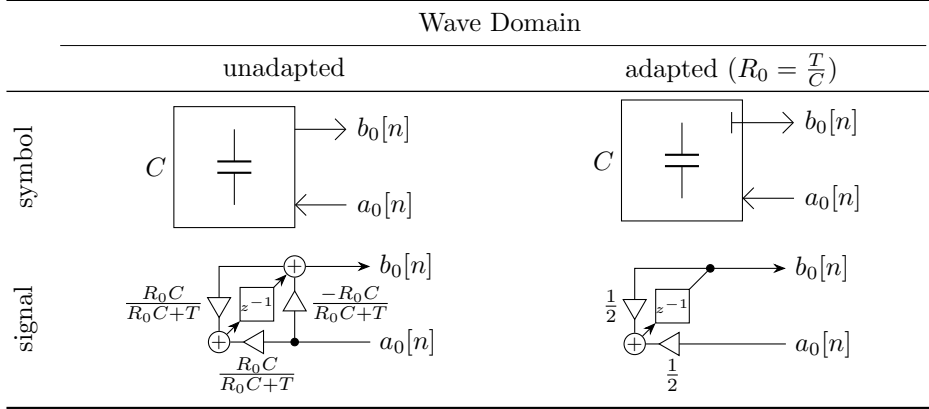


Figure 1.16: Wave-Domain Representations of a Capacitor, Discretized Using Backward Euler.

discrete-time wave domain equation

$$b_0[n] = \frac{R_0 C}{T + R_0 C} b_0[n-1] + \frac{T - R_0 C}{T + R_0 C} a_0[n] + \frac{R_0 C}{T + R_0 C} a_0[n-1]. \quad (1.67)$$

This discretization is adapted by  $R_0 = T/C$ , which yields the adapted difference equation

$$b_0[n] = \frac{1}{2} b_0[n-1] + \frac{1}{2} a_0[n-1]. \quad (1.68)$$

Notice that as with the Warped Bilinear Transform, the adaptation criteria is different than for the Bilinear Transform. Unlike with either version of the Bilinear Transform, the difference equation is now a first order IIR filter, albeit one with the special property that the delay-free feedforward gain is constrained to be 0.

The adapted and unadapted Wave Digital Filter symbols and adapted and unadapted Wave Digital Filter signal-flow diagrams for the capacitor discretized using Backward Euler are shown in Figure 1.16.

### $\alpha$ Transform

Here we explore another discretization scheme, which we call the “ $\alpha$  Transform”:

$$s = f_\alpha(z^{-1}) = \frac{\frac{1+\alpha}{T} - \frac{1+\alpha}{T} z^{-1}}{1 + \alpha z^{-1}}. \quad (1.69)$$

This transform is parameterized by a parameter  $\alpha$ . It was explored in the context of Kirchhoff-domain circuit modeling in [155] and can be considered a compromise between the Bilinear Transform and Backwards Euler. Indeed it includes Backward Euler ( $\alpha = 0$ ), the Bilinear Transform ( $\alpha = 1.0$ ), and even Forward Euler ( $\alpha \rightarrow \infty$ ) as special cases. The concept of compromising between Backward

Euler and the Bilinear Transform has been explored in other contexts [156]; the  $\alpha$  Transform defined in 1.69 is related by frequency scaling and a transformation of the parameterization to other known discretization schemes, including the “ $\alpha$ -Approximation” [157] and the “Al-Alaoui Operator” [158].

As a conformal mapping, the  $\alpha$  Transform maps dc on the  $s$  plane  $z = 1$  and  $s \rightarrow \infty$  to the point  $z = -\alpha$ . This is shown in Figure 1.13d [155]. This can be seen as a parameterization of the the transform’s denominator pole as well as a frequency scaling by  $\frac{1+\alpha}{T}$ .

Wave Domain		
symbol	unadapted	adapted ( $R_0 = \frac{T}{C(1+\alpha)}$ )
$C$		
signal		

Figure 1.17: Wave-Domain Representations of a Capacitor, Discretized Using the  $\alpha$  Transform.

Applying the  $\alpha$ -Transform discretization to the continuous-time, wave-domain capacitor equation (1.52) and collecting terms

$$H_0(z^{-1}) = \frac{B_0(z^{-1})}{A_0(z^{-1})} = \frac{(T - R_0C(1 + \alpha)) + (T\alpha + R_0C(1 + \alpha))z^{-1}}{(T + R_0C(1 + \alpha)) + (T\alpha + R_0C(1 - \alpha))z^{-1}} \quad (1.70)$$

then taking the inverse  $z$ -transform and solving for the reflected wave  $b_0[n]$  yields the unadapted discrete-time wave domain equation

$$b_0[n] = \frac{R_0C(1 + \alpha) - T\alpha}{R_0C(1 + \alpha) + T} b_0[n - 1] + \frac{-R_0C(1 + \alpha) + T}{R_0C(1 + \alpha) + T} a_0[n] + \frac{R_0C(1 + \alpha) + T\alpha}{R_0C(1 + \alpha) + T} a_0[n - 1]. \quad (1.71)$$

This discretization is adapted by  $R_0 = \frac{T}{C(1+\alpha)}$ , which yields the adapted difference equation

$$b_0[n] = \frac{1 - \alpha}{2} b_0[n - 1] + \frac{1 + \alpha}{2} a_0[n - 1]. \quad (1.72)$$

Again, the difference equation is a first-order IIR filter. The  $\alpha$  transform is intended to operate in the range  $\alpha \in [0, 1]$  (bracketed by Backward Euler and the Bilinear Transform) and to a lesser extent the range  $\alpha \in [1, \infty]$  (bracketed by Bilinear Transform and Forward Euler). Values of  $\alpha < 0$  may be interesting as well, although they lack an interpretation as a compromise between known discretizations. The only condition that must be respected is that  $\alpha \neq -1$ ; if  $\alpha = -1$  were allowed

it would correspond to an adaptation criteria of  $R_0 = \infty$ , which is disallowed for causing a non-invertible wave definition. At the same time it would correspond to a mapping from the entire left half  $s$  plane to the single point  $z = 1$  on the  $z$  plane; a nonsensical situation that would collocate all poles and zeros of the system.

The adapted and unadapted Wave Digital Filter symbols and adapted and unadapted Wave Digital Filter signal-flow diagrams for the capacitor discretized using the  $\alpha$  Transform are shown in Figure 1.17.

### Möbius Transform

The  $\alpha$  Transform contains the three most well-known discretization schemes—Backwards Euler, Bilinear Transform, and Forwards Euler—as special cases. Still, an even more general conformal mapping exists. This mapping is called the Möbius Transform and is defined by [155]

$$s = f_M(z^{-1}) = \frac{a_M + b_M z^{-1}}{c_M + d_M z^{-1}}. \quad (1.73)$$

The Möbius Transform is parameterized by four parameters  $a_M$ ,  $b_M$ ,  $c_M$ , and  $d_M$ ; it is simply an application of the Möbius Transform from the study of conformal mapping [159] to the problem of discretization.

Wave Domain		
	unadapted	adapted ( $R_0 = \frac{c_M}{C a_M}$ )
symbol	$C$ 	$C$ 
signal		

Figure 1.18: Wave-Domain Representations of a Capacitor, Discretized Using the Möbius Transform.

Applying the Möbius Transform discretization to the continuous-time, wave-domain capacitor equation (1.52) and collecting terms

$$H_0(z^{-1}) = \frac{B_0(z^{-1})}{A_0(z^{-1})} = \frac{(c_M - R_0 C a_M) + (d_M - R_0 C b_M) z^{-1}}{(c_M + R_0 C a_M) + (d_M + R_0 C b_M) z^{-1}} \quad (1.74)$$

then taking the inverse  $z$ -transform and solving for the reflected wave  $b_0[n]$  yields the unadapted

discrete-time wave domain equation

$$b_0[n] = -\frac{d_M + R_0 C b_M}{c_M + R_0 C a_M} b_0[n-1] + \frac{c_M - R_0 C a_M}{c_M + R_0 C a_M} a_0[n] + \frac{d_M - R_0 C b_M}{c_M + R_0 C a_M} a_0[n-1]. \quad (1.75)$$

This discretization is adapted by  $R_0 = \frac{c_M}{C a_M}$ , which yields the adapted difference equation

$$b_0[n] = -\frac{a_M d_M + b_M c_M}{2 a_M c_M} b_0[n-1] + \frac{a_M d_M - b_M c_M}{2 a_M c_M} a_0[n-1]. \quad (1.76)$$

This very general result contains all of the previously discussed discretization techniques as special cases as well as the fully class of transforms parameterized by  $a_M$ ,  $b_M$ ,  $c_M$ , and  $d_M$ . This class is constrained by a few special cases. The transform must satisfy  $a_M \neq 0$  (to avoid the disallowed adaptation  $R_0 = \infty$ ) and  $c_M \neq 0$  (to avoid the disallowed adaptation  $R_0 = 0$ ).

It is fascinating that the condition  $a_M \neq 0$  can also be interpreted as a structural restriction that disqualifies all fully explicit discretization methods (such as Forward Euler). Ironically, although the central concept of the Wave Digital Filter approach is choosing port resistances to create fully local, fully explicit building blocks, the chosen discretization method must itself be implicit!

The adapted and unadapted Wave Digital Filter symbols and adapted and unadapted Wave Digital Filter signal-flow diagrams for the capacitor discretized using the Möbius Transform are shown in Figure 1.18.

### 1.3.2 Inductor

The behavior of a linear inductor with inductance  $L$  is modeled by the differential equation

$$v_0(t) = L \frac{di_0(t)}{dt} \quad (1.77)$$

which relates the port voltage  $v_0(t)$  to the time derivative of port current  $\frac{di_0(t)}{dt}$  by the inductance  $L$ . In the Laplace domain, this relationship is

$$V_0(s) = L s I_0(s). \quad (1.78)$$

Plugging the parametric wave definition (1.9) into the Kirchhoff-domain inductor equation (1.78)

$$\frac{1}{2} R_0^{1-\rho} A_0(s) + \frac{1}{2} R_0^{1-\rho} B_0(s) = \frac{1}{2} R_0^{-\rho} L s A_0(s) - \frac{1}{2} R_0^{-\rho} L s B_0(s) \quad (1.79)$$

and solving for the reflected wave  $B_0(s)$  yields the Laplace- and wave-domain transfer function

$$H_0(s) = \frac{B_0(s)}{A_0(s)} = \frac{L s - R_0}{L s + R_0}. \quad (1.80)$$

### Bilinear Transform

Just like the capacitor, the inductor's continuous-time transfer function 1.80 is discretized using  $s \rightarrow z$  mappings. Again we begin with the Bilinear Transform.

	Kirchhoff domain	Wave Domain	
		unadapted	adapted ( $R_0 = \frac{2L}{T}$ )
symbol			
signal			

Figure 1.19: Kirchhoff- and Wave-Domain Representations of a Inductor One-Port, Discretized Using the Bilinear Transform.

Applying the BLT to the continuous-time, wave-domain inductor equation (1.80) and collecting terms

$$H_0(z^{-1}) = \frac{B_0(z^{-1})}{A_0(z^{-1})} = \frac{(2L - R_0 T) + (-2L - 2R_0 T) z^{-1}}{(2L + R_0 T) + (-2L + R_0 T) z^{-1}} \quad (1.81)$$

then taking the inverse  $z$ -transform and solving for the reflected wave  $b_0[n]$  yields the unadapted discrete-time wave-domain equation

$$b_0[n] = \frac{2L - R_0 T}{2L + R_0 T} b_0[n-1] + \frac{2L - R_0 T}{2L + R_0 T} a_0[n] - a_0[n-1]. \quad (1.82)$$

This discretization is adapted by  $R_0 = \frac{2L}{T}$ , which yields the adapted difference equation

$$b_0[n] = -a_0[n-1]. \quad (1.83)$$

Similar to the capacitor, the adapted Wave Digital Filter inductor is simply a unit delay with a sign inversion when it is discretized using the trapezoidal rule / BLT.

The symbol and port definition for an inductor, adapted and unadapted Wave Digital Filter symbols, and adapted and unadapted Wave Digital Filter signal-flow diagrams for the Bilinear Transform discretization are shown in Figure 1.19.

### Warped Bilinear Transform

Again, the Warped Bilinear Transform  $z$ -plane transfer function is identical to the unwarped case, except that  $T$  is replaced by  $T'$

$$H_0(z^{-1}) = \frac{B_0(z^{-1})}{A_0(z^{-1})} = \frac{(2L - R_0T') + (-2L - 2R_0T')z^{-1}}{(2L + R_0T') + (-2L + R_0T')z^{-1}}. \quad (1.84)$$

Again this results in a difference equation

$$b_0[n] = \frac{2L - R_0T'}{2L + R_0T'} b_0[n-1] + \frac{2L - R_0T'}{2L + R_0T'} a_0[n] - a_0[n-1] \quad (1.85)$$

which is now adapted by  $R_0 = \frac{2L}{T'}$ , yielding the adapted difference equation

$$b_0[n] = -a_0[n-1]. \quad (1.86)$$

Again, only the adaptation is affected by the warping.

Wave Domain		
symbol	unadapted	adapted ( $R_0 = \frac{2L}{T'}$ )
$L$		
signal		

Figure 1.20: Wave-Domain Representations of an Inductor, Discretized Using the *Warped Bilinear Transform*.

The adapted and unadapted Wave Digital Filter symbols and adapted and unadapted Wave Digital Filter signal-flow diagrams for the inductor discretized using the Warped Bilinear Transform are shown in Figure 1.20.

### Backwards Euler

Applying Backwards Euler to the continuous-time, wave-domain inductor equation (1.80) and collecting terms

$$H_0(z^{-1}) = \frac{B_0(z^{-1})}{A_0(z^{-1})} = \frac{(L - R_0T) + (-L)z^{-1}}{(L + R_0T) + (-L)z^{-1}} \quad (1.87)$$

then taking the inverse  $z$ -transform and solving for the reflected wave  $b_0[n]$  yields the unadapted discrete-time wave domain equation

$$b_0[n] = \frac{L}{L + R_0 T} b_0[n - 1] + \frac{L - R_0 T}{L + R_0 T} a_0[n] + \frac{L}{L + R_0 T} a_0[n - 1]. \quad (1.88)$$

This discretization is adapted by  $R_0 = \frac{L}{T}$ , which yields that adapted difference equation

$$b_0[n] = \frac{1}{2} b_0[n - 1] - \frac{1}{2} a_0[n - 1]. \quad (1.89)$$

Wave Domain		
symbol	unadapted	adapted ( $R_0 = \frac{L}{T}$ )
$L$		
signal		

Figure 1.21: Wave-Domain Representations of an Inductor, Discretized Using Backward Euler.

The adapted and unadapted Wave Digital Filter symbols and adapted and unadapted Wave Digital Filter signal-flow diagrams for the inductor discretized using Backward Euler are shown in Figure 1.21.

### $\alpha$ Transform

Applying the  $\alpha$  Transform discretization to the continuous-time, wave-domain inductor equation (1.80) and collecting terms

$$H_0(z^{-1}) = \frac{B_0(z^{-1})}{A_0(z^{-1})} = \frac{(L(1 + \alpha) - R_0 T) + (-L(1 + \alpha) - R_0 T\alpha) z^{-1}}{(L(1 + \alpha) + R_0 T) + (-L(1 + \alpha) + R_0 T\alpha) z^{-1}} \quad (1.90)$$

then taking the inverse  $z$ -transform and solving for the reflected wave  $b_0[n]$  yields the unadapted discrete-time wave domain equation

$$b_0[n] = \frac{L(1 + \alpha) - R_0 T\alpha}{L(1 + \alpha) + R_0 T} b_0[n - 1] + \frac{L(1 + \alpha) - R_0 T}{L(1 + \alpha) + R_0 T} a_0[n] + \frac{L(1 + \alpha) + R_0 T\alpha}{L(1 + \alpha) + R_0 T} a_0[n - 1]. \quad (1.91)$$

This discretization is adapted by  $R_0 = \frac{L(1+\alpha)}{T}$ , which yields the adapted difference equation

$$b_0[n] = \frac{1-\alpha}{2} b_0[n-1] - \frac{1+\alpha}{2} a_0[n-1]. \quad (1.92)$$

		Wave Domain
symbol	unadapted	adapted ( $R_0 = \frac{L(1+\alpha)}{T}$ )
signal		
	$\frac{L(1+\alpha)-R_0T\alpha}{L(1+\alpha)+R_0T}$ $\frac{L(1+\alpha)+R_0T\alpha}{L(1+\alpha)+R_0T}$	$\frac{1-\alpha}{2}$ $\frac{1+\alpha}{2}$

Figure 1.22: Wave-Domain Representations of an Inductor, Discretized Using the  $\alpha$  Transform.

The adapted and unadapted Wave Digital Filter symbols and adapted and unadapted Wave Digital Filter signal-flow diagrams for the inductor discretized using the  $\alpha$  Transform are shown in Figure 1.22.

### Möbius Transform

Applying the Möbius Transform discretization to the continuous-time, wave-domain inductor equation (1.80) and collecting terms

$$H_0(z^{-1}) = \frac{B_0(z^{-1})}{A_0(z^{-1})} = \frac{(La_M - R_0c_M) + (Lb_M - R_0d_M)z^{-1}}{(La_M + R_0c_M) + (Lb_M + R_0d_M)z^{-1}} \quad (1.93)$$

then taking the inverse  $z$ -transform and solving for the reflected wave  $b_0[n]$  yields the unadapted discrete-time wave domain equation

$$b_0[n] = -\frac{Lb_M + R_0d_M}{La_M + R_0c_M} b_0[n-1] + \frac{La_M - R_0c_M}{La_M + R_0c_M} a_0[n] + \frac{Lb_M - R_0d_M}{La_M + R_0c_M} a_0[n-1]. \quad (1.94)$$

This discretization is adapted by  $R_0 = \frac{La_M}{c_M}$ , which yields the adapted difference equation

$$b_0[n] = -\frac{b_M c_M + a_M d_M}{2a_M c_M} b_0[n-1] + \frac{b_M c_M - a_M d_M}{2a_M c_M} a_0[n-1]. \quad (1.95)$$

This time, the transform must satisfy  $a_M \neq 0$  (to avoid the disallowed adaptation  $R_0 = 0$ ) and  $c_M \neq 0$  (to avoid the disallowed adaptation  $R_0 = \infty$ ). Again, the condition  $a_M \neq 0$  can also be

interpreted as a structural restriction that disqualifies all fully explicit discretization methods (such as Forward Euler).

Wave Domain		
symbol	unadapted	adapted ( $R_0 = \frac{La_M}{c_M}$ )
$L$		
signal	$-\frac{Lb_M + R_0 d_M}{La_M + R_0 c_M} z^{-1} + \frac{La_M - R_0 c_M}{La_M + R_0 c_M}$ $+\frac{Lb_M - R_0 d_M}{La_M + R_0 c_M} a_0[n]$	$-\frac{b_M c_M + a_M d_M}{2a_M c_M} z^{-1} + \frac{b_M c_M - a_M d_M}{2a_M c_M}$ $a_0[n]$

Figure 1.23: Wave-Domain Representations of an Inductor, Discretized Using the Möbius Transform.

The adapted and unadapted Wave Digital Filter symbols and adapted and unadapted Wave Digital Filter signal-flow diagrams for the inductor discretized using the Möbius are shown in Figure 1.23.

### 1.3.3 Choosing a Discretization Method

The choice of discretization method is an important one, and we've explored a number of options for Wave Digital Filter discretization of capacitors and inductors. These include Backwards Euler, the Bilinear Transform, the Warped Bilinear Transform, the  $\alpha$  Transform, and the Möbius Transform.

The Bilinear Transform and the Warped Bilinear Transform are the most commonly used discretization methods. Indeed they are order-preserving, stability-preserving, and the Bilinear Transform is 2nd-order accurate. When a frequency response has an important feature, the warping control of the Warped Bilinear Transform is a useful way to map the frequency of that one feature exactly.

However, in nonlinear simulations the Bilinear Transform is known to suffer from spurious high-frequency oscillations [146, 160, 161, 162, 155]. These relate to the motion of instantaneous highly-damped poles, which “clump up” near the image of  $s \rightarrow \infty$  on the  $z$  plane. Since that image is at Nyquist for the Bilinear Transform, it is unsurprising that it could create high-frequency oscillations.

Using Backwards Euler can often alleviate this issue—its image of  $s \rightarrow \infty$  is at  $z = 0$ , the most damped possible location. Using the  $\alpha$  Transform, it is possible to compromise between these two extremes, possibly with the goal of satisfying an instantaneous pole damping monotonicity condition [155]. In Chapter 3 we'll show a case study where this degree of control becomes important. The Möbius Transform is an even wider class of transforms that encompasses all these approaches

and others, e.g., the recently-proposed application of the Fractional Bilinear Transform [163] (with the fractional delay realized with first-order Lagrange interpolation) and the AL-Alaoui operator to Wave Digital Filter modeling [164, 165]. Although not yet widely in use, the Möbius Transform has a high potential. In fact, since linear multistep methods above order 2 cannot be A-stable (a concept known as the “second Dahlquist Barrier” [153]), the Möbius transform is likely the most broad generalization of the highest order linear multistep methods that can achieve guaranteed passivity, an important Wave Digital Filter concept. Although we won’t demonstrate it here, it is quite possible to use higher order linear multistep methods, such as the family of Gear’s methods (also known as Backward Differentiation Formulas [166]), to discretize capacitors and inductors in the Wave Digital Filter context [167, 160, 168]. However, due to the Dahlquist barrier it appears they cannot be guaranteed passive. For this reason, discretizations that mesh philosophically with the Wave Digital Filter approach will likely all be special cases of the Möbius Transform approach.

Here, we’ve shown that although discretization schemes besides the Bilinear Transform are not often considered in the Wave Digital Filter context, all these transforms are viable. Another contribution of this section is the discovery of the fascinating condition that Wave Digital Filter discretization schemes, by construction, must be implicit—fully explicit schemes like Forward Euler ruin the chance for adaptation and hence cannot be used.

## 1.4 Two-Ports

More complicated than one-ports are *two-ports*. Luckily, they are usually just algebraic (not reactive), so issues of discretization can be set aside.<sup>5</sup>

Typically, circuit two-ports are described in the Kirchhoff domain by two equations. Certain standard definitions based on amplifier  $y$ -,  $z$ -,  $h$ -, and  $g$ -parameters are often used, and indeed we will derive Wave Digital Filter adaptors based on those models later in this Section. However, for the purposes of derivation, we will simply use linear algebra on a very general Kirchhoff-domain matrix equation to solve for the scattering parameters of each two-port. This general Kirchhoff-domain matrix expression is

$$\begin{bmatrix} x_{00} & x_{01} \\ x_{10} & x_{11} \end{bmatrix} \begin{bmatrix} v_0 \\ v_1 \end{bmatrix} + \begin{bmatrix} y_{00} & y_{01} \\ y_{10} & y_{11} \end{bmatrix} \begin{bmatrix} i_0 \\ i_1 \end{bmatrix} = \begin{bmatrix} 0 \\ 0 \end{bmatrix}, \quad (1.96)$$

or, in vector-matrix form

$$\mathbf{X}\mathbf{v} + \mathbf{Y}\mathbf{i} = \mathbf{0}. \quad (1.97)$$

---

<sup>5</sup>A two-port known as the Generalized Immittance Converter (GIC) [148, p. 37] which may involve embedded reactances is indeed involved in one thread of Wave Digital Filter research (e.g., [169, 170, 171, 165]), but is not important to audio circuitry and will not be considered further here.

Plugging the parametric wave definition (1.9) into this equation

$$\mathbf{X} \left( \frac{1}{2} \mathbf{R}^{1-\rho} \mathbf{a} + \frac{1}{2} \mathbf{R}^{1-\rho} \mathbf{b} \right) + \mathbf{Y} \left( \frac{1}{2} \mathbf{R}^{-\rho} \mathbf{a} - \frac{1}{2} \mathbf{R}^{-\rho} \mathbf{b} \right) = \mathbf{0} \quad (1.98)$$

and solving for  $\mathbf{b}$  yields the unadapted wave-domain equation

$$\mathbf{b} = -(\mathbf{X}\mathbf{R}^{1-\rho} - \mathbf{Y}\mathbf{R}^{-\rho})^{-1} (\mathbf{X}\mathbf{R}^{1-\rho} + \mathbf{Y}\mathbf{R}^{-\rho}) \mathbf{a} \quad (1.99)$$

which means the scattering matrix is defined

$$\mathbf{S} = -(\mathbf{X}\mathbf{R}^{1-\rho} - \mathbf{Y}\mathbf{R}^{-\rho})^{-1} (\mathbf{X}\mathbf{R}^{1-\rho} + \mathbf{Y}\mathbf{R}^{-\rho}) . \quad (1.100)$$

In the rest of this section, we will discuss important electrical two-ports, including parallel adaptors, series adaptors (inverters), series and parallel adaptors containing absorbed sources, transformers, controlled sources (voltage-controlled voltage source, voltage-controlled current source, current-controlled voltage source, and current-controlled current source), ideal voltage, current, and power converters, unit elements, quasi-reciprocal lines (QUARLs), gyrators, dualizers, mutators, nullors, and  $y$ -,  $z$ -,  $h$ -, and  $h$ -parameter models.

### 1.4.1 Simple Two-Port Connections

The simplest two-ports are connections between ports. There are two kinds of connections, series and parallel. In the Wave Digital Filter context, a standard connection is a two-port parallel connection; hence the two-port series connection is also Wave Digital Filter *inverter*. We will find at the end of these derivations that the scattering matrix of an adapted parallel connection is simply an identity matrix—for this reason two-port parallel adaptors are almost never even notated, but rather just implied. Two-port series adaptors should be notated, since their adapted scattering matrix involves sign inversions.

#### Two-Port Parallel Adaptor

When two ports are in parallel, their voltages are equal and their currents are opposite

$$v_0 = v_1 \quad (1.101)$$

$$i_0 = -i_1 . \quad (1.102)$$

The symbol and port definition for a two-port parallel adaptor, adapted and unadapted Wave Digital Filter symbols, and adapted and unadapted Wave Digital Filter signal-flow diagrams are shown in Figure 1.24.

	Kirchhoff domain	Wave Domain
symbol		unadapted      adapted ( $R_0 = R_1$ )
$v_0$		
$v_0 \leftarrow v_1$		
$i_0 \leftarrow \square_{-1} i_1$		

Figure 1.24: Kirchhoff- and Wave-Domain Representations of a Two-Port Parallel Connection.

Plugging the parametric wave definition (1.9) into the Kirchhoff-domain parallel adaptor equations (1.101)–(1.102) and solving for the reflected waves  $\begin{bmatrix} b_0 & b_1 \end{bmatrix}^\top$  yields the unadapted wave-domain equation

$$\begin{bmatrix} b_0 \\ b_1 \end{bmatrix} = \begin{bmatrix} -\frac{R_0-R_1}{R_0+R_1} & \frac{2R_0^{\rho}R_1^{1-\rho}}{R_0+R_1} \\ \frac{2R_0^{1-\rho}R_1^{\rho}}{R_0+R_1} & \frac{R_0-R_1}{R_0+R_1} \end{bmatrix} \begin{bmatrix} a_0 \\ a_1 \end{bmatrix}. \quad (1.103)$$

To adapt port 0 of the adaptor, we must find the value of  $R_0$  that sets  $-\frac{R_0-R_1}{R_0+R_1} = 0$ . This is satisfied by  $R_0 = R_1$  and produces the adapted wave-domain equation

$$\begin{bmatrix} b_0 \\ b_1 \end{bmatrix} = \begin{bmatrix} 0 & 1 \\ 1 & 0 \end{bmatrix} \begin{bmatrix} a_0 \\ a_1 \end{bmatrix}. \quad (1.104)$$

This is identical to the criteria for adapting port 1.

The adapted two-port parallel connection is special because it is just a connection between ports. So, usually two-port parallel connections are not even drawn in an adaptor structure. Still, you may occasionally find a reason to use the two-port parallel adaptor as the root of a Wave Digital Filter tree.

### Two-Port Series Adaptor / Inverter

The derivation of the two-port series adaptor proceeds in a very similar fashion to the two-port parallel adaptor. When two ports are in series, their voltages are opposite and their currents are

equal

$$v_0 = -v_1 \quad (1.105)$$

$$i_0 = i_1. \quad (1.106)$$

The symbol and port definition for a two-port series adaptor, adapted and unadapted Wave Digital Filter symbols, and adapted and unadapted Wave Digital Filter signal-flow diagrams are shown in Figure 1.25.

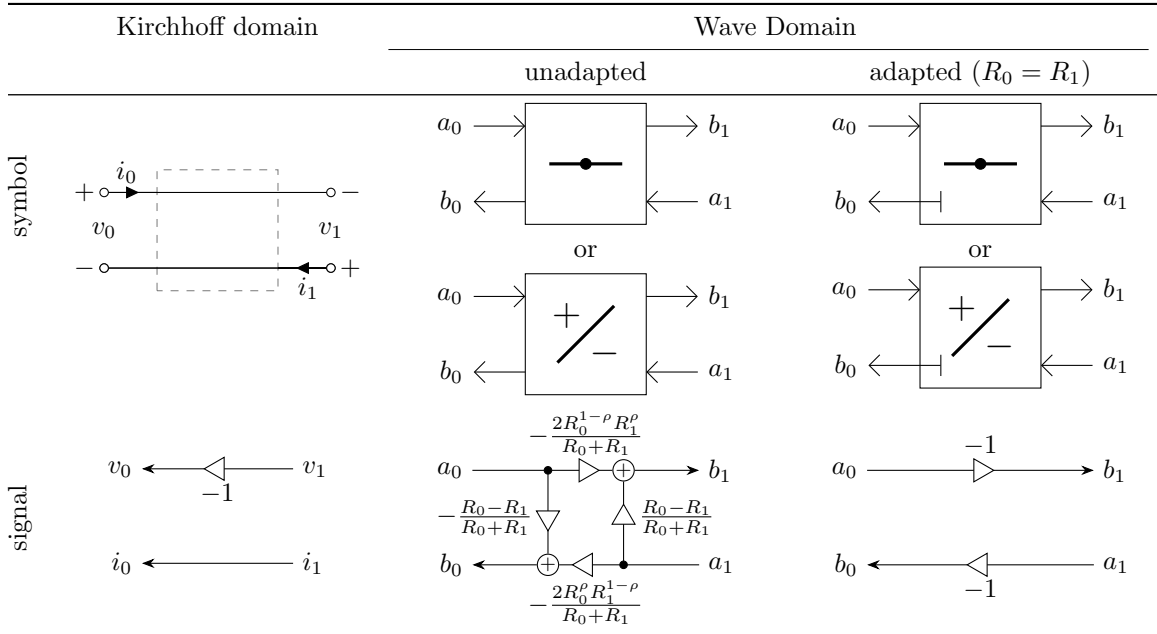


Figure 1.25: Kirchhoff- and Wave-Domain Representations of a Two-Port Series Connection (Inverter).

Plugging the parametric wave definition (1.9) into the Kirchhoff-domain series adaptor equation (1.105)–(1.106) and solving for the reflected waves  $[b_0 \ b_1]^\top$  yields the unadapted wave-domain equation

$$\begin{bmatrix} b_0 \\ b_1 \end{bmatrix} = \begin{bmatrix} -\frac{R_0-R_1}{R_0+R_1} & -\frac{2R_0^\rho R_1^{1-\rho}}{R_0+R_1} \\ -\frac{2R_0^{1-\rho}R_1^\rho}{R_0+R_1} & \frac{R_0-R_1}{R_0+R_1} \end{bmatrix} \begin{bmatrix} a_0 \\ a_1 \end{bmatrix}. \quad (1.107)$$

To adapt port 0 of the series adaptor, we must find the value of  $R_0$  that sets  $-\frac{R_0-R_1}{R_0+R_1} = 0$ . This is satisfied by  $R_0 = R_1$  and produces the adapted wave-domain equation

$$\begin{bmatrix} b_0 \\ b_1 \end{bmatrix} = \begin{bmatrix} 0 & -1 \\ -1 & 0 \end{bmatrix} \begin{bmatrix} a_0 \\ a_1 \end{bmatrix}. \quad (1.108)$$

Again this is identical to the criteria for adapting port 1.

Notice that the two-port series adaptor is very similar to the two-port parallel adaptor, differing only by a sign inversion on the antidiagonal scattering matrix entries. In fact series adaptors are the dual of parallel adaptors and can be realized through certain transpositional properties by a series adaptor and sign inversions (and vice versa) [172]. Although the two-port series adaptor may appear as a root element, its normal use is as a *polarity inverter* [173]. Many audio circuits have a single input and a single output, and are ac-coupled; for these circuits getting the polarity of ports correct is often not important and at worst could case a sign flip in the output signal. However, in more complicated circuits, especially those involving nonlinearities, incorrect polarities can be disasterous and completely change the behavior of a circuit [174, 175, 173, 176]. The systematic use of the two-port series adaptor / inverter will be illustrated later in the case study of this Chapter.

#### 1.4.2 Two-Port Series/Parallel Adaptors Containing Sources

Here we consider two-port series adaptors with absorbed ideal current sources and two-port parallel adaptors with absorbed ideal voltage sources [6]. These two-ports are essential for creating realizable Wave Digital Filter trees out of reference circuits with multiple sources without altering the reference circuit by adding extra resistances. This hints at broader issues of realizability due to multiple nonadaptable linear electrical one-ports. An alternate and more comprehensive strategy for handling multiple nonadaptable linear elements will be presented at the end of Chapter 2.

##### Two-Port Parallel Adaptor + Ideal Current Source

When two ports are in parallel with an ideal current source  $j$ , the two port current and the source current sum to zero and the voltages currents are equal

$$v_0 = v_1 \quad (1.109)$$

$$i_0 + i_1 + j = 0. \quad (1.110)$$

The symbol and port definition for a two-port parallel adaptor with an absorbed current source, adapted and unadapted Wave Digital Filter symbols, and adapted and unadapted Wave Digital Filter signal-flow diagrams are shown in Figure 1.26.

Plugging the parametric wave definition (1.9) into the Kirchhoff-domain equations (1.109)–(1.110) and solving for the reflected waves  $\begin{bmatrix} b_0 & b_1 \end{bmatrix}^\top$  yields the unadapted wave-domain equation

$$\begin{bmatrix} b_0 \\ b_1 \end{bmatrix} = \begin{bmatrix} -\frac{R_0 - R_1}{R_0 + R_1} & \frac{2R_0^\rho R_1^{1-\rho}}{R_0 + R_1} \\ \frac{2R_0^{1-\rho} R_1^\rho}{R_0 + R_1} & \frac{R_0 - R_1}{R_0 + R_1} \end{bmatrix} \begin{bmatrix} a_0 \\ a_1 \end{bmatrix} + \begin{bmatrix} 2 \frac{R_0^\rho R_1}{R_0 + R_1} \\ 2 \frac{R_0 R_1^\rho}{R_0 + R_1} \end{bmatrix} j. \quad (1.111)$$

Exactly like in the normal two-port parallel adaptor, to adapt port 0 of the adaptor, we must find

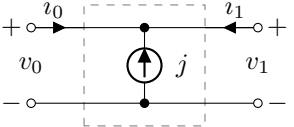
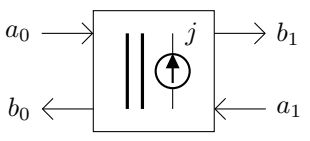
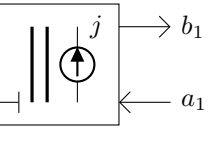
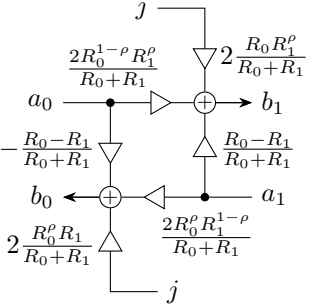
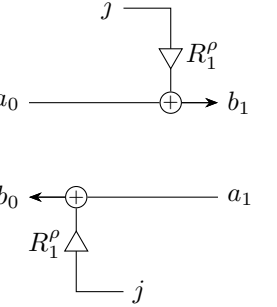
Kirchhoff domain	Wave Domain	
symbol	unadapted	adapted ( $R_0 = R_1$ )
	 $\begin{aligned} v_0 &\leftarrow v_1 \\ i_0 &\leftarrow -1 \end{aligned}$ $\begin{aligned} i_0 &\leftarrow +1 \\ j &\leftarrow \end{aligned}$	
		

Figure 1.26: Kirchhoff- and Wave-Domain Representations of a Two-Port Parallel Connection Including an Ideal Current Source.

the value of  $R_0$  that sets  $-\frac{R_0-R_1}{R_0+R_1} = 0$ . This is satisfied by  $R_0 = R_1$  and produces the adapted wave-domain equation

$$\begin{bmatrix} b_0 \\ b_1 \end{bmatrix} = \begin{bmatrix} 0 & 1 \\ 1 & 0 \end{bmatrix} \begin{bmatrix} a_0 \\ a_1 \end{bmatrix} + \begin{bmatrix} R_1^\rho \\ R_1^\rho \end{bmatrix} j. \quad (1.112)$$

Again this is identical to the criteria for adapting port 1.

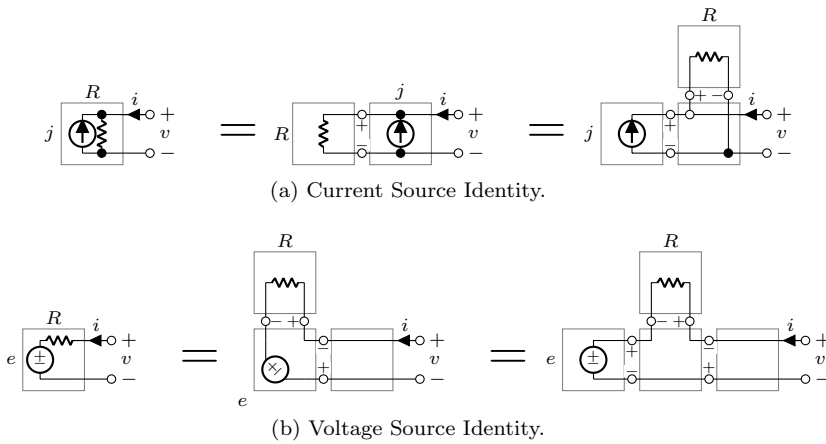


Figure 1.27: Current and Voltage Source Identities.

Arguably, as shown in Figure 1.27a, we can view resistive current sources as a combination of a

resistor with a parallel adaptor with an absorbed current source.

### Two-Port Series Adaptor + Ideal Voltage Source

When two ports are in series with an ideal voltage source  $e$ , the two port voltages and the source voltage sum to zero and the port currents are equal

$$v_0 + v_1 + e = 0 \quad (1.113)$$

$$i_0 = i_1. \quad (1.114)$$

Take note that we diverge slightly from how this adaptor is defined in [6], arguing that their port polarity actually reflects a parallel connection. The symbol and port definition for a two-port series adaptor with absorbed voltage source, adapted and unadapted Wave Digital Filter symbols, and adapted and unadapted Wave Digital Filter signal-flow diagrams are shown in Figure 1.28.

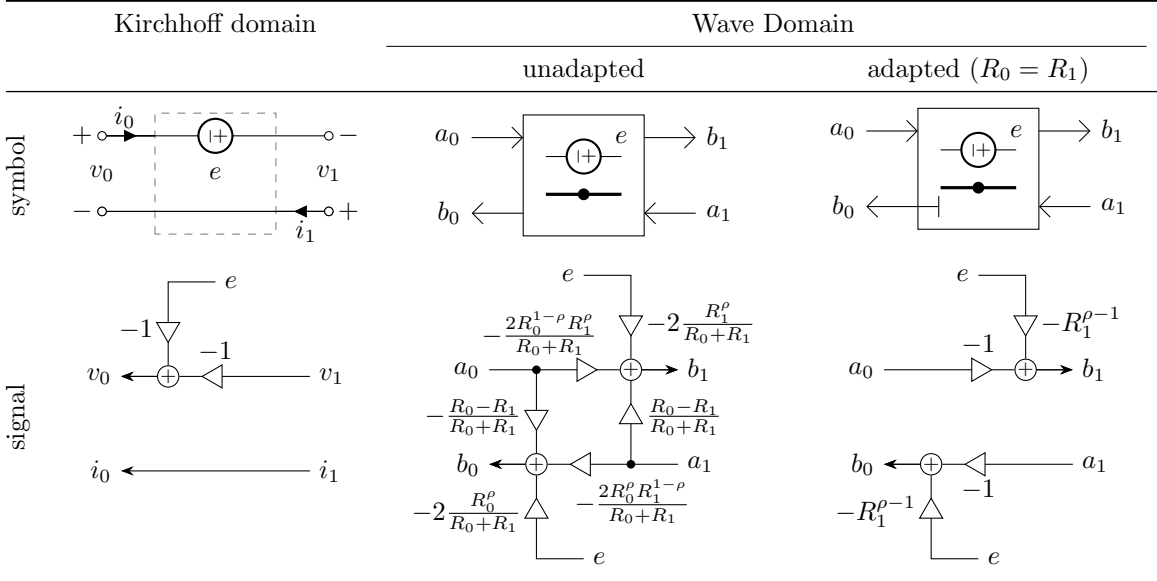


Figure 1.28: Kirchhoff- and Wave-Domain Representations of a Two-Port Series Connection Including an Ideal Voltage Source.

Plugging the parametric wave definition (1.9) into the Kirchhoff-domain parallel adaptor equations (1.113)–(1.114) and solving for the reflected waves  $\begin{bmatrix} b_0 & b_1 \end{bmatrix}^\top$  yields the unadapted wave-domain equation

$$\begin{bmatrix} b_0 \\ b_1 \end{bmatrix} = \begin{bmatrix} -\frac{R_0-R_1}{R_0+R_1} & -\frac{2R_0^\rho R_1^{1-\rho}}{R_0+R_1} \\ -\frac{2R_0^{1-\rho} R_1^\rho}{R_0+R_1} & \frac{R_0-R_1}{R_0+R_1} \end{bmatrix} \begin{bmatrix} a_0 \\ a_1 \end{bmatrix} + \begin{bmatrix} -2\frac{R_0^\rho}{R_0+R_1} \\ -2\frac{R_1^\rho}{R_0+R_1} \end{bmatrix} e. \quad (1.115)$$

Exactly like in the normal two-port series adaptor, to adapt port 0 of the adaptor, we must find

the value of  $R_0$  that sets  $-\frac{R_0 - R_1}{R_0 + R_1} = 0$ . This is satisfied by  $R_0 = R_1$  and produces the adapted wave-domain equation

$$\begin{bmatrix} b_0 \\ b_1 \end{bmatrix} = \begin{bmatrix} 0 & -1 \\ -1 & 0 \end{bmatrix} \begin{bmatrix} a_0 \\ a_1 \end{bmatrix} + \begin{bmatrix} -R_1^{\rho-1} \\ -R_1^{\rho-1} \end{bmatrix} e. \quad (1.116)$$

Again this is identical to the criteria for adapting port 1.

Arguably, as shown in Figure 1.27b, we can view resistive voltage sources as a combination of a resistor with a series adaptor with an absorbed voltage source, and an inverter.

### 1.4.3 Ideal Transformer

We define the ideal transformer (sometimes more specifically called the “ideal real transformer” [148]) as the linear two-port device that relates the port voltages and currents at two ports according to

$$v_0 = n v_1 \quad (1.117)$$

$$i_1 = -n i_0, \quad (1.118)$$

where  $n$  is the “turns ratio,” the ratio between windings on the primary and secondary coils. This definition uses sign conventions that conform with the standard port definition (currents pointing inwards on the positive terminals). Sometimes a cascade definition is used [177], which emphasizes how a transformer transforms an impedance that it is attached to.

$$v_0 = n v_1 \quad (1.119)$$

$$i_1 = n i_0. \quad (1.120)$$

In this work, we will always use the first transformer definition (1.117)–(1.118). To use this derivation for a transformer using the sign conventions of (1.119)–(1.120), it suffices to put our derived Wave Digital Filter transformer in series with a Wave Digital Filter inverter, i.e., a two-port series adaptor §1.4.1. The symbol and port definition for an ideal transformer, adapted and unadapted Wave Digital Filter symbols, and adapted and unadapted Wave Digital Filter signal-flow diagrams are shown in Figure 1.29.

Plugging the parametric wave definition (1.9) into the Kirchhoff-domain transformer equations (1.117)–(1.118) and solving for the reflected waves  $\begin{bmatrix} b_0 & b_1 \end{bmatrix}^\top$  yields the unadapted wave-domain equation

$$\begin{bmatrix} b_0 \\ b_1 \end{bmatrix} = \begin{bmatrix} -\frac{R_0 - n^2 R_1}{R_0 + n^2 R_1} & \frac{2nR_0^\rho R_1^{1-\rho}}{R_0 + n^2 R_1} \\ \frac{2nR_0^{1-\rho} R_1^\rho}{R_0 + n^2 R_1} & \frac{R_0 - n^2 R_1}{R_0 + n^2 R_1} \end{bmatrix} \begin{bmatrix} a_0 \\ a_1 \end{bmatrix}. \quad (1.121)$$

To adapt port 0 of the transformer adaptor, we must find the value of  $R_0$  that sets  $-\frac{R_0 - n^2 R_1}{R_0 + n^2 R_1} = 0$ .

symbol	Kirchhoff domain	Wave Domain	
		unadapted	adapted ( $R_0 = n^2 R_1$ )
$v_0$			
$v_0$	$v_0 \leftarrow \begin{array}{c} n \\ \searrow \swarrow \end{array} v_1$	$a_0 \rightarrow \begin{array}{c} n : 1 \\ \searrow \swarrow \end{array} b_1$	$a_0 \rightarrow \begin{array}{c} n^{1-2\rho} \\ \searrow \swarrow \end{array} b_1$
$i_0$	$i_0 \rightarrow \begin{array}{c} -n \\ \searrow \swarrow \end{array} i_1$	$b_0 \leftarrow \begin{array}{c} \frac{2nR_0^{1-\rho}R_1^\rho}{R_0+n^2R_1} \\ \searrow \swarrow \end{array} a_1$	$b_0 \leftarrow \begin{array}{c} n^{2\rho-1} \\ \searrow \swarrow \end{array} a_1$

Figure 1.29: Kirchhoff- and Wave-Domain Representations of a Two-Port Transformer.

This is satisfied by  $R_0 = n^2 R_1$  and produces the adapted wave-domain equation

$$\begin{bmatrix} b_0 \\ b_1 \end{bmatrix} = \begin{bmatrix} 0 & n^{2\rho-1} \\ n^{1-2\rho} & 0 \end{bmatrix} \begin{bmatrix} a_0 \\ a_1 \end{bmatrix}. \quad (1.122)$$

Port 1 is adapted in the same way, although the criteria would rather be written  $R_1 = \frac{1}{n^2} R_0$ .

### Active Transformer

A non-passive generalization of the ideal transformer is called the “active transformer” [148, pp. 42–43]. The active transformer is characterized by two different turns ratios  $\gamma_1$  and  $\gamma_2$

$$v_0 = \gamma_1 v_1 \quad (1.123)$$

$$i_1 = -\gamma_2 i_0. \quad (1.124)$$

The symbol and port definition for an active transformer, adapted and unadapted Wave Digital Filter symbols, and adapted and unadapted Wave Digital Filter signal-flow diagrams are shown in Figure 1.30.

Plugging the parametric wave definition (1.9) into the Kirchhoff-domain active transformer equations (1.123)–(1.124) and solving for the reflected waves  $[b_0 \ b_1]^\top$  yields the unadapted wave-domain equation

$$\begin{bmatrix} b_0 \\ b_1 \end{bmatrix} = \begin{bmatrix} -\frac{R_0-\gamma_1\gamma_2R_1}{R_0+\gamma_1\gamma_2R_1} & \frac{2\gamma_1R_0^\rho R_1^{1-\rho}}{R_0+\gamma_1\gamma_2R_1} \\ \frac{2\gamma_2R_0^{1-\rho}R_1^\rho}{R_0+\gamma_1\gamma_2R_1} & \frac{R_0-\gamma_1\gamma_2R_1}{R_0+\gamma_1\gamma_2R_1} \end{bmatrix} \begin{bmatrix} a_0 \\ a_1 \end{bmatrix}. \quad (1.125)$$

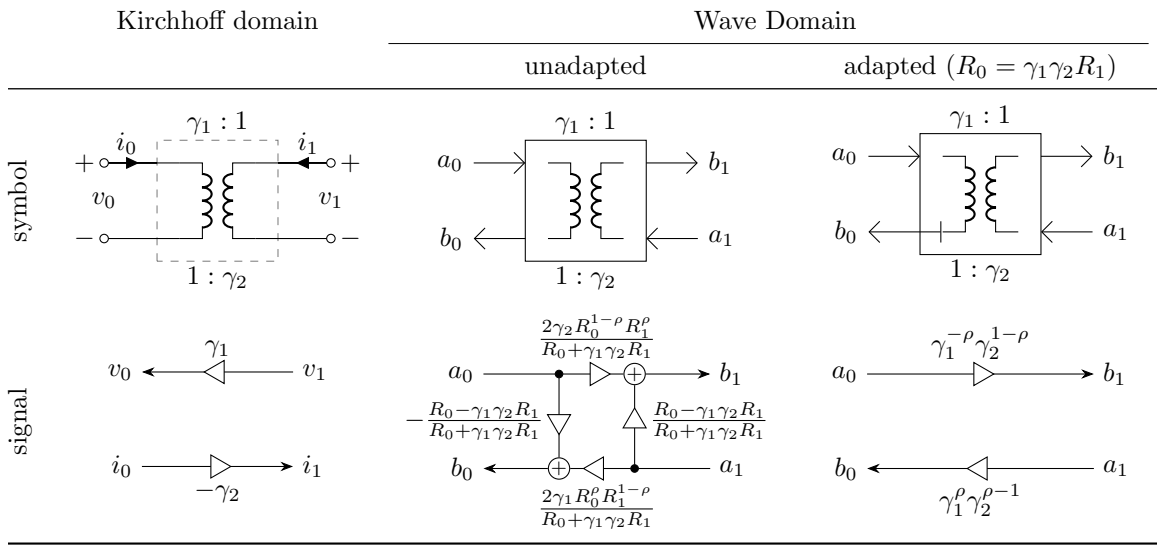


Figure 1.30: Kirchhoff- and Wave-Domain Representations of a Two-Port Active Transformer.

Port 0 of the active transformer is adapted by  $R_0 = \gamma_1 \gamma_2 R_1$ , yielding the adapted scattering matrix

$$\begin{bmatrix} b_0 \\ b_1 \end{bmatrix} = \begin{bmatrix} 0 & \gamma_1^\rho \gamma_2^{\rho-1} \\ \gamma_1^{-\rho} \gamma_2^{1-\rho} & 0 \end{bmatrix} \begin{bmatrix} a_0 \\ a_1 \end{bmatrix}. \quad (1.126)$$

Port 1 is adapted in the same way, although the criteria would rather be written  $R_1 = \frac{1}{\gamma_1 \gamma_2} R_0$ .

An even more general case involving complex values is known as the ideal complex transformer (also known as the “generalized ideal transformer” [178]), where  $\gamma_1$  and  $\gamma_2$  may be complex and  $\gamma_2 = \gamma_1^*$ , the complex conjugate of  $\gamma_1$ .

#### 1.4.4 Controlled Sources

Another important class of electrical two-ports are controlled sources. These include the Voltage-Controlled Voltage Source (VCVS), the Voltage-Controlled Current Source (VCCS), the Current-Controlled Voltage Source (CCVS), and the Current-Controlled Current Source (CCCS). In electrical circuits controlled sources are used to model amplification, connections between subcircuits, and as part of device macromodeling. They are also the building blocks of the  $y$ -,  $z$ -,  $h$ -, and  $g$ -parameter amplifier two-ports discussed later in this Chapter. In audio circuitry they are an essential part of modeling operational amplifiers and linearized transistor and tube amplifiers [141, 179].

Here we consider the feedforward case, where each of the two ports connect to a different subcircuit with no feedback between them. This is important for studying feedforward cascades of independent subcircuits, but many audio circuits are designed on principles of amplifier feedback

and do not have this property. However, we will find that two-port ideal controlled sources in feed-forward arrangements cannot be natively accommodated into Wave Digital Filters since neither of their two ports are adaptable. A work-around is explained after the four controlled sources are introduced.

Handling the case involving feedback around the two ports is one of the major contributions of this dissertation and is handled in Chapter 2.

### Voltage-Controlled Voltage Source

An ideal Voltage-Controlled Voltage Source (VCVS) is defined by [148, p. 27]

$$v_1 = \mu v_0 \quad (1.127)$$

$$i_0 = 0, \quad (1.128)$$

where  $\mu$  is the voltage gain factor. The symbol and port definition for a VCVS, unadapted Wave Digital Filter symbols, and unadapted Wave Digital Filter signal-flow diagrams are shown in Figure 1.31.

	Kirchhoff domain	Wave Domain	
symbol		unadapted	adapted

Figure 1.31: Kirchhoff- and Wave-Domain Representations of a Voltage-Controlled Voltage Source (VCVS).

Plugging the parametric wave definition (1.9) into the Kirchhoff-domain VCVS equations (1.127)–(1.128) and solving for the reflected waves  $\begin{bmatrix} b_0 & b_1 \end{bmatrix}^\top$  yields the unadapted wave-domain equation

$$\begin{bmatrix} b_0 \\ b_1 \end{bmatrix} = \begin{bmatrix} 1 & 0 \\ 2\mu R_0^{1-p} R_1^p - 1 & -1 \end{bmatrix} \begin{bmatrix} a_0 \\ a_1 \end{bmatrix}. \quad (1.129)$$

Since the diagonal entries of the scattering matrix are 1 and  $-1$ , they are not parameterized by either port resistance  $R_0$  or  $R_1$ . So, neither diagonal entry of the scattering matrix can be set to

zero by choice of port resistance and hence neither port can be adapted. This is a result of the fact that port 0 “sees” an open circuit, which we earlier showed is nonadaptable, and port 1 “sees” an ideal voltage source, which we earlier showed is nonadaptable.

### Voltage-Controlled Current Source

An ideal Voltage-Controlled Current Source (VCCS) is defined by [148, p. 26]

$$i_1 = g v_0 \quad (1.130)$$

$$i_0 = 0, \quad (1.131)$$

where  $g$  is the transfer admittance gain factor. The symbol and port definition for VCCS, unadapted Wave Digital Filter symbols, and unadapted Wave Digital Filter signal-flow diagrams are shown in Figure 1.32.

	Kirchhoff domain	Wave Domain	
symbol		unadapted	adapted
			N/A
			N/A

Figure 1.32: Kirchhoff- and Wave-Domain Representations of a Voltage-Controlled Current Source (VCCS).

Plugging the parametric wave definition (1.9) into the Kirchhoff-domain VCCS equations (1.130)–(1.131) and solving for the reflected waves  $\begin{bmatrix} b_0 & b_1 \end{bmatrix}^\top$  yields the unadapted wave-domain equation

$$\begin{bmatrix} b_0 \\ b_1 \end{bmatrix} = \begin{bmatrix} 1 & 0 \\ -2gR_0^{1-p}R_1^p & 1 \end{bmatrix} \begin{bmatrix} a_0 \\ a_1 \end{bmatrix}. \quad (1.132)$$

Since the diagonal entries of the scattering matrix are both 1, they are not parameterized by either port resistance  $R_0$  or  $R_1$ . Again, neither port can be adapted. This is a result of the fact that port 0 “sees” an nonadaptable open circuit, and port 1 “sees” an nonadaptable ideal current source.

### Current-Controlled Voltage Source

An ideal Current-Controlled Voltage Source (CCVS) is defined by [148, p. 26]

$$v_1 = r i_0 \quad (1.133)$$

$$v_0 = 0, \quad (1.134)$$

where  $r$  is the transfer impedance gain factor. The symbol and port definition for a CCVS, unadapted Wave Digital Filter symbols, and unadapted Wave Digital Filter signal-flow diagrams are shown in Figure 1.33.

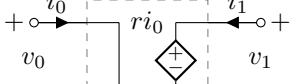
symbol	Kirchhoff domain	Wave Domain	
		unadapted	adapted
 $v_0$ $i_0$ $v_1$ $i_1$ $v_0$ $i_0$ $v_1$ $i_1$	 $a_0 \rightarrow [ri_0] \rightarrow b_1$ $b_0 \leftarrow$	N/A	
$v_0$ $i_0$ $v_1$ $i_1$ $i_0 \rightarrow r \rightarrow v_1$	 $a_0 \rightarrow [2rR_0^{-\rho} R_1^{\rho-1}] \rightarrow b_1$ $b_0 \leftarrow$	N/A	

Figure 1.33: Kirchhoff- and Wave-Domain Representations of a Current-Controlled Voltage Source (CCVS).

Plugging the parametric wave definition (1.9) into the Kirchhoff-domain CCVS equations (1.133)–(1.134) and solving for the reflected waves  $\begin{bmatrix} b_0 & b_1 \end{bmatrix}^\top$  yields the unadapted wave-domain equation

$$\begin{bmatrix} b_0 \\ b_1 \end{bmatrix} = \begin{bmatrix} -1 & 0 \\ 2rR_0^{-\rho} R_1^{\rho-1} & -1 \end{bmatrix} \begin{bmatrix} a_0 \\ a_1 \end{bmatrix}. \quad (1.135)$$

Since the diagonal entries of the scattering matrix are both  $-1$ , they are not parameterized by either port resistance  $R_0$  or  $R_1$ . Again, neither port can be adapted. This is a result of the fact that port 0 “sees” an nonadaptable short circuit, and port 1 “sees” an nonadaptable ideal voltage source.

### Current-Controlled Current Source

An ideal Current-Controlled Current Source (CCCS) is defined by [148, p. 27]

$$i_1 = \alpha i_0 \quad (1.136)$$

$$v_0 = 0, \quad (1.137)$$

where  $\alpha$  is the current gain factor. The symbol and port definition for a CCCS, unadapted Wave Digital Filter symbols, and unadapted Wave Digital Filter signal-flow diagrams are shown in Figure 1.34.

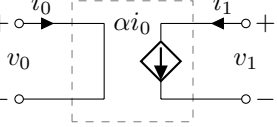
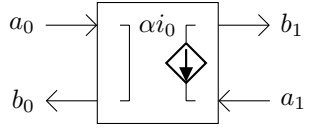
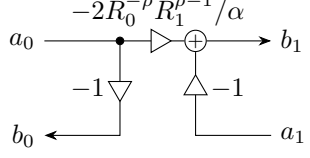
	Kirchhoff domain	Wave Domain	
symbol		unadapted	adapted
			N/A
$v_0 \leftarrow 0$			N/A
$i_0 \rightarrow \alpha \rightarrow i_1$			

Figure 1.34: Kirchhoff- and Wave-Domain Representations of a Current-Controlled Current Source (CCCS).

Plugging the parametric wave definition (1.9) into the Kirchhoff-domain CCCS equations (1.136)–(1.137) and solving for the reflected waves  $\begin{bmatrix} b_0 & b_1 \end{bmatrix}^\top$  yields the unadapted wave-domain equation

$$\begin{bmatrix} b_0 \\ b_1 \end{bmatrix} = \begin{bmatrix} -1 & 0 \\ 2R_0^{-\rho} R_1^{\rho-1}/\alpha & -1 \end{bmatrix} \begin{bmatrix} a_0 \\ a_1 \end{bmatrix}. \quad (1.138)$$

Since the diagonal entries of the scattering matrix are both  $-1$ , they are not parameterized by either port resistance  $R_0$  or  $R_1$ . Again, neither port can be adapted. This is a result of the fact that port 0 “sees” an nonadaptable short circuit, and port 1 “sees” an nonadaptable ideal current source.

### Using Controlled Sources

Since both ports of each of the four ideal controlled sources are nonadaptable, the four ideal controlled sources are only suitable for inclusion at the root of Wave Digital Filter trees. So, it is common to break the controlled sources conceptually into a voltage or current read off of a short circuit or

open circuit in one Wave Digital Filter tree, which controls (according to  $\mu$ ,  $g$ ,  $r$ , or  $\alpha$ ) the voltage or current of a normal ideal source in another Wave Digital Filter tree. Since there is no reverse transmission in any of their scattering matrices (all of them have  $s_{01} = 0$ ), there is only a unilateral flow of information at play. To free up the root of these two trees for other nonadaptable elements, it is common to pull the voltage or current off of another appropriate port in the first tree, rather than explicitly include a short or open circuit. Similarly, if the ideal voltage or current source in the second tree can be associated with a series or parallel resistance, or absorbed into a series or parallel adaptor (as discussed in §1.4.2), it can also be relieved of its restriction to the root of the second tree, freeing that location up for another nonadaptable circuit element.

If its not possible to pull voltages or currents off of other circuit elements, or to associate the ideal sources with series or parallel resistances or absorb them into series or parallel adaptors, it may be appropriate to make small modifications to the reference circuit to ease these realizability concerns. A short circuit may be replaced by a very small (e.g.,  $1\Omega$ ) resistor. An open circuit may be replaced by a very large (e.g.,  $1000\times$  larger than the largest resistance in the circuit [146]). A small resistor may be added in series to an ideal voltage source to make it adaptable, and likewise a large resistor may be added in parallel with an ideal current source to make it adaptable. Although these tricks will decrease the accuracy of any simulation slightly, they are very practical and also have the nice property of being incrementally passive—they involve only the introduction of simple passive electrical elements (resistors) into the reference circuit.

### 1.4.5 Ideal Converters

A family of unusual linear two-port devices are known as ideal converters [148, pp. 43–45], including the Ideal Voltage Converter (IVC), the Ideal Current Converter (ICC), and the Ideal Power Converter (IPC), which are useful for the analysis and synthesis of active networks. The ideal voltage and current converters can also be seen as impedance converters [180]. In the analysis of power systems, ideal converters are sometimes defined in a different way, where power is conserved [181].

#### Ideal Voltage Converter (IVC)

The Ideal Voltage Converter (IVC) is defined by the transmission matrix relationship

$$v_0 = k v_1 \tag{1.139}$$

$$i_0 = -i_1 , \tag{1.140}$$

where  $k$  is the voltage gain factor. The symbol and port definition for an IVC, adapted and unadapted Wave Digital Filter symbols, and adapted and unadapted Wave Digital Filter signal-flow diagrams are shown in Figure 1.35.

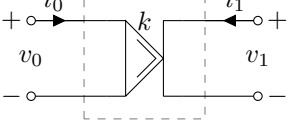
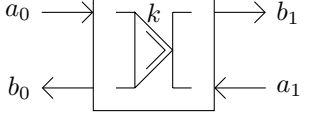
	Kirchhoff domain	Wave Domain
symbol		unadapted      adapted ( $R_0 = k R_1$ )
$i_0$		
$v_0$	$v_0 \xrightarrow{k} v_1$	$a_0 \xrightarrow{\frac{2R_0^{1-\rho}R_1^\rho}{R_0+kR_1}} b_1$
$i_1$	$i_0 \xrightarrow{-1} i_1$	$b_0 \xleftarrow{\frac{R_0-kR_1}{R_0+kR_1}} a_1$
		$a_0 \xrightarrow{\frac{2kR_0^\rho R_1^{1-\rho}}{R_0+kR_1}} b_1$
		$b_0 \xleftarrow{k^{-\rho}} a_1$

Figure 1.35: Kirchhoff- and Wave-Domain Representations of an Ideal Voltage Converter Two-Port.

Plugging the parametric wave definition (1.9) into the Kirchhoff-domain IVC equations (1.139)–(1.140) and solving for the reflected waves  $\begin{bmatrix} b_0 & b_1 \end{bmatrix}^\top$  yields the unadapted wave-domain equation

$$\begin{bmatrix} b_0 \\ b_1 \end{bmatrix} = \begin{bmatrix} \frac{R_0-kR_1}{R_0+kR_1} & \frac{2kR_0^\rho R_1^{1-\rho}}{R_0+kR_1} \\ \frac{2R_0^{1-\rho}R_1^\rho}{R_0+kR_1} & -\frac{R_0-kR_1}{R_0+kR_1} \end{bmatrix} \begin{bmatrix} a_0 \\ a_1 \end{bmatrix}. \quad (1.141)$$

Port 0 is adapted by  $R_0 = k R_1$ , yielding the adapted wave-domain equation

$$\begin{bmatrix} b_0 \\ b_1 \end{bmatrix} = \begin{bmatrix} 0 & k^\rho \\ k^{-\rho} & 0 \end{bmatrix} \begin{bmatrix} a_0 \\ a_1 \end{bmatrix}. \quad (1.142)$$

Port 1 is adapted in the same way, although the criteria would rather be written  $R_1 = \frac{1}{k} R_0$ .

### Ideal Current Converter (ICC)

The Ideal Current Converter (ICC) is defined by the transmission matrix relationship

$$v_0 = v_1 \quad (1.143)$$

$$i_0 = -\beta i_1, \quad (1.144)$$

where  $\beta$  is the current gain factor. The symbol and port definition for an ICC, adapted and unadapted Wave Digital Filter symbols, and adapted and unadapted Wave Digital Filter signal-flow diagrams are shown in Figure 1.36.

	Kirchhoff domain	Wave Domain
symbol		unadapted adapted ( $R_0 = R_1/\beta$ )
signal		
	$v_0 \longrightarrow v_1$	$a_0 \longrightarrow b_1$
	$i_0 \longrightarrow -\beta i_1$	$b_0 \longleftarrow \frac{2R_0^{1-\rho}R_1^\rho}{\beta R_0+R_1} a_1$

Figure 1.36: Kirchhoff- and Wave-Domain Representations of an Ideal Current Converter Two-Port.

Plugging the parametric wave definition (1.9) into the Kirchhoff-domain ICC equations (1.143)–(1.144) and solving for the reflected waves  $\begin{bmatrix} b_0 & b_1 \end{bmatrix}^\top$  yields the unadapted wave-domain equation

$$\begin{bmatrix} b_0 \\ b_1 \end{bmatrix} = \begin{bmatrix} -\frac{\beta R_0 - R_1}{\beta R_0 + R_1} & \frac{2\beta R_0^\rho R_1^{1-\rho}}{\beta R_0 + R_1} \\ \frac{2R_0^{1-\rho}R_1^\rho}{\beta R_0 + R_1} & \frac{\beta R_0 - R_1}{\beta R_0 + R_1} \end{bmatrix} \begin{bmatrix} a_0 \\ a_1 \end{bmatrix}. \quad (1.145)$$

Port 0 is adapted by  $R_0 = R_1/\beta$ , yielding the adapted wave-domain equation

$$\begin{bmatrix} b_0 \\ b_1 \end{bmatrix} = \begin{bmatrix} 0 & \beta^{1-\rho} \\ \beta^{\rho-1} & 0 \end{bmatrix} \begin{bmatrix} a_0 \\ a_1 \end{bmatrix}. \quad (1.146)$$

Port 1 is adapted in the same way, although the criteria would rather be written  $R_1 = \beta R_0$ .

### Ideal Power Converter (IPC)

The Ideal Power Converter (IPC) is defined by the transmission matrix relationship

$$v_0 = m v_1 \quad (1.147)$$

$$i_0 = -m i_1, \quad (1.148)$$

where  $m$  is the power gain factor. The symbol and port definition for an IPC, and adapted and unadapted Wave Digital Filter signal-flow diagrams are shown in Figure 1.37.

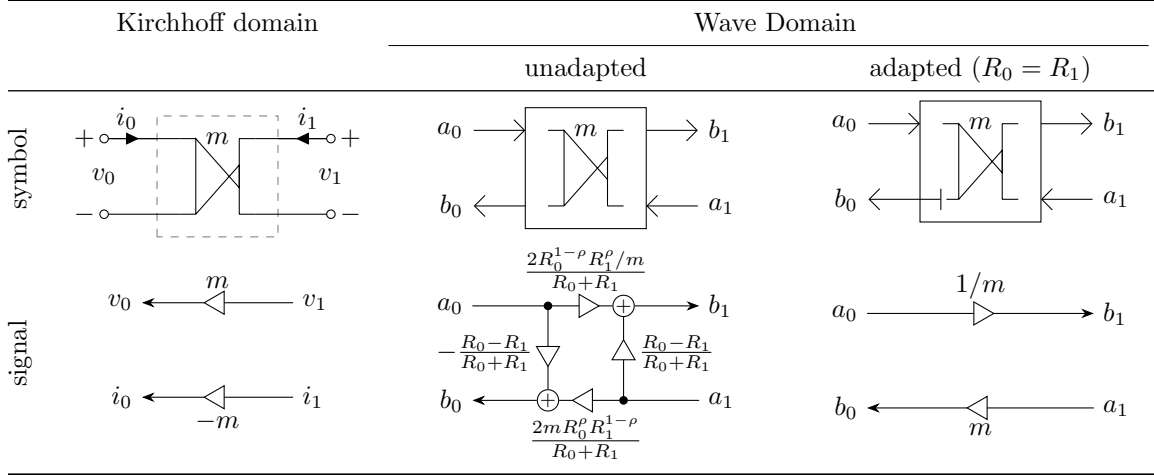


Figure 1.37: Kirchhoff- and Wave-Domain Representations of an Ideal Power Converter Two-Port.

Plugging the parametric wave definition (1.9) into the Kirchhoff-domain IPC equations (1.147)–(1.148) and solving for the reflected waves  $\begin{bmatrix} b_0 & b_1 \end{bmatrix}^\top$  yields the unadapted wave-domain equation

$$\begin{bmatrix} b_0 \\ b_1 \end{bmatrix} = \begin{bmatrix} -\frac{R_0-R_1}{R_0+R_1} & \frac{2R_0^\rho R_1^{1-\rho} m}{R_0+R_1} \\ \frac{2R_0^{1-\rho} R_1^\rho / m}{R_0+R_1} & \frac{R_0-R_1}{R_0+R_1} \end{bmatrix} \begin{bmatrix} a_0 \\ a_1 \end{bmatrix}. \quad (1.149)$$

Port 0 is adapted by  $R_0 = R_1$ , yielding the adapted wave-domain equation

$$\begin{bmatrix} b_0 \\ b_1 \end{bmatrix} = \begin{bmatrix} 0 & m \\ 1/m & 0 \end{bmatrix} \begin{bmatrix} a_0 \\ a_1 \end{bmatrix}. \quad (1.150)$$

Port 1 is adapted in the same way.

#### 1.4.6 Unit Element and QUARLs

Unit elements are reciprocal wave-domain delays with a delay length of  $T/2$  in each direction and a characteristic impedance  $R_0$ , a special case of a transmission line. They are an important concept in microwave engineering and in the early days of Wave Digital Filters, before the adaptation concept had matured [91], they were used between stages of the Wave Digital Filter to break delay-free loops. Wave Digital Filters based explicitly on “unit element filters” have also been developed (e.g., [88, 182]). A Quasi-Reciprocal Line (QUARL) is a generalization of the Unit Element, where the average delay length is still  $T/2$  but the wave delay length in each direction are not the same [5]. Since transmission lines don’t appear in standard audio circuits, we won’t consider Unit Elements or QUARLs further here—information on their application can be found in the Wave Digital Filter [5]

and microwave engineering literatures.

### 1.4.7 Gyrator

A gyrator is defined by its open-circuit impedance matrix [148, 145]

$$v_0 = -r i_1 \quad (1.151)$$

$$v_1 = r i_0 \quad (1.152)$$

which is parameterized by the “gyration resistance”  $r$ . Although  $r$  relates variables on different ports, it does indeed relate currents to voltages, so the “resistance” designation is appropriate. Gyrators are lossless but nonreciprocal. The gyrator is sometimes defined equivalently by its chain matrix [5]

$$\begin{aligned} v_0 &= -r i_1 \\ i_0 &= 1/r v_1 \end{aligned} \longleftrightarrow \begin{bmatrix} v_0 \\ i_0 \end{bmatrix} = \begin{bmatrix} 0 & -r \\ 1/r & 0 \end{bmatrix} \begin{bmatrix} v_1 \\ -i_1 \end{bmatrix}. \quad (1.153)$$

The symbol and port definition for a two-port gyrator, adapted and unadapted Wave Digital Filter symbols, and adapted and unadapted Wave Digital Filter signal-flow diagrams are shown in Figure 1.38.

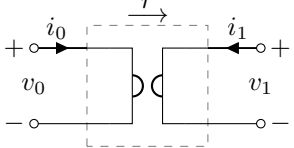
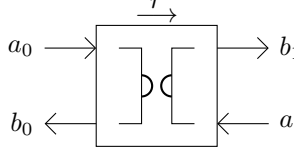
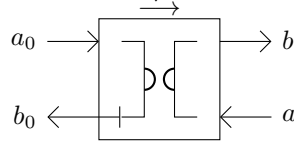
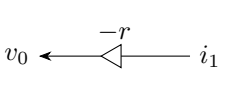
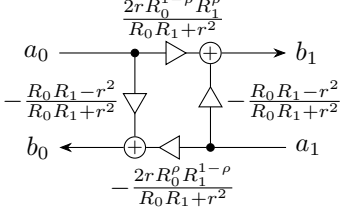
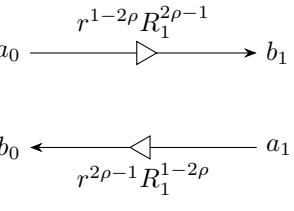
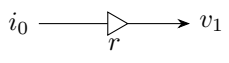
	Kirchhoff domain	Wave Domain	
symbol		unadapted	adapted ( $R_0 = r^2/R_1$ )
signal			
			
			

Figure 1.38: Kirchhoff- and Wave-Domain Representations of a Two-Port Gyrator.

Plugging the parametric wave definition (1.9) into the Kirchhoff-domain gyrator equations (1.151)–(1.152) and solving for the reflected waves  $\begin{bmatrix} b_0 & b_1 \end{bmatrix}^\top$  yields the unadapted wave-domain equation

$$\begin{bmatrix} b_0 \\ b_1 \end{bmatrix} = \begin{bmatrix} -\frac{R_0 R_1 - r^2}{R_0 R_1 + r^2} & -\frac{2r R_0^\rho R_1^{1-\rho}}{R_0 R_1 + r^2} \\ \frac{2r R_0^{1-\rho} R_1^\rho}{R_0 R_1 + r^2} & -\frac{R_0 R_1 - r^2}{R_0 R_1 + r^2} \end{bmatrix} \begin{bmatrix} a_0 \\ a_1 \end{bmatrix}. \quad (1.154)$$

Port 0 is adapted by  $R_0 = r^2/R_1$ , yielding the adapted wave-domain equation

$$\begin{bmatrix} b_0 \\ b_1 \end{bmatrix} = \begin{bmatrix} 0 & r^{2\rho-1} R_1^{1-2\rho} \\ r^{1-2\rho} R_1^{2\rho-1} & 0 \end{bmatrix} \begin{bmatrix} a_0 \\ a_1 \end{bmatrix}. \quad (1.155)$$

Port 1 is adapted in the same way, although the criteria would rather be written  $R_1 = r^2/R_0$ .

### Active Gyrator

Gyrators are sometimes known as “ideal gyrators” [148, p. 47] to distinguish them from the distinct so-called “active gyrator” [183]. A generalization of the gyrator concept, active gyrators are defined by open-circuit impedance matrix

$$v_0 = -r_0 i_1 \quad (1.156)$$

$$v_1 = r_1 i_0, \quad (1.157)$$

where  $r_0$  and  $r_1$  are two different real positive gyration constants. Unlike the ideal gyrator, active gyrators are not passive. The symbol and port definition for a two-port active gyrator, adapted and unadapted Wave Digital Filter symbols, and adapted and unadapted Wave Digital Filter signal-flow diagrams are shown in Figure 1.39.

Plugging the parametric wave definition (1.9) into the Kirchhoff-domain active gyrator equations (1.156)–(1.157) and solving for the reflected waves  $\begin{bmatrix} b_0 & b_1 \end{bmatrix}^\top$  yields the unadapted wave-domain equation

$$\begin{bmatrix} b_0 \\ b_1 \end{bmatrix} = \begin{bmatrix} -\frac{R_0 R_1 - r_0 r_1}{R_0 R_1 + r_0 r_1} & -\frac{2r_0 R_0^\rho R_1^{1-\rho}}{R_0 R_1 + r_0 r_1} \\ \frac{2r_1 R_0^{1-\rho} R_1^\rho}{R_0 R_1 + r_0 r_1} & -\frac{R_0 R_1 - r_0 r_1}{R_0 R_1 + r_0 r_1} \end{bmatrix} \begin{bmatrix} a_0 \\ a_1 \end{bmatrix}. \quad (1.158)$$

Port 0 is adapted by  $R_0 = r_0 r_1 / R_1$ , yielding the adapted wave-domain equation

$$\begin{bmatrix} b_0 \\ b_1 \end{bmatrix} = \begin{bmatrix} 0 & -r_0^\rho r_1^{\rho-1} R_1^{1-2\rho} \\ r_0^{-\rho} r_1^{1-\rho} R_1^{2\rho-1} & 0 \end{bmatrix} \begin{bmatrix} a_0 \\ a_1 \end{bmatrix}. \quad (1.159)$$

Port 1 is adapted in the same way, although the criteria would rather be written  $R_1 = r_0 r_1 / R_0$ .

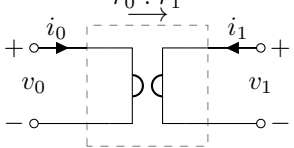
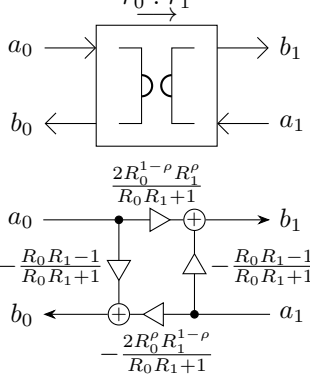
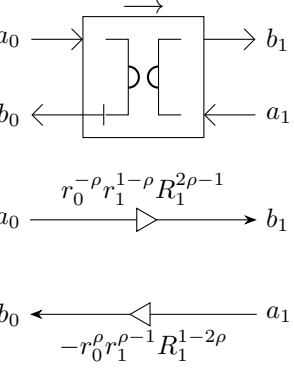
symbol	Kirchhoff domain	Wave Domain	
		unadapted	adapted ( $R_0 = r_0 r_1 / R_1$ )
signal	 $v_0 \leftarrow -r_0 i_1$ $i_0 \rightarrow r_1 v_1$		

Figure 1.39: Kirchhoff- and Wave-Domain Representations of a Two-Port Active Gyrator.

#### 1.4.8 Changes of Variables

Some circuit elements deal explicitly with changes of physical variables. These include the “Dualizer,” which exchanges the role of voltage and current between its two ports, and the “Mutator,” which is used to change from standard Kirchhoff variables onto other variable planes related by differentiation or integration of voltage or current, such as the voltage–charge plane (useful for nonlinear capacitor modeling) or the flux–current plane (useful for nonlinear inductor modeling)..

##### Dualizer

The two-port known as the “dualizer” exchanges the role of voltage and current between its two ports [143], i.e.,

$$v_0 = -i_1 \quad (1.160)$$

$$v_1 = i_0. \quad (1.161)$$

It is equivalent to a gyrator with  $r = 1$ . Exchanging the role of voltage and current is the same as saying it changes whatever it is connected to into its dual [6]. Gyrators are equivalent to the cascade of a dualizer and a transformer with turns ratio  $r$  (the gyration resistance) [97]<sup>6</sup>. The symbol and port definition for a dualizer, adapted and unadapted Wave Digital Filter symbols, and adapted and unadapted Wave Digital Filter signal-flow diagrams are shown in Figure 1.40.

Plugging the parametric wave definition (1.9) into the dualizer equations (1.160)–(1.161) and

<sup>6</sup><https://ccrma.stanford.edu/~jos/pasp/Gyrators.html>

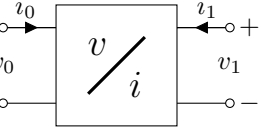
	Kirchhoff domain	Wave Domain
symbol		unadapted      adapted ( $R_0 = 1/R_1$ )
		
$v_0$	$i_0$	$a_0$
$v_1$	$i_1$	$b_1$
		$b_0$
	$v_0 \leftarrow -1 \cdot i_1$	$a_1 \leftarrow -\frac{R_0 R_1 - r^2}{R_0 R_1 + r^2} b_1$
	$i_0 \rightarrow v_1$	$b_0 \leftarrow \frac{2r R_0^{1-\rho} R_1^\rho}{R_0 R_1 + r^2} a_0 + \frac{2r R_0^\rho R_1^{1-\rho}}{R_0 R_1 + r^2} b_1$
		$a_1 \leftarrow -\frac{R_0 R_1 - r^2}{R_0 R_1 + r^2} b_0$
		$b_0 \leftarrow -\frac{2r R_0^\rho R_1^{1-\rho}}{R_0 R_1 + r^2} a_1$

Figure 1.40: Kirchhoff- and Wave-Domain Representations of a Two-Port Dualizer.

solving for the reflected waves  $\begin{bmatrix} b_0 & b_1 \end{bmatrix}^\top$  yields the unadapted wave-domain equation

$$\begin{bmatrix} b_0 \\ b_1 \end{bmatrix} = \begin{bmatrix} -\frac{R_0 R_1 - 1}{R_0 R_1 + 1} & -\frac{2R_0^\rho R_1^{1-\rho}}{R_0 R_1 + 1} \\ \frac{2R_0^{1-\rho} R_1^\rho}{R_0 R_1 + 1} & -\frac{R_0 R_1 - 1}{R_0 R_1 + 1} \end{bmatrix} \begin{bmatrix} a_0 \\ a_1 \end{bmatrix}. \quad (1.162)$$

Port 0 is adapted by  $R_0 = 1/R_1$ , yielding the adapted wave-domain equation

$$\begin{bmatrix} b_0 \\ b_1 \end{bmatrix} = \begin{bmatrix} 0 & 1 \\ 1 & 0 \end{bmatrix} \begin{bmatrix} a_0 \\ a_1 \end{bmatrix}. \quad (1.163)$$

Port 1 is adapted in the same way, although the criteria would rather be written  $R_1 = 1/R_0$ .

### Mutator

Another two-port that deals with changes of variables is the “mutator.” Mutators change the port variables from standard Kirchhoff variables at one port to other variable planes related by differentiation or integration of voltage or current, such as the voltage–charge ( $v$ – $q$ ) plane (useful for nonlinear capacitor modeling) or the flux–current ( $\phi$ – $i$ ) plane (useful for nonlinear inductor modeling). From the impedance transformation standpoint, these can be seen as transforming capacitors (“ $R$ – $C$  mutator”) or inductors (“ $R$ – $L$  mutator”) effectively into resistors. This is useful for making Wave Digital Filters of nonlinear capacitors modeled as algebraic nonlinearities on the  $v$ – $q$  plane and nonlinear inductors modeled as algebraic nonlinearities on the  $\phi$ – $i$  plane [167, 184]. Even “ $R$ – $M$  mutators” for accommodating memristors or frequency-dependent negative resistors (FDNRs) have been considered [185]. Mutators are a special case of a more broad class of adaptors

called “dynamic scattering junctions” (DSJs), adaptors which involve memory [186, 185, 98, 187, 6].

### 1.4.9 Nullor

Nullors were introduced by Tellegen (who called them “universal amplifiers”) in 1954 [188]. The name “nullor” is due to a 1964 paper of Carlin’s [147]. Nullors are two-port devices that combine a nullator at one port and a norator at a second port. The symbol and port definition for a nullor is shown in Figure 1.41.<sup>7</sup>

	Kirchhoff domain	Wave Domain	
		unadapted	adapted
symbol		N/A	N/A
signal	$0 \longrightarrow v_0(t)$ $0 \longrightarrow i_0(t)$	N/A	N/A

Figure 1.41: Kirchhoff- and Wave-Domain Representations of a Two-Port Nullor.

Nullors are useful in ideal modeling of operational amplifiers and other amplifiers. Examples of how to model ideal Operational Inverting Amplifiers, Operational Voltage Amplifiers (standard op-amp), Operational Current Amplifiers, and Operational Floating Amplifiers [189] are shown in Figure 1.42.

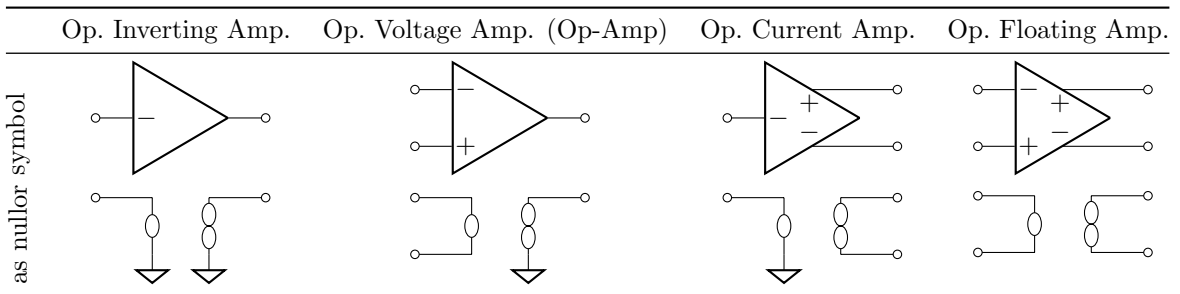


Figure 1.42: Four Types of Operational Amplifiers and Their Ideal Equivalents Using a Nullor.

Nullors can also be used to model ideal transistors [190, 191]. An ideal transistor realized as a nullor shown in Figure 1.43 [145, pp. 102–103].

Nullors are also used in theorems on equivalences between other ideal two-ports [145]. An extensive bibliography on nullors is given in [192].

<sup>7</sup>Thanks to Michael Olsen for providing the code to draw nullators and norators.

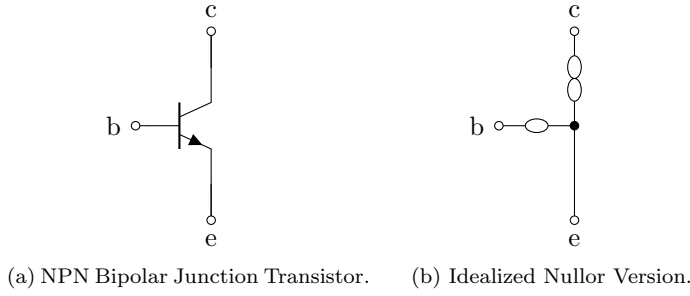


Figure 1.43: NPN Bipolar Junction Transistor and its Idealized Nullor Equivalent.

Nullors have an all-zero chain matrix description

$$\begin{bmatrix} v_0 \\ i_0 \end{bmatrix} = \begin{bmatrix} 0 & 0 \\ 0 & 0 \end{bmatrix} \begin{bmatrix} v_1 \\ -i_1 \end{bmatrix}. \quad (1.164)$$

Attempting to find a scattering matrix from this by plugging the parametric wave definition (1.9) and solving for the vector of reflected waves  $\begin{bmatrix} b_0 & b_1 \end{bmatrix}^\top$  will fail since the derivation would involve inverting a singular (all-zero) matrix. Therefore, the nullor cannot be represented directly as a two-port Wave Digital Filter building block. For a vector-space-based proof of this see [147].

These means that a nullor two-port, even an unadapted one, cannot be used in Wave Digital Filter modeling. Luckily, nullors should never really be seen in feedforward arrangements due to their status as models of ideal amplification. In Chapter 2 we will introduce techniques for accommodating any number of nullors in feedback arrangements.

#### 1.4.10 Two-Ports Based on $y$ , $z$ , $h$ , and $g$ Parameters

Sometimes two-ports are characterized based on their admittance ( $y$ ), impedance ( $z$ ), hybrid ( $h$ ), or inverse hybrid ( $g$ ) parameters. Each of these characterizations can also be represented by an equivalent circuit [193]. These are related to the “two-port” method of Wave Digital Filter synthesis [124, 116]. In this section we’ll derive the scattering matrix for the equivalent circuit of each amplifier parameterization, yielding four different special Wave Digital Filter adaptors.

##### $y$ Parameters

The  $y$ -parameter (i.e., short circuit admittance) characterization of a two-port is given by

$$\begin{bmatrix} i_1 \\ i_2 \end{bmatrix} = \begin{bmatrix} y_{11} & y_{12} \\ y_{21} & y_{22} \end{bmatrix} \begin{bmatrix} v_1 \\ v_2 \end{bmatrix}. \quad (1.165)$$

The symbol and port definition for a  $y$ -parameter two-port, adapted and unadapted Wave Digital Filter symbols, and adapted and unadapted Wave Digital Filter signal-flow diagrams are shown in Figure 1.44.

Matrix Description	Equivalent Circuit
$\begin{bmatrix} i_1 \\ i_2 \end{bmatrix} = \begin{bmatrix} y_{11} & y_{12} \\ y_{21} & y_{22} \end{bmatrix} \begin{bmatrix} v_1 \\ v_2 \end{bmatrix}$	

Figure 1.44:  $y$ -Parameter Amplifier.

Plugging the parametric wave definition (1.9) yields an unadapted wave-domain equation

$$\begin{bmatrix} b_1 \\ b_2 \end{bmatrix} = \begin{bmatrix} -\frac{y_{11}R_1 + (y_{11}y_{22} - y_{12}y_{21})R_1R_2 - y_{22}R_2 - 1}{y_{11}R_1 + (y_{11}y_{22} - y_{12}y_{21})R_1R_2 + y_{22}R_2 + 1} & -\frac{2y_{12}R_1^\rho R_2^{1-\rho}}{y_{11}R_1 + (y_{11}y_{22} - y_{12}y_{21})R_1R_2 + y_{22}R_2 + 1} \\ -\frac{2y_{21}R_1^{1-\rho}R_2^\rho}{y_{11}R_1 + (y_{11}y_{22} - y_{12}y_{21})R_1R_2 + y_{22}R_2 + 1} & -\frac{-y_{11}R_1 + (y_{11}y_{22} - y_{12}y_{21})R_1R_2 + y_{22}R_2 - 1}{y_{11}R_1 + (y_{11}y_{22} - y_{12}y_{21})R_1R_2 + y_{22}R_2 + 1} \end{bmatrix} \begin{bmatrix} a_1 \\ a_2 \end{bmatrix}. \quad (1.166)$$

Port 1 can be adapted by setting  $R_1 = \frac{R_2y_{22}+1}{y_{11}+R_2y_{11}y_{22}-R_2y_{12}y_{21}}$ , yielding the adapted wave-domain equation

$$\begin{bmatrix} b_1 \\ b_2 \end{bmatrix} = \begin{bmatrix} 0 & -\frac{R_2^{1-\rho}y_{12}}{(y_{11}+R_2y_{11}y_{22}-R_2y_{12}y_{21})^\rho(R_2y_{22}+1)^{1-\rho}} \\ -\frac{R_2^\rho y_{21}}{(y_{11}+R_2y_{11}y_{22}-R_2y_{12}y_{21})^{1-\rho}(R_2y_{22}+1)^\rho} & \frac{-y_{11}R_2^{1-\rho}y_{22}+y_{12}y_{21}R_2^2y_{22}+y_{11}}{(y_{11}+R_2y_{11}y_{22}-R_2y_{12}y_{21})(R_2y_{22}+1)} \end{bmatrix} \begin{bmatrix} a_1 \\ a_2 \end{bmatrix}. \quad (1.167)$$

Port 2 can be adapted by setting  $R_2 = \frac{R_1y_{11}+1}{y_{22}+R_1y_{11}y_{22}-R_1y_{12}y_{21}}$ , yielding the adapted wave domain equation

$$\begin{bmatrix} b_1 \\ b_2 \end{bmatrix} = \begin{bmatrix} -\frac{y_{22}R_1^2y_{11}^2+y_{12}y_{21}R_1^2y_{11}+y_{22}}{(y_{22}+R_1y_{11}y_{22}-R_1y_{12}y_{21})(R_1y_{11}+1)} & -\frac{R_1^\rho y_{12}}{(y_{22}+R_1y_{11}y_{22}-R_1y_{12}y_{21})^{1-\rho}(R_1y_{11}+1)^\rho} \\ -\frac{R_1^{1-\rho}y_{21}}{(y_{22}+R_1y_{11}y_{22}-R_1y_{12}y_{21})^\rho(R_1y_{11}+1)^{1-\rho}} & 0 \end{bmatrix} \begin{bmatrix} a_1 \\ a_2 \end{bmatrix}. \quad (1.168)$$

### $z$ Parameters

The  $z$ -parameter (i.e., open circuit impedance) characterization of a two-port is given by

$$\begin{bmatrix} v_1 \\ v_2 \end{bmatrix} = \begin{bmatrix} z_{11} & z_{12} \\ z_{21} & z_{22} \end{bmatrix} \begin{bmatrix} i_1 \\ i_2 \end{bmatrix}. \quad (1.169)$$

The symbol and port definition for a  $z$ -parameter two-port, adapted and unadapted Wave Digital Filter symbols, and adapted and unadapted Wave Digital Filter signal-flow diagrams are shown in Figure 1.45.

Matrix Description	Equivalent Circuit
$\begin{bmatrix} v_1 \\ v_2 \end{bmatrix} = \begin{bmatrix} z_{11} & z_{12} \\ z_{21} & z_{22} \end{bmatrix} \begin{bmatrix} i_1 \\ i_2 \end{bmatrix}$	

Figure 1.45:  $z$ -Parameter Amplifier.

Plugging the parametric wave definition (1.9) yields an unadapted wave-domain equation

$$\begin{bmatrix} b_1 \\ b_2 \end{bmatrix} = \begin{bmatrix} \frac{-R_1 R_2 + R_2 z_{11} - R_1 z_{22} + z_{11} z_{22} - z_{12} z_{21}}{R_1 R_2 + R_2 z_{11} + R_1 z_{22} + z_{11} z_{22} - z_{12} z_{21}} & \frac{2R_1^\rho R_2^{1-\rho} z_{12}}{R_1 R_2 + R_2 z_{11} + R_1 z_{22} + z_{11} z_{22} - z_{12} z_{21}} \\ \frac{2R_1^{1-\rho} R_2^\rho z_{21}}{R_1 R_2 + R_2 z_{11} + R_1 z_{22} + z_{11} z_{22} - z_{12} z_{21}} & \frac{-R_1 R_2 - R_2 z_{11} + R_1 z_{22} + z_{11} z_{22} - z_{12} z_{21}}{R_1 R_2 + R_2 z_{11} + R_1 z_{22} + z_{11} z_{22} - z_{12} z_{21}} \end{bmatrix} \begin{bmatrix} a_1 \\ a_2 \end{bmatrix}. \quad (1.170)$$

Port 1 can be adapted by setting  $R_1 = \frac{R_2 z_{11} + z_{11} z_{22} - z_{12} z_{21}}{R_2 + z_{22}}$ , yielding the adapted wave domain equation

$$\begin{bmatrix} b_1 \\ b_2 \end{bmatrix} = \begin{bmatrix} 0 & \frac{R_2^{1-\rho} z_{12}}{(R_2 z_{11} + z_{11} z_{22} - z_{12} z_{21})^{1-\rho} (R_2 + z_{22})^\rho} \\ \frac{R_2^\rho z_{21}}{(R_2 z_{11} + z_{11} z_{22} - z_{12} z_{21})^\rho (R_2 + z_{22})^{1-\rho}} & \frac{z_{11} R_2^2 - z_{11} z_{22}^2 + z_{12} z_{21} z_{22}}{(R_2 z_{11} + z_{11} z_{22} - z_{12} z_{21})(R_2 + z_{22})} \end{bmatrix} \begin{bmatrix} a_1 \\ a_2 \end{bmatrix}. \quad (1.171)$$

Port 2 can be adapted by setting  $R_2 = \frac{R_1 z_{22} + z_{11} z_{22} - z_{12} z_{21}}{R_1 + z_{11}}$ , yielding the adapted wave domain equation

$$\begin{bmatrix} b_1 \\ b_2 \end{bmatrix} = \begin{bmatrix} -\frac{z_{22} R_1^2 - z_{22} z_{11}^2 + z_{12} z_{21} z_{11}}{(R_1 z_{22} + z_{11} z_{22} - z_{12} z_{21})(R_1 + z_{11})} & \frac{R_1^\rho z_{12}}{(R_1 z_{22} + z_{11} z_{22} - z_{12} z_{21})^\rho (R_1 + z_{11})^{1-\rho}} \\ \frac{R_1^{1-\rho} z_{21}}{(R_1 z_{22} + z_{11} z_{22} - z_{12} z_{21})^{1-\rho} (R_1 + z_{11})^\rho} & 0 \end{bmatrix} \begin{bmatrix} a_1 \\ a_2 \end{bmatrix}. \quad (1.172)$$

## $h$ Parameters

The  $h$ -parameter (i.e., hybrid) characterization of a two-port is given by

$$\begin{bmatrix} v_1 \\ i_2 \end{bmatrix} = \begin{bmatrix} h_{11} & h_{12} \\ h_{21} & h_{22} \end{bmatrix} \begin{bmatrix} i_1 \\ v_2 \end{bmatrix}. \quad (1.173)$$

The symbol and port definition for a  $h$ -parameter two-port, adapted and unadapted Wave Digital Filter symbols, and adapted and unadapted Wave Digital Filter signal-flow diagrams are shown in Figure 1.46.

Matrix Description	Equivalent Circuit
$\begin{bmatrix} v_1 \\ i_2 \end{bmatrix} = \begin{bmatrix} h_{11} & h_{12} \\ h_{21} & h_{22} \end{bmatrix} \begin{bmatrix} i_1 \\ v_2 \end{bmatrix}$	

Figure 1.46:  $h$ -Parameter Amplifier.

Plugging the parametric wave definition (1.9) yields an unadapted wave-domain equation

$$\begin{bmatrix} b_1 \\ b_2 \end{bmatrix} = \begin{bmatrix} \frac{-R_1+h_{11}-R_1R_2h_{22}+R_2h_{11}h_{22}-R_2h_{12}h_{21}}{R_1+h_{11}+R_1R_2h_{22}+R_2h_{11}h_{22}-R_2h_{12}h_{21}} & \frac{2R_1^\rho R_2^{1-\rho}h_{12}}{R_1+h_{11}+R_1R_2h_{22}+R_2h_{11}h_{22}-R_2h_{12}h_{21}} \\ \frac{2R_1^{1-\rho}R_2^\rho h_{21}}{R_1+h_{11}+R_1R_2h_{22}+R_2h_{11}h_{22}-R_2h_{12}h_{21}} & \frac{R_1+h_{11}-R_1R_2h_{22}-R_2h_{11}h_{22}+R_2h_{12}h_{21}}{R_1+h_{11}+R_1R_2h_{22}+R_2h_{11}h_{22}-R_2h_{12}h_{21}} \end{bmatrix} \begin{bmatrix} a_1 \\ a_2 \end{bmatrix}. \quad (1.174)$$

Port 1 can be adapted by setting  $R_1 = \frac{h_{11}+R_2(h_{11}h_{22}-h_{12}h_{21})}{R_2h_{22}+1}$ , yielding the adapted wave domain equation

$$\begin{bmatrix} b_1 \\ b_2 \end{bmatrix} = \begin{bmatrix} 0 & \frac{R_2^{1-\rho}h_{12}}{(h_{11}+R_2h_{11}h_{22}-R_2h_{12}h_{21})^{1-\rho}(R_2h_{22}+1)^\rho} \\ -\frac{R_2^\rho h_{21}}{(h_{11}+R_2h_{11}h_{22}-R_2h_{12}h_{21})^\rho(R_2h_{22}+1)^{1-\rho}} & \frac{-h_{11}R_2^2h_{22}^2+h_{12}h_{21}R_2^2h_{22}+h_{11}}{(h_{11}+R_2h_{11}h_{22}-R_2h_{12}h_{21})(R_2h_{22}+1)} \end{bmatrix} \begin{bmatrix} a_1 \\ a_2 \end{bmatrix}. \quad (1.175)$$

Port 2 can be adapted by setting  $R_2 = \frac{R_1+h_{11}}{R_1h_{22}+h_{11}h_{22}-h_{12}h_{21}}$ , yielding the adapted wave domain equation

$$\begin{bmatrix} b_1 \\ b_2 \end{bmatrix} = \begin{bmatrix} -\frac{h_{22}R_1^2-h_{22}h_{11}^2+h_{12}h_{21}h_{11}}{(R_1h_{22}+h_{11}h_{22}-h_{12}h_{21})(R_1+h_{11})} & \frac{R_1^\rho h_{12}}{(R_1h_{22}+h_{11}h_{22}-h_{12}h_{21})^{1-\rho}(R_1+h_{11})^\rho} \\ -\frac{R_1^{1-\rho}h_{21}}{(R_1h_{22}+h_{11}h_{22}-h_{12}h_{21})^\rho(R_1+h_{11})^{1-\rho}} & 0 \end{bmatrix} \begin{bmatrix} a_1 \\ a_2 \end{bmatrix}. \quad (1.176)$$

### $g$ Parameters

The  $g$ -parameter (i.e., inverse hybrid) characterization of a two-port is given by

$$\begin{bmatrix} i_1 \\ v_2 \end{bmatrix} = \begin{bmatrix} g_{11} & g_{12} \\ g_{21} & g_{22} \end{bmatrix} \begin{bmatrix} v_1 \\ i_2 \end{bmatrix}. \quad (1.177)$$

The symbol and port definition for a  $g$ -parameter two-port, adapted and unadapted Wave Digital Filter symbols, and adapted and unadapted Wave Digital Filter signal-flow diagrams are shown in Figure 1.47.

Plugging the parametric wave definition (1.9) yields an unadapted wave-domain equation

$$\begin{bmatrix} b_1 \\ b_2 \end{bmatrix} = \begin{bmatrix} \frac{R_2-g_{22}+R_1R_2g_{11}-R_1g_{11}g_{22}+R_1g_{12}g_{21}}{R_2+g_{22}+R_1R_2g_{11}+R_1g_{11}g_{22}-R_1g_{12}g_{21}} & \frac{2R_1^\rho R_2^{1-\rho}g_{12}}{R_2+g_{22}+R_1R_2g_{11}+R_1g_{11}g_{22}-R_1g_{12}g_{21}} \\ \frac{2R_1^{1-\rho}R_2^\rho g_{21}}{R_2+g_{22}+R_1R_2g_{11}+R_1g_{11}g_{22}-R_1g_{12}g_{21}} & \frac{-R_2+g_{22}-R_1R_2g_{11}+R_1g_{11}g_{22}-R_1g_{12}g_{21}}{R_2+g_{22}+R_1R_2g_{11}+R_1g_{11}g_{22}-R_1g_{12}g_{21}} \end{bmatrix} \begin{bmatrix} a_1 \\ a_2 \end{bmatrix}. \quad (1.178)$$

Matrix Description	Equivalent Circuit
$\begin{bmatrix} i_1 \\ v_2 \end{bmatrix} = \begin{bmatrix} g_{11} & g_{12} \\ g_{21} & g_{22} \end{bmatrix} \begin{bmatrix} v_1 \\ i_2 \end{bmatrix}$	

Figure 1.47:  $g$ -Parameter Amplifier.

Port 1 can be adapted by setting  $R_1 = \frac{R_2 + g_{22}}{R_2 g_{11} + g_{11} g_{22} - g_{12} g_{21}}$ , yielding the adapted wave domain equation

$$\begin{bmatrix} b_1 \\ b_2 \end{bmatrix} = \begin{bmatrix} 0 & -\frac{R_2^{1-\rho} g_{12}}{(R_2 g_{11} + g_{11} g_{22} - g_{12} g_{21})^\rho (R_2 + g_{22})^{1-\rho}} \\ \frac{R_2^\rho g_{21}}{(R_2 g_{11} + g_{11} g_{22} - g_{12} g_{21})^{1-\rho} (R_2 + g_{22})^\rho} & -\frac{g_{11} R_2^2 - g_{11} g_{22}^2 + g_{12} g_{21} g_{22}}{(R_2 g_{11} + g_{11} g_{22} - g_{12} g_{21})(R_2 + g_{22})} \end{bmatrix} \begin{bmatrix} a_1 \\ a_2 \end{bmatrix}. \quad (1.179)$$

Port 2 can be adapted by setting  $R_2 = \frac{R_1(g_{11}g_{22}-g_{12}g_{21})+g_{22}}{R_1g_{11}+1}$ , yielding the adapted wave domain equation

$$\begin{bmatrix} b_1 \\ b_2 \end{bmatrix} = \begin{bmatrix} \frac{-g_{22} R_1^2 g_{11}^2 + g_{12} g_{21} R_1^2 g_{11} + g_{22}}{(g_{22} + R_1 g_{11} g_{22} - R_1 g_{12} g_{21})(R_1 g_{11} + 1)} & -\frac{R_1^\rho g_{12}}{(g_{22} + R_1 g_{11} g_{22} - R_1 g_{12} g_{21})^\rho (R_1 g_{11} + 1)^{1-\rho}} \\ \frac{R_1^{1-\rho} g_{21}}{(g_{22} + R_1 g_{11} g_{22} - R_1 g_{12} g_{21})^{1-\rho} (R_1 g_{11} + 1)^\rho} & 0 \end{bmatrix} \begin{bmatrix} a_1 \\ a_2 \end{bmatrix}. \quad (1.180)$$

## 1.5 Three-Ports

The most common and important types of connections in Wave Digital Filters are three-port series and parallel connections. The topology of ladder circuits and other simple circuits are composed entirely of three-port series and parallel connections. Another type of three-port connection is a circulator, a special device defined directly in the wave domain.

### 1.5.1 Three-Port Parallel Adaptor

Considering three ports 0, 1, and 2 in parallel, the following Kirchhoff domain constraints apply by definition

$$\begin{aligned} v_0 &= v_1 = v_2 \\ i_0 + i_1 + i_2 &= 0 \end{aligned} \quad . \quad (1.181)$$

Rewriting this in matrix form

$$\begin{bmatrix} 1 & -1 & 0 \\ 0 & 1 & -1 \\ 0 & 0 & 0 \end{bmatrix} \begin{bmatrix} v_0 \\ v_1 \\ v_2 \end{bmatrix} + \begin{bmatrix} 0 & 0 & 0 \\ 0 & 0 & 0 \\ 1 & 1 & 1 \end{bmatrix} \begin{bmatrix} i_0 \\ i_1 \\ i_2 \end{bmatrix} = \begin{bmatrix} 0 \\ 0 \\ 0 \end{bmatrix}, \quad (1.182)$$

symbol	Kirchhoff domain	Wave Domain	
		unadapted	adapted ( $R_0 = \frac{1}{1/R_1+1/R_2}$ )

Figure 1.48: Kirchhoff- and Wave-Domain Representations of Three-Port Parallel Connection.

Plugging the parametric wave definition (1.9), and solving for the vector of reflected waves  $\begin{bmatrix} b_0 & b_1 & b_2 \end{bmatrix}^\top$  yields

$$\begin{bmatrix} b_0 \\ b_1 \\ b_2 \end{bmatrix} = \begin{bmatrix} -\frac{R_0 R_1 + R_0 R_2 - R_1 R_2}{R_0 R_1 + R_0 R_2 + R_1 R_2} & \frac{2 R_0^\rho R_1^{1-\rho} R_2}{R_0 R_1 + R_0 R_2 + R_1 R_2} & \frac{2 R_0^\rho R_1 R_2^{1-\rho}}{R_0 R_1 + R_0 R_2 + R_1 R_2} \\ \frac{2 R_0^{1-\rho} R_1^\rho R_2}{R_0 R_1 + R_0 R_2 + R_1 R_2} & -\frac{R_0 R_1 - R_0 R_2 + R_1 R_2}{R_0 R_1 + R_0 R_2 + R_1 R_2} & \frac{2 R_0 R_1^\rho R_2^{1-\rho}}{R_0 R_1 + R_0 R_2 + R_1 R_2} \\ \frac{2 R_0^{1-\rho} R_1 R_2^\rho}{R_0 R_1 + R_0 R_2 + R_1 R_2} & \frac{2 R_0 R_1^{1-\rho} R_2^\rho}{R_0 R_1 + R_0 R_2 + R_1 R_2} & -\frac{R_0 R_1 + R_0 R_2 + R_1 R_2}{R_0 R_1 + R_0 R_2 + R_1 R_2} \end{bmatrix} \begin{bmatrix} a_0 \\ a_1 \\ a_2 \end{bmatrix}. \quad (1.183)$$

Port 0 can be adapted by setting  $R_0 = \frac{1}{1/R_1+1/R_2}$ , yielding the adapted scattering matrix

$$\begin{bmatrix} b_0 \\ b_1 \\ b_2 \end{bmatrix} = \begin{bmatrix} 0 & \frac{R_2^\rho}{(R_1+R_2)^\rho} & \frac{R_1^\rho}{(R_1+R_2)^\rho} \\ \frac{R_2^{1-\rho}}{(R_1+R_2)^{1-\rho}} & -\frac{R_1}{R_1+R_2} & \frac{R_1^\rho R_2^{1-\rho}}{R_1+R_2} \\ \frac{R_1^{1-\rho}}{(R_1+R_2)^{1-\rho}} & \frac{R_1^{1-\rho} R_2^\rho}{R_1+R_2} & -\frac{R_2}{R_1+R_2} \end{bmatrix} \begin{bmatrix} a_0 \\ a_1 \\ a_2 \end{bmatrix}. \quad (1.184)$$

Notice that the adaptation criteria can be more elegantly written in terms of port conductances:  $G_0 = G_1 + G_2$ . Thinking from the perspective of impedance matching, this adaptation criteria means that port 0 “sees” the parallel combination of  $R_1$  and  $R_2$ . Alternatively, port 1 can be adapted by  $G_1 = G_0 + G_2$  or port 2 can be adapted by  $G_2 = G_0 + G_1$ .

The symbol and port definition for a three-port parallel adaptor, adapted and unadapted Wave Digital Filter symbols, and adapted and unadapted Wave Digital Filter signal-flow diagrams are shown in Figure 1.48.

### 1.5.2 Three-Port Series Adaptor

Considering three ports 0, 1, and 2 in series, the following Kirchhoff domain constraints apply by definition

$$\begin{aligned} i_0 &= i_1 = i_2 \\ v_0 + v_1 + v_2 &= 0 \end{aligned} \quad (1.185)$$

Rewriting this in matrix form

$$\begin{bmatrix} 1 & 1 & 1 \\ 0 & 0 & 0 \\ 0 & 0 & 0 \end{bmatrix} \begin{bmatrix} v_0 \\ v_1 \\ v_2 \end{bmatrix} + \begin{bmatrix} 0 & 0 & 0 \\ 1 & -1 & 0 \\ 0 & 1 & -1 \end{bmatrix} \begin{bmatrix} i_0 \\ i_1 \\ i_2 \end{bmatrix} = \begin{bmatrix} 0 \\ 0 \\ 0 \end{bmatrix}, \quad (1.186)$$

symbol	Kirchhoff domain	Wave Domain	
		unadapted	adapted ( $R_0 = R_1 + R_2$ )

Figure 1.49: Kirchhoff- and Wave-Domain Representations of Three-Port Series Connection.

Plugging the parametric wave definition (1.9), and solving for the vector of reflected waves  $\begin{bmatrix} b_0 & b_1 & b_2 \end{bmatrix}^\top$  yields

$$\begin{bmatrix} b_0 \\ b_1 \\ b_2 \end{bmatrix} = \begin{bmatrix} -R_0 + R_1 + R_2 & -\frac{2R_0^\rho R_1^{1-\rho}}{R_0 + R_1 + R_2} & -\frac{R_0^\rho R_2^{1-\rho}}{R_0 + R_1 + R_2} \\ \frac{-2R_0^{1-\rho} R_1^\rho}{R_0 + R_1 + R_2} & \frac{R_0 - R_1 + R_2}{R_0 + R_1 + R_2} & -\frac{2R_1^\rho R_2^{1-\rho}}{R_0 + R_1 + R_2} \\ -\frac{2R_0^\rho R_2^\rho}{R_0 + R_1 + R_2} & -\frac{2R_1^{1-\rho} R_2^\rho}{R_0 + R_1 + R_2} & \frac{R_0 + R_1 - R_2}{R_0 + R_1 + R_2} \end{bmatrix} \begin{bmatrix} a_0 \\ a_1 \\ a_2 \end{bmatrix}. \quad (1.187)$$

Port 0 can be adapted by setting  $R_0 = R_1 + R_2$ , yielding the adapted scattering matrix

$$\begin{bmatrix} b_0 \\ b_1 \\ b_2 \end{bmatrix} = \begin{bmatrix} 0 & -\frac{R_1^{1-\rho}}{(R_1+R_2)^{\rho-1}} & -\frac{R_2^{1-\rho}}{(R_1+R_2)^{\rho-1}} \\ -\frac{R_1^\rho}{(R_1+R_2)^{\rho-1}} & \frac{R_2}{R_1+R_2} & \frac{R_1^\rho R_2^{1-\rho}}{R_1+R_2} \\ -\frac{R_2^\rho}{(R_1+R_2)^{\rho-1}} & -\frac{R_1^{1-\rho} R_2^\rho}{R_1+R_2} & \frac{R_1}{R_1+R_2} \end{bmatrix} \begin{bmatrix} a_0 \\ a_1 \\ a_2 \end{bmatrix}. \quad (1.188)$$

Thinking from the perspective of impedance matching, this adaptation criteria means that port 0

“sees” the series combination of  $R_1$  and  $R_2$ . Alternatively, port 1 can be adapted by  $R_1 = R_0 + R_2$  or port 2 can be adapted by  $R_2 = R_0 + R_1$ .

The symbol and port definition for a three-port series adaptor, adapted and unadapted Wave Digital Filter symbols, and adapted and unadapted Wave Digital Filter signal-flow diagrams are shown in Figure 1.49.

The series adaptor is the dual of the parallel adaptor; they can also be realized using the other by leveraging certain transpositional identities [172].

### 1.5.3 Three-Port Circulator

Circulators are special three-port devices from microwave electronics that are defined in the wave domain by

$$\begin{bmatrix} b_0 \\ b_1 \\ b_2 \end{bmatrix} = \begin{bmatrix} 0 & 0 & 1 \\ 1 & 0 & 0 \\ 0 & 1 & 0 \end{bmatrix} \begin{bmatrix} a_0 \\ a_1 \\ a_2 \end{bmatrix}. \quad (1.189)$$

Uniquely, circulators are defined as having equal port resistances at all ports

$$R_0 = R_1 = R_2. \quad (1.190)$$

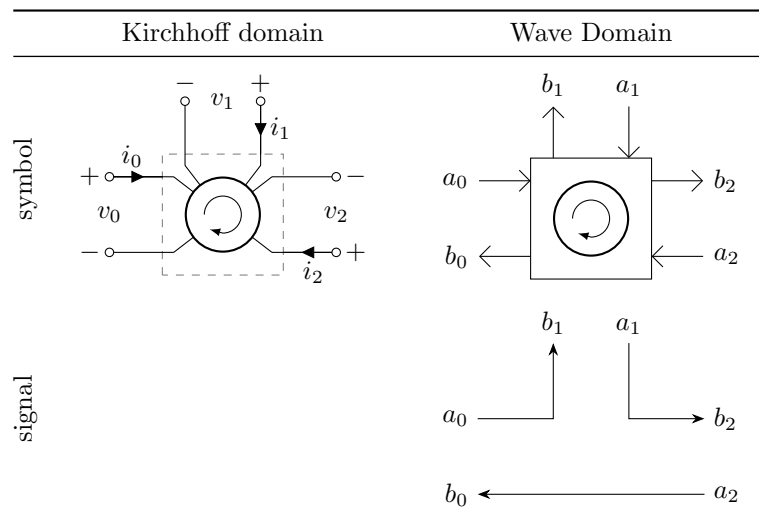


Figure 1.50: Kirchhoff- and Wave-Domain Representations of Three-Port Circulator.

Consider a three-port circulator’s role in a Wave Digital Filter tree. One port faces up the tree and two ports face down the tree. Typically, the upward-facing port resistance is chosen based on the two downward-facing ports to adapt the upwards-facing port. Because of the unique nature of the circulator’s scattering matrix, we can think about adaptation of the circulator’s upwards-facing port

in a different way. Recall that adaptation means that the reflected wave at the upwards-facing port does not depend instantaneously on the incident wave at the upwards-facing port. For a circulator this means that at least one of the delay-free paths at the downwards-facing ports must be broken. This can be accomplished by setting the circulator's port resistance equal to the port resistance of either of the elements below the circulator in the tree.

Circulators are occasionally used for the design of filters in the Wave Digital Filter domain, e.g., [5, 194, 195, 196, p. 287].

The symbol and port definition for a three-port circulator, Wave Digital Filter symbol, and Wave Digital Filter signal-flow diagrams are shown in Figure 1.50.

## 1.6 *N*-Ports

So far we have discussed three-port series adaptors, parallel adaptors, and circulators. In this section we will study Wave Digital Filter connections with *more* than three ports, and how they can be decomposed into three-port adaptors. Sometimes, a connection of many three-port adaptors is called a “macroadaptor” [6].

### 1.6.1 *N*-Port Parallel Adaptors

A very convenient property of Wave Digital Filter parallel adaptors is that *N*-port parallel adaptors can be realized with  $N - 2$  three-port parallel adaptors. This is always less expensive computationally than realizing the adaptor as an *N*-port scattering matrix [102], and leads to a certain elegance in implementation as well. This decomposition is illustrated for the four-port and *N*-port cases in Figure 1.51.

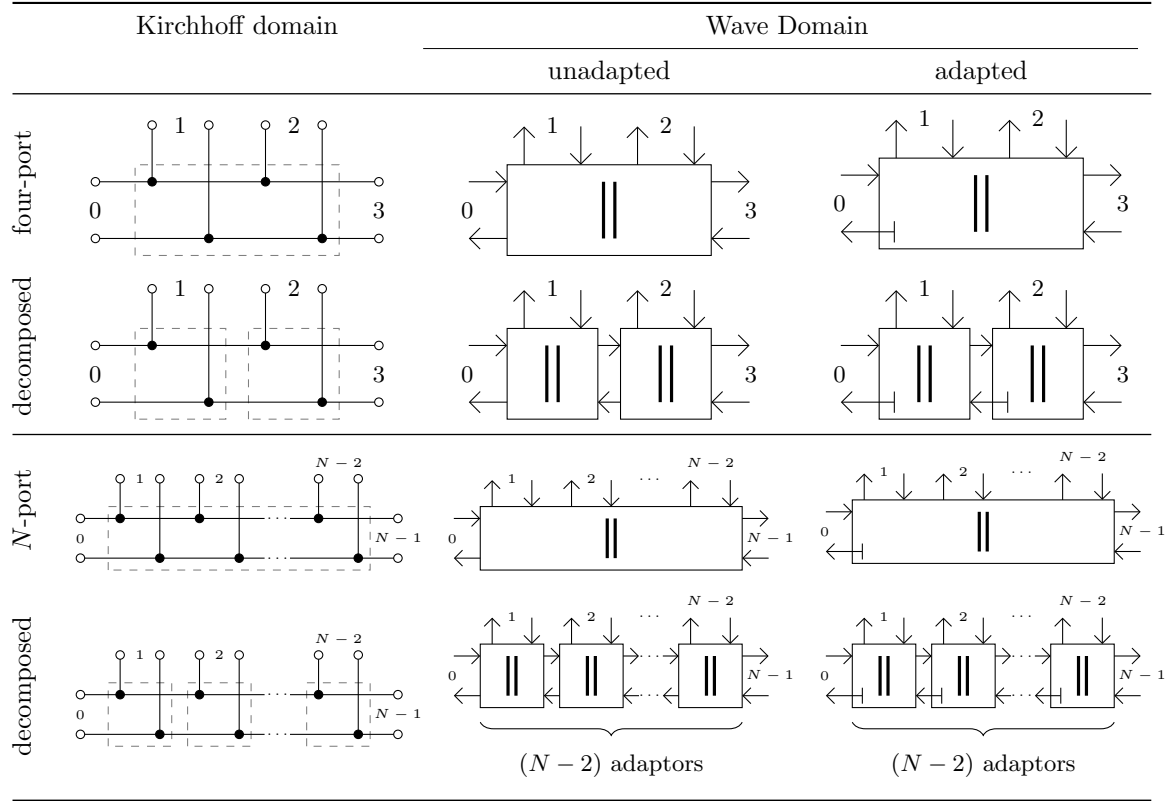


Figure 1.51: Decomposing Parallel Connections into Three-Port Parallel Connections, Including Four-Port (Top) and  $N$ -Port (Bottom) Cases.

### 1.6.2 $N$ -Port Series Adaptors

The dual of this property is that  $N$ -port series adaptors can be realized with  $N - 2$  three-port series adaptors. Again, this is less expensive computationally than realizing the  $N$ -port adaptor directly. This is illustrated for the four-port and  $N$ -port cases in Figure 1.52.

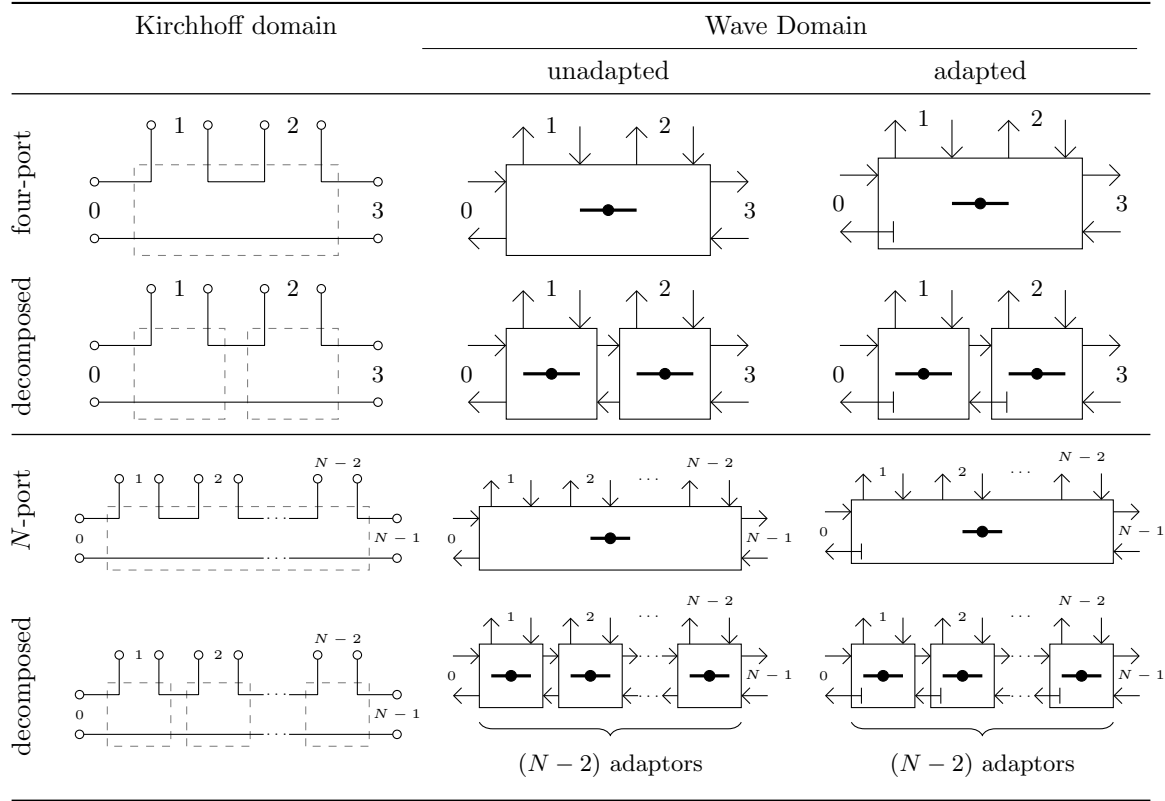


Figure 1.52: Decomposing Series Connections into Three-Port Series Connections. Including Four-port and  $N$ -Port Cases.

### 1.6.3 $N$ -Port Circulator

Just like series adaptors and parallel adaptors, an  $N$ -port circulator can be simply<sup>8</sup> be realized using  $N - 2$  three-port circulators. For circulators, computational complexity is not much of an issue. Circulators are essentially free to implement since their scattering matrices only take the values 0 and 1. For this reason, although it nicely continues the trend of series and parallel adaptors, the decomposition of  $N$ -port circulators into three-ports is largely a theoretical curiosity and has no real practical implications.

<sup>8</sup>even “trivial” [5]

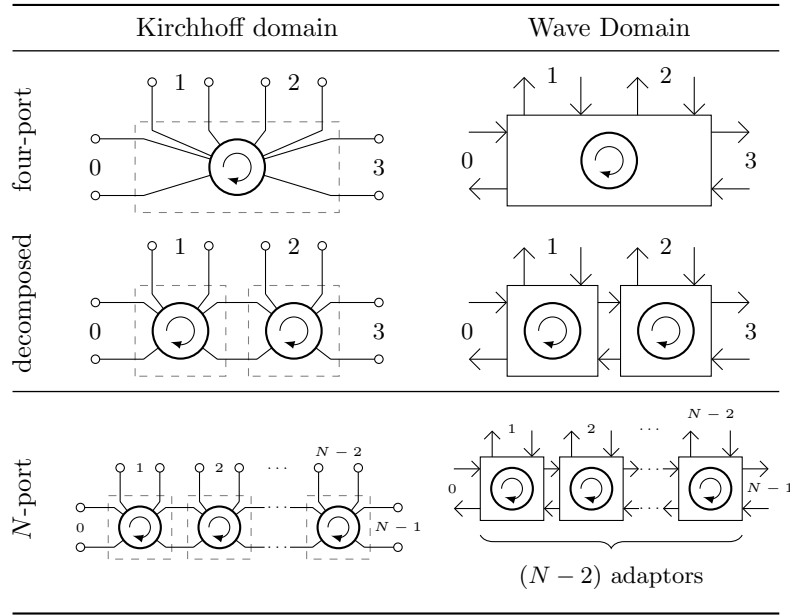


Figure 1.53: Decomposing Circulators into Three-Port Circulators. Including Four-port and  $N$ -Port Cases.

#### 1.6.4 $\mathcal{R}$ -Type

Not every  $N$ -port topological connection can be decomposed into series and parallel connections. Indeed, there exists an *infinitely large* class of  $N$ -port junctions called  $\mathcal{R}$ -type connections, which can be automatically detected in the context of Wave Digital Filter structures using a graph-theoretic technique based on SPQR trees [197, 198].  $\mathcal{R}$ -type adaptors include pure junctions as well as junctions that have absorbed multiport linear elements. To handle  $\mathcal{R}$ -type adaptors in general, we require a method for *deriving* their scattering matrices as well as *adapting* them. This will be the subject of the following chapter, Chapter 2. Their implications for accommodating multiple nonlinearities in Wave Digital Filter structures is the subject of Chapter 4.

## 1.7 Case Study: TR-808 Output Filter

To illustrate the principles and techniques of this first chapter, we'll conclude with a real-world case study. This study will show how to create a wave digital filter simulation of one part of the Roland TR-808 Bass Drum circuit: its tone stage. The schematic for the tone stage is shown in Figure 1.54a.

The tone stage is composed of numerous passive electrical elements: resistors  $R_{171}$ ,  $R_{172}$ ,  $R_{173}$ ,  $R_{174}$ ,  $R_{176}$ , and  $R_{177}$ ; potentiometers  $VR_4$  and  $VR_5$ ; capacitors  $C_{45}$ ,  $C_{47}$ ,  $C_{48}$ ,  $C_{49}$ ,  $C_{50}$ ; and one NPN BJT transistor  $Q_{44}$ . The transistor is biased by two power rails labeled  $B2$  and  $-B2$  in the service notes, which we will treat as ideal  $\pm 15$  V voltage sources. Component values are given in

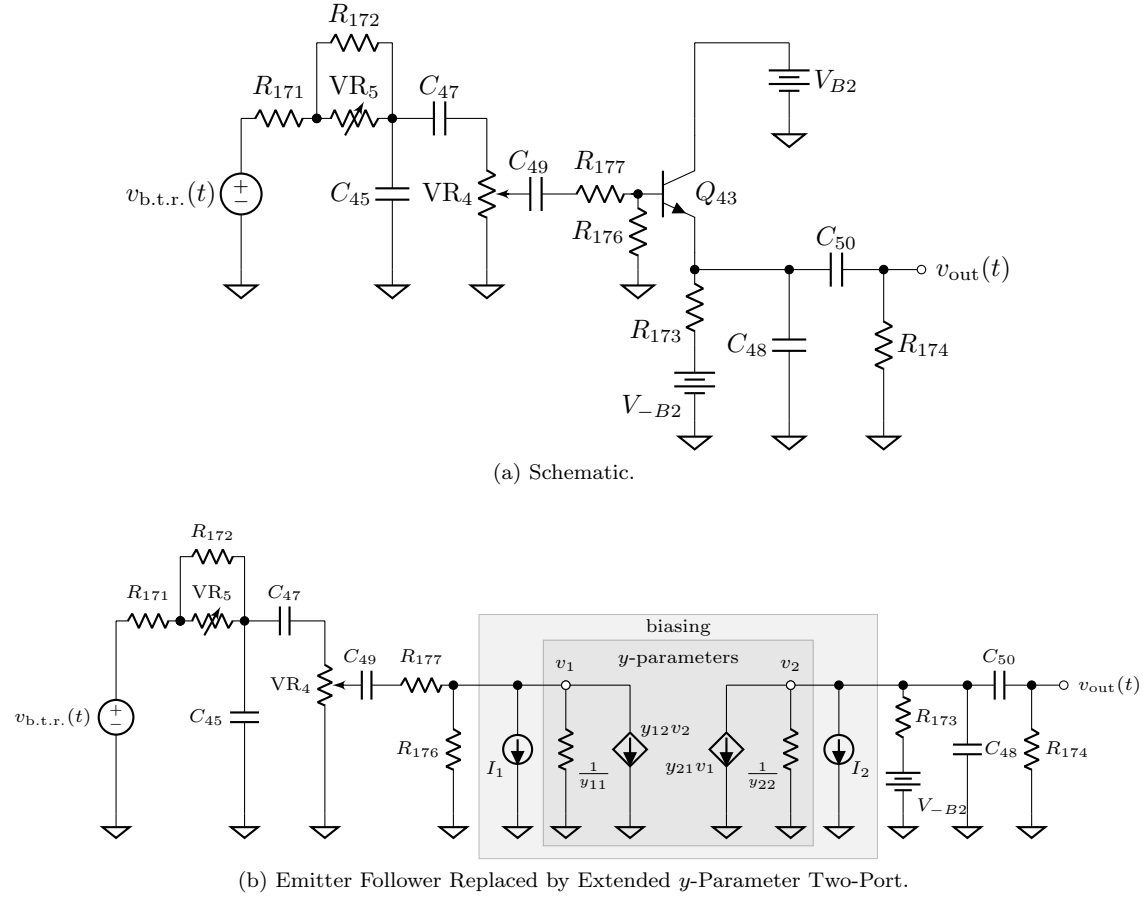


Figure 1.54: TR-808 Bass Drum Output Filter.

Table 1.1a.

The input to the tone stage is the output of the op-amp involved in the bridged-T network, which we will treat here as an ideal voltage source  $V_{b.t.r.}$ . Breaking a circuit into sub-circuits at the output of an op-amp is typical technique that will be familiar to circuit designers. Conceptually, this is a good assumption because the input impedance of the circuit stage which is being drive is almost always much higher than the output impedance of the op-amp. Even beyond this familiar assumption, when we assume that the op-amp involved in the bridged-T network is ideal (an assumption that will indeed make much later on in Chapter 4), this separation is actually a perfect circuit-theoretic equivalence. We will develop this equivalence in the section of Chapter 2 which deals with the theoretical circuit elements known as nullators, norators, and nullors, and their use in modeling ideal op-amps in negative feedback and ideal transistor amplifiers.

The output  $v_{out}$  from the tone stage is taken as the voltage across resistor  $R_{174}$ . In the real circuit, the bass drum tone stage is followed by a summing amplifier that sums together contributions from

Table 1.1: TR-808 Bass Drum Component Names and Values For Extended Two-Port  $y$ -Parameter Model. Derived quantities ( $1/y_{11}$  and  $1/y_{22}$ ) are given as well.

(a) Component Values.			(b) $y$ Parameters and DC Source Values.	
Component	Value	Note	Name	Value
$R_{171}$	$220\ \Omega$		$y_{11}$	$0.261\ 273\ \text{mS}$
$R_{172}$	$10\ \text{k}\Omega$		$y_{12}$	$-2.612\ 73 \times 10^{-4}$
$R_{173}$	$6.8\ \text{k}\Omega$		$y_{21}$	$-7.864\ 31 \times 10^{-2}$
$R_{174}$	$100\ \text{k}\Omega$		$y_{22}$	$78.6431\ \text{mS}$
$R_{176}$	$100\ \text{k}\Omega$		$I_1$	$-0.169\ 104\ \text{mA}$
$R_{177}$	$82\ \text{k}\Omega$		$I_2$	$50.9002\ \text{mA}$
VR <sub>4</sub>	$100\ \text{k}\Omega$	max value	$1/y_{11}$	$3.827\ 42\ \text{k}\Omega$
VR <sub>5</sub>	$10\ \text{k}\Omega$	max value	$1/y_{22}$	$12.7157\ \Omega$
$C_{45}$	$0.1\ \mu\text{F}$			
$C_{47}$	$0.47\ \mu\text{F}$			
$C_{48}$	$220\ \text{pF}$			
$C_{49}$	$0.47\ \mu\text{F}$			
$C_{50}$	$1\ \mu\text{F}$			
$V_{B2}$	$15\ \text{V}$			
$V_{-B2}$	$-15\ \text{V}$			
Transistor	2N3904	substitute for 2SC945(P)		
$I_s$	$10\ \text{fA}$	saturation current		
$\beta_F$	300	forward current gain		
$\beta_R$	4	reverse current gain		
$V_T$	$25.85\ \text{mV}$	thermal voltage		

all of the TR-808's voices.

The behavior of the tone stage is parameterized by a volume knob (the potentiometer VR<sub>4</sub>) and a tone knob (potentiometer VR<sub>5</sub>). In our analysis and simulation we will treat the tone knob as a single resistor  $(1 - c)\text{VR}_4$ , where  $c \in [0, 1]$  is the position of the tone knob and VR<sub>4</sub> is the maximum value of the potentiometer. We will treat the volume knob as two resistors, one with the value  $(1 - l)\text{VR}_5$  and one with the value  $l\ \text{VR}_5$ , where  $l \in [0, 1]$  is the position of the volume knob and VR<sub>5</sub> is the maximum value of the potentiometer.<sup>9</sup>

The service notes [135] give some clue as to the behavior of each part of the circuit. Ignoring loading between stages and making some simplifications, it is possible to break down the tone stage into five sub-stages:

1. A tone sub-stage (first order lowpass filter) composed of  $R_{171}$ ,  $R_{172}$ , VR<sub>5</sub>, and  $C_{45}$ ;

<sup>9</sup>Rather than having a linear relationship between knob position and resistance, VR<sub>4</sub> and VR<sub>5</sub> actually have “(A)” and “(C)” tapers, respectively [135]. Since we are only concerned with the simulation of the circuit’s dynamics, not the precise mapping from control parameters to reference circuit values, we are going to ignore this fact. In practice, one should measure the “(A)” and “(C)” tapers to find the functions mapping  $c$  and  $l$  to the three resistances.

2. A volume stage (first order highpass filter) composed of  $VR_4$  and  $C_{47}$ ;
3. A highpass stage (first order highpass filter) composed of  $R_{176}$ ,  $R_{177}$ , and  $C_{49}$ ;
4. A buffer stage (unity gain emitter follower) composed of the transistor,  $R_{173}$ ,  $C_{48}$ ,  $V_{-B2}$ , and  $V_{B2}$ ; and
5. An output stage (first order highpass filter) composed of  $C_{50}$  and  $R_{174}$ .

Although this sort of breakdown gives us a good intuition about the behavior of the circuit, an ad hoc simulation designed directly from this simplified analysis will suffer from significant errors.

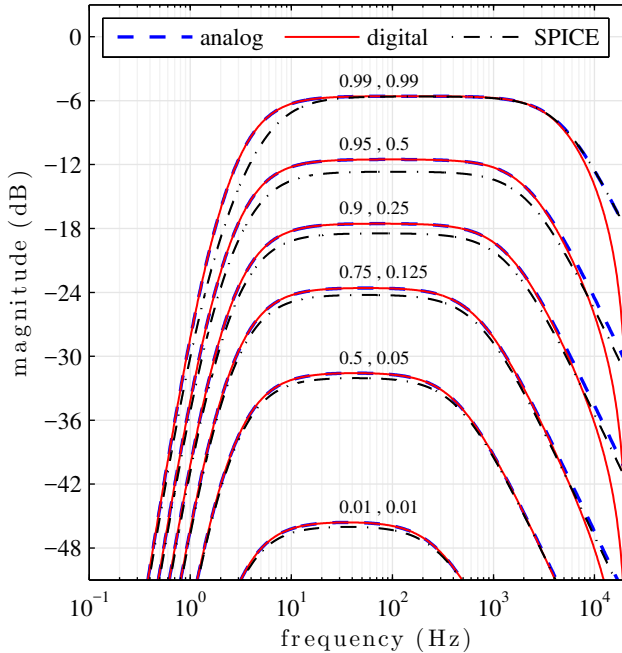


Figure 1.55: Overall Magnitude Response for Simplified TR-808 Bass Drum Output Filter at Various Tone and Volume Knob Settings, Comparison to Continuous-Time Magnitude Response and SPICE. Above each set of traces the pair of tone and level controls  $c, l \in [0 \dots 1]$  is shown.

Figure 1.55 compares the magnitude response of a digital simulation implemented directly from this analysis to a SPICE simulation (treated as the ground truth). Six different combinations of the tone and volume knob pairs  $\{c, l\}$  are shown. Of course the digital simulation suffers from a well-known frequency distortion at high frequencies [155]. However, even at low frequencies there are significant errors in the digital simulation. This is a direct result of the inaccuracy of the assumptions that enabled the analysis above. The derivation of this style of digital simulation is explained in a previous study on the TR-808 bass drum [2] and detailed further in Appendix §B.

These errors motivate the need for a better approach. In the rest of this case study, we'll detail how to build a Wave Digital Filter from the TR-808 Bass Drum tone stage which does not require analysis of the stages of the circuit and will not suffer from the same errors as the simplified model.

Most of the electrical components of the Bass Drum Tone Stage and their interconnection topology can be modeled using the standard Wave Digital Filter building blocks including resistors, discretized capacitors, series adaptors, and parallel adaptors which were developed in this chapter and have been known in the literature since the earliest days of Wave Digital Filters. The part of the circuit which deserves special treatment is the single transistor  $Q_{44}$ . Transistors are three-terminal nonlinear devices which we have not discussed yet. The basics of transistor modeling alongside novel contributions for handling transistorized circuits 4.

In the rest of this case study, we will first create a very-nearly-equivalent *linear* reference circuit by linearizing the transistor. Second, we will develop a Wave Digital Filter block diagram from the circuit schematic. Finally, the model will be compared to SPICE simulation and simulations based on ad-hoc simplified models. It will be seen that the Wave Digital Filter model enjoys a nearly exact match to SPICE simulation under the entire range of simulation conditions and does not suffer from low-frequency errors like the ad-hoc simplified model.

To prepare a reference circuit that is suitable for linear Wave Digital Filter modeling, we first take the schematic shown in Figure 1.54a and replace the emitter follower [199, p. 65] with an appropriate linearization. The linearization involves replacing the transistor and voltage source  $V_{B2}$  with a  $y$ -parameter two port and two dc current sources  $I_1$  and  $I_2$  and is shown in Figure 1.54b. The  $y$  parameters and current source values produced by this derivation are given in Table 1.1b. The derivation of this linearization is a little involved and is detailed in Appendix §A. For now, it suffices to say that for this emitter follower, the combination of the  $y$ -parameter two port and the two current sources shown in Figure 1.54b is nearly equivalent for reasonable input signals.<sup>10</sup>

Rearranging the linearized reference circuit (Figure 1.54b) to highlight the underlying circuit topology yields Figure 1.56. Notice again that the tone potentiometer appears as a single resistor with value  $(1 - c)VR_5$  and the volume potentiometer appears as two resistors with values  $(1 - l)VR_4$  and  $l VR_4$ . Resistor  $R_{176}$  happens to be in parallel with current source  $I_1$  in the reference circuit, and here they are merged together into a resistive current source. In this Figure the polarity of each port is indicated with a pair of + and - terminals. The polarity of series and parallel connections has been chosen to respect the Wave Digital Filter convention. As a result, in four cases connected elements have mismatched polarities. These are resolved by the empty-looking two-port elements with mismatched polarities on the two ports.

The structure of the Wave Digital Filter simulation is shown in Figure 1.57 and is completely isomorphic to Figure 1.56. The  $y$ -parameter two-port is treated like any other Wave Digital Filter

---

<sup>10</sup>With the volume and tone knobs turned all the way up ( $c = 1$ ,  $l = 1$ ), input signals with amplitudes above 25 V will “rail” the amplifier. Considering that the tone stage is fed by a stage that is itself powered by  $\pm 15$  V (and hence shouldn't produce output outside that range), the railing condition should never occur in practice.

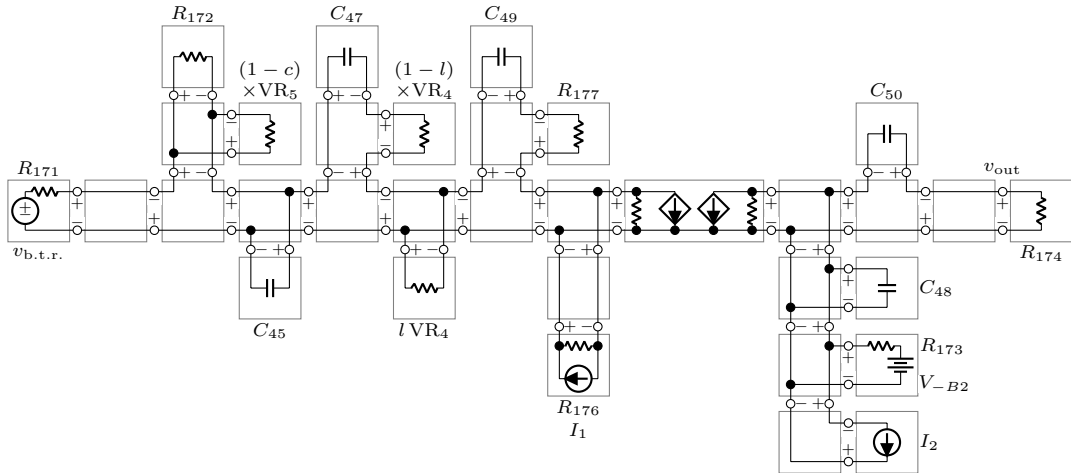


Figure 1.56: TR-808 Bass Drum Output Filter, Rearranged to Highlight Topology.

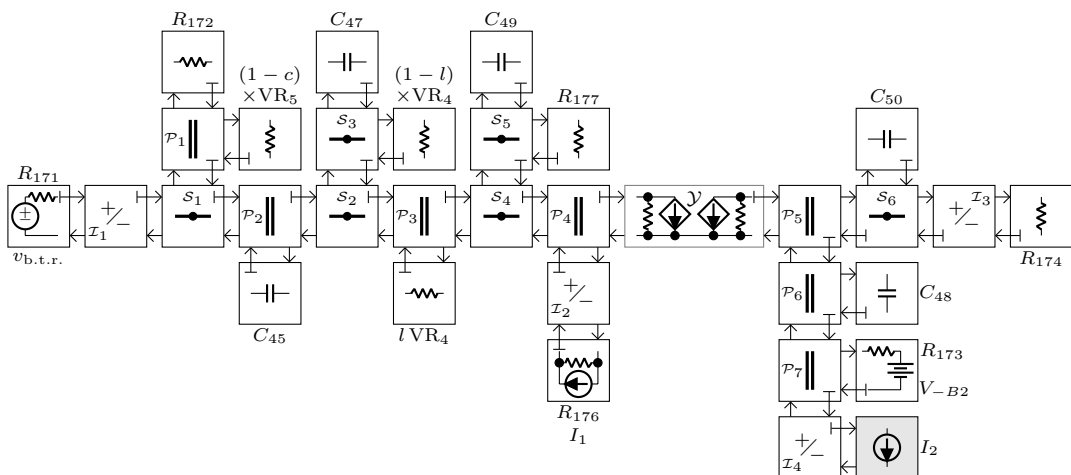


Figure 1.57: TR-808 Bass Drum Output Filter, Wave Digital Filter structure, root element highlighted.

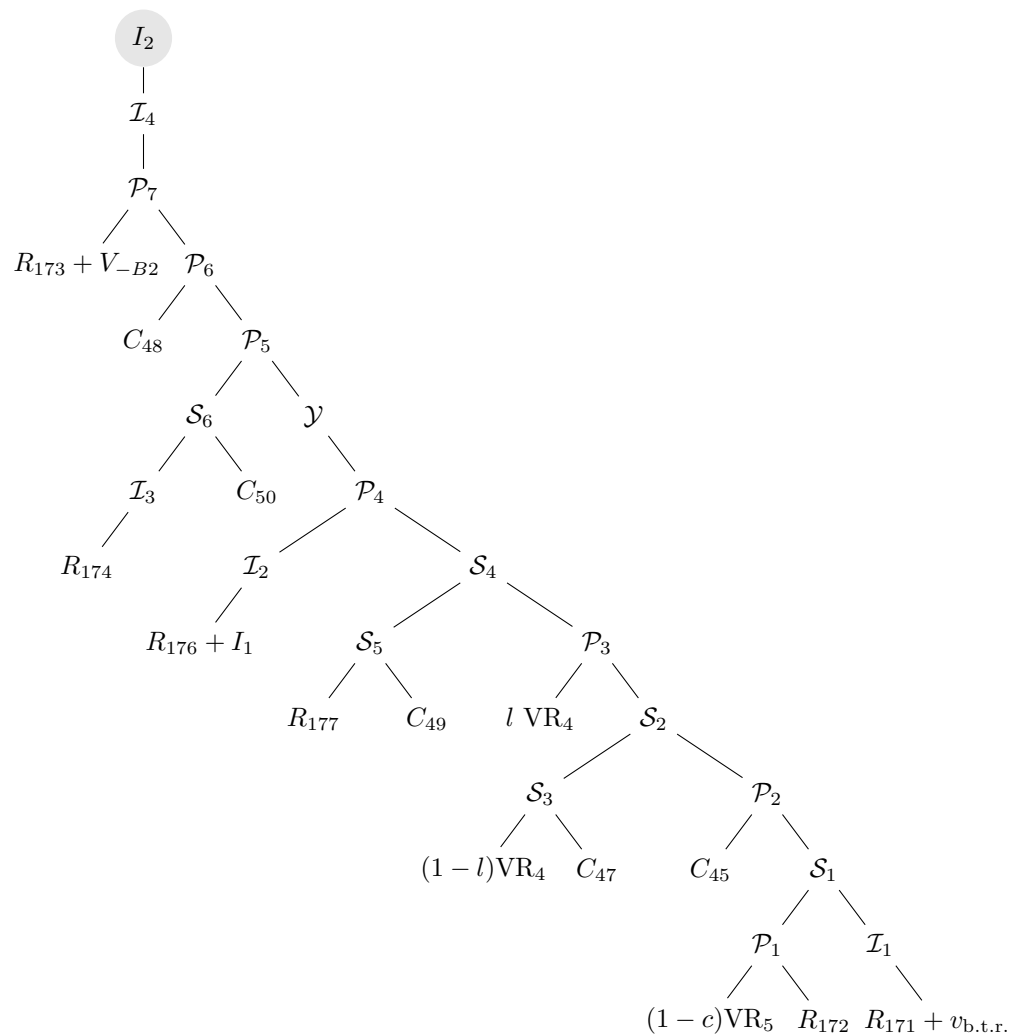


Figure 1.58: Connection Tree for TR-808 Bass Drum.

element using the techniques detailed in §1.4.10 and its right-facing port is adapted. Following the notational tradition established by Fettweis and others, in a Wave Digital Filter diagram like this, the arrows represent signal flow, and the arrows starting with a perpendicular bar represent adaptation. The only non-adaptable element in this reference circuit is current source  $I_2$ . Since it cannot be adapted, it will be designated as the root of the Wave Digital Filter tree (indicated by shading). The tree structure is determined by the direction of adaptation of each block—the direction of adaptation always points towards the root of the tree. A diagram showing the tree structure explicitly is shown in Figure 1.58.

Figure 1.59 compares the magnitude response of a SPICE simulation, the simplified model (Appendix §B), and our Wave Digital Filter model. For the simplified model and the Wave Digital Filter, a sampling rate of  $f_s = 44\,100$  Hz was used.

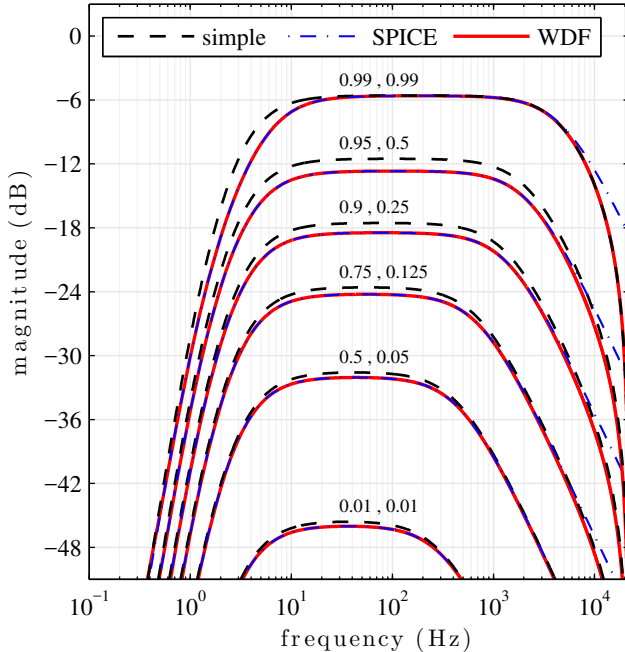


Figure 1.59: Overall Magnitude Response for TR-808 Bass Drum Tone, Level, and Output Buffer at Various Tone and Volume Knob Settings, Comparison to Simplified Model and SPICE. Above each set of traces the pair of tone and level controls  $c, l \in [0 \cdots 1]$  is shown.

To obtain the SPICE magnitude response, the standard `.ac` command was used.

The simplified model magnitude response comes directly from evaluation of its  $z$ -plane transfer function.

To measure the magnitude response, the Wave Digital Filter model is first run with dc inputs for 16 s to be completely sure that the correct operating point is established. Then, a single unit voltage impulse is sent in. The transient response is measured for 1 s, letting the impulse response

decay “sufficiently to zero.” Taking the Discrete Fourier Transform (DFT) of the impulse response yields the magnitude response.

While the simplified model suffers from significant low-frequency errors, the Wave Digital Filter model enjoys a nearly perfect match to SPICE at low frequencies. Both experience the expected frequency distortion at high frequencies due to the Bilinear Transform. Of course, this could be easily mitigated through oversampling. This simulation confirms the usefulness of the Wave Digital Filter approach for modeling the Output Filter. Notably, we never had to derive the transfer function of the circuit (which would have been miserable) or make any simplifying assumptions about the circuit beyond linearizing the transistor.

## 1.8 Review

In this Chapter, we’ve introduced the basic principles of Wave Digital Filter modeling for linear circuits, enumerated the basic one-, two-, and three-port linear electrical devices and topological connections, including  $y$ -,  $z$ -,  $h$ -, and  $g$ -parameter two-port models which have apparently not been treated in the Wave Digital Filter context before. For all these building blocks, we’ve derived their Wave Digital Filter models and adaptation criteria when possible, and demonstrated the Wave Digital Filter approach to modeling with a case study on the TR-808 Bass Drum’s Output Filter.

We’ve given emphasis to a new parametric wave definition that encompasses the standard voltage, power, and current waves as special cases. In our discussion of capacitor and inductor modeling, we’ve emphasized the potential for using discretization methods other than the standard Bilinear Transform, including the Warped Bilinear Transform, Backwards Euler, the  $\alpha$  Transform, and the general Möbius Transform which encompasses the others as special cases. An interesting result of the Möbius Transform derivation is the finding that fully explicit methods such as Forward Euler cannot be used in the Wave Digital Filter context.

With these approaches we can build Wave Digital Filter models of any linear circuit whose topology can be decomposed entirely into series and parallel connections. This is an important class of circuits which encompasses, e.g., standard ladder circuits.

However these techniques can still not be applied to model all circuits, not even all linear circuits. Circuits involving complex topologies are not handled. Two-port devices that are not in feed-forward arrangement are not handled. Circuits involving operational amplifiers in feedback arrangement are not handled. Although we’ve discussed tricks for adding resistances to aid realizability in the presence of multiple linear nonadaptable elements, these tricks in general add some error to the simulation. New techniques for handling these issues will be the subject of Chapter 2.

Looking ahead to nonlinear circuit modeling, techniques for handling circuits with a single nonlinearity will be reviewed and extended in Chapter 3 and a novel technique for handling circuits with multiple nonlinearities will be the subject of Chapter 4.



## Chapter 2

# Topological Advances for Wave Digital Filters

In this chapter we will consider linear electrical circuits which cannot be handled using the methods of Chapter 1. Specifically we take aim at circuits involving arbitrarily complex topologies which cannot be decomposed into series and parallel adaptors, multiport linear amplifiers in feedback topologies, operational amplifiers, and multiple nonadaptable linear elements. Some of the work in this chapter appeared previously in conference proceedings [141, 154].

In the analysis and synthesis of classical networks there is a heavy focus on ladder circuits (composed of “series- and shunt-connected” networks), or more generally series-parallel networks; the driving point impedance of these networks can be represented as a continued fraction [129, pp. 28–31]. In this context, the driving point impedance of general structures which cannot be decomposed into series and parallel connections has to be approached by writing the circuit equations on the loop/mesh or node basis [129, pp. 31–35]. The theory of Wave Digital Filters inherits much from classical network theory; the work in this chapter can be seen as the Wave Digital Filter reflection of the extension of classical network theory to general (non-series-parallel) networks.

This chapter is structured as follows. In §2.1 previous work on this class of circuits is reviewed. In §2.2 a method is proposed that can handle complicated topologies that can’t be decomposed into series and parallel connections, including those with absorbed multiport linear elements like transformers, controlled sources, nullors, gyrators, etc. In §2.3 a second complementary method is proposed which can handle multiple linear nonadaptable elements (e.g., open circuits, closed circuits, ideal sources, switches). In §2.4, case studies on various Bridged-T circuits are given which illustrate these techniques. §2.5 reviews the capabilities and limitations of the presented techniques and points towards the next steps (nonlinear circuits).

## 2.1 Previous Work

In this Section we'll review related work on handling complicated topologies in the Wave Digital Filter context. We'll begin with a review of the method of Martens and Meerkötter (§2.1.1), which can handle reciprocal circuits. This method and other ad hoc approaches have been used to discretize certain special adaptors from the field of network synthesis (§2.1.2). Following that we'll mention one class of operational amplifier circuits which have been handled in the literature, as well as other ad hoc examples of op amp modeling (§2.1.3). One research thread forces series and parallel topologies onto circuits with complicated topologies, resulting in non-tree-like structures that must be resolved with global iteration (§2.1.4). The techniques we'll propose later in this chapter rely rather on an SPQR-decomposition of circuit graphs; finally we'll review relevant work on SPQR tree decompositions in the Wave Digital Filter context (§2.1.5).

### 2.1.1 Martens and Meerkötter

The simplest class of circuits which cannot be handled with the methods of Chapter 1 are circuits with complicated topologies which cannot be decomposed into series and parallel connections. The issue of complicated topologies was first recognized by Martens and Meerkötter [200], who use a graph-theoretic approach to finding the scattering matrix of an adaptor with a complicated topology, relying crucially on the orthogonality of the circuit and cutset matrix for part of their derivation. In the literature, there exist derivations for particular special adaptors corresponding to standard sections from network synthesis, some of which are based on [200]. For voltage-wave scattering matrices derived from reciprocal junctions, a technique has been proposed for reducing the computational cost [201].

The main limitation of this method is that because it relies on the orthogonality of the circuit and cutset matrix, it is only valid for pure junctions and those which only have absorbed reciprocal devices (e.g. transformers). Common audio circuit devices like operational amplifiers, controlled sources, and nullors cannot be accommodated.

### 2.1.2 Special Adaptors

There are certain special two-port circuit topologies that come from classical network synthesis (e.g., the Bott–Duffin procedure for network synthesis of positive real functions [129]) and that cannot be handled with standard Wave Digital Filter techniques. Wave Digital Filter designers were interested in designing digital filters that inherited the same properties as the circuits built out of these two-ports and developed special adaptors for those topologies, sometimes using the method of [200].

The simplest of these special two-ports devices is the “lattice” topology, shown in Figure 2.1a, which interfaces two external ports to a “lattice” of four impedances, two of which have the same

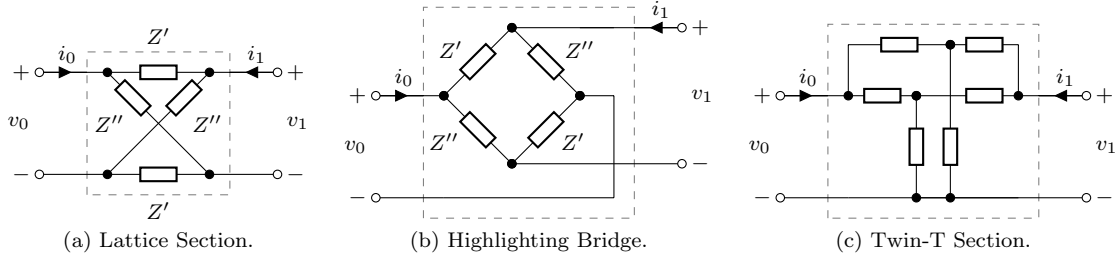


Figure 2.1: Lattice Section, Bridged-T Section, and Twin-T Section.

values as the other two. We note that a lattice topology is identical to a Bridged-T topology (shown in Figure 2.1b), although bridge sections don't typically have any restrictions on component equivalences. Lattice networks are useful in communications systems and are an important building block in network theory [129, pp. 337–338]. Fettweis designed a Wave Digital Filter adaptor to accommodate lattice topologies, which uniquely exploits the equivalence between the connected impedances in the lattice topology to eliminate two of the six ports from the analog prototype [128], [5, pp. 288–289]. A related two-port is the Twin-T network, shown in Figure 2.1c, which interfaces two external ports to six impedances. Twin-T and related structures are of interest in impedance measuring instruments and are capable of synthesizing imaginary or complex transmission zeros without the use of inductors [129, p. 323]. To accommodate these structures in a Wave Digital Filter, Lê designed an adaptor [202] using the method of [200].

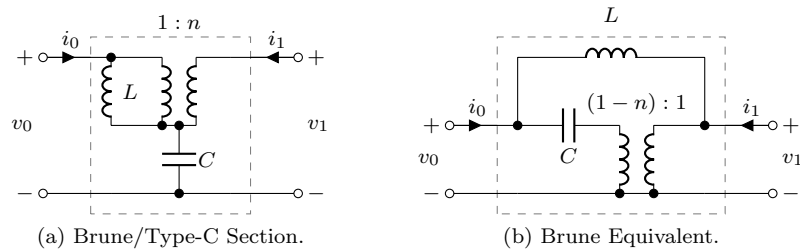


Figure 2.2: Brune/Type-C Section and Brune Equivalent.

More complicated special two-ports incorporate transformers. A foundational network synthesis section is the Brune / Type-C section<sup>1</sup>, shown in Figure 2.2a, for which Lê and others have derived Wave Digital Filter adaptors. An “equivalent form” Brune adaptor, shown in Figure 2.2b, with a different topology and different transformer turns ratio also exists, in circuit and Wave Digital Filter form [202, 203, 204, 205, 206, 207, 208]. One of the first special adaptors to be recognized in the Wave Digital Filter context is the Jaumann structure, shown in Figure 2.3a [209, 197, 198].

<sup>1</sup>The designation depends on the sign of the transformer turns ratio.

Fahmy and others have derived Wave Digital Filter adaptors from the D-type section, shown in Figure 2.3b [210, 202, 203, 208].

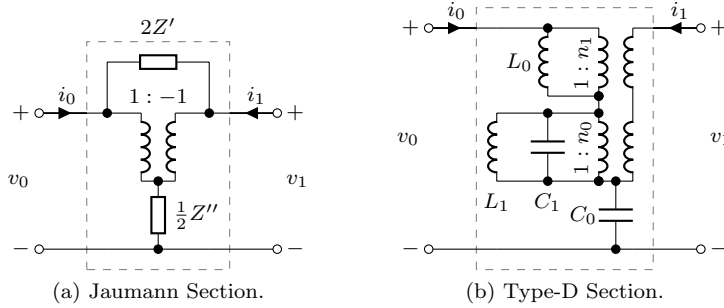


Figure 2.3: Jaumann Section and Type-D Section.

Even more complicated are the adaptors which incorporate gyrators in addition to transformers. Since gyrators are not reciprocal, the method of [200] is no longer an appropriate way of discretizing these topologies. Suzuki developed a Wave Digital Filter adaptor for the E-type section and the Richards sections, shown in Figure 2.4 [205, 208].

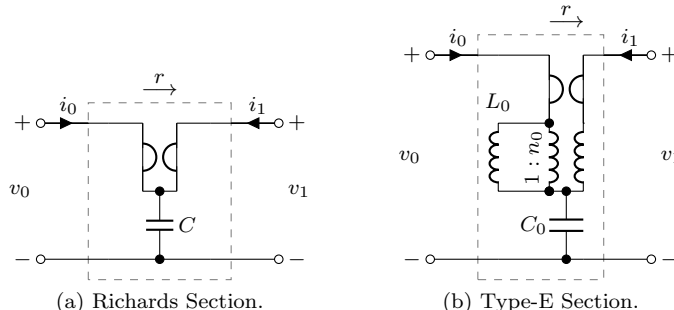


Figure 2.4: Type-E Section and Richards Equivalent.

The two-port sections we've mentioned come from network synthesis but are actually not common in audio circuitry.<sup>2</sup> The main limitation of these approaches is that they are only valid for circuits which happen to use the derived adaptors.

### 2.1.3 Circuits Involving Operational Amplifiers

The operational amplifier is an important electrical device which is common in audio circuits, but hasn't been treated in detail in the Wave Digital Filter context. Here we'll review two ad hoc approach to modeling op-amp circuits, implications for their extensions, and their ultimate limitations.

<sup>2</sup>In drum machine circuits like the Korg Mini Pops-120 [211], Twin-T topologies are used with operational amplifiers to form ringing bandpass filters, just like the Bridged-T in the TR-808 Bass Drum.

### Op-Amp Differential Amplifier Topologies

In [212], Paiva *et al.* show how to model a class of audio circuits involving an operational amplifier. For their modeling approach to work, a few criteria must be satisfied. First, the op-amp must be modeled as *ideal*, i.e., the output terminal will source or sink as much current as is necessary and float to whatever voltage is necessary to ensure that the two input terminals have an equal voltage ( $v_+ = v_-$ ) without drawing any current ( $i_+ = i_- = 0$ ). Second, the op-amp circuit must have a differential amplifier topology. Finally, although it is easy to imagine extensions of their method to multiple operational amplifiers in feedforward combinations, circuits involving multiple operational amplifiers with global feedback are not handled, as they will produce a nonrealizable Wave Digital Filter structure.

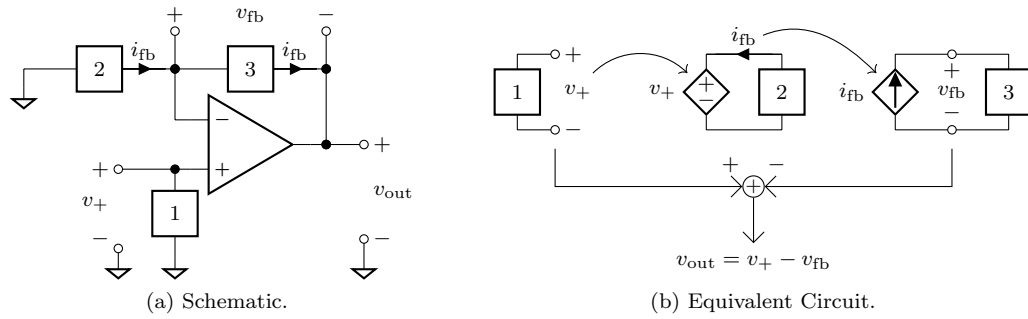


Figure 2.5: Op-amp Differential Amplifier Topology and Equivalent Circuit.

An outline of their approach is shown in Figure 2.5, where the boxes labeled 1, 2, and 3 represent individual one-ports or more complicated networks with a single external port. In short, their approach involves application of Kirchhoff's circuit laws to the schematic shown in Figure 2.5a to rearrange it into an equivalent circuit shown in Figure 2.5b, which can be realized as three separated Wave Digital Filter trees. This approach is justified in the following way. Since under the ideal op-amp assumption, the positive op-amp input terminal does not draw any current, it is possible to replace the two input terminals with a voltage-controlled voltage source (VCVS), shearing off block 1 into its own subcircuit. Again, since the negative op-amp input terminal does not draw any current, the current  $i_{fb}$  flowing through block 2 will flow entirely into block 3; this relationship is replaced by a current-controlled current source (CCCS), again shearing off block 2 and the VCVS into its own subcircuit. Since the controlled sources only ever represent the forward flow of information from subcircuit to subcircuit, this equivalent circuit can easily be modeled as three separate Wave Digital Filter trees. Finally, we notice that by polling the voltage off of blocks 1 and 3, the output voltage can be reconstructed as  $v_{out} = v_+ - v_{fb}$ .

This approach is in fact sufficient to model certain circuits based on operational amplifiers. Paiva *et al.* show applications to noninverting distortion circuits (e.g., the Ibanez Tube Screamer)

and inverting distortion circuits (e.g., the Marshall 4100 JCM900 Hi Gain Dual Reverb preamplifier) [212]. We show a few other examples in Figure 2.6, including an op-amp-based inverting amplifier (Figure 2.6a), non-inverting amplifier (Figure 2.6b), integrator (Figure 2.6c), differentiator (Figure 2.6d), and adder/subtractor (Figure 2.6e) [213]. Notice that in all these cases it is possible to group collections of components together so that the topology matches that of Figure 2.5a.

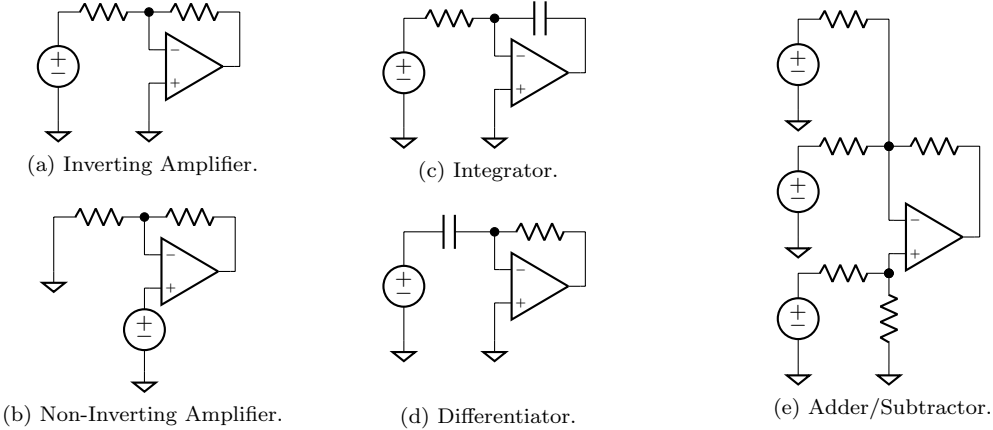


Figure 2.6: Op-Amp-Based Filters Which can be Framed as Differential Amplifiers: Inverting and Non-Inverting Amplifiers, Integrator, Differentiator, and Adder/Subtractor.

However, this approach is still limited in what types of reference circuits it can handle. First, it cannot be used on any circuits where the op-amps are not assumed ideal—op-amp non-idealities are often considered important and op-amps are often modeled using complex *macromodels* [214, 215, 216, 193] rather than ideal assumptions. Second, it cannot be used on any circuits which do not have differential amplifier topology. Examples of these types of circuits are easily found among standard filter topologies. Examples include the Sallen-Key family of filters (e.g., Figure 2.7a) [217, 218, 219] and the Multiple-Feedback family of filters (e.g., Figure 2.7b) [219]. Circuits involving multiple op-amps in a feedback arrangement are also common—an example is the classic State-Variable Filter (e.g., Figure 2.7c) [220, 199]. Notice specifically that although the State-Variable Filter is composed entirely out of smaller building blocks (two Integrators and an Adder/Subtractor) which are possible to handle using [212], their combination is not. Other standard filter topologies including the Delyannis family [221, 222, 219], the Fliege topology [219], op-amp-based biquads [223, 222], and op-amp-based circuits for synthesizing inductors, gyrators, etc. [148, 222] also fall into this category. The Bridged-T Resonator in the TR-808 bass Drum is another op-amp based circuit which cannot be classified into differential amplifier topology and requires a more general approach to model as a Wave Digital Filter.

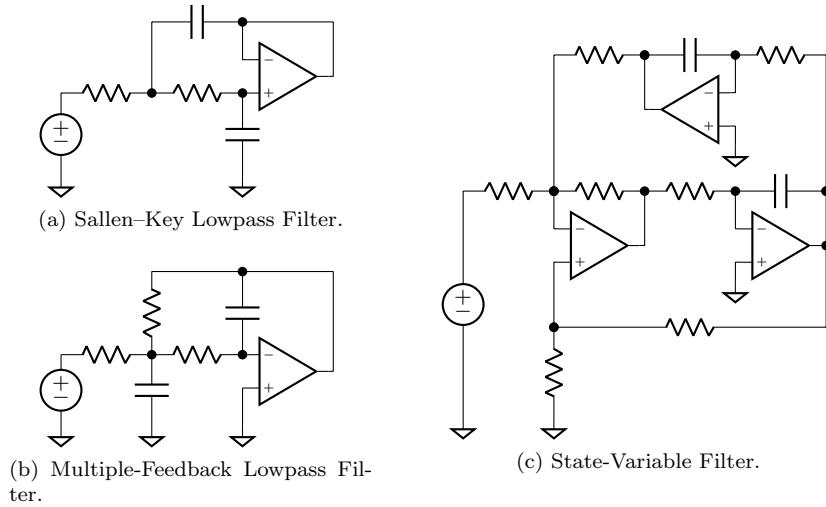


Figure 2.7: Op-Amp-Based Filters Which can't be Framed as Differential Amplifiers: Sallen-Key Lowpass Filter, Multiple-Feedback (MFB) Lowpass Filter, and State-Variable Filter (SVF).

### Ad hoc op-amp model

In [6], De Sanctis and Sarti show an ad hoc model of a comparator-configured op-amp-based astable multivibrator configured to produce square and sawtooth waves. Although this is an efficient and ingenious model of the circuit, it relies on a number of assumptions and simplifications. As in [212], the op-amp is used to separate the circuit into two subcircuits. Since the op-amp is configured as a comparator, it is modeled as a nonlinearly-controlled voltage-controlled voltage source. Two diodes are not explicitly incorporated into the model, but rather their behavior is abstracted as a switch. Finally, since the circuit relies on feedback principles to operate, the assumption of a feedforward flow of information is broken and an ad hoc unit delay is inserted to aid realizability.

#### 2.1.4 Methods Involving Global Iteration or “Dynamic Adaptation”

Recently, Schwerdtfeger and Kummert have approached complicated topologies by *forcing* series and parallel structures onto these topologies, which alters the global structure of the Wave Digital Filter simulation from a Connection Tree to a non-tree-like structure. In these cases the structure cannot be rendered realizable using adaptation. To ensure a realizable structure, extra unit delays are added [224, 225], and the error that these extra delays introduce is eliminated through global iteration on the structure [226]. These techniques have been applied to, e.g., active ladder circuits [227].

The main limitations of these approaches are that there is no systematic procedure for deriving the original structure and that they fail to localize the complicated topology to one part of the structure; rather they may involve global iteration.

In a related work [228], Bernardini and Sarti propose a method of accommodating multiple

nonadaptable elements without localizing them to the tree of the Wave Digital Filter structure. Although their approach is designed for use with nonlinear one-ports, it could have implications for accomodating multiple linear one-ports. They use a technique of “dynamic adaptation” which introduces some error into the simulation.

### 2.1.5 SPQR Tree

To uncover tree-like adaptor structures in circuits with complicated topologies, Fränken *et al.* proposed a technique based on the *SPQR tree* formalism from graph theory [197, 198]. Given a reference circuit, which may contain linear multiport elements and complicated topologies, Fränken *et al.* start by creating a connected graph representing the reference circuit. In this graph, graph nodes correspond to circuit nodes and graph edges correspond to ports in the circuits, i.e., these graph edges correspond to one-port circuit elements (resistors, capacitors, inductors, etc.) or ports of a linear multiport element (transformer, controlled source, etc.). Then, standard graph separation algorithms which find “split components” are used to decompose the connected graph into a tree structure: the *SPQR* tree. For realizability reasons, we must ensure that these graph separation algorithms will not separate edges that correspond to a single multiport circuit element. This can be avoided by pre-processing the graph structure with so-called *replacement graphs* before applying a separation algorithm [198]. A minimal suitable replacement graph includes the addition of 3 fictitious nodes to each multiport element, and fictitious edges connecting each one of them to every node in the multiport element; this is sufficient to ensure that graph separation algorithms will not break apart the multiport linear element.

In the SPQR tree, nodes represent topological entities in the graph with detected split components, and edges represent virtual edges in the split components.  $\mathcal{S}$ ,  $\mathcal{P}$ , and  $\mathcal{R}$  nodes correspond directly to familiar **S**eries adaptors, **P**arallel adaptors, and the less well-known family of **R**igid or “strongly connected” adaptors.  $\mathcal{Q}$  nodes correspond to single component ports. This process highlights the fact that series and parallel adaptors are *not* sufficient to represent all linear circuit topologies, not even those without multiport elements. A result of using replacement graphs, multiport linear elements will commonly “clump up” inside of  $\mathcal{R}$ -type nodes. The idea of sources absorbed into adaptors is not necessarily new [6], but generalizing the concept in light of formal graph decomposition methods is crucial to our approach.

In the proposed approaches which will be discussed in the following section, these techniques are used to discover the global Wave Digital Filter structure of a reference circuit. The proposed approach to modeling circuits with multiple nonadaptable linear elements makes special use of the replacement graph technique to localize nonadaptable linear elements to one part of the Wave Digital Filter structure.

As an example of how the method of Fränken *et al.* can be applied to derive Wave Digital Filter adaptor structures, we consider two circuits: the Fender Bassman tone stack and the active tone

stage from the Ibanez Tube Screamer. The Bassman derivation demonstrates the basic application of the technique and the more complicated Tube Screamer derivation demonstrates the application replacement graph technique. Full details on the Wave Digital Filter simulations of these circuit are given in [141].

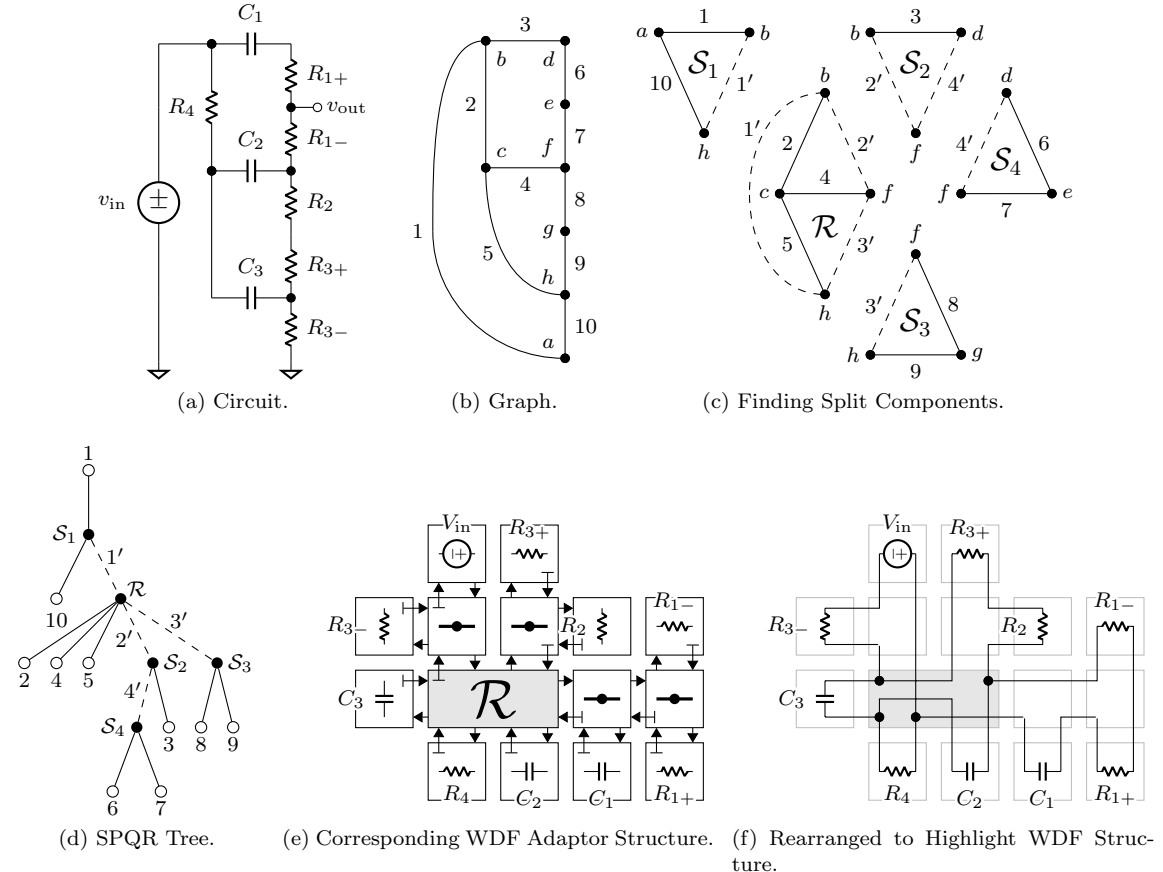


Figure 2.8: Deriving a Wave Digital Filter Adaptor Structure for the Fender Bassman Tone Stack.

First, consider the Fender Bassman tone stack circuit [141], shown in Figure 2.8a.<sup>3</sup> Yeh and Smith studied the Bassman tone stack by deriving its transfer function [47]. Although they suggested that it could potentially be implemented as a Wave Digital Filter, that would have been a daunting task at the time, since the Bassman tone stack circuit (Fig. 2.8a) can't be decomposed into a tree of series and parallel adaptors. Until now simulation of this circuit as a Wave Digital Filter would require the use of component consolidation [102] or topological transformations such as the  $Y-\Delta$  ("wye-delta") transformation [229]. To derive a Wave Digital Filter adaptor structure for this circuit, first a graph representing this circuit is formed (Fig. 2.8b). In this graph, nodes correspond to circuit nodes and

<sup>3</sup> $R_1$ ,  $R_2$ , and  $R_3$  are high, low, and mid tone control potentiometers.

are each assigned a lowercase letter. Graph edges correspond to ports in the circuit and are each assigned an Arabic numeral. For this graph representation, we follow the procedure of Fränken *et al.* [198] to find split components (Fig. 2.8c). This yields four series connections and a 6-port  $\mathcal{R}$ -type connection. We designate the voltage source (edge 1) as the root of the tree for realizability reasons—an ideal voltage source cannot be adapted and must be a root element. From here, an SPQR tree can be formed (Fig. 2.8d). A Wave Digital Filter adaptor structure follows by identity from this SPQR tree (Fig. 2.8e). This adaptor structure contains one  $\mathcal{R}$ -type adaptor, corresponding to the  $\mathcal{R}$ -type connection in Fig. 2.8c. A rearranged version of Fig. 2.8a which highlights the derived adaptor structure is shown in Fig. 2.8f.

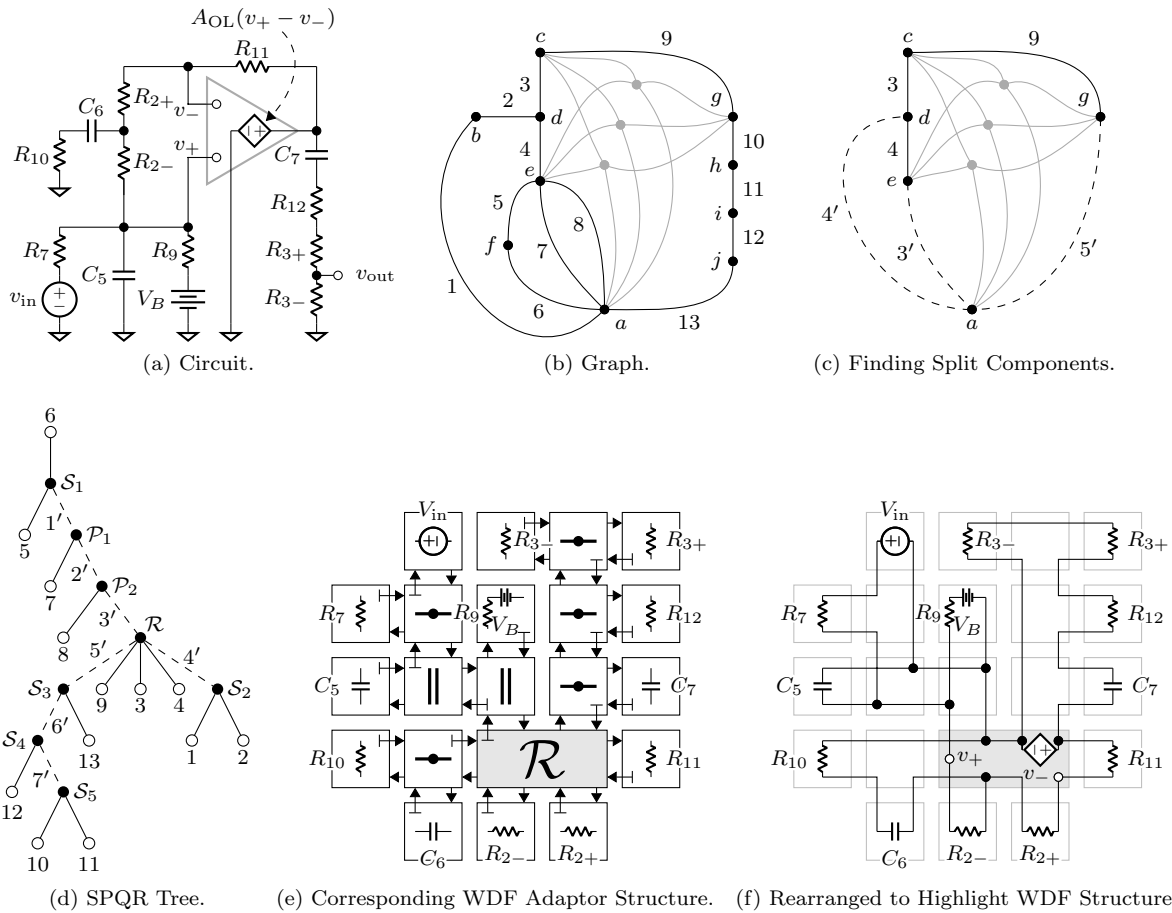


Figure 2.9: Deriving a Wave Digital Filter Adaptor Structure for the Tube Screamer Tone/Volume Stage.

Second, consider the active tone/volume stage of the Ibanez Tube Screamer distortion pedal [141].<sup>4</sup>

<sup>4</sup>  $R_2$  and  $R_3$  are tone and volume control potentiometers.

This circuit is based around an op-amp, and since it does not have a differential amplifier topology the approach of §2.1.3 cannot be used. In the circuit (Fig. 2.9a), the op-amp is treated as ideal, i.e., as a voltage-controlled voltage source that relates the output voltage to the differential input voltage  $v_+ - v_-$  by a large open-loop gain  $A_{OL}$ . A graph (Fig. 2.9b) is formed by the *replacement graph* method of Fränken *et al.* [198]; nameless replacement graph nodes and edges are indicated in gray. Detail on the resulting  $\mathcal{R}$ -type topology is shown in Fig. 2.9c; remaining standard series and parallel structures are not shown. As before, the split component search yields an SPQR tree (Fig. 2.9d) and corresponding Wave Digital Filter adaptor structure (Fig. 2.9e). Notice in Fig. 2.9f that the controlled source has been absorbed into the  $\mathcal{R}$ -type adaptor.

The work of Fränken *et al.* yields critical insights about the existence of complicated topologies and the implications of multiport linear elements like transformers and controlled sources on circuit topology. However, they don't mention how to derive the scattering behavior of the  $\mathcal{R}$ -type adaptors, meaning that the method does not in practice yield an actual signal processing algorithm, but only the global Wave Digital Filter structure. Solving this issue is a central contribution of this dissertation, and is explained in the next section.

## 2.2 Proposed method

Here we propose a systematic approach for deriving the scattering matrix of any  $\mathcal{R}$ -type adaptor. This method is fully general, covering  $\mathcal{R}$ -type adaptors with any topology, absorbed multiport linear elements including controlled sources and even absorbed nullors, which are used for ideal op-amp modeling and other reasons. It works by combining the Modified Nodal Analysis (MNA) circuit simulation formalism with the Wave Digital Filter wave definition. The original presentation of this approach in [141, 230, 231, 179] focused on the common voltage wave case. Here we extend that approach to the parametric wave case.

First, we observe a structure inherent in the parametric wave definition. Recall the parametric wave definition and its inverse for a vector of ports

$$\begin{aligned} \mathbf{a} &= \mathbf{R}^{\rho-1}\mathbf{v} + \mathbf{R}^{\rho}\mathbf{i} & \mathbf{v} &= \frac{1}{2}\mathbf{R}^{1-\rho}\mathbf{a} + \frac{1}{2}\mathbf{R}^{1-\rho}\mathbf{b} \\ \mathbf{b} &= \mathbf{R}^{\rho-1}\mathbf{v} - \mathbf{R}^{\rho}\mathbf{i} & \mathbf{i} &= \frac{1}{2}\mathbf{R}^{-\rho}\mathbf{a} - \frac{1}{2}\mathbf{R}^{-\rho}\mathbf{b} \end{aligned} \quad (2.1)$$

Our goal is to derive the scattering relationship  $\mathbf{b} = \mathbf{S}\mathbf{a}$ . By trying to combine these equations to find a scattering relationship, we get close but do not succeed

$$\mathbf{b} = \mathbf{a} - 2\mathbf{R}^{\rho}\mathbf{i}. \quad (2.2)$$

To succeed in finding the scattering relationship, we have to find a way to eliminate the port current

vector  $\mathbf{i}$  from (2.2), replacing it by some function of the incident wave vector  $\mathbf{a}$ . This should be a linear relationship of the form

$$\mathbf{i} = \mathbf{Q}\mathbf{a}, \quad (2.3)$$

which suggest a scattering relationship of the form

$$\mathbf{b} = \mathbf{S}\mathbf{a}, \quad \mathbf{S} = \mathbf{I} - 2\mathbf{R}^\rho\mathbf{Q}. \quad (2.4)$$

Our task, then, is finding  $\mathbf{Q}$  in a systematic way for any  $\mathcal{R}$ -type adaptor.

### 2.2.1 Thévenin Adaptors

To figure out how to solve this problem in a general way, we need a general way of writing out the equations that describe the  $\mathcal{R}$ -type adaptor. Since all of the classical circuit equation formulations are written in the Kirchhoff domain, we start by representing the  $\mathcal{R}$ -type adaptors and the incident and reflected waves at each port exclusively in the Kirchhoff domain. The circuit internals of any  $\mathcal{R}$ -type adaptor, including any absorbed multiport linear elements, are already described in the Kirchhoff domain; we only need to figure out how to represent the incident and reflected waves at each port in the Kirchhoff domain.

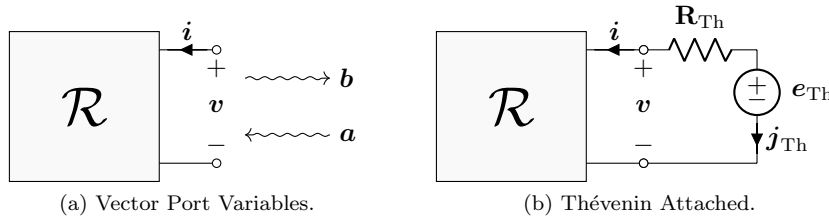


Figure 2.10: Instantaneous Thévenin Port Equivalents.

This problem can be seen as finding the correct parameters (source value and resistance) of Thévenin sources attached to each port. Considering all ports at once, they are characterized by a vector of Thévenin voltage source values  $\mathbf{e}_{\text{Th}}$  and a diagonal matrix of Thévenin resistances  $\mathbf{R}_{\text{Th}}$ . The branch constituent equation of the Thévenin resistors is given by

$$\mathbf{R}_{\text{Th}}^{-1}(\mathbf{e}_{\text{Th}} - \mathbf{v}) = \mathbf{i}. \quad (2.5)$$

Plugging in the parametric wave definition

$$\mathbf{R}_{\text{Th}}^{-1} \left( \mathbf{e}_{\text{Th}} - \frac{1}{2} \mathbf{R}^{1-\rho} \mathbf{a} - \frac{1}{2} \mathbf{R}^{1-\rho} \mathbf{b} \right) = \frac{1}{2} \mathbf{R}^{-\rho} \mathbf{a} - \frac{1}{2} \mathbf{R}^{-\rho} \mathbf{b} \quad (2.6)$$

and rearranging yields

$$\mathbf{e}_{\text{Th}} = \frac{1}{2} (\mathbf{R}^{1-\rho} + \mathbf{R}_{\text{Th}} \mathbf{R}^{-\rho}) \mathbf{a} + \frac{1}{2} (\mathbf{R}^{1-\rho} - \mathbf{R}_{\text{Th}} \mathbf{R}^{-\rho}) \mathbf{b}. \quad (2.7)$$

Setting the Thévenin resistances equal to the port resistances ( $\mathbf{R}_{\text{Th}} = \mathbf{R}$ ) eliminates  $\mathbf{b}$  from this equation, yielding an equation directly relating the Thévenin source values to the incident wave values,  $\mathbf{e}_{\text{Th}} = \mathbf{R}^{1-\rho} \mathbf{a}$ . So, finally, the way that the Thévenin values are related to port values is given by

$$\mathbf{R}_{\text{Th}} = \mathbf{R} \quad (2.8)$$

$$\mathbf{e}_{\text{Th}} = \mathbf{R}^{1-\rho} \mathbf{a}. \quad (2.9)$$

We also note that the current flowing through the voltage sources is the opposite of the port current

$$\mathbf{j}_{\text{Th}} = -\mathbf{i}. \quad (2.10)$$

### 2.2.2 Modified Nodal Analysis

Now that we have the **R**-type adaptor and the variables at the ports themselves represented in the Kirchhoff domain, we need to find a systematic way of writing the circuit equations and using it to find  $\mathbf{Q}$ . A circuit equation formalism from the literature called *Modified Nodal Analysis* (MNA) [232, 52, 233] is suitable for this purpose. Modified Nodal Analysis sets up a system of equations of the form

$$\underbrace{\begin{bmatrix} \mathbf{Y} & \mathbf{A} \\ \mathbf{B} & \mathbf{D} \end{bmatrix}}_{\text{MNA matrix } \mathbf{X}} \begin{bmatrix} \mathbf{v}_n \\ \mathbf{j} \end{bmatrix} = \begin{bmatrix} \mathbf{i}_s \\ \mathbf{e} \end{bmatrix}, \quad (2.11)$$

where  $\mathbf{X}$  partitions  $\mathbf{Y}$ ,  $\mathbf{A}$ ,  $\mathbf{B}$ , and  $\mathbf{D}$  define the relationship among node voltages  $\mathbf{v}_n$ , voltage source branch currents  $\mathbf{j}$ , current source values  $\mathbf{i}_s$  and voltage source values  $\mathbf{e}$ . The top partition of the matrix equation embodies Kirchhoff's Current Laws at each node of the circuit and the bottom partition represents certain branch relationships like the definitions of voltage sources. For our purposes, we'll be partitioning the vector  $\mathbf{j}$  into two parts as  $\mathbf{j} = [\mathbf{j}_{\text{Th}}^{\top} \quad \mathbf{j}_{\text{etc}}^{\top}]^{\top}$ , and the vector  $\mathbf{e}$  into two parts as  $\mathbf{e} = [\mathbf{e}_{\text{Th}}^{\top} \quad \mathbf{0}]^{\top}$  so the Modified Nodal Analysis system of equations will look more specifically like

$$\underbrace{\begin{bmatrix} \mathbf{Y} & \mathbf{A}_1 & \mathbf{A}_2 \\ \mathbf{B}_1 & \mathbf{D}_{11} & \mathbf{D}_{12} \\ \mathbf{B}_2 & \mathbf{D}_{21} & \mathbf{D}_{22} \end{bmatrix}}_{\text{MNA matrix } \mathbf{X}} \begin{bmatrix} \mathbf{v}_n \\ \mathbf{j}_{\text{Th}} \\ \mathbf{j}_{\text{etc}} \end{bmatrix} = \begin{bmatrix} \mathbf{i}_s \\ \mathbf{e}_{\text{Th}} \\ \mathbf{0} \end{bmatrix}. \quad (2.12)$$

This allows us to explicitly separate the relevant port variables  $e_{\text{Th}}$  and  $j_{\text{Th}}$  in the equation. Now we assume that our circuit will only be composed of elements coming from the Thévenin sources (ideal voltage sources and resistors), and potentially absorbed multiport linear elements (VCVSs, CCVSs, VCCSs, CCCSs, transformers, and nullors). The lack of independent ideal current sources means that  $\mathbf{i}_s = \mathbf{0}$ . Recalling also (2.8)–(2.10), the MNA system looks like

$$\underbrace{\begin{bmatrix} \mathbf{Y} & \mathbf{A}_1 & \mathbf{A}_2 \\ \mathbf{B}_1 & \mathbf{D}_{11} & \mathbf{D}_{12} \\ \mathbf{B}_2 & \mathbf{D}_{21} & \mathbf{D}_{22} \end{bmatrix}}_{\text{MNA matrix } \mathbf{X}} \begin{bmatrix} \mathbf{v}_n \\ -\mathbf{i} \\ \mathbf{j}_{\text{etc}} \end{bmatrix} = \begin{bmatrix} \mathbf{0} \\ \mathbf{R}^{1-\rho} \mathbf{a} \\ \mathbf{0} \end{bmatrix}. \quad (2.13)$$

Now by inverting  $\mathbf{X}$ , we can solve for  $\begin{bmatrix} \mathbf{v}_n^\top & -\mathbf{i}^\top & \mathbf{j}_{\text{etc}}^\top \end{bmatrix}^\top$

$$\begin{bmatrix} \mathbf{v}_n \\ -\mathbf{i} \\ \mathbf{j}_{\text{etc}} \end{bmatrix} = \mathbf{X}^{-1} \begin{bmatrix} \mathbf{0} \\ \mathbf{R}^{1-\rho} \mathbf{a} \\ \mathbf{0} \end{bmatrix}. \quad (2.14)$$

The middle set of equations relates  $\mathbf{i}$  and  $\mathbf{a}$

$$-\mathbf{i} = \begin{bmatrix} \mathbf{0} & \mathbf{I} & \mathbf{0} \end{bmatrix} \mathbf{X}^{-1} \begin{bmatrix} \mathbf{0} \\ \mathbf{I} \\ \mathbf{0} \end{bmatrix} \mathbf{R}^{1-\rho} \mathbf{a} \quad (2.15)$$

which finally gives us the relationship we've been looking for (2.3)

$$\mathbf{i} = \underbrace{\left( - \begin{bmatrix} \mathbf{0} & \mathbf{I} & \mathbf{0} \end{bmatrix} \mathbf{X}^{-1} \begin{bmatrix} \mathbf{0} \\ \mathbf{I} \\ \mathbf{0} \end{bmatrix} \mathbf{R}^{1-\rho} \right)}_{\text{matrix } \mathbf{Q}} \mathbf{a}. \quad (2.16)$$

Plugging this relationship into (2.4) finally gives us our scattering matrix

$$\mathbf{b} = \mathbf{S}\mathbf{a} \quad , \quad \mathbf{S} = \mathbf{I} + 2\mathbf{R}^\rho \begin{bmatrix} \mathbf{0} & \mathbf{I} & \mathbf{0} \end{bmatrix} \mathbf{X}^{-1} \begin{bmatrix} \mathbf{0} \\ \mathbf{I} \\ \mathbf{0} \end{bmatrix} \mathbf{R}^{1-\rho}. \quad (2.17)$$

### 2.2.3 Stamping

Now that we have an equation for the scattering matrix of any arbitrary  $\mathbf{R}$ -type adaptor, we only need to populate the partitions of  $\mathbf{X}$ : matrices  $\mathbf{Y}$ ,  $\mathbf{A}$ ,  $\mathbf{B}$ , and  $\mathbf{D}$ . Although it is certainly possible to do by

manually inspecting the circuit, satisfying Kirchhoff's Current Laws in the top partition and branch voltage definitions in the bottom two partitions, that can be quite tedious. Luckily the Modified Nodal Analysis framework provides a systematic and even automatic approach to accomplish this called *element stamps* [232], which are also sometimes called “MNA by inspection” [52] and “MNA templates” [57, 58]. The use of element stamps greatly simplifies the process of populating  $\mathbf{X}$ .

First, an index is assigned to each node in the circuit. Second, the contribution of each circuit element is added into  $\mathbf{X}$  one by one. This is done by consulting an element stamp table which shows how each circuit element contributes to  $\mathbf{X}$  according to the electrical values, node indices, matrix locations, values to be added to those locations to satisfy Kirchhoff's laws. Circuit elements which can entirely be described by their admittances only end up contributing to  $\mathbf{Y}$ . Other elements like ideal voltage sources and VCVSs can contribute to  $\mathbf{A}$ ,  $\mathbf{B}$ , and even  $\mathbf{D}$ . These elements must in fact be stamped in the correct order, since the very existence of these elements is what determines the ordering of elements in most of  $\mathbf{X}$ ; for our purposes first the Thévenin voltage sources are added in the same order as the ports are ordered in the relationship  $\mathbf{b} = \mathbf{Sa}$ , then transformers, controlled sources, and nullors (in any order).

The element stamps which we'll need to refer to in this dissertation, including the resistor, the ideal voltage source, the VCVS, and the nullor, are shown in Table 2.1. A full listing of element stamps is given in the literature [232, 52, 233, 57, 58]. Besides the resistor, ideal voltage source, VCVS, and nullor, the most important element stamps for the purposes of deriving the scattering matrices of  $\mathcal{R}$ -type adaptors are those for the CCVS, VCCS, CCCS, and the ideal transformer.

Table 2.1: Some Modified Nodal Analysis Element Stamps.

	resistor	voltage source	VCVS	nullor
symbol				
stamp	$i \begin{bmatrix} i & j \\ G & -G \\ j & G \end{bmatrix}$ next $i \begin{bmatrix} i & j & n \\ -G & -G & 1 \\ j & G & -1 \end{bmatrix} = \begin{bmatrix} \text{source} \\ E \end{bmatrix}$	$j \begin{bmatrix} i & j & n \\ -1 & -1 & -1 \end{bmatrix}$ next $j \begin{bmatrix} i & j & n \\ -1 & -1 & -1 \end{bmatrix} = \begin{bmatrix} \text{source} \\ 0 \end{bmatrix}$	$i \begin{bmatrix} i & j & k & l & n \\ -\mu & \mu & 1 & -1 & -1 \end{bmatrix} = \begin{bmatrix} \text{source} \\ 0 \end{bmatrix}$ next $i \begin{bmatrix} i & j & n \\ -1 & -1 & -1 \end{bmatrix} = \begin{bmatrix} \text{source} \\ 0 \end{bmatrix}$	$j \begin{bmatrix} i & j & n \\ -1 & -1 & -1 \end{bmatrix} = \begin{bmatrix} \text{source} \\ 0 \end{bmatrix}$

A fine point of Modified Nodal Analysis is the existence and implication of the *datum node*. If every node is included in (2.12), then  $\mathbf{X}$  will be singular and hence noninvertible. This is a consequence of the fact that the number of independent Kirchhoff's Circuit Law equations in any circuit is always one less than the number of nodes [234]. To remove the redundant information, any node in the circuit is designated as the *datum node*, and its row and column are removed from the Modified Nodal Analysis equation (2.11). To be clear, *any* node in the circuit can be designated

as the datum node, but to preserve the intuitive interpretation of node voltages, we may often find that the ground node is chosen as the datum node.

### 2.2.4 Adaptation

$\mathcal{R}$ -type adaptors are suitable for use in a Wave Digital Filter tree just like series and parallel adaptors. Recall that in a standard Wave Digital Filter, we always need to ensure that the port facing towards the root of the tree is reflection-free, i.e., the reflected wave at that port does not depend instantaneously on the incident wave at that port. For an  $\mathcal{R}$ -type adaptor, this is accomplished just as with the traditional three-port series and parallel adaptors. For a port  $n$  that we must adapt, we simply solve for the value of  $R_n$  which accomplishes  $s_{nn} = 0$ , where  $s_{nn}$  is the diagonal entry of  $\mathbf{S}$  corresponding to the contribution of the incident wave  $a_n$  to the refected wave  $b_n$ .

## 2.3 Resolving Multiple Linear Nonadaptable Elements

In addition to its utility in accommodating complicated  $\mathcal{R}$ -type topologies and multiport linear elements in feedback, the method of the previous section enables two other contributions of this dissertation. One of those enables a Wave Digital Filter to accommodate multiple *linear* nonadaptable elements grouped together at the root of the tree and is the subject of this section. The other enables a Wave Digital Filter to accommodate multiple *nonlinear* elements grouped together at the root of a tree and is the subject of Chapter 4.

In Chapter 1 we mentioned that the classical Wave Digital Filter approach is only valid for circuits with a single nonadaptable element, such as an ideal current source, ideal voltage source, open circuit, short circuit, switch, or one-port nonlinearity. In this Section we'll propose a method for accommodating multiple linear one-ports at the root of a Wave Digital Filter tree. This method first appeared in [154], where Werner, Dunkel, and Germain used it to model the Vibrato/Chorus circuit from the Hammond Organ.

In the literature, issues of accommodating multiple linear elements have not received a lot of attention. This may be because the issue can often be sidestepped (at the cost of introducing some error) in one of two ways. One tactic is to alter the reference circuit so that these nonadaptable elements become adaptable. It is common to approximate ideal voltage sources as resistive voltage sources with small series resistances and to approximate ideal current sources as resistive current sources with large parallel resistances. The same principle can be used to approximate short circuits or the closed state of switches as small resistances and to approximate open circuits or the open state of switches as large resistances. A second tactic is to assemble the Wave Digital Filter structure as if the elements were adaptable, and then introduce fictitious unit delays to resolve the delay-free loops through the nonadaptable elements. Fettweis used this approach [88] before developing reflection-free ports [91], and it is still common in Virtual Analog [235, 236, 175]. Of course, altering the

reference circuit through these tactics introduces error and can have adverse effects on stability.

We'll start by explaining how the problem can be framed, i.e., how the global Wave Digital Filter block diagram can be derived (§2.3.1). This generates a global structure with an  $\mathcal{R}$ -type topology at the root interfacing the multiple nonadaptable linear elements to the rest of the circuit. An exact method for resolving this structure is presented (§2.3.2). Finally, a case study applying this method to the Hammond Organ Vibrato/Chorus circuit [154] is reviewed briefly in §2.3.3.

### 2.3.1 Configure Structure Using Replacement Graphs

To begin, we must configure the global structure of the simulation. The goal of this setup is to group all of the nonadaptable linear elements in one part of the simulation while still decomposing the circuit into the smallest pieces as possible, respecting the modularity principle of Wave Digital Filters. To group the nonadaptable linear elements together, we return to the replacement graph technique of Fränken, Ochs, and Ochs (§2.1.5). In this context, rather than using a replacement graph for each multiport linear element, one single replacement graph is introduced for the collection of all nonadaptable linear elements.

This yields a global structure with all nonadaptable linear elements grouped at the top of the tree, an  $\mathcal{R}$ -type adaptor which interfaces these nonadaptable linear elements to the rest of the circuit, and a collection of one or more Wave Digital Filter trees below. These Wave Digital Filter trees may contain any normal linear Wave Digital Filter elements and can be handled with standard techniques. These trees may even contain other  $\mathcal{R}$ -type adaptors each with an adapted upwards-facing port, which can be handled with the proposed method from the previous section (2.2).

The combination of the nonadaptable elements at the root and the  $\mathcal{R}$ -type adaptor that interfaces them to the Wave Digital Filter trees cannot be handled with standard techniques, however. The reason is that the  $\mathcal{R}$ -type adaptor has more than one upwards-facing port and can hence not be adapted. Therefore it and everything above it cannot be rendered realizable by standard techniques, i.e., choosing proper port resistances. Resolving this combination is at the crux of the proposed technique.

### 2.3.2 Resolve Root

The  $\mathcal{R}$ -type adaptor in this context has “external” ports with incident waves  $\mathbf{a}_e$  and reflected waves  $\mathbf{b}_e$  facing the rest of the circuit and “internal” ports with incident waves  $\mathbf{a}_i$  and reflected waves  $\mathbf{b}_i$  facing the nonadaptable linear elements, related by the scattering relationship

$$\begin{bmatrix} \mathbf{b}_i \\ \mathbf{b}_e \end{bmatrix} = \begin{bmatrix} \mathbf{S}_{11} & \mathbf{S}_{12} \\ \mathbf{S}_{21} & \mathbf{S}_{22} \end{bmatrix} \begin{bmatrix} \mathbf{a}_i \\ \mathbf{a}_e \end{bmatrix} \quad (2.18)$$

The scattering matrix values are derived using the proposed Modified-Nodal-Analysis-based method from §2.2. In this context, however, since the  $\mathcal{R}$ -type adaptor has more than one upwards-facing port, we cannot hope to adapt those ports. So, the upwards facing port resistances are completely arbitrary; we arbitrarily always choose  $1\text{k}\Omega$ .

The vector of nonadaptable linear elements relates the incident waves  $\mathbf{a}_r$  and inputs  $\mathbf{x}_r$  to reflected waves  $\mathbf{b}_r$  by

$$\mathbf{b}_r = \Phi \mathbf{a}_r + \Psi \mathbf{x}_r, \quad (2.19)$$

where  $\Phi$  and  $\Psi$  embody the wave-domain behavior of the linear elements.  $\mathbf{a}_r$  and  $\mathbf{b}_r$  are related to the  $\mathbf{a}_i$  and  $\mathbf{b}_i$  by

$$\mathbf{a}_r = \mathbf{b}_i \quad \text{and} \quad \mathbf{a}_i = \mathbf{b}_r. \quad (2.20)$$

This can be represented in the signal-flow sense by Figure 2.11a. Notice that this structure is not realizable due to a delay-free loop (in red).

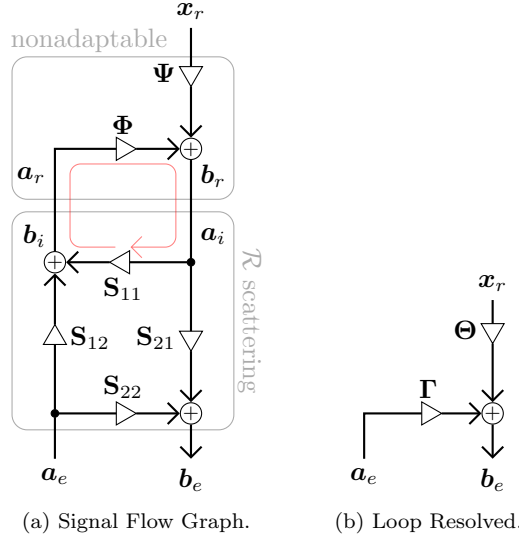


Figure 2.11: Framework Signal Flow Graphs, Derived and Resolved.  $\mathbf{a}_E$  is supplied by and  $\mathbf{b}_E$  delivered to classical WDF subtrees below.

Combining (2.18), (2.19), and (2.20) and solving for  $\mathbf{b}_e$  yields<sup>5</sup>

$$\begin{aligned} \mathbf{b}_e &= \Gamma \mathbf{a}_e + \Theta \mathbf{x}_r \quad \text{with} \\ \Gamma &= \mathbf{S}_{21} (\mathbf{I} - \Phi \mathbf{S}_{11})^{-1} \mathbf{S}_{12} + \mathbf{S}_{22} \\ \Theta &= \mathbf{S}_{21} (\mathbf{I} - \Phi \mathbf{S}_{11})^{-1} \Psi. \end{aligned} \quad (2.21)$$

Now, given a set vector of incident waves  $\mathbf{a}_e$  supplied by the trees below the  $\mathcal{R}$ -type adaptor and a

---

<sup>5</sup>Thank you to Jingjie Zhang for catching a typographical error in [154].

vector of inputs  $\mathbf{x}_r$ , the set of reflected waves can immediately be found using (2.21). This is shown in the signal flow sense in Figure 2.11b.

### 2.3.3 Example Application

An example application of this approach is given in [154], where Werner, Dunkel, and Germain model the Hammond Organ Vibrato/Chorus circuit using the Wave Digital Filter approach. This circuit has two nonadaptable linear elements, an ideal voltage source and an ideal switch. The circuit, a rearranged version highlighting the circuit's underlying topology, and its block diagram representation as a Wave Digital Filter are shown in Figure 2.12—full details of this modeling approach are given in [154].

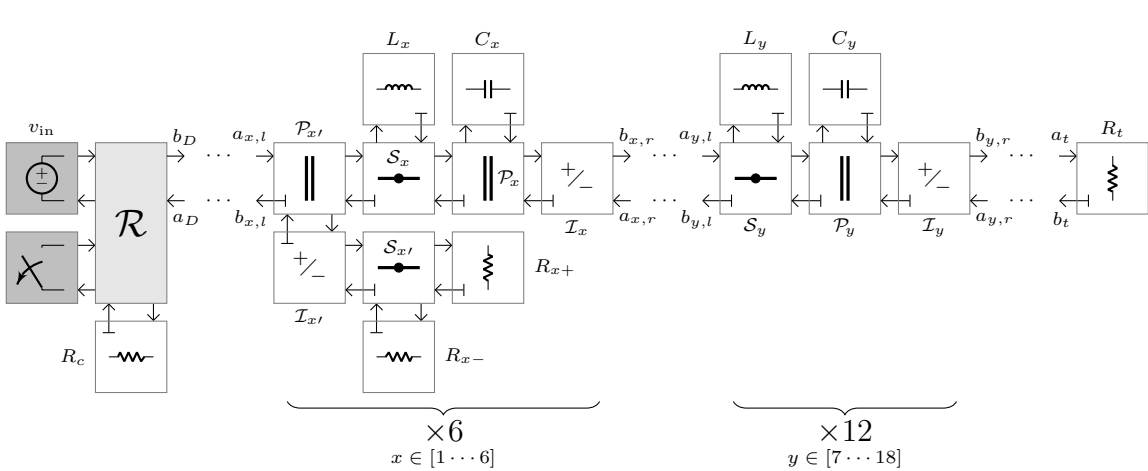
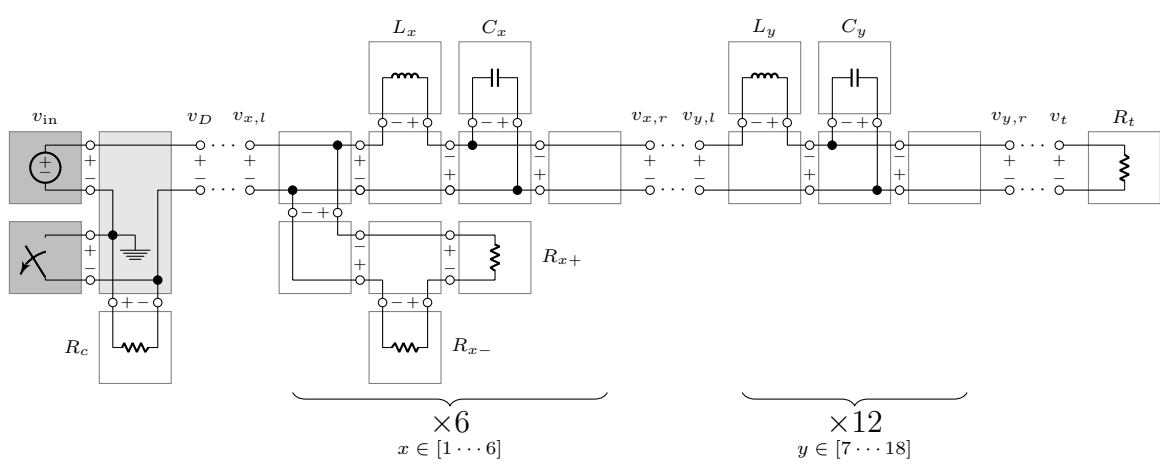
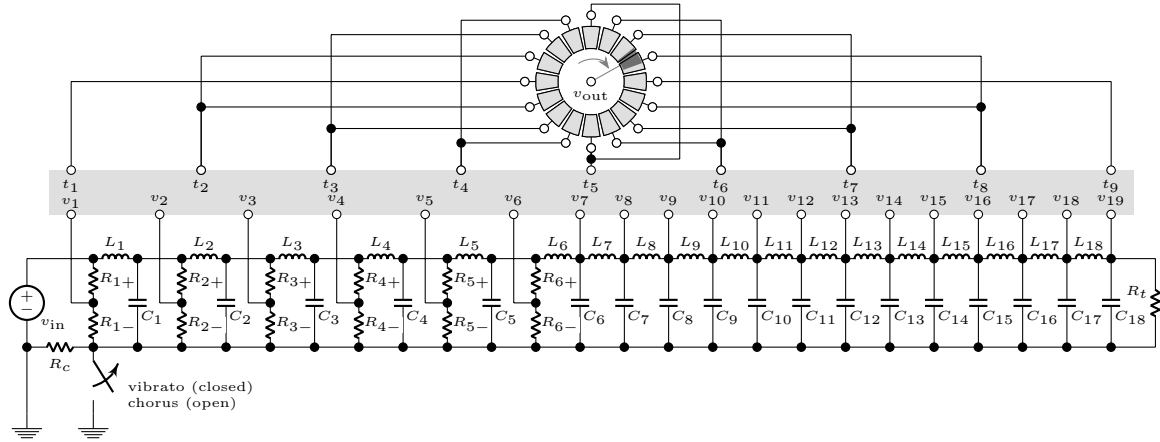


Figure 2.12: Overview of Modeling Approach to Hammond Organ Vibrato/Chorus Circuit.

## 2.4 Case Studies

In this Section, case studies demonstrating the application of the proposed approach (§2.2) to circuits with complicated topologies and multiport elements in feedback are shown. The examples are all simplified models of the Nonlinear Bridged-T Resonator from the TR-808 Bass Drum. First we'll start with a Passive Bridged-T Filter (§2.4.1). Adding an operational amplifier, we'll study two versions of the basic linear Bridged-T Resonator (§2.4.2), one where the op-amp is modeled using a nullor and one where it is modeled using a simple linear macromodel. Finally, we'll study a version of the Bridged-T Resonator which includes an additional op-amp feedback buffer (§2.4.3), again considering both nullor and the macromodel varieties. For the first three of these case studies we'll show experimental verification against theoretical continuous-time transfer functions, confirming the validity of the proposed approach.

### 2.4.1 Passive Bridged-T Filter

Bridged-T networks (Figure 2.13a) are passive networks used in measurement of resistance at radio frequencies [237] and as a component of sinusoidal oscillators [238]. They are also used in various voices of the TR-808, including the Bass Drum. Here we begin by studying a Passive Bridged-T Filter outside of the context of the op-amp. This Passive Bridged-T Filter, shown in Figure 2.13b is formed by adding a voltage source  $v_{in}$  and a large load resistor  $R_L$  to the two resistors  $R_1$  and  $R_2$  and the two capacitors  $C_1$  and  $C_2$  of the Bridged-T Network in Figure 2.13a.

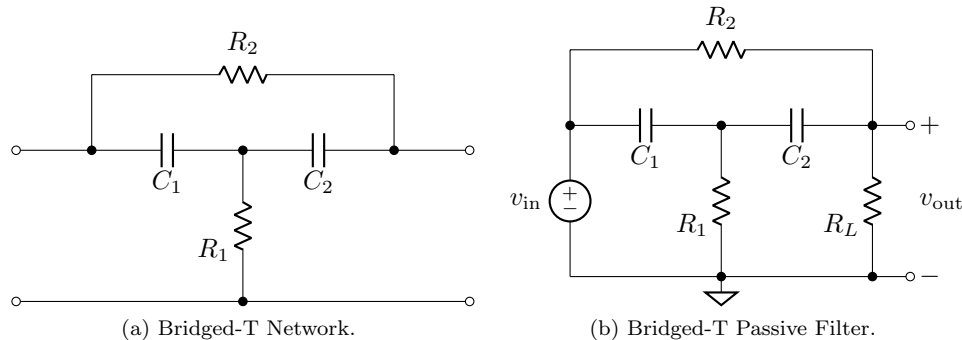


Figure 2.13: Passive Bridged-T Circuit.

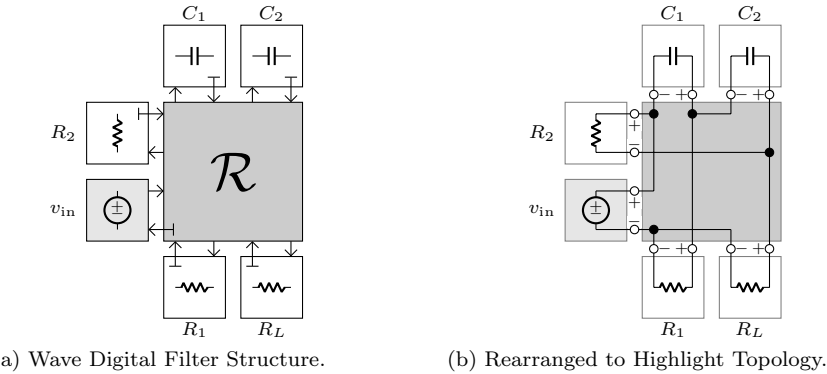
Since Bridged-T Networks are used in a variety of TR-808 voices, we'll study simplified versions of all of these voices at the same time. The relationship between the component values of each of the voices and the generic Bridged-T Filter are given in Table 2.2. In all cases the load resistor is assumed to have a value of  $R_L = 1 \text{ M}\Omega$ . The Tom and Conga voices have a rather complicated arrangement of resistors, a potentiometer, and a diode in place of  $R_1$ . For this study we linearize the

diode around dc to arrive at a range of values (depending on the tuning potentiometer setting) of  $R_1$  for the Toms and Congas. Details of this derivation are given in Appendix §C.

Table 2.2: Bridged-T Resonator Values for Various TR-808 Voices.

TR-808 Voice		$R_1$ Name	Value	$R_2$ Name	Value	$C_1$ Name	Value	$C_2$ Name	Value
Bass Drum		$R_{165} + R_{166}$	53.8 kΩ	$R_{167}$	1 MΩ	$C_{41}$	0.015 μF	$C_{42}$	0.015 μF
Snare Drum (low)		$R_{196}$	680 Ω	$R_{197}$	820 kΩ	$C_{58}$	0.027 μF	$C_{59}$	0.027 μF
Snare Drum (high)		$R_{195}$	2.2 kΩ	$R_{198}$	1 MΩ	$C_{60}$	0.0068 μF	$C_{61}$	0.0068 μF
Low Tom		$R_{eq,low}$	333.3–500 Ω	$R_{228}$	820 kΩ	$C_{76}$	0.056 μF	$C_{77} + C_{78}$	0.059 μF
Low Conga		$R_{eq,low}$	333.3–500 Ω	$R_{228}$	820 kΩ	$C_{76}$	0.056 μF	$C_{78}$	0.012 μF
Mid Tom		$R_{eq,mid}$	333.3–500 Ω	$R_{257}$	820 kΩ	$C_{89} + C_{90}$	0.0352 μF	$C_{91} + C_{92}$	0.039 μF
Mid Conga		$R_{eq,mid}$	333.3–500 Ω	$R_{257}$	820 kΩ	$C_{90}$	0.027 μF	$C_{92}$	0.012 μF
High Tom		$R_{eq,high}$	333.3–500 Ω	$R_{284}$	820 kΩ	$C_{103}$	0.027 μF	$C_{104} + C_{105}$	0.0276 μF
High Conga		$R_{eq,high}$	333.3–500 Ω	$R_{284}$	820 kΩ	$C_{103}$	0.027 μF	$C_{105}$	0.0056 μF
Rimshot / Clave (low)		$R_{315}$	5.6 kΩ	$R_{316}$	1 MΩ	$C_{116}$	0.0047 μF	$C_{115}$	0.0047 μF
Clave (high)		$R_{312}$	1 kΩ	$R_{308}$	820 kΩ	$C_{119}$	0.0022 μF	$C_{117}$	0.0022 μF

To create a Wave Digital Filter from the Bridged-T Filter in Figure 2.13b, we begin by applying the process of Fränken *et al.* [197, 198] and arrive at the Wave Digital Filter structure shown in Figure 2.14a. A rearranged version of the reference circuit that highlights how this structure arises is shown in Figure 2.14b.



(a) Wave Digital Filter Structure.

(b) Rearranged to Highlight Topology.

Figure 2.14: Passive Bridged-T Filter: Rearranged to Highlight Topology, and Wave Digital Filter Structure.

The explicit tree structure of this Wave Digital Filter simulation is shown in Figure 2.15.

For the Wave Digital Filter, we'll use the standard bilinear transform for discretizing the capacitors. In Figure 2.14a, the only Wave Digital Filter building block which does not have a classical realization is the  $\mathcal{R}$ -type adaptor. We denote the six ports of the  $\mathcal{R}$ -type adaptors by the letters  $A, B, C, D, E$ , and  $F$ , proceeding clockwise from the port connected to  $v_{in}$ . So, these ports have port voltages  $\mathbf{v} = [v_A \ v_B \ v_C \ v_D \ v_E \ v_F]^T$ , port currents  $\mathbf{i} = [i_A \ i_B \ i_C \ i_D \ i_E \ i_F]^T$ , incident waves  $\mathbf{a} = [a_A \ a_B \ a_C \ a_D \ a_E \ a_F]^T$ , reflected waves  $\mathbf{b} = [b_A \ b_B \ b_C \ b_D \ b_E \ b_F]^T$ , and

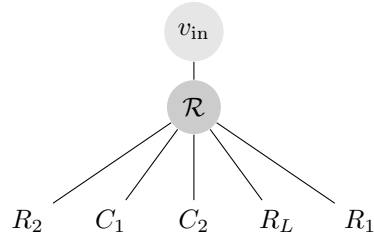


Figure 2.15: Connection Tree for Passive Bridged-T Filter.

a diagonal port resistance matrix  $\mathbf{R} = \text{diag}\left(\begin{bmatrix} R_A & R_B & R_C & R_D & R_E & R_F \end{bmatrix}\right)$ . To find its scattering matrix, we apply the proposed method of §2.2 to find the  $6 \times 6$  matrix  $\mathbf{S}$  describing  $\mathbf{b} = \mathbf{Sa}$ . This starts by adding a Thévenin equivalent to each port and labeling each of the 10 nodes in the circuit as shown in Figure 2.16.

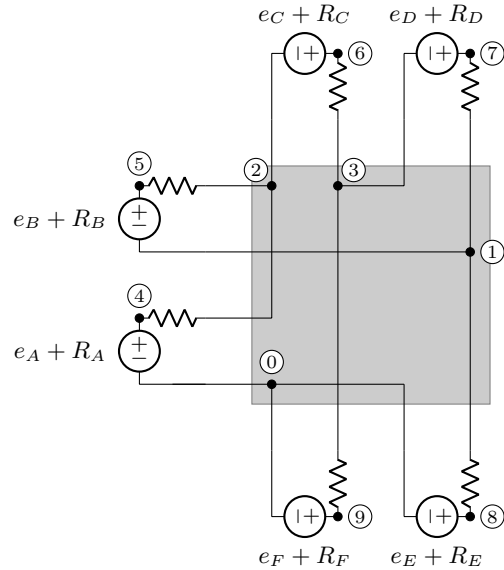


Figure 2.16: Bridged-T Filter, Thévenin Equivalents Attached.

The element stamp method is used to form a system of equations describing the circuit in Figure 2.16; the results of this process are shown in Figure 2.17. Note that here the datum node has not yet been removed. Plugging the Modified Nodal Analysis matrix into (2.17) yields the scattering matrix, which is adapted by choosing a value of  $R_A$  that sets  $s_{AA} = 0$ .

To show that this discretization approach has worked, we'll compare against the theoretical transfer function of the Passive Bridged-T Filter. The continuous-time transfer function of the

$$\begin{array}{c|ccccc|ccccc|cccc}
 & \textcircled{0} & \textcircled{1} & \textcircled{2} & \textcircled{3} & \textcircled{4} & \textcircled{5} & \textcircled{6} & \textcircled{7} & \textcircled{8} & \textcircled{9} & A & B & C & D & E & F \\
 \textcircled{0} & 0 & 0 & 0 & 0 & 0 & 0 & 0 & 0 & 0 & -1 & 0 & 0 & 0 & -1 & -1 \\
 \textcircled{1} & 0 & G_D + G_E & 0 & 0 & 0 & 0 & -G_D - G_E & 0 & 0 & 0 & -1 & 0 & 0 & 0 & 0 & 0 \\
 \textcircled{2} & 0 & 0 & G_A + G_B & 0 & -G_A - G_B & 0 & 0 & 0 & 0 & 0 & 0 & -1 & 0 & 0 & 0 & 0 \\
 \textcircled{3} & 0 & 0 & 0 & G_C + G_F & 0 & 0 & -G_C & 0 & 0 & -G_F & 0 & 0 & -1 & 0 & 0 & 0 \\
 \textcircled{4} & 0 & 0 & -G_A & 0 & G_A & 0 & 0 & 0 & 0 & 1 & 0 & 0 & 0 & 0 & 0 & 0 \\
 \textcircled{5} & 0 & 0 & -G_B & 0 & 0 & G_B & 0 & 0 & 0 & 0 & 1 & 0 & 0 & 0 & 0 & 0 \\
 \textcircled{6} & 0 & 0 & 0 & -G_C & 0 & 0 & G_C & 0 & 0 & 0 & 0 & 0 & 1 & 0 & 0 & 0 \\
 \textcircled{7} & 0 & -G_D & 0 & 0 & 0 & 0 & G_D & 0 & 0 & 0 & 0 & 0 & 0 & 1 & 0 & 0 \\
 \textcircled{8} & 0 & -G_E & 0 & 0 & 0 & 0 & 0 & G_E & 0 & 0 & 0 & 0 & 0 & 0 & 1 & 0 \\
 \textcircled{9} & 0 & 0 & 0 & -G_F & 0 & 0 & 0 & 0 & G_F & 0 & 0 & 0 & 0 & 0 & 0 & 1 & 0 \\
 \hline
 A & -1 & 0 & 0 & 0 & 1 & 0 & 0 & 0 & 0 & 0 & 0 & 0 & 0 & 0 & 0 & 0 & 0 \\
 B & 0 & -1 & 0 & 0 & 0 & 1 & 0 & 0 & 0 & 0 & 0 & 0 & 0 & 0 & 0 & 0 & 0 \\
 C & 0 & 0 & -1 & 0 & 0 & 0 & 1 & 0 & 0 & 0 & 0 & 0 & 0 & 0 & 0 & 0 & 0 \\
 D & 0 & 0 & 0 & -1 & 0 & 0 & 0 & 1 & 0 & 0 & 0 & 0 & 0 & 0 & 0 & 0 & 0 \\
 E & -1 & 0 & 0 & 0 & 0 & 0 & 0 & 1 & 0 & 0 & 0 & 0 & 0 & 0 & 0 & 0 & 0 \\
 F & -1 & 0 & 0 & 0 & 0 & 0 & 0 & 0 & 1 & 0 & 0 & 0 & 0 & 0 & 0 & 0 & 0
 \end{array} = \begin{bmatrix} v_0 \\ v_1 \\ v_2 \\ v_3 \\ v_4 \\ v_5 \\ v_6 \\ v_7 \\ v_8 \\ v_9 \\ j_A \\ j_B \\ j_C \\ j_D \\ j_E \\ j_F \end{bmatrix} = \begin{bmatrix} 0 \\ 0 \\ 0 \\ 0 \\ 0 \\ 0 \\ 0 \\ 0 \\ 0 \\ 0 \\ e_A \\ e_B \\ e_C \\ e_D \\ e_E \\ e_F \end{bmatrix} \quad (2.22)$$

Figure 2.17: Forming MNA matrix  $\mathbf{X}$ .

passive Bridged-T Filter is

$$H_{\text{PBT}}(s) = \frac{V_{\text{out}}(s)}{V_{\text{in}}(s)} = \frac{(R_1 R_2 C_1 C_2) s^2 + (R_1 (C_1 + C_2)) s + 1}{(R_1 R_2 C_1 C_2) s^2 + \left(R_1 \left(\frac{R_2}{R_L} + 1\right) (C_1 + C_2) + R_2 C_2\right) s + \left(\frac{R_2}{R_L} + 1\right)}. \quad (2.23)$$

The derivation of this ideal response is given in Appendix §C.1.

The continuous-time magnitude responses of each of the Passive Bridged-T Filters with component values given in Table 2.2 are shown in Figure 2.18. The continuous-time magnitude responses are found by evaluating the transfer function (2.23) along the  $j\Omega$  axis. The magnitude response of the Wave Digital Filter is found by measuring a 1 s long impulse response which has decayed “sufficiently to zero”, and taking the magnitude of its frequency response. There is good agreement between the theoretical responses predicted by (2.23) and the Wave Digital Filter, although it is possible to see some of the expected (due to the Bilinear Transform) frequency warping at high frequencies. Notice that these filters are notch filters, the opposite of the behavior we’ll see once the Bridged-T Network is placed in the negative feedback path of an op-amp.

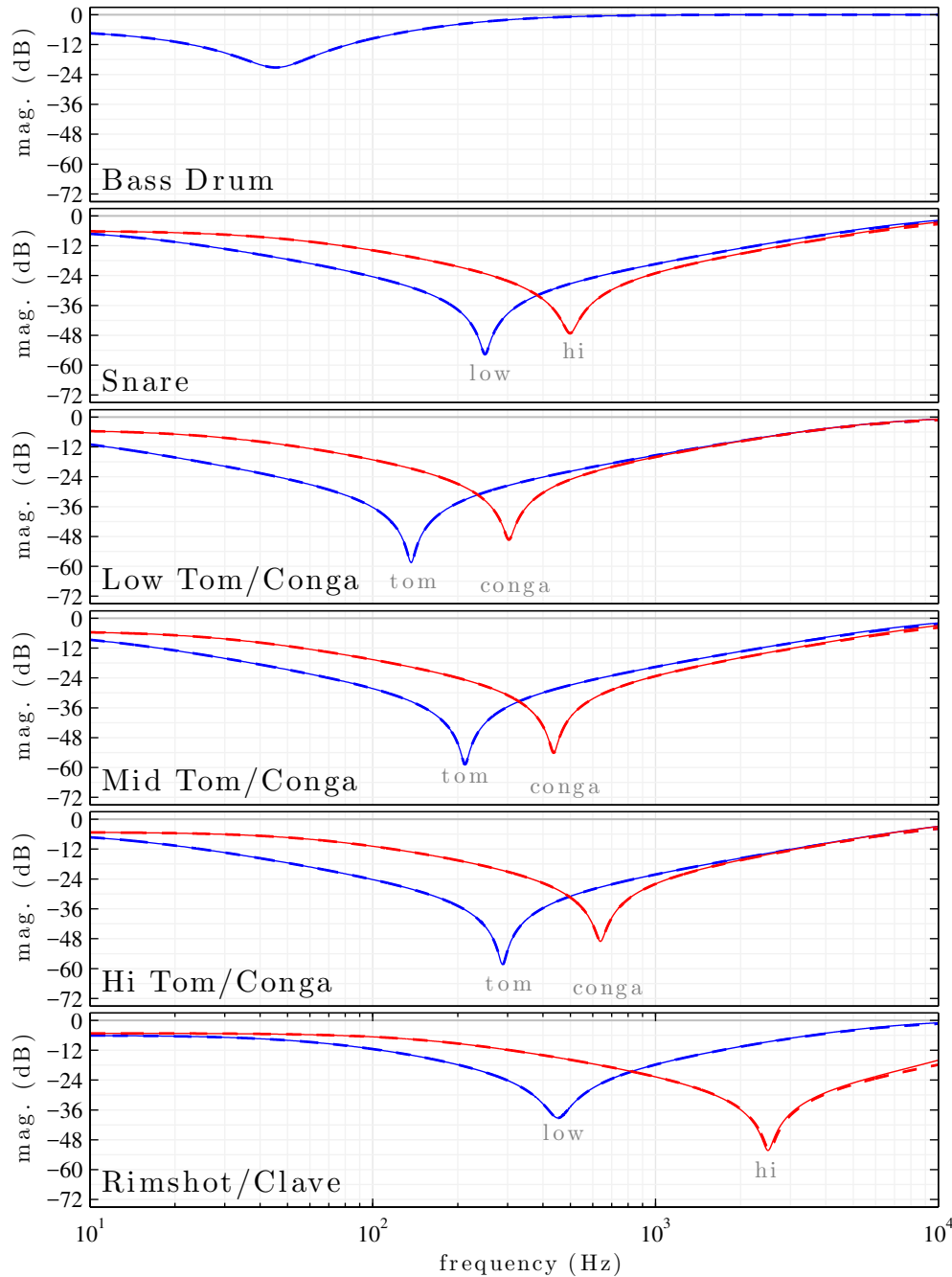


Figure 2.18: Various Passive Bridged-T Filter Magnitude Responses. Tom and Congas are assumed to be tuned to their lowest setting (see Appendix §C). Dashed lines are ideal continuous-time magnitude responses and solid lines are Wave Digital Filter responses.

### 2.4.2 Bridged-T Resonator

As a second case study, we consider a Bridged-T Network in the negative feedback path of an op amp, as shown in Figure 2.19a. We call this circuit the “Bridged-T Resonator” since it creates a resonant bandpass filter. This is a simplified version of the circuits used in the TR-808 and other analog drum machines to make decaying sinusoids mimicking drum sounds. The most notable example for our purposes is the Bass Drum circuit, although we’ll study Bridged-T Resonators using circuit values from all of the TR-808’s relevant voice circuits.

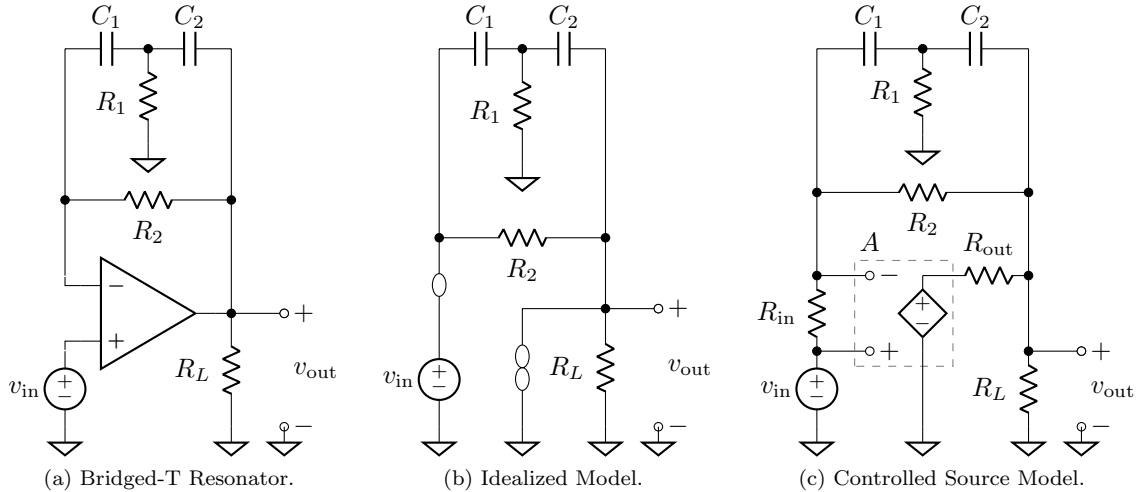


Figure 2.19: Bridged-T Resonator Schematic, Nullor- and Controlled-Source-Based Models.

Since the circuit includes an operational amplifier, we need to choose a model for the operational amplifier before proceeding. In this case study we’ll consider two cases: the idealized case where the operational amplifier is replaced by a nullor (§2.4.2) and a case using a simple op-amp macromodel involving a finite-gain VCVS and input and output resistances (§2.4.2). More complicated op-amp macromodels are certainly possible; a study on the Bridged-T Resonator that uses a very complex linear macromodel involving input offset voltage, input bias currents, input offset current, common-mode and differential impedances, common-mode and differential gains, dominant pole / gain-bandwidth effect, and output resistance is given in [179]. More complicated nonlinear macromodels which include nonlinear behaviors like slew-rate limiting and transfer, input, and output nonlinearities [239] are often included in op-amp macromodels alongside device-level models of differential transistor input stage [216].

### Ideal Op-amp

We'll start with the ideal case, where the operational amplifier is replaced by a nullor. This circuit is shown in Figure 2.19b. To create a Wave Digital Filter from the Bridged-T Resonator, we begin by applying the process of Fränken *et al.* [197, 198] and arrive at the Wave Digital Filter structure shown in Figure 2.20a. Notice that the two ports of the nullor are constrained to the same adaptor; this is accomplished by using the replacement graph technique of [198]. A rearranged version of the reference circuit that highlights how this structure arises is shown in Figure 2.20b.

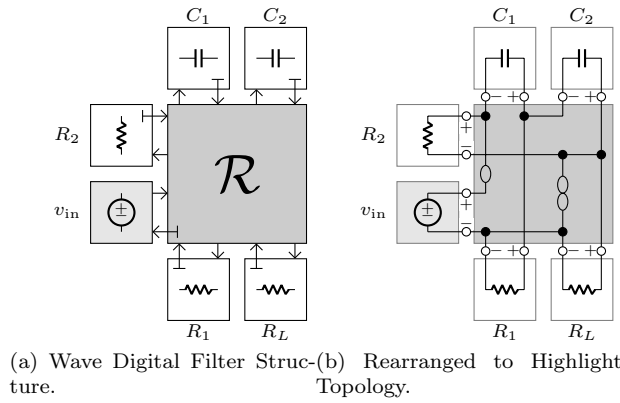


Figure 2.20: Idealized (Nullor-Based) Bridged-T Resonator Circuit: Rearranged to Highlight Topology, and Wave Digital Filter Structure.

The explicit tree structure of this Wave Digital Filter simulation is shown in Figure 2.21.

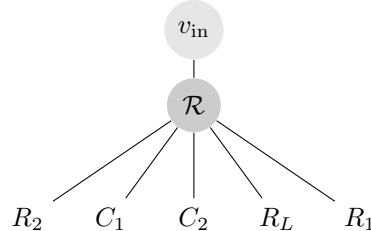


Figure 2.21: Connection Tree for Idealized (Nullor-Based) Bridged-T Resonator Circuit.

Again, to find its scattering matrix, we apply the proposed method of §2.2 to find the  $6 \times 6$  matrix  $\mathbf{S}$  describing  $\mathbf{b} = \mathbf{Sa}$ . This starts by adding a Thévenin equivalent to each port and labeling each of the 11 nodes in the circuit as shown in Figure 2.22.

The element stamp method is used to form a system of equations describing the circuit in Figure 2.22; the results of this process are shown in Figure 2.23. Note that here the datum node has not yet been removed. Plugging the Modified Nodal Analysis matrix into (2.17) yields the scattering matrix, which is adapted by choosing a value of  $R_A$  that sets  $s_{AA} = 0$ .

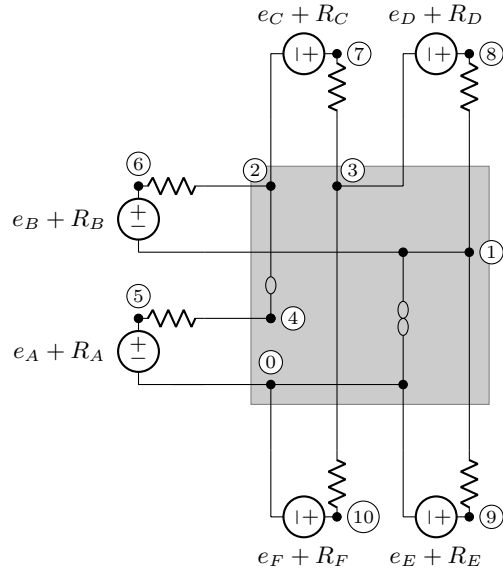


Figure 2.22: Idealized (Nullor-Based) Bridged-T Resonator, Thévenin Equivalents Attached.

$$\begin{array}{ccccccccc}
\textcircled{0} & 0 & 0 & 0 & 0 & 0 & 0 & 0 & 0 \\
\textcircled{1} & 0 & G_D + G_E & 0 & 0 & 0 & 0 & -G_D - G_E & 0 \\
\textcircled{2} & 0 & 0 & G_B & 0 & 0 & 0 & -G_B & 0 \\
\textcircled{3} & 0 & 0 & 0 & G_C + G_F & 0 & 0 & -G_C & 0 \\
\textcircled{4} & 0 & 0 & 0 & 0 & G_A - G_A & 0 & 0 & 0 \\
\textcircled{5} & 0 & 0 & 0 & 0 & -G_A & G_A & 0 & 0 \\
\textcircled{6} & 0 & 0 & -G_B & 0 & 0 & 0 & G_B & 0 \\
\textcircled{7} & 0 & 0 & 0 & -G_C & 0 & 0 & 0 & G_C \\
\textcircled{8} & 0 & -G_D & 0 & 0 & 0 & 0 & G_D & 0 \\
\textcircled{9} & 0 & -G_E & 0 & 0 & 0 & 0 & 0 & G_E \\
\textcircled{10} & 0 & 0 & 0 & -G_F & 0 & 0 & 0 & 0
\end{array}
\quad
\begin{array}{ccccccccc}
A & -1 & 0 & 0 & 0 & 1 & 0 & 0 & 0 \\
B & 0 & -1 & 0 & 0 & 0 & 1 & 0 & 0 \\
C & 0 & 0 & -1 & 0 & 0 & 0 & 1 & 0 \\
D & 0 & 0 & 0 & -1 & 0 & 0 & 0 & 1 \\
E & -1 & 0 & 0 & 0 & 0 & 0 & 0 & 0 \\
F & -1 & 0 & 0 & 0 & 0 & 0 & 0 & 0 \\
\text{nul} & 0 & 0 & 1 & 0 & -1 & 0 & 0 & 0
\end{array}
\quad
\begin{array}{ccccccccc}
A & -1 & 0 & 0 & 0 & -1 & -1 & -1 \\
B & 0 & -1 & 0 & 0 & 0 & 0 & 1 \\
C & 0 & 0 & -1 & 0 & 0 & 0 & 0 \\
D & 0 & 0 & 0 & -1 & 0 & 0 & 0 \\
E & 0 & 0 & -1 & 0 & 0 & 0 & 0 \\
F & 0 & 0 & 0 & 0 & -1 & 0 & 0 \\
\text{nor} & 0 & 0 & 0 & 0 & 0 & 0 & 0
\end{array}
\quad
\begin{array}{c}
v_0 \\
v_1 \\
v_2 \\
v_3 \\
v_4 \\
v_5 \\
v_6 \\
v_7 \\
v_8 \\
v_9 \\
v_{10}
\end{array}
\quad
\begin{array}{c}
0 \\
0 \\
0 \\
0 \\
0 \\
0 \\
0 \\
0 \\
0 \\
0 \\
0
\end{array}
\quad
\begin{array}{c}
e_A \\
e_B \\
e_C \\
e_D \\
e_E \\
e_F \\
0
\end{array}
\quad
\begin{array}{c}
= \\
(2.24)
\end{array}$$

Figure 2.23: Forming MNA matrix  $\mathbf{X}$ .

To show that this discretization approach has worked, we'll compare against the theoretical transfer function of the Bridged-T Resonator. The continuous-time transfer function of the Bridged-T Resonator is

$$H_{\text{BTR}}(s) = \frac{V_{\text{out}}(s)}{V_{\text{in}}(s)} = \frac{(R_1 R_2 C_1 C_2) s^2 + (R_1 (C_1 + C_2) + R_2 C_1) s + 1}{(R_1 R_2 C_1 C_2) s^2 + (R_1 (C_1 + C_2)) s + 1}. \quad (2.25)$$

The response is characterized by three parameters, center frequency  $f_c$ , quality factor  $Q$ , and peak of the magnitude response  $H_{\text{peak}}$ , which are given in terms of the circuit values  $R_1$ ,  $R_2$ ,  $C_1$ , and  $C_2$  by

$$f_c = \frac{1}{2\pi\sqrt{R_1 R_2 C_1 C_2}} \quad (2.26)$$

$$H_{\text{peak}} = \frac{R_1 (C_1 + C_2) + R_2 C_1}{R_1 (C_1 + C_2)} = 1 + \frac{R_2 C_1}{R_1 (C_1 + C_2)} \quad (2.27)$$

$$Q = \frac{\sqrt{R_2/R_1}}{\sqrt{C_1/C_2} + \sqrt{C_2/C_1}}. \quad (2.28)$$

A more detailed derivation of this response and its properties is given in Appendix §C.2.

The continuous-time magnitude responses of each of the Bridged-T Resonators with component values given in Table 2.2 are shown in Figure 2.24. The continuous-time magnitude responses are found by evaluating the transfer function (2.25) along the  $j\Omega$  axis. The magnitude response of the Wave Digital Filter is found by measuring a 1 s long impulse response which has decayed “sufficiently to zero”, and taking the magnitude of its frequency response. There is good agreement between the theoretical responses predicted by (2.25) and the Wave Digital Filter, although it is possible to see some of the expected (due to the Bilinear Transform) frequency warping at high frequencies. Notice that these are all bandpass responses.

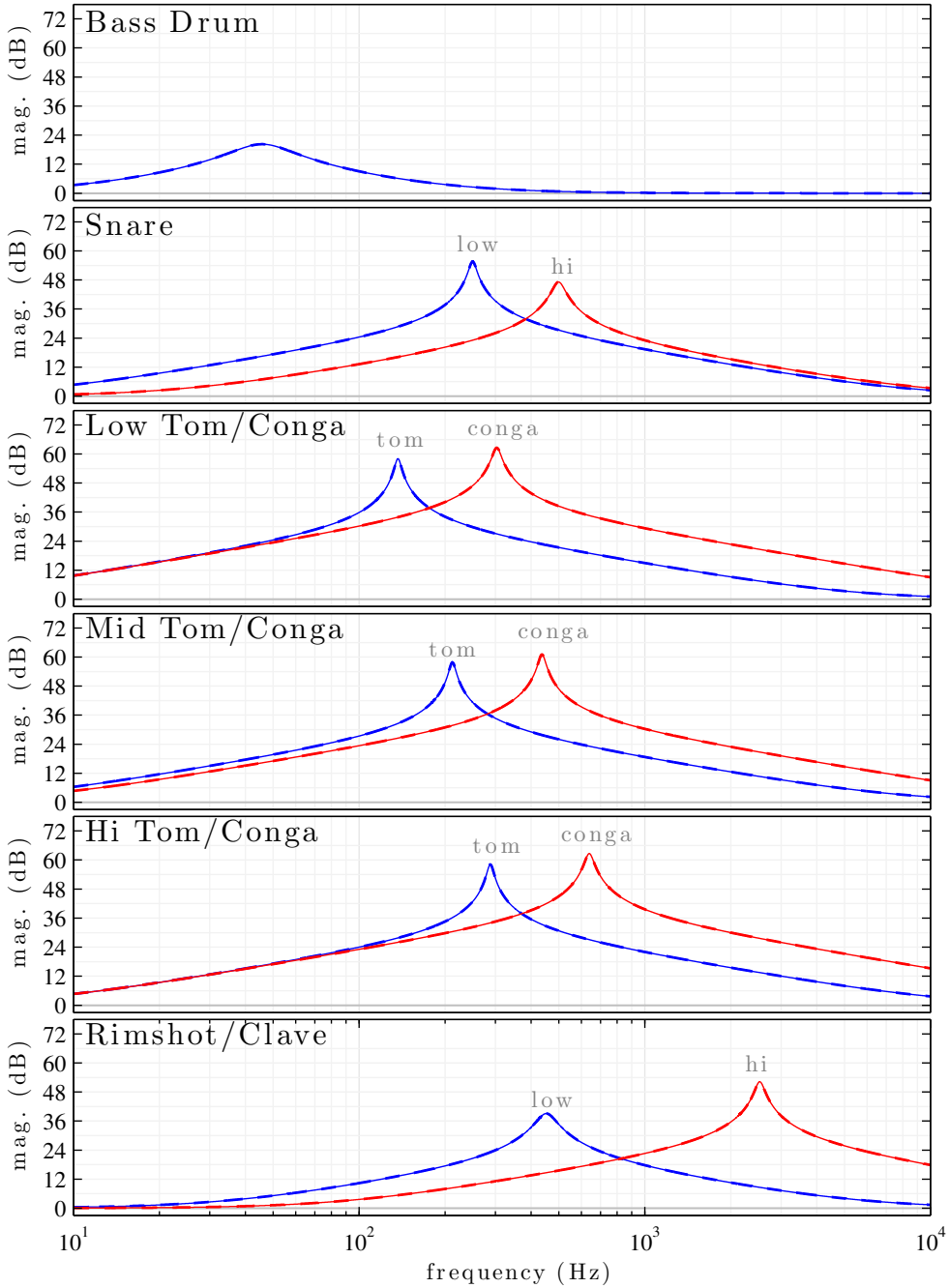


Figure 2.24: Various Bridged-T Resonator Magnitude Responses. Tom and Congas are assumed to be tuned to their lowest setting (see Appendix §C). Dashed lines are ideal continuous-time magnitude responses and solid lines are Wave Digital Filter responses.

### Macromodel

The same approach is taken to model a version of the Bridged-T Resonator, shown in Figure 2.19c, which uses a simple macromodel to model a non-ideal operational amplifier. To give an overview of this approach, consider the Wave Digital Filter structure found using [198] (Figure 2.25a), a rearranged version of the reference circuit emphasizing that underlying topology (Figure 2.25b), and the explicit tree structure of the resulting Wave Digital Filter (Figure 2.26). Notice that the two ports of the VCVS are constrained to the same adaptor; this is accomplished by using the replacement graph technique of [198].

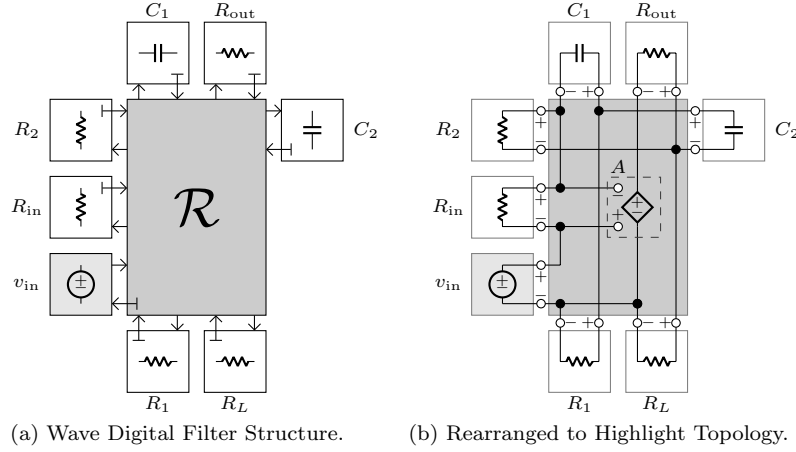


Figure 2.25: Non-Ideal (Controlled-Source-Based) Bridged-T Resonator Circuit: Rearranged to Highlight Topology, and Wave Digital Filter Structure.

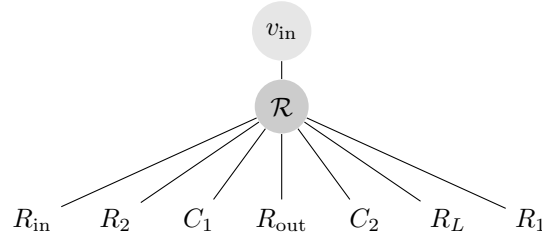


Figure 2.26: Connection Tree for Non-Ideal (Controlled-Source-Based) Bridged-T Resonator Circuit.

### 2.4.3 Bridged-T Resonator With Feedback

In the context of the actual drum machine circuit, these Bridged-T Resonators do not always appear in isolation. In the bass drum, toms/congas, and rimshot/clave circuit they appear in feedback with active op-amp based networks. Here we consider a version of the Bridged-T Resonator that is even

closer to the real circuit from the TR-808 Bass Drum which incorporates an op-amp based feedback stage, shown in Figure 2.27. Here we'll consider the component values used in the TR-808 Bass Drum, shown in Table 2.3.

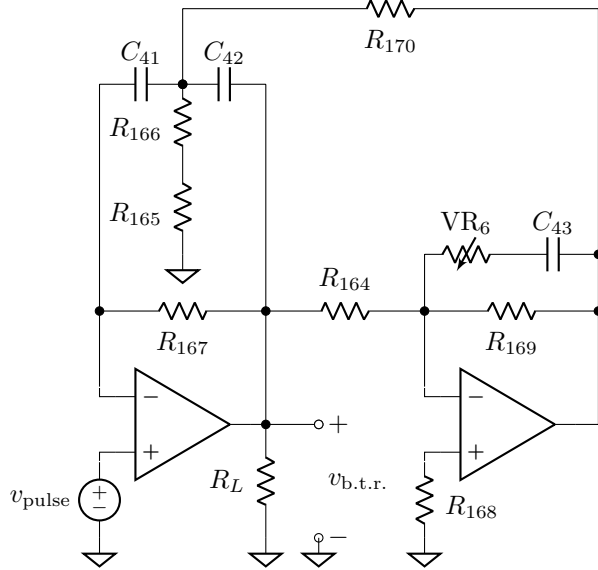


Figure 2.27: Bridged-T Resonator with Feedback Schematic.

Table 2.3: TR-808 Bass Drum, Bridged-T Resonator With Feedback.

Component	Value	Note
$R_{164}$	47 k $\Omega$	
$R_{165}$	47 k $\Omega$	
$R_{166}$	6.8 k $\Omega$	
$R_{167}$	1 M $\Omega$	
$R_{168}$	22 k $\Omega$	
$R_{169}$	47 k $\Omega$	
$R_{170}$	470 k $\Omega$	
VR <sub>6</sub>	500 k $\Omega$	max value
$C_{41}$	0.015 $\mu$ F	
$C_{42}$	0.015 $\mu$ F	
$C_{43}$	33 $\mu$ F	

Although we've shown detailed examples of how to apply our proposed technique to circuits involving  $\mathcal{R}$ -type adaptors involving a single absorbed multiport element (one example using a nullor and one example using a VCVS), there is nothing to prohibit us from using these techniques on circuits involving more than one. Here we'll briefly sketch Wave Digital Filter simulations of two versions of the Bridged-T Resonator with Feedback, one where the op-amps are modeled by nullors

and one where the op-amps are modeled by simple linear macromodels.

### Ideal op-amps

Here we sketch the approach used to model a version of the Bridged-T Resonator, shown in Figure 2.28, which uses nullors to model the two ideal operational amplifiers. Consider the Wave Digital Filter structure found using [198] (Figure 2.29a), a rearranged version of the reference circuit emphasizing that underlying topology (Figure 2.29b), and the explicit tree structure of the resulting Wave Digital Filter (Figure 2.30). Notice that the two ports of each nullor are constrained to the same adaptor. The replacement graph technique of [198] is used to form *two* replacement graphs, one for each of the nullors. It is only a coincidence that the topology of the circuit ends up forcing those two into the same adaptor.

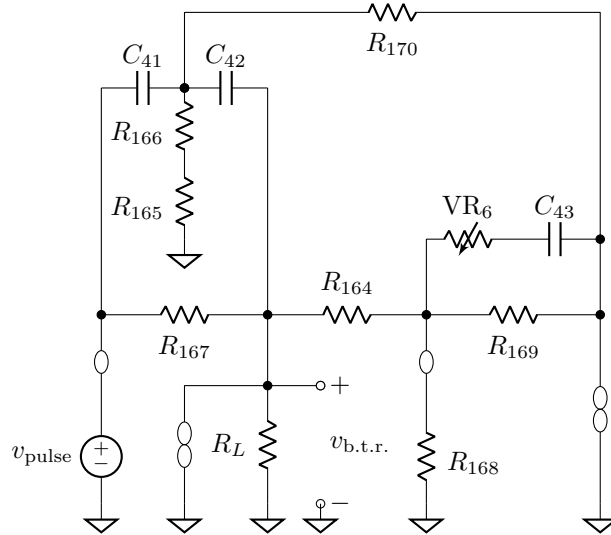


Figure 2.28: Bridged-T Resonator with Feedback, Idealized (Nullor-Based) Model.

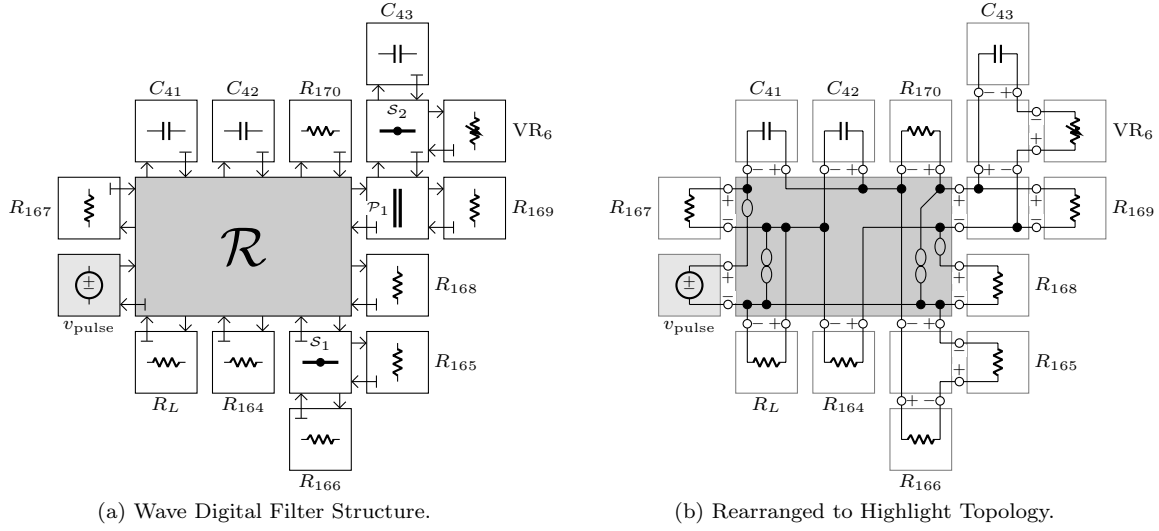


Figure 2.29: Nullor-Based Bridged-T Resonator Circuit with Feedback Stage: Rearranged to Highlight Topology, and Wave Digital Filter Structure.

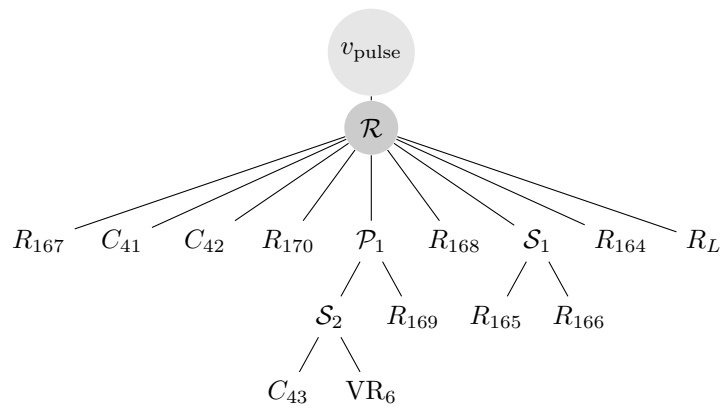


Figure 2.30: Connection Tree for Nullor-Based Bridged-T Resonator Circuit with Feedback.

### Macromodels

Here we sketch the approach used to model a version of the Bridged-T Resonator, shown in Figure 2.31, which uses simple linear macromodels to model the two operational amplifiers. Consider the Wave Digital Filter structure found using [198] (Figure 2.32a), a rearranged version of the reference circuit emphasizing that underlying topology (Figure 2.32b), and the explicit tree structure of the resulting Wave Digital Filter (Figure 2.33). Notice that the two ports of each VCVs are constrained to the same adaptor. The replacement graph technique of [198] is used to form *two* replacement graphs, one for each of the VCVSs. It is only a coincidence that the topology of the circuit ends up forcing those two into the same adaptor.

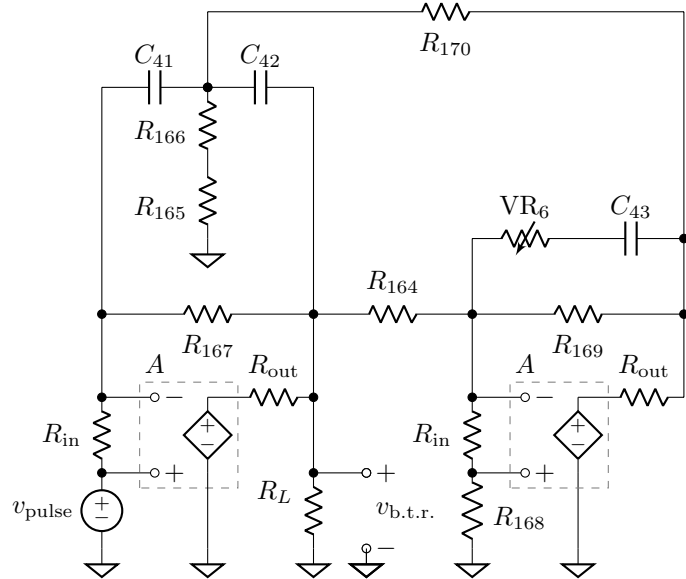
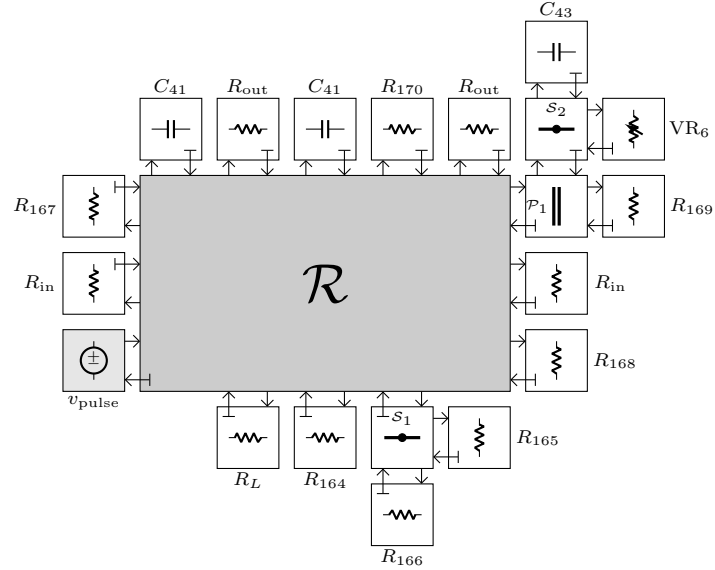
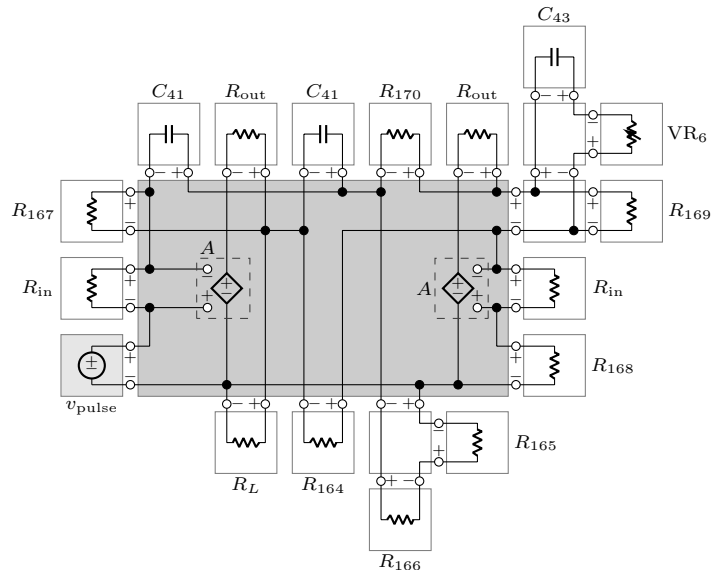


Figure 2.31: Bridged-T Resonator with Feedback, Non-Ideal (Controlled-Source-Based) Model.



(a) Wave Digital Filter Structure.



(b) Rearranged to Highlight Topology.

Figure 2.32: Controlled-Source-Based Bridged-T Resonator Circuit with Feedback: Rearranged to Highlight Topology, and Wave Digital Filter Structure.

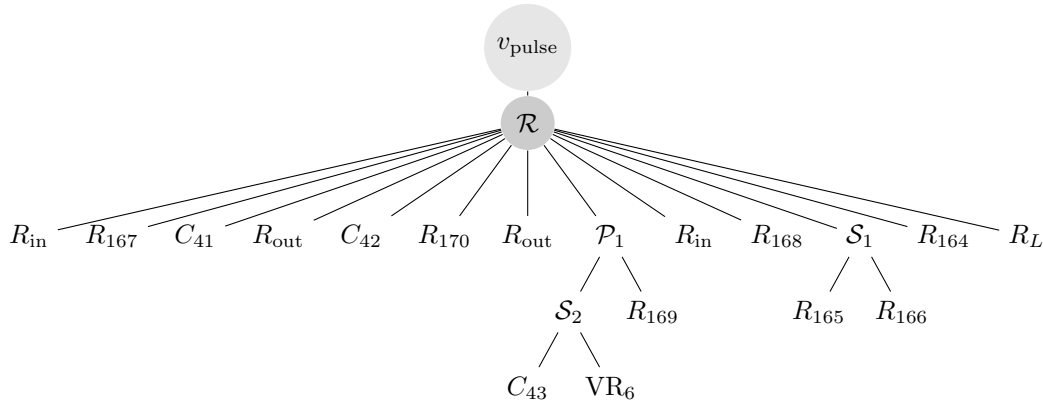


Figure 2.33: Connection Tree for Controlled-Source-Based Bridged-T Resonator with Feedback.

## 2.5 Conclusion

In this Chapter, we've reviewed previous work on trying to accommodate complicated topologies in Wave Digital Filter modeling, proposed a technique for deriving the scattering matrices of arbitrary  $\mathcal{R}$ -type adaptors which may have absorbed linear multiports, and proposed a technique for handling multiple linear nonadaptable elements collected at the root of a Wave Digital Filter tree.

With these proposed techniques, it is now possible to accommodate linear circuits including arbitrarily complex topologies in Wave Digital Filter modeling. These may include absorbed multiport nonlinear elements like controlled sources, transformers, and nullors in feedback arrangements, a very common case in audio circuitry. They may also include multiple nonadaptable linear elements. Beyond the case studies in this Chapter, circuits whose Wave Digital Filter simulation has been enabled by these proposed techniques include the Fender Bassman tone stacks [141], the Tube Screamer tone stage [141], more complicated op-amp macromodels [179], and the Hammond Organ vibrato/chorus circuit [154].

However, until this point in Chapters 1–2 we have only considered *linear* circuit elements. Nonlinear circuit devices like diodes, transistors, and triodes are very important parts of audio circuits, and require special treatment in the context of Wave Digital Filter modeling. In Chapter 3 we will review the standard handling of nonlinearities in the literature, pointing out serious limitations. In Chapter 4 it will be shown how we can leverage the proposed method presented in this Chapter (§2.2) to handle Wave Digital Filters with multiple nonlinearities in a very general way.



## Chapter 3

# One-Port Nonlinearities in Wave Digital Filters

In this chapter we will consider electrical circuits which involve one single nonlinear electrical device, e.g. a diode, and strategies for Wave Digital Filter modeling of this class of circuits. This is a narrow but important class of circuits which have been the most rigorously studied in the Wave Digital Filter context. Circuits involving a one-port nonlinearity which have been modeled using Wave Digital Filters include guitar distortion pedals [212, 240], diode clippers [241, 242, 243], simple oscillators [132], and envelope followers [6]. In addition to their use in electronic circuit modeling, these techniques have been used in Wave Digital modeling of lumped mechanical systems with a single nonlinearity. Researchers including Pedersini *et al.* [111, 244], De Sanctis *et al.* [98, 140, 6], and Bilbao *et al.* [109, 113] grafted Wave Digital Filter models of one-port nonlinear *mechanical* systems onto digital waveguide networks [143, 96, 97]. This trend continued in the *block-based modeling* research thread, e.g., [245, 100, 102, 101].

The structure of this chapter is as follows. We'll begin with a review of the basic model for the most important one-port nonlinearity in audio circuits: the diode (3.1). Then we will review the literature on Wave Digital Filter modeling of circuits with a single nonlinear device (§3.2). Following that, we'll demonstrate one-port nonlinearity modeling in a simulation of the TR-808's Bass Drum's Pulse Shaper circuit (§3.3). We'll conclude with a review of one-port nonlinear modeling and a discussion of its limitations (§3.4).

### 3.1 Diode Modeling

The most important one-port nonlinear device in common use in audio circuits is the diode, whose symbol and port variables are shown in Figure 3.1. In audio circuits, diodes are used as switches, in

“clippers” where they are used to limit a voltage excursion, and elsewhere.

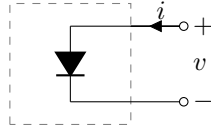


Figure 3.1: A Diode.

The behavior of a diode is described in the Kirchhoff domain by the Shockley ideal diode equation [246, 247]

$$i = I_s \left( e^{\frac{v}{V_T}} - 1 \right), \quad (3.1)$$

which is parameterized by the thermal voltage  $V_T$  and the reverse-bias saturation current  $I_s$ . Assuming a thermal voltage of  $V_T = 25.85 \text{ mV}$  and a reverse-bias saturation current of  $I_s = 2.52 \text{ nA}$ , this  $v$ - $i$  characteristic is shown in Figure 3.2. Because of the exponential in (3.1), the structure of the  $v$ - $i$  characteristic is not very visible on a linear scale (Figure 3.2a). To show this structure more clearly, Figure 3.2b shows the same characteristic with both the positive and negative currents plotted on a log scale. To allow this representation, currents below the threshold  $|i| < 0.1 \text{ nA}$  are not shown.

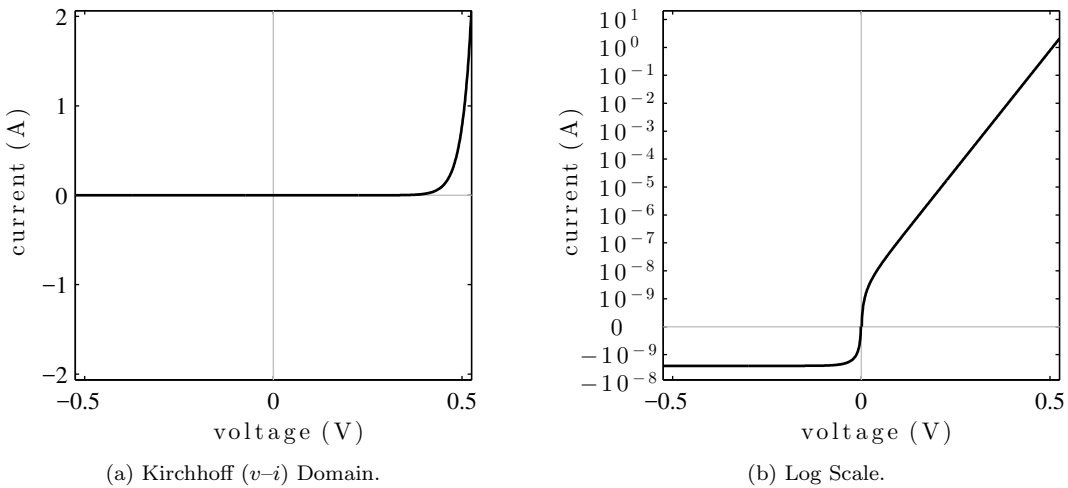


Figure 3.2: Diode Kirchhoff-Domain  $v$ - $i$  Characteristic, and Log-Scaled Version to Show Structure.

More complicated models of diodes may include series resistances, junction capacitances, etc., but we will not be discussing those models.

## 3.2 Previous Work

In this section we'll review previous work on Wave Digital Filter modeling of circuits with a single nonlinearity. Figuring out how to accommodate an element in a Wave Digital Filter structure involves answering three questions:

1. What is the input–output relationship of the device in the wave ( $a-b$ ) domain?
2. Can the device be adapted, and if so how is it adapted? and
3. Where in the Wave Digital Filter tree is the device allowed to be placed?

In the case of a single nonlinearity, the answer to the second question is simply “no,” and hence the answer to the third question is “only at the root.” Because of this, most of the research around one-port nonlinearities has focused on different ways of handling the input–output relationship in the wave domain.

After explaining the role of a single nonlinearity in a global Wave Digital Filter structure (§3.2.1), we'll review strategies for handling one-port nonlinearities, including interpolated table lookups and piecewise linear models (§3.2.2), iterative schemes (§3.2.3), and analytical solutions to certain nonlinearities (§3.2.4). These strategies can be applied to single nonlinearities, as well as multiple nonlinearities which can be topologically consolidated into a single one-port (§3.2.5) and certain simplified multiport nonlinear elements (§3.2.6).

### 3.2.1 Connection Tree

When a circuit has one nonlinear circuit element, it is always placed at the root of the tree in a Wave Digital Filter simulation.<sup>1</sup> Recall that a realizable Wave Digital Filter structure is created by arranging the circuit and its topology into a tree structure called a Connection Tree. To make that structure realizable, every upwards-facing port in the tree has to be “adapted,” i.e., its port resistance is chosen so that the reflected (upwards facing) wave at that port does not depend instantaneously on the incident (downwards facing) wave at that port. The root element does not have an upwards-facing port, so it is not adaptable. Typically, nonlinear devices are not suitable for inclusion as leaves in a Wave Digital Filter tree because they cannot be easily adapted. In circuit terms, this is because the incremental resistance of a one-port nonlinearity depends on the incident wave hitting that nonlinearity, thus the port resistance (equal to the incremental resistance) required for adaptation depends on the incident wave, but the incident wave hitting the nonlinearity depends in turn on the port resistance. This implicit relationship implicates the dynamics of potentially the entire Wave Digital Filter tree and cannot be resolved with standard techniques (although we'll discuss work in

---

<sup>1</sup>Recently, Bernardini and Sarti investigated “dynamic adaptation” of nonlinear one-ports, allowing them to be placed as leaves in a Wave Digital Filter tree [228]. Since this relates to accommodating multiple nonlinearities rather than a single nonlinearity, it will be reviewed more in Chapter 4.

that direction in §3.2.3). This means that the only appropriate place for a nonlinear circuit element in a classical Wave Digital Filter is at the root of the tree [185, 132].

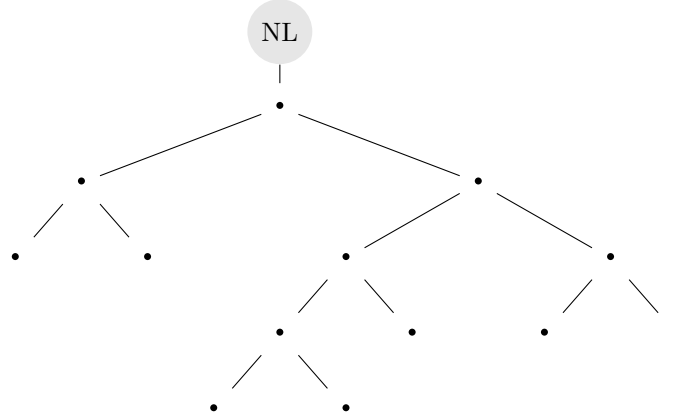


Figure 3.3: Example Connection Tree with Single Nonlinearity.

An example of a connection tree structure with a nonlinearity at the root is shown in Figure 3.3.

### 3.2.2 Piecewise Linear Models

The first researchers to study nonlinearities in the context of Wave Digital Filters were Meerkötter and Scholz [248]. They realized that:

1. On a structural level, a single nonlinear device could be accommodated in a Wave Digital Filter tree (at the root); and
2. Nonlinear devices with piecewise-linear  $v-i$  characteristics could be solved in the wave domain.

They represented piecewise-linear characteristics with Chua's "canonic" representation [249], and studied in particular an "ideal diode" with no current flowing for negative voltages and no voltage developing for positive currents and a piecewise linear active resistance, also known as "Chua's diode." An ideal diode can be represented in the Kirchhoff domain by

$$\begin{cases} i = 0 & \text{when } v \leq 0 \\ v = 0 & \text{when } i \geq 0 \end{cases} \quad (3.2)$$

and in the wave domain by

$$b = -|a|. \quad (3.3)$$

Their particular piecewise linear resistance is represented in the Kirchhoff domain by the canonic representation

$$i = G_1 v + \frac{1}{2} (G_2 - G_1) (|v + v_0| - |v - v_0|) \quad (3.4)$$

with constants  $G_1 = -500 \mu\text{S}$ ,  $G_2 = -800 \mu\text{S}$ , and  $v_0 = 1 \text{ V}$ . In the wave domain (using the value of  $R = 569.2 \Omega$  which is appropriate for their circuit), this is transformed to

$$b = \varrho_1 a + \frac{1}{2} (\varrho_2 - \varrho_1) (|a + a_0| - |a - a_0|) \quad (3.5)$$

with constants  $\varrho_1$ ,  $\varrho_2$ , and  $a_0$  derived from the Kirchhoff-domain constants according to

$$\varrho_1 = \frac{1 - G_1 R}{1 + G_1 R} = 1.7956 \quad (3.6)$$

$$\varrho_2 = \frac{1 - G_2 R}{1 + G_1 R} = 2.6722 \quad (3.7)$$

$$a_0 = v_0 (1 + G_2 R) = 0.5447 \text{ V}. \quad (3.8)$$

Details on generalizing this approach to any number of piecewise-linear segments are given in their paper [248]. The Kirchhoff-domain  $v$ - $i$  and wave domain  $a$ - $b$  characteristics of the “ideal diode” and “Chua’s diode” are shown in Figure 3.4 [248]. For the ideal diode the two line segments are labeled  $A$  and  $B$  and for Chua’s diode they are labeled  $A$ ,  $B$ , and  $C$ , to show the correspondence between the characteristics in the Kichhoff and the wave domains.

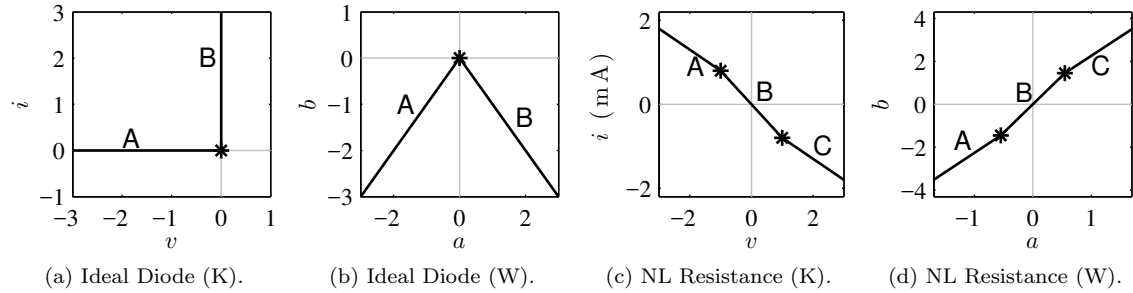


Figure 3.4: Ideal Diode and Piecewise-Linear Active Resistor (“Chua’s diode”), Representations in the Kirchhoff and Wave Domains. The ideal diode is transformed to the wave domain using a port resistance of  $R = 1 \Omega$ , and the piecewise-linear resistance is transformed to the wave domain using  $R = 569.2 \Omega$ .

Meerkötter and Scholz used their technique to simulate a version of Chua’s circuit [250], shown in Figure 3.5a with component values enumerated in Figure 3.5b. Here, the boxed resistor represents the piecewise linear nonlinear resistor “Chua’s diode” discussed above. The Wave Digital Filter structure of their simulation, in our notation, is shown in Figure 3.5c and a version of the circuit rearranged to highlight this topology is shown in Figure 3.5d. A diagram of the explicit tree structure of this Wave Digital Filter is shown in Figure 3.6.

Their structural insight forms the basis for all subsequent work on handling a single nonlinearity in a Wave Digital Filter tree, and their method for handling piecewise-linear  $v$ - $i$  characteristics set

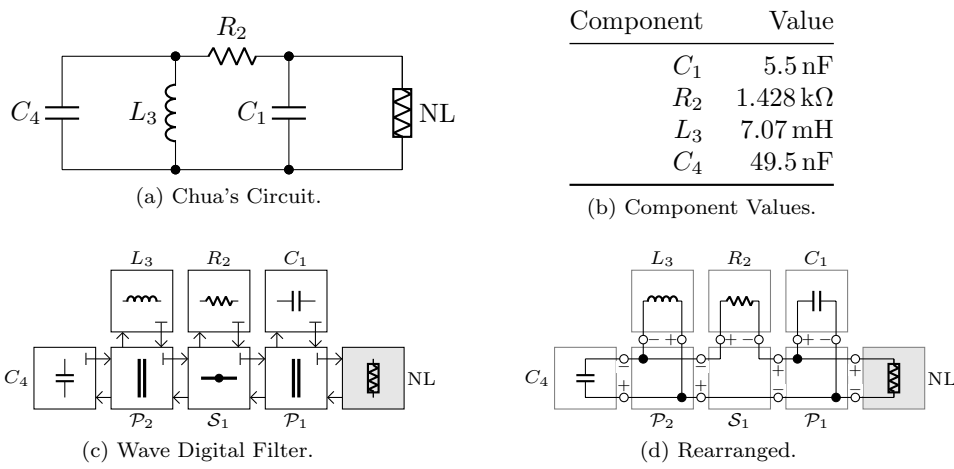


Figure 3.5: Chua's Circuit Schematic, Component Values, Wave Digital Filter, and Rearranged to Highlight Topology.

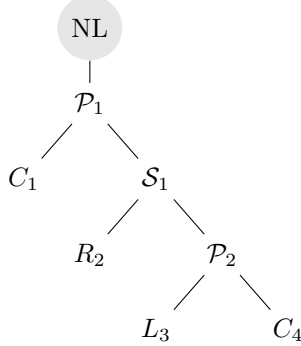


Figure 3.6: Chua's Circuit Connection Tree.

up a variety of other modeling techniques.

Felderhoff built on their work, recognizing that it could be applied to nonlinear devices with piecewise-linear  $v-q$  characteristics (nonlinear capacitor) [167, 184]. Sarti and De Poli had the insight [185] that the two-port adaptor used in [184, 186] to affect a change of variables around a nonlinear capacitor is the digital counterpart to the *mutator* two-port from analog circuit theory. So, the two-port adaptor can be called a mutator in the Wave Digital Filter context as well. They used the *mutator* concept to formalize the study of nonlinear reactances “with memory” [186, 185], extending the approach of Felderhoff to consider nonlinear  $\phi-i$  characteristics (nonlinear inductor) and even nonlinear memristors [251].<sup>2</sup>

<sup>2</sup>More exotic models of nonlinear inductors exist, for instance the Jiles–Atherton model, which has been used in Virtual Analog [78, 61, 77] although not in the Wave Digital Filter context.

Piecewise linear modeling can be considered the same as interpolating linearly between a tabulated solution. The difference is only slight and philosophical. Piecewise linear modeling assumes an instantaneous circuit characteristic made up of line segments—in the Virtual Analog context, this is in practice probably an approximation of a curved characteristic like the Shockley diode model. Tabulation and interpolation stores exact solutions to certain points along the curve and interpolates to approximate the solutions in between. The difference is that one approach introduces error in the model approximation and then solves the model perfectly, and one solves the model perfectly (offline) and then introduces error approximating solutions between tabulated values. This error can be considered to have an energetic interpretation. It is common practice in the Wave Digital Filter approach to circuit modeling to attempt to ensure that simplifications or numerical aspects of the simulation are incrementally passive<sup>3</sup> [92], i.e., that the simplification or numerical error always corresponds to a loss of energy in the reference circuit. This has important implications for stability and the suppression of limit cycles and other spurious oscillations [5, 252]. In [253], Werner and Smith give recommendations on interpolation and extrapolation strategies to ensure passivity of one-port tabulated nonlinearities.

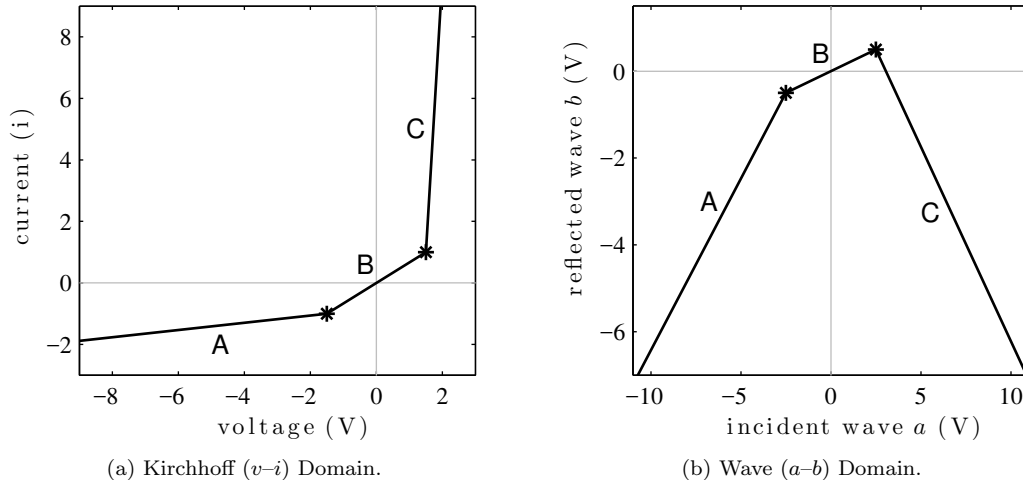


Figure 3.7: Piecewise Linear Kirchhoff- and Wave-Domain Characteristics ( $R = 1$ ).

To sketch the piecewise linear modeling approach originated by Meerkötter and Scholz, we'll study a vaguely-diode-like piecewise linear resistance with three segments. The  $v-i$  characteristic is shown in Figure 3.7a. Plugging in the voltage wave definition yields an  $a-b$  characteristic shown in Figure 3.7b. In both cases the line segments are labeled  $A$ ,  $B$ , and  $C$  to show the correspondence between the Kirchhoff and wave domains.

Since each segment is linear, it “looks” like a Thévenin or Norton source with the appropriate

---

<sup>3</sup>The term in most Wave Digital Filter literature is actually “incrementally pseudopassive”.

source value and resistance. Conceptually, accommodating a piecewise-linear characteristic in Wave Digital Filter involves two steps. First, we need to figure out which segment we are on. Second, we need to solve for the reflected wave as a function of the incident wave, for that segment. Figuring out which segment we are on is simple; since the  $a$ - $b$  characteristic is functional, the correct segment is uniquely determined by the incident wave  $a$ . Once we know which segment we are on, that segment can be solved in the wave domain just like the corresponding Thévenin (§1.2.4) or Norton source (§1.2.5). Full details are given in [248] and elaborated on in [185].

### 3.2.3 Iterative Schemes

Although piecewise linear characteristics can be handled with the techniques just discussed, most one-ports that we care about in Virtual Analog, e.g., diodes, are defined rather with more complicated  $v$ - $i$  characteristics that don't have a piecewise-linear representation. In general, plugging wave definitions into a Kirchhoff-domain nonlinear equation will produce an equation relating the incident and reflected waves  $a$  and  $b$  which can't be solved analytically for  $b$ . Since the root element must solve the relationship  $b = f(a)$ , this is an issue. One way to address that problem is to solve for the relationship iteratively. The first use of this approach in the Virtual Analog literature is by Yeh and Smith, who solved an implicit diode pair wave domain characteristic using numerical methods [59, 229, 7].

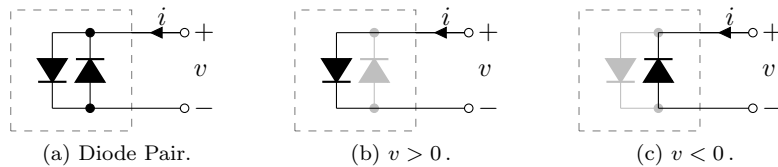


Figure 3.8: Diode Pair and Two Orientation-Dependent Simplified Versions.

To sketch this approach, we'll study a diode clipper pair as in [59]. A diode clipper pair, shown in Figure 3.8a, is described in the Kirchhoff domain by the application of two instances of Shockley's ideal diode law (3.1), yielding the equation

$$i = I_s \left( e^{\frac{v}{V_T}} - e^{-\frac{v}{V_T}} \right). \quad (3.9)$$

This  $v$ - $i$  characteristic is shown in Figure 3.9a. Plugging in the voltage wave definition

$$\frac{a}{2R} - \frac{b}{2R} = I_s \left( e^{\frac{a+b}{2V_T}} - e^{-\frac{a+b}{2V_T}} \right) \quad (3.10)$$

and rearranging to form a zero-finding equation yields

$$0 = 2RI_s \left( e^{\frac{a+b}{2V_T}} - e^{-\frac{a+b}{2V_T}} \right) - a + b. \quad (3.11)$$

The wave-domain ( $a-b$ ) characteristic is shown in Figure 3.9b.

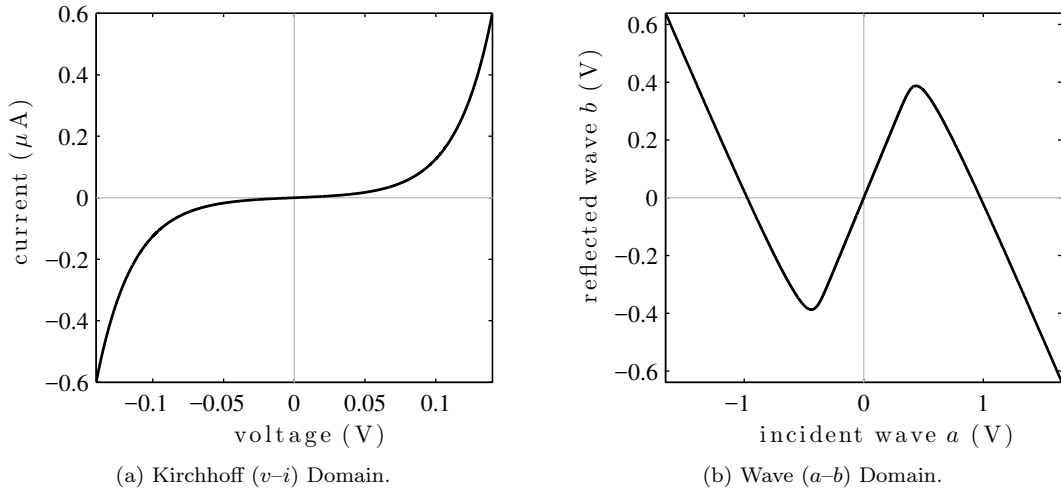


Figure 3.9: Diode Pair Kirchhoff- and Wave-Domain Characteristics ( $R = 1$ ).

Although the  $a-b$  characteristic is functional (there is one  $b$  value for each  $a$  value), it is not possible to rearrange (3.11) to solve for  $b$  analytically. However, it is possible to use a Newton–Raphson solver to solve the zero-finding equation (3.11), either offline to populate a table or online as solutions are needed. Specifically, the Wave Digital Filter tree will provide an incident wave  $a$  to the root, this value is plugged in to (3.11), and then (3.11) is solved iteratively for  $b$  using Newton–Raphson iteration.

### 3.2.4 Analytic Solutions

Although in general we can't depend on finding analytic solutions to nonlinearities in the wave domain, certain classes of nonlinear equations can indeed be solved analytically. We've already discussed piecewise-linear relationships which remain piecewise linear in the wave domain and can be solved analytically at the root of a Wave Digital Filter tree. Here we mention the most important nonlinear one-port for Virtual Analog applications: the diode. Paiva *et al.* showed that the wave-domain equation for a diode can be solved exactly using a special function called the *Lambert W* function [212].

The Lambert  $W$  function has been used previously in Virtual Analog [254, 253] and for many other applications [255]. The Lambert  $W$  function can be used to solve equations in one of these

forms [255, 256]

$$\ln(A + Bx) + Cx = \ln(D) \quad (3.12)$$

$$(A + Bx)e^{Cx} = D \quad (3.13)$$

using

$$x = \frac{1}{C}\mathcal{W}\left(\frac{CD}{B}e^{AC/B}\right) - \frac{A}{B}. \quad (3.14)$$

To use the Lambert  $\mathcal{W}$  equation to solve the Shockley ideal diode equation in the wave domain, we reframe (3.1) in the form of (3.13):

$$(a + 2RI_s - b)e^{-\frac{1}{2V_T}b} = 2RI_se^{\frac{a}{2V_T}}. \quad (3.15)$$

The coefficients of (3.13), with  $x = b$ , are

$$A = a + 2RI_s \quad (3.16)$$

$$B = -1 \quad (3.17)$$

$$C = -\frac{1}{2V_T} \quad (3.18)$$

$$D = 2RI_se^{\frac{a}{2V_T}}. \quad (3.19)$$

Plugging (3.16)–(3.19) into (3.14) yields

$$b = a + 2RI_s - 2V_T\mathcal{W}\left(\frac{RI_s}{V_T}e^{\frac{a+RI_s}{V_T}}\right), \quad (3.20)$$

an explicit wave domain equation.

### 3.2.5 Consolidated One-Port Combinations

The techniques discussed so far are intended to accommodate a single one-port nonlinear device in a Wave Digital Filter tree. Luckily, in audio circuits, combinations of one-port devices which form a larger consolidated one-port are common. Good examples are found in guitar distortion circuits. Single or multiple diodes are found in each direction in stock guitar pedals; adding or removing diodes is common in aftermarket modifications. Diode clippers have been extensively studied in Virtual Analog [257, 258, 59, 259, 229, 7, 23, 260, 63, 57, 73, 19, 61, 212, 261, 62, 225, 2, 231, 155, 241].

Paiva *et al.* showed that their analytic solution to a single diode can be leveraged to produce an analytic approximation for a diode pair: two diodes in parallel, facing in opposite directions. In short, the reverse-biased diode is assumed to not contribute to the solution, forming two configurations shown in Figure 3.8b ( $v > 0$ ) and Figure 3.8c ( $v < 0$ ); in each case the gray diode is neglected. Under this assumption, the Lambert- $\mathcal{W}$ -based analytic solution is used for the remaining single diode in

the proper orientation [212], yielding

$$b = \operatorname{sgn}(a) \left[ |a| + 2RI_s - 2V_T \mathcal{W} \left( \frac{RI_s}{V_T} e^{\frac{|a|+RI_s}{V_T}} \right) \right]. \quad (3.21)$$

Werner *et al.* improved this model, mitigating the error somewhat with a second Lambert  $\mathcal{W}$  function evaluation [240], according to

$$b = \operatorname{sgn}(a) \left[ |a| - 2V_T \left( \mathcal{W} \left( \frac{RI_s}{V_T} e^{\frac{|a|+RI_s}{V_T}} \right) + \mathcal{W} \left( -\frac{RI_s}{V_T} e^{-\frac{|a|+RI_s}{V_T}} \right) \right) \right]. \quad (3.22)$$

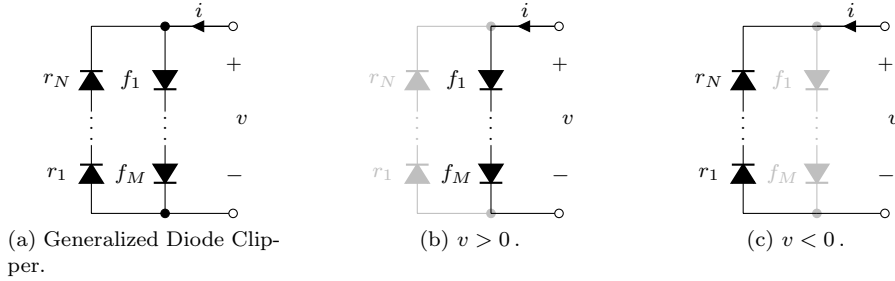


Figure 3.10: Generalized Diode Clippers and Two Orientation-Dependent Simplified Versions.

Werner *et al.* further generalized this approach to diode clippers with any number of diodes in each direction [240]. Denoting the number of diodes in the forwards orientation by  $M$  and the number of diodes in the reverse orientation by  $N$ , a generalized diode clipper (Figure 3.10a) is described in the Kirchhoff domain by

$$i = I_s \left( e^{\frac{v}{MV_T}} - e^{-\frac{v}{NV_T}} \right). \quad (3.23)$$

It is possible to simply neglect the negatively-biased branch (Figures 3.10b–3.10c), but again this introduces some error. In the wave domain, Werner *et al.* propose a model with somewhat mitigated error using two Lambert  $\mathcal{W}$  solves

$$b = a - 2\lambda V_T \left[ \mu_0 \mathcal{W} \left( \frac{RI_s}{\mu_0 V_T} e^{\frac{\lambda a}{\mu_0 V_T}} \right) + \mu_1 \mathcal{W} \left( -\frac{RI_s}{\mu_1 V_T} e^{-\frac{\lambda a}{\mu_1 V_T}} \right) \right]. \quad (3.24)$$

Here, factors  $\mu_0$  and  $\mu_1$  account for the  $M$  forward and  $N$  reverse diodes according to

$$\mu_0 = \begin{cases} M & , a \geq 0 \\ N & , a < 0 \end{cases} \quad \text{and} \quad \mu_1 = \begin{cases} N & , a \geq 0 \\ M & , a < 0 \end{cases}. \quad (3.25)$$

### 3.2.6 Simplified Multiports

Similarly to how one-port techniques can be leveraged to handle multiple one-port nonlinearities so long as they can be consolidated into a single one-port, one-port techniques can also sometimes be used to handle certain multiport nonlinear devices, provided the devices can be judiciously approximated. Two varieties of approximation are called cross-controlled models and simplified multiports.

Karjalainen and Pakarinen showed how the triode in a triode amplification stage can be modeled as a one-port nonlinearity with a “cross control” [174]. They assume that the grid current of the triode is zero, and replace the triode with a special grid-to-cathode one-port junction, whose characteristic is cross-controlled by the grid voltage. For realizability, they delay the grid voltage by one sample, adding a fictitious unit delay. In [175], they refine this model by not neglecting grid current for positive grid voltages. In [6], De Sanctis and Sarti propose a cross-controlled model for a transistor-based amplifier circuit.

In [262], Bernardini *et al.* propose an analytic approximation technique for handling circuits with multiple nonlinearities which extends the approach of [212]. Essentially, only the most important nonlinear junction is considered in a circuit at any point in time. Considering a wide class of diode- and transistor-based circuits, specifically an “extended Ebers–Moll” class of transistor topologies with a port between each transistor terminal and feedback ports between each of three pairs of terminals, they use the Lambert  $\mathcal{W}$  function to solve these simplified circuits analytically [262].

## 3.3 Case Study

To illustrate the application of Wave Digital Filter modeling to a circuit with a single nonlinearity, we’ll conclude with a real-world case study. This study will show how to create a Wave Digital Filter simulation of one part of the Roland TR-808 Bass Drum circuit: its Pulse Shaper. The schematic for the Pulse Shaper is shown in Figure 3.11a.

The Pulse Shaper is composed of a few passive electrical elements: resistors  $R_{162}$  and  $R_{163}$ ; capacitor  $C_{40}$ , and diode  $D_{53}$ . The electrical component values are shown in Table 3.1. The input to the Pulse Shaper is the rectangular pulse input  $v_{\text{in}}$ . The Pulse Shaper does not have any parametric control, but it must handle a variety of input pulses. During operation, 1 ms rectangular pulses are delivered to the Pulse Shaper by the sequencer, through some trigger logic which sets the amplitude of the pulse according to a global accent level on the TR-808 sequencer. This level is normally 4 V, but the accented level can be anywhere between 4–14 V. The output  $v_{\text{pulse}}$  is taken as the voltage across the resistor  $R_{162}$  and is delivered to the Bridged-T Resonator; splitting the circuit at this location is a fine assumption because it is the positive input terminal to an op-amp. Assuming the op-amp acts ideal, it therefore does not load the output of the Pulse Shaper at all.

Rearranging the reference circuit (Figure 3.11a) to highlight the underlying circuit topology yields Figure 3.11b, which matches the overall structure of the Wave Digital Filter simulation shown

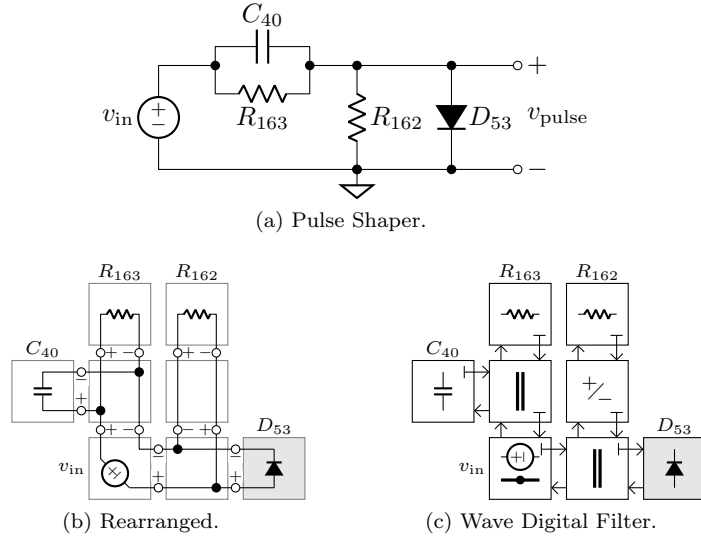


Figure 3.11: Pulse Shaper Schematic, Rearranged to Highlight Topology, and Wave Digital Filter.

Table 3.1: Pulse Shaper Component Values.

Component	Value	Note
$R_{162}$	$4.7 \text{ k}\Omega$	
$R_{163}$	$100 \text{ k}\Omega$	
$C_{40}$	$0.015 \mu\text{F}$	
Diode	1N4148	substitute for IS2473
$I_s$	$2.52 \text{ nA}$	saturation current
$V_T$	$25.85 \text{ mV}$	thermal voltage

in Figure 3.11c. A diagram explicitly showing the tree structure of this simulation is shown in Figure 3.12. A few aspects of this Wave Digital Filter deserve special explanation. The circuit contains both a non-adaptable linear element (ideal voltage source  $v_{\text{in}}$ ) and a one-port nonlinear element (diode  $D_{53}$ ), both of which seem like they have to be at the root of the tree. Luckily  $v_{\text{in}}$  can be absorbed into the series adaptor  $\mathcal{S}_1$  and handled using the technique from §1.4.2. The inverter  $\mathcal{I}_1$  is present only to ensure that the polarity of the output voltage (which is taken off of  $R_{162}$ ) is correct. The diode is implemented using a Lambert  $\mathcal{W}$  solve, using the technique of [212].

Surprisingly, the capacitor  $C_{40}$  in the Pulse Shaper circuit requires special treatment. Figure 3.13 shows a transient simulation in response to a 4 V pulse input (shown in the top panel). The next three panels show traces for  $v_{\text{out}}$ , comparing a reference SPICE simulation to three different capacitor discretization strategies: the Bilinear Transform, the  $\alpha$  Transform with  $\alpha = 0.029$ , and Backwards Euler. Notice that the standard discretization choice, Bilinear Transform, has a disastrously bad fit to the SPICE simulation. This is related to the high frequency oscillation that others have

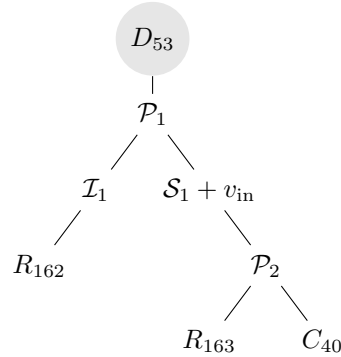


Figure 3.12: Connection Tree for Pulse Shaper Circuit.

noticed in the context of trapezoidal integration [146, 160, 161, 162, 155]. However, since this circuit operates the diode as a switch, the “high-frequency oscillation” sometimes seen when using trapezoidal integration on circuits with nonlinearities disengages the diode after one sample. Once the diode is disengaged, the circuit starts discharging just as it did after the rising edge. This accounts for the wrong polarity, after one sample, of the simulation using the Bilinear Transform. As suggested in [155], using Backwards Euler does indeed ameliorate the issue; however a brute-force test across  $\alpha \in [0, 1]$  finds that  $\alpha = 0.029$  minimizes the root-mean-square error of the simulation while also ensuring that the response to the falling edge doesn’t have any oscillation. Therefore, we use the  $\alpha = 0.029$  discretization in modeling the Pulse Shaper.

The transient response of each of the discretization strategies to a wider range of pulses with amplitudes  $\in [4.0, 6.5, 9.0, 11.5, 14.0]$  V is shown in Figure 3.14. Notice that the Bilinear Transform behaves poorly across the entire range of input pulse amplitudes and that Backwards Euler and the  $\alpha = 0.029$  Transform match well across the entire range of input pulse amplitudes.

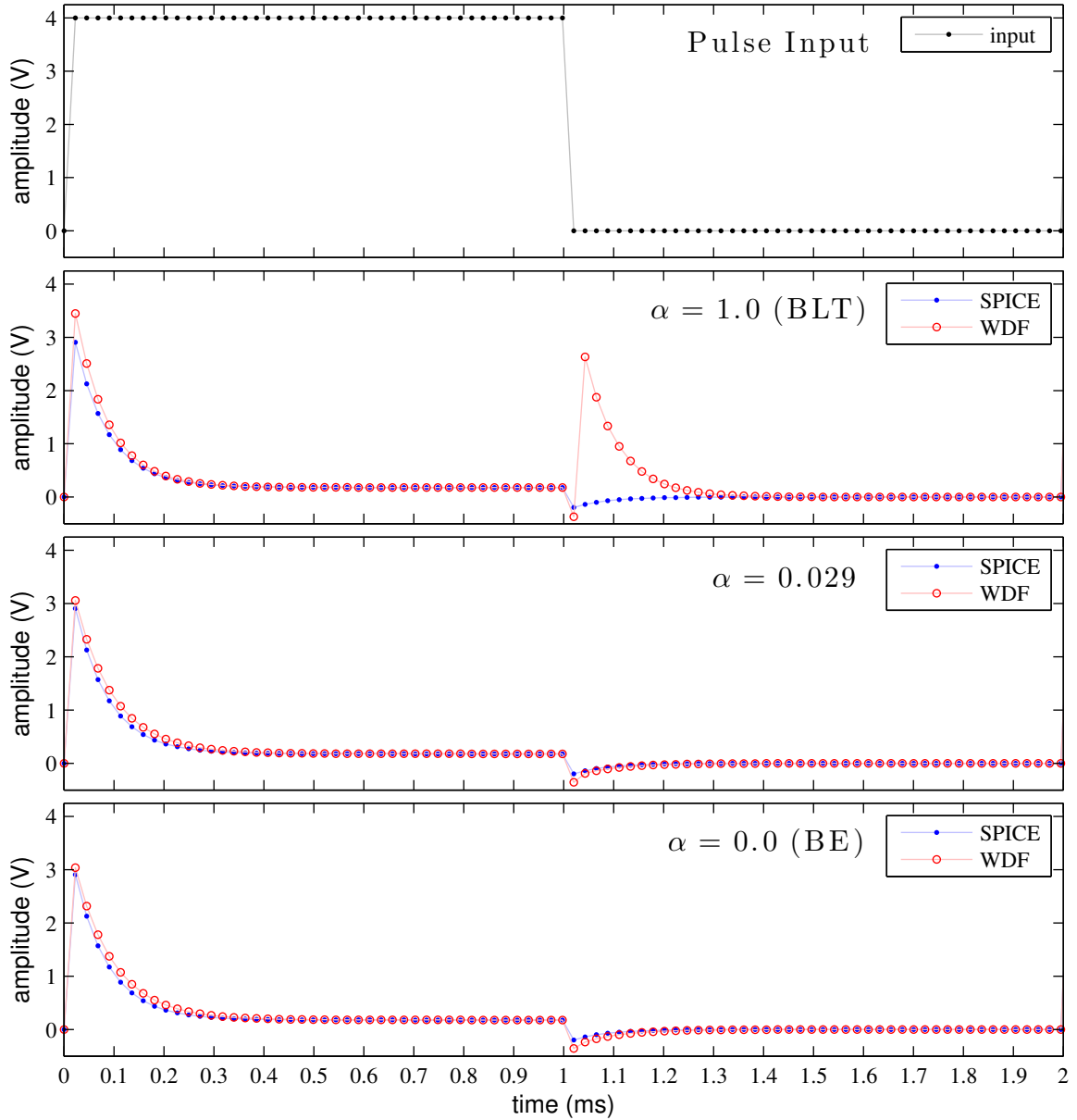


Figure 3.13: Time Domain Response (Voltage Aver  $R_{162}$ ) of the Pulse Shaper in Response to an Input Pulse (Top). Three Different Discretizations are Shown:  $\alpha = 1.0$  (Bilinear Transform / Trapezoidal Rule),  $\alpha = 0.029$ , and  $\alpha = 0.0$  (Backward Euler).

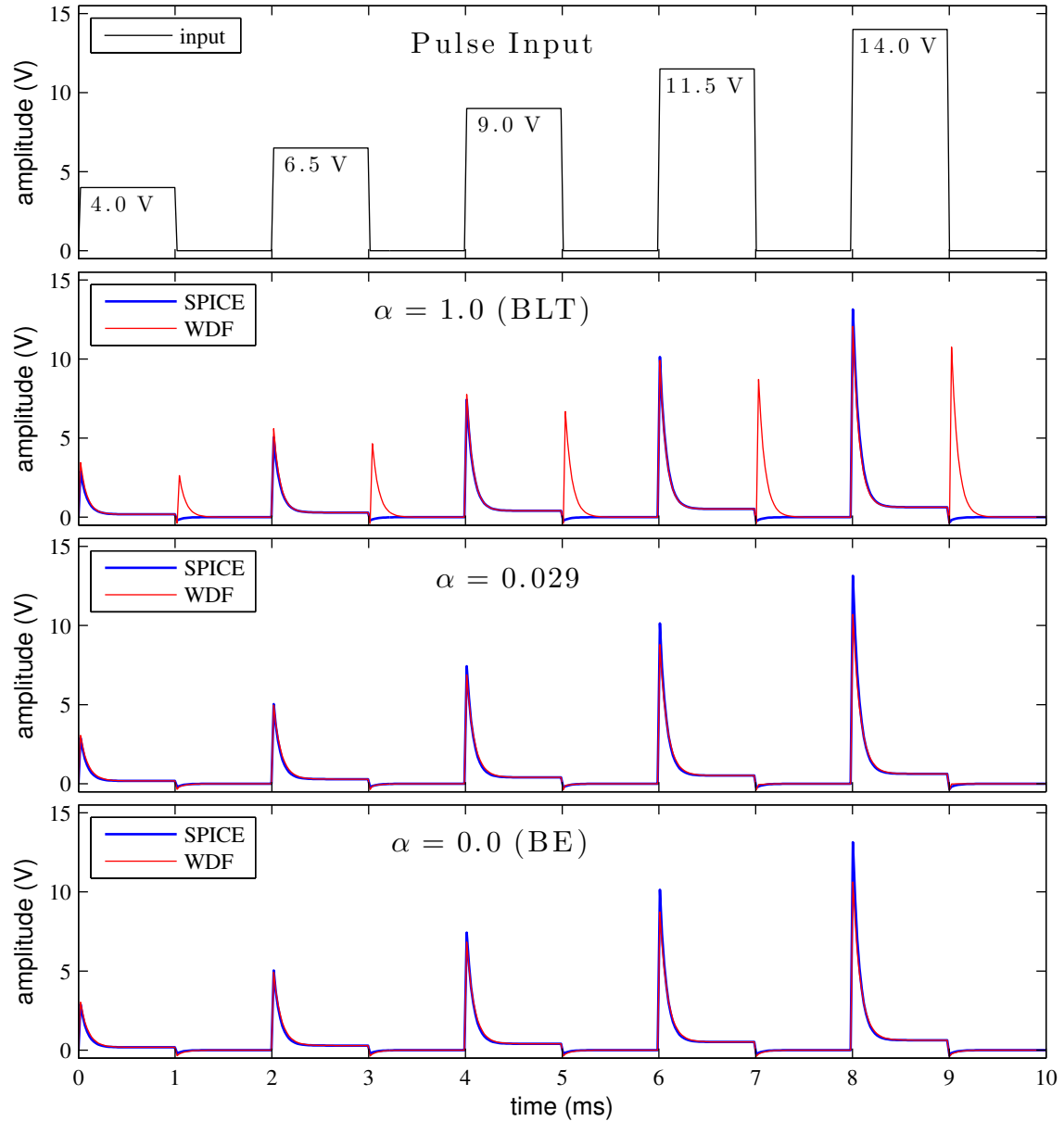


Figure 3.14: Time Domain Response (Voltage Over  $R_{162}$ ) of the Pulse Shaper in Response to a Family of Input Pulses of Different Amplitudes  $\in [4.0, 6.5, 9.0, 11.5, 14.0]$  V (Top). Three Different Discretizations are Shown:  $\alpha = 1.0$  (Bilinear Transform / Trapezoidal Rule),  $\alpha = 0.029$ , and  $\alpha = 0.0$  (Backward Euler).

## 3.4 Review

Methods for modeling one-port nonlinearities in a Wave Digital Filter are quite mature. In terms of the one-port nonlinearity's place in a Wave Digital Filter tree, it can always be safely placed at the root of the tree. Modeling one-port nonlinearities in the wave domain can be accomplished with a few different methods. We've reviewed the important Virtual Analog approaches to modeling single nonlinearities, including how those techniques can be used for simplified models of certain multiport nonlinearities. These techniques are sufficient for Wave Digital Filter modeling of most circuits that involve one nonlinearity. Tabulation or piecewise-linear modeling is neither expensive in terms of storage nor in terms of runtime computational complexity, and in practice seems to work just fine for one-dimensional nonlinear functions.

To show these techniques in action, we've studied the Pulse Shaper from the TR-808 Bass Drum, placing a special emphasis on the interaction between the diode nonlinearity and the chosen discretization scheme for the capacitor. In fact, the typical choice of the Bilinear Transform proves ill-suited to this problem, and we make recourse to the  $\alpha$  Transform discussed in Chapter 1 to reduce the simulation error. We emphasize that dealing with this interesting case did not require a modification to the treatment of the nonlinearity, but rather a non-standard approach to discretizing the reactive part of the circuit.

The main limitation of the techniques discussed in this chapter is that they only target circuits with a single nonlinearity. Most audio circuits involve several nonlinear circuit elements, so the problem of modeling a circuit with only a single nonlinearity can be considered oversimplified compared to most Virtual Analog applications. The problem of handling multiple nonlinearities is unsurprisingly much more complex. A novel approach to handling multiple nonlinearities is the subject of the final Chapter.



## Chapter 4

# Advances to Wave Digital Filters With Multiple Nonlinearities

In this chapter we will consider the general case of electrical circuits involving more than one nonlinear port with any topology. Some of the work in this chapter appeared previously in conference proceedings [230, 231]. This is the most important class of audio circuits, and has received the most attention from the Virtual Analog research community. This proposed approach to Wave Digital Filter modeling is general enough that it can be used on any standard audio circuit.

The chapter is structured as follows. In §4.1, the basics of nonlinear electrical device modeling are reviewed. In §4.2, previous work on Wave Digital Filter modeling of circuits with more than one nonlinearity is outlined. In §4.3, we propose a novel technique for Wave Digital Filter modeling of circuits with multiple nonlinearities. In §4.4, two cases studies on the TR-808 Bass Drum's Envelope Generator and Nonlinear Bridged-T Resonator illustrate the proposed technique in action. Finally §4.5 contains some commentary on the proposed approach.

### 4.1 Nonlinear Devices

Nonlinear circuits with more than one nonlinearity may involve one-port nonlinearities like the diode as well as multiport nonlinear device. The most important multiport nonlinear devices for audio circuits are triodes and transistors. Here we'll review the basic models of these devices, with a special focus on the NPN Bipolar Junction Transistors (NPN BJT) which will be used in both of the case studies at the end of the Chapter.

### 4.1.1 Transistor Modeling

Transistors are the basic building blocks of modern audio circuits. Many different kinds of transistors exist, but the most important ones for audio circuits are Bipolar Junction Transistors (BJT) and Field-Effect Transistors (FET). Here we'll introduce these devices, showing their schematic symbols, mentioning some of their uses, and reviewing their basic Kirchhoff-domain models which are commonly used to in audio. We will focus on NPN BJTs, but will also mention PNP BJTs and MOSFETs along the way.

#### NPN BJT

NPN Bipolar Junction Transistors (NPN BJTs) are common in audio circuits, where they are used in audio amplifiers (common emitter, common collector, common base, emitter follower, etc. [199]), as switches, and in more complicated applications. We've already seen an example in Chapter 1 of an NPN BJT being used in an emitter follower amplifier as part of the TR-808 Bass Drum's Output Filter, and we will see it again in the case studies at the end of this chapter, where the TR-808 Bass Drum's envelope generator uses two NPN BJTs and its Nonlinear Bridged-T Resonator uses one NPN BJT.

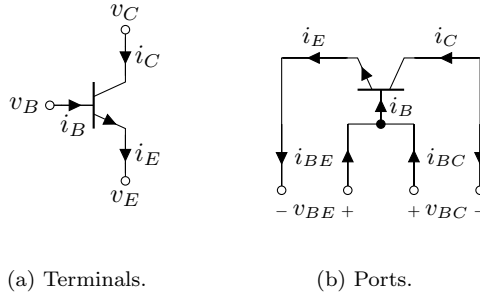


Figure 4.1: Symbol of NPN Bipolar Junction Transistor with Terminal Voltages and Branch Currents Labeled, and One Way of Viewing it From a Port-Wise Perspective.

An NPN BJT has three terminals, a base ( $B$ ), collector ( $C$ ) and emitter ( $E$ ). The symbol for an NPN BJT is shown in Figure 4.1a, with terminal voltages  $v_B$ ,  $v_C$ , and  $v_E$  and branch currents  $i_B$ ,  $i_C$ , and  $i_E$  labeled. The simplest model of an NPN BJT in the Kirchhoff domain is given by the Ebers–Moll model [263]. The Ebers–Moll model gives the currents  $i_B$ ,  $i_C$ , and  $i_E$  as a function of the voltage drops  $v_{BE} = v_B - v_E$  and  $v_{BC} = v_B - v_C$  and is parameterized by the transistor parameters  $I_s$  (saturation current),  $\beta_F$  (forward current gain), and  $\beta_R$  (reverse current gain) as well as the thermal voltage  $V_T$ . Derived quantities  $\alpha_F = \beta_F/(1 + \beta_F)$  and  $\alpha_R = \beta_R/(1 + \beta_R)$  are also

used to make the expressions more compact. The Ebers–Moll model is

$$i_E = \frac{I_s}{\alpha_F} \left( e^{v_{BE}/V_T} - 1 \right) - I_s \left( e^{v_{BC}/V_T} - 1 \right) \quad (4.1)$$

$$i_C = I_s \left( e^{v_{BE}/V_T} - 1 \right) - \frac{I_s}{\alpha_R} \left( e^{v_{BC}/V_T} - 1 \right) \quad (4.2)$$

$$i_B = \frac{I_s}{\beta_F} \left( e^{v_{BE}/V_T} - 1 \right) + \frac{I_s}{\beta_R} \left( e^{v_{BC}/V_T} - 1 \right). \quad (4.3)$$

In the Wave Digital Filter context, we will always be thinking in terms of ports rather than individual terminals, so the three terminals will need to be paired off to form two ports. Since the Ebers–Moll model (4.1)–(4.3) is derived in terms of voltage drops, it is natural to choose those voltage drops  $v_{BE}$  and  $v_{BC}$  as the port voltages and define the port currents  $i_{BE}$  and  $i_{BC}$  in terms of  $i_B$ ,  $i_C$ , and  $i_E$  in the appropriate way. This port-wise way of viewing an NPN BJT is shown in Figure 4.1b. For this port definition, port voltages and currents are given in terms of terminal voltages and branch currents according to

$$v_{BE} = v_B - v_E \quad (4.4)$$

$$v_{BC} = v_B - v_C \quad (4.5)$$

$$i_{BE} = i_E \quad (4.6)$$

$$i_{BC} = -i_C, \quad (4.7)$$

which yields a description for the port currents in terms of the port voltages

$$i_{BE} = \frac{I_s}{\alpha_F} \left( e^{v_{BE}/V_T} - 1 \right) - I_s \left( e^{v_{BC}/V_T} - 1 \right) \quad (4.8)$$

$$i_{BC} = -I_s \left( e^{v_{BE}/V_T} - 1 \right) + \frac{I_s}{\alpha_R} \left( e^{v_{BC}/V_T} - 1 \right). \quad (4.9)$$

Although this may be the most natural way to think of an NPN BJT in terms of ports, mathematically there should be  $3 \times 2 \times 2 = 12$  different ways to define the ports of any three-terminal device.

More complicated models of NPN BJTs exist. Some can be viewed as extensions of the Ebers–Moll model and some work on different principles though reduce back to the Ebers–Moll model under simplifying assumptions [247]. Here we'll mention a few, using equivalent circuit representations for the models rather than dealing with the unwieldy equations directly. The equivalent circuit of the Ebers–Moll model of the NPN BJT is shown in Figure 4.2a. This model can be refined to more accurately reflect the behavior of the real device (this is more important at high frequencies) by adding small series resistances at each terminal and depletion (Miller) capacitances across the  $p$ – $n$  junctions [52, 247]; this is shown in Figure 4.2b. A special base-width modulation effect called the Early Effect [247, 263] can be represented as another controlled source and refines the model further,

as shown in Figure 4.2c. The Gummel–Poon model [264, 247] shown in Figure 4.2d is even more refined.

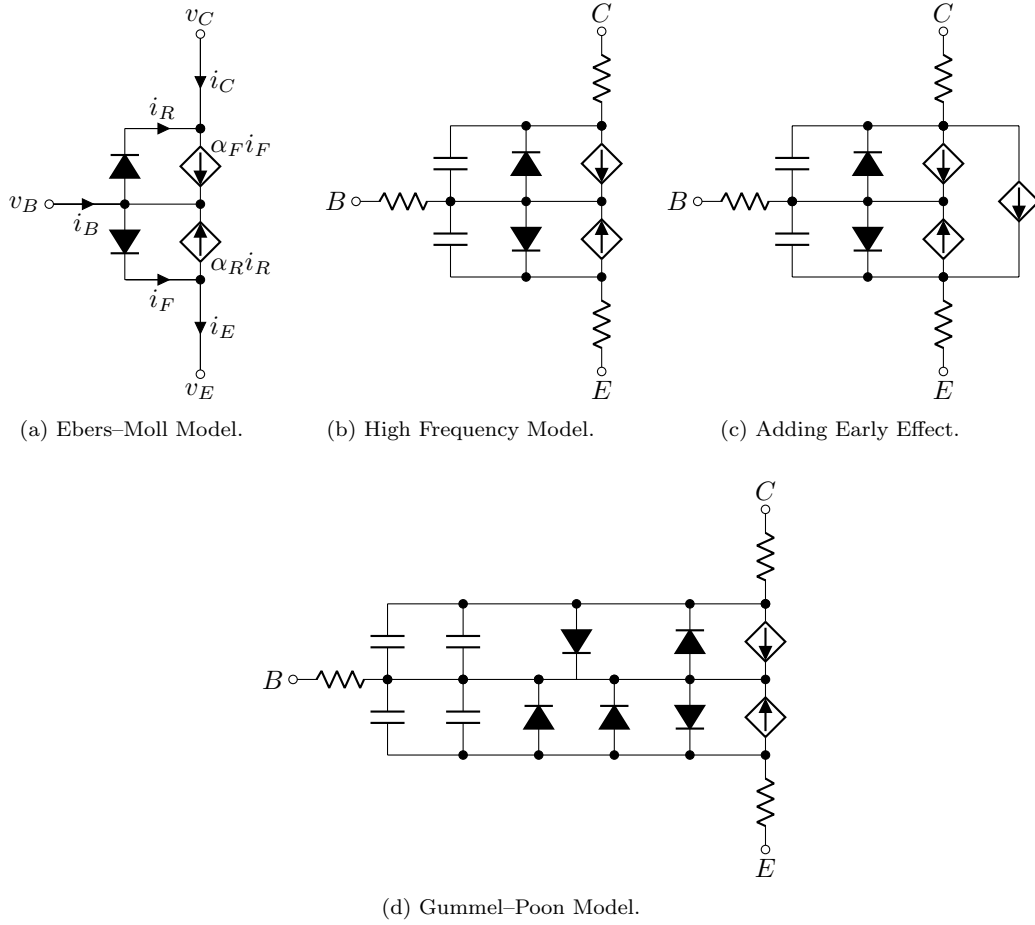


Figure 4.2: Different Equivalent Circuit Models of NPN BJTs.

Although these models are more refined than the Ebers–Moll mode, they can be unwieldy to use because they require a large number (up to 25) parameters to be specified [247], which are neither typically provided by transistor manufacturers nor very simple to measure. For simplicity, we will only use the basic Ebers–Moll model in this dissertation.

### PNP BJT

Another type of Bipolar Junction Transistor is the *PNP BJT*. Like its NPN cousin, this device has three terminals, a base (*B*), collector (*C*) and emitter (*E*). The symbol for an PNP BJT is shown in Figure 4.3, with terminal voltages  $v_B$ ,  $v_C$ , and  $v_E$  and branch currents  $i_B$ ,  $i_C$ , and  $i_E$  labeled.

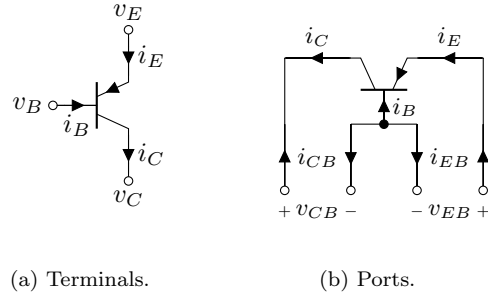


Figure 4.3: Symbol of PNP Bipolar Junction Transistor with Terminal Voltages and Branch Currents Labeled, and One Way of Viewing it from a Port-Wise Perspective.

The only difference between the PNP and the NPN BJTs is the orientation of the  $p-n$  junctions in the device. This means that the port voltages have flipped signs, or that orientation of the elements in the equivalent circuit have all flipped polarities. Because of this similarity, the PNP BJT can be modeled using the same approaches as the NPN BJT.

The PNP BJT's Kirchhoff-domain description is given by the Ebers–Moll model as

$$i_E = \frac{I_s}{\alpha_F} \left( e^{v_{EB}/V_T} - 1 \right) - I_s \left( e^{v_{CB}/V_T} - 1 \right) \quad (4.10)$$

$$i_C = I_s \left( e^{v_{EB}/V_T} - 1 \right) - \frac{I_s}{\alpha_R} \left( e^{v_{CB}/V_T} - 1 \right) \quad (4.11)$$

$$i_B = \frac{I_s}{\beta_F} \left( e^{v_{EB}/V_T} - 1 \right) + \frac{I_s}{\beta_R} \left( e^{v_{CB}/V_T} - 1 \right). \quad (4.12)$$

Grouping the terminals in a port-wise fashion as with the NPN transistor (but with flipped polarity), as shown in Figure 4.3b, port voltages and currents are given in terms of terminal voltages and branch currents according to

$$v_{EB} = v_E - v_B \quad (4.13)$$

$$v_{CB} = v_C - v_B \quad (4.14)$$

$$i_{EB} = i_E \quad (4.15)$$

$$i_{CB} = -i_C, \quad (4.16)$$

which yields a description for the port currents in terms of the port voltages for a PNP transistor,

given by

$$i_{EB} = \frac{I_s}{\alpha_F} \left( e^{v_{EB}/V_T} - 1 \right) - I_s \left( e^{v_{CB}/V_T} - 1 \right) \quad (4.17)$$

$$i_{CB} = -I_s \left( e^{v_{EB}/V_T} - 1 \right) + \frac{I_s}{\alpha_R} \left( e^{v_{CB}/V_T} - 1 \right). \quad (4.18)$$

The more advanced models for the PNP transistor will be identical to those for the NPN transistor, making the proper exchange of terminals and change of polarity for the diodes and controlled sources.

## MOSFET

Another important type of transistor for audio circuits is the Metal-Oxide-Semiconductor Field-Effect Transistor (MOSFET) [247], which can also be used, e.g., in switching and amplification applications, or as a sort of voltage-controlled resistor [71].

A MOSFET has three terminals, a gate ( $G$ ), drain ( $D$ ) and source ( $S$ ). The simplest model of a MOSFET in the Kirchhoff domain is the Shichman–Hodges model [265], which is also used in SPICE modeling [146, pp. 102–103]. The Shichman–Hodges model gives the currents  $i_G$ ,  $i_D$ , and  $i_S$  as a function of the voltage drops  $v_{GS} = v_G - v_S$  and  $v_{DS} = v_D - v_S$  and is parameterized by a number of parameters.

More complicated models of MOSFETs [146] and models of other transistors exist, but are outside the scope of our consideration.

### 4.1.2 Triode Modeling

Triodes are important three-terminal electronic devices that were used heavily in the early days of audio circuitry. Important basic applications include simple amplifiers (e.g. common-cathode). In audio, their most famous use is as an essential part of guitar amplifiers, where their operation and peculiarities are believed to be responsible for much of the essence of an amplifier’s sound [13].

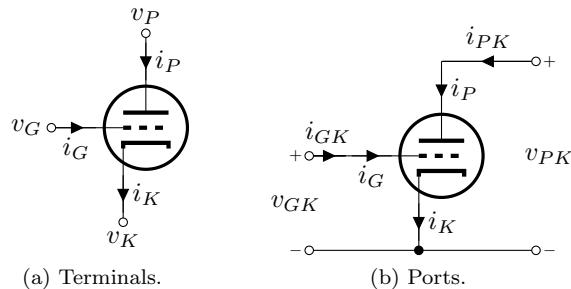


Figure 4.4: Symbol of a Triode with Terminal Voltages and Branch Currents Labeled, and One Way of Viewing it From a Port-Wise Perspective.

A triode has three terminals, a grid ( $G$ ), cathode ( $K$ ) and plate ( $P$ ). The symbol for a triode is shown in Figure 4.1a, with terminal voltages  $v_G$ ,  $v_K$ , and  $v_P$  and branch currents  $i_G$ ,  $i_K$ , and  $i_P$  labeled.

Triode modeling is an active area of research; here we'll mention only a few. Some early models, such as Sjursen's model, were intended for use in SPICE simulations [266]. A model which has been used in the Virtual Analog context [267] is Koren's model [268]. Cardarilli offers a refined model [269], and Dempwolf and Zölzer offer a physically-motivated triode model [70] which has been verified in the context of a state-space-based Virtual Analog simulation of a common-cathode amplifier [63]. Here as an example we'll briefly review the Dempwolf model, which has been used in Wave Digital Filter modeling of the Preamplifier stage of the Fender Bassman 5F6-A [270].

Dempwolf's model gives the cathode and grid currents  $i_P$  and  $i_G$  as a function of the terminal voltages  $v_{GK}$  and  $v_{PK}$

$$i_P = G \left( \log \left( 1 + \exp \left( C \left( \frac{1}{\mu} v_{PK} + v_{GK} \right) \right) \right) \frac{1}{C} \right)^\gamma \quad (4.19)$$

$$i_G = G_G \left( \log \left( 1 + \exp \left( C_G \cdot v_{GK} \right) \right) \frac{1}{C_G} \right)^\xi, \quad (4.20)$$

parameterized by amplification factor  $\mu$ , permeances  $G$  and  $G_G$ , exponents  $\gamma$  and  $\xi$ , adaption factors  $C$  and  $C_G$ , and a current constant  $I_{G0}$  [70]. Using the same logic as for the BJTs, we can choose the Grid–Cathode and Plate–Cathode junctions as the two ports of the device, finding a simple relationship between the basic Kirchhoff domain behavior and the port behavior

$$i_{GK} = G_G \left( \log \left( 1 + \exp \left( C_G \cdot v_{GK} \right) \right) \frac{1}{C_G} \right)^\xi \quad (4.21)$$

$$i_{PK} = G \left( \log \left( 1 + \exp \left( C \left( \frac{1}{\mu} v_{PK} + v_{GK} \right) \right) \right) \frac{1}{C} \right)^\gamma. \quad (4.22)$$

Again, other combinations of terminals and polarities are possible, but this one has the most natural fit with the model's original expression.

## 4.2 Previous Work

Even though models for common nonlinear devices (some of which we discussed above) are well known, incorporating more than one nonlinear port into a Wave Digital Filter simulation is not simple. The reason for this is that nonlinear devices in general cannot be adapted, and hence are only suitable for inclusion at the root of the Wave Digital Filter structure. Since in the classical approach there is only one root element in the tree, the approach described in Chapter 3 cannot be used and other approaches must be explored.

Trying to solve this problem for different specific cases and classes of circuits has been a major

focus of Wave Digital Filter research in the Virtual Analog community. In this Section we'll review previous work on this issue, covering approaches based on inserting fictitious unit delays and cross-controlled models of the nonlinearities (§4.2.1), iterative methods (§4.2.2), and methods based on simplifying or linearizing the collection of nonlinearities (§4.2.3). Finally the affordances and limitations of these approaches are reviewed (§4.2.4).

#### 4.2.1 Fictitious Delays and Cross-Control Models

In the earliest days of Wave Digital Filters, the concept of adaptation had not been developed yet, and unit elements had to be inserted between stages of ladder circuits to render their Wave Digital Filter simulations computable [87, 88]. When dealing with multiple nonadaptable nonlinear elements, a similar strategy has been used. This approach to modeling a circuit with multiple nonlinearities is to first design a Wave Digital Filter structure with no special regard for computability of nonlinearities, allow all but one of those nonlinearities to exist at leaves in the Wave Digital Filter tree, and then add a fictitious unit delay after the reflected wave of each nonlinearity. This solves the computability problem, but at the cost of potentially significant error coming from the fictitious unit delays. Remember that in a normal Wave Digital Filter, capacitors and inductors turn into unit delays or unit delays with a sign flip. Therefore adding fictitious unit delays is somewhat akin to adding extra reactances. A more theoretical development in this direction is the “dynamic adaption” approach proposed by Bernardini and Sarti [228]. Rather than inserting fictitious unit delays in the wave signal flow path, this can be seen as inserting fictitious unit delays in the calculation of the port resistance necessary to “adapt” one-port nonlinearities which normally cannot be adapted; the use of power wave in their approach is essential to avoid altering the stored energy in the circuit as the port resistances change.

The technique of adding ad hoc unit delays has been used, e.g., for modeling nonlinear transmission lines which include numerous nonlinear capacitances [271], nonlinear audio transformers which include nonlinear resistances and capacitances in the transformer core model as well as in winding models [236], and the Fairchild 670 Limiter which includes four triodes [272]. In [272], unit elements are used to separate the “push” and “pull” halves of the amplifier, as well as *within* the model of each triode, which is implemented as a “cross-control” model [174, 175].

In [174], Karjalainen and Pakarinen modeled a single triode amplifier using a “cross-control” model for the triode. Rather than using a full model of the triode, they make the assumption that the grid current is zero, splitting the circuit into two stages. In the second stage, the assumption of zero grid current allows them to treat the triode as a one-port plate–cathode nonlinearity which is parameterized by the grid–cathode voltage. Even splitting the circuit into two disjunct stages, the cathode voltage depends instantaneously on the behavior of the plate–cathode nonlinearity, setting up a delay-free loop. This is resolved by inserting an ad hoc unit delay. This model has been used in modeling the output chain of a tube amplifier [273]. Pakarinen and Karjalainen further extended

this approach to incorporating a triode by relaxing the assumption of zero grid current [175]. This approach does, however, retain the ad hoc unit delay in the calculation of the grid–cathode voltage. This model has also been implemented as a Csound opcode by Fink and Rabenstein [274]. Cross-controlled models have also been proposed for NPN BJTs. De Sanctis and Sarti propose a model for an NPN BJT-based common-emitter amplifier which ignores the base current of the BJT, framing it rather as a voltage-controlled current source, where  $i_C$  is controlled by  $v_{BE}$  [6].

### 4.2.2 Iteration

In [176], D’Angelo *et al.* propose further refinements to [174, 175], eliminating the need for the ad hoc unit delay inside of the triode model. Rather, they resolve the implicit relationship inside the triode using a special secant-method-derived iterative method which is designed specifically to work with the Cardarilli triode model [269]. They demonstrate this refinement on a common-cathode triode amplifier case study, showing reduced error compared to the previous methods. Conceptually, a crucial part of their approach is that the memoryless nonlinearity is indeed modeled by a memoryless model; previous approaches added fictitious memory to the triode models through the use of ad hoc unit delays.

Another approach to iterative solution of structures which involve delay-free loops has been proposed by Schwerdtfeger and Kummert, who show applications to a class of ladder circuits [227] and to diode clippers [225, 226]. Related work shows the application of the same method to circuits with non-tree-like arrangements of series and parallel adaptors [224]; in their formulation the use of  $\mathcal{R}$ -type adaptors is not considered. Their approach amounts to inserting ad-hoc unit delays, but viewing them as a multidimensional extension to a second time dimension and using global iteration on the Wave Digital Filter structure to iteratively eliminate the effect of the extra delays. A Lipschitz-criterion-based look at contractivity properties of certain Wave Digital Filter elements is said to guarantee the convergence of this algorithm. Here the choice of port impedance at ports where the fictitious delays are inserted is very influential on the rate of convergence; Newton–Raphson- and pseudo-secant-based iterative methods are proposed to speed up the convergence [226].

### 4.2.3 Linearization and Simplified Models

An approach to handling multiple nonlinearities called “Simplified Models” was proposed by Bernardini *et al.* [262]. In this approach, a class of nonlinearities based on combinations of diodes and BJTs in certain topology<sup>1</sup> are approximated and solved using the Lambert  $\mathcal{W}$  function; they show applications to a range of circuits including a transformerless ring modulator [275], a half-wave rectifier, an electrical damper [276, 277], and common collector, common emitter, and common base BJT amplifiers. For the BJTs, only the most important nonlinear port is considered to conduct at any

---

<sup>1</sup>Each of the three terminals of the BJT is considered to have a port to ground and each pair of terminals is considered to have a port between them: the so-called “Extended Ebers–Moll” Model [262].

one time and the others are neglected, leaving behind a single  $p$ - $n$  junction (equivalent to a diode) that can be solved using advanced versions of the method of [212].

Sometimes, certain nonlinear devices can be linearized (that is, viewed as linear around their operating point) without affecting the accuracy of the simulation. This technique was proposed for Wave Digital Filters in the power electronics context by Fiedler and Grotstollen [278, 279] and in the Virtual Analog context by De Sanctis and Sarti [6]. We used it in our Chapter 1 case study on the TR-808 Bass Drum Output Filter, linearizing the emitter-follower to create a completely linear reference circuit to model.

A more complicated version of linearization is building piecewise linear models, which generalize the approach of [248] to multiport devices. This approach can be used to model networks of idealized diodes [278, 279] and devices with curved characteristics approximated by breakpoints [276, 280, 277].

#### 4.2.4 Evaluation of Previous Work

The body of work on modeling nonlinear devices in the Wave Digital Filter context is quite diverse and exploits a variety of techniques as appropriate. We can even imagine combining these methods to get even better behavior, e.g., combining the linearization approach with the Simplified Model approach by linearizing the less-conducting nonlinear ports rather than neglecting them entirely. Most of the approaches we've reviewed show accurate behavior in case studies on appropriate circuits, demonstrating that these approaches can be quite useful. Although these approaches can be useful for certain circuits, they face a number of limitations. All of these approaches face at least one of the following issues:

1. They involve fictitious ad hoc delays which introduce error and can affect the stability of the simulation;
2. The nonlinear devices are simplified or neglected, affecting the accuracy of the simulation;
3. The difficult part of the problem is not localized to one part of the Wave Digital Filter simulation; or
4. The dimensionality of the nonlinear part of the problem is related to the topology of the problem, rather than solely to the number of nonlinearities in the circuit.

The first two issues relate mainly to the *accuracy* of the simulation and can sometimes be avoided through skillful engineering choices. The last two issues are far more serious, since they relate to some of the fundamental assumptions of the Wave Digital Filter approach and the potential for setting up and solving a Wave Digital Filter simulation of any circuit in a generalized way. So, the most important limitation which all of these approaches suffer from is that none of the approaches is applicable to a very wide range of circuits. Some of the techniques are designed to work for only a single type of nonlinearity or even a single circuit and hence cannot be considered very extensible to

the general case of the arbitrary circuits which may be encountered by the Virtual Analog algorithm designer..

A generalized approach is desirable for a number of reasons. First, understanding a general theory widens the range of circuits which can be modeled. Second, I propose that the best starting place for Virtual Analog circuit simulation is understanding how to model a circuit exactly, with no simplifications. After that model is established, simplifications can be made to the structure to reduce the computational complexity. However, with the current state of the art it is neither possible to build a block diagram of a Wave Digital Filter for any arbitrary structure, nor is it known in a general way what mathematical relationships should exist inside of certain blocks that may arise in Wave Digital Filter structures, like  $\mathcal{R}$ -type adaptors and nonlinearities. Finally, someday we may hope to model complicated circuits using Wave Digital Filters in an *automated* fashion. For this to be possible, Wave Digital Filter modeling approaches must be *systematized*; in an automatically-generated structure it will not be possible to rely on the ad hoc application of specialized domain knowledge about the circuit or the trade-offs of various macro-level simplifications in designing the simulation.

### 4.3 Proposed Method

Here we propose a systematic approach to Wave Digital Filter modeling of circuits which involve more than one nonlinearity. On a structural level, this approach is very general and has no theoretical limit to the number of nonlinearities that can be accommodated. On a computational level, the complexity of the nonlinear part of the approach is related to the number of nonlinearities in the circuit, not the complexity of the topology. Unlike many of the approaches in literature, where it is common to consider certain types of circuits like circuits with feedback as special unhandled cases [6, 176], our approach is fully general and does not require treating any type of circuit topology as a special case.

The proposed approach works by collecting all nonlinearities together into a vector, interfacing that vector of nonlinearities to the rest of the circuit (which has a standard Wave Digital Filter tree structure) with an  $\mathcal{R}$ -type adaptor, and resolving the implicit relationship between the vector of nonlinearities and the  $\mathcal{R}$ -type adaptor using methods like table lookup or Newton–Raphson iteration. The original presentation of this approach in [230, 231] focused on the common voltage wave case. Here we extend that approach to the parametric wave case.

To present our approach in more detail, we'll first explain how the global Wave Digital Filter structure can be derived by grouping the nonlinearities (§4.3.1). This generates a global structure with an  $\mathcal{R}$ -type topology interfacing the multiple nonlinear (and nonadaptable) elements to the rest of the circuit; its mathematical description is then described (§4.3.2). Two methods, one based on table lookup and one based on Newton–Raphson iteration, are proposed for resolving the

implicit loop inside this structure (§4.3.3). Finally, the system matrices  $\mathbf{S}$  and  $\mathbf{C}$  are populated by solving the scattering relationship of the  $\mathcal{R}$ -type topology and applying the definition of wave variables to interface the Kirchhoff variables of the nonlinearity with the wave variables of the  $\mathcal{R}$ -type adaptor (§4.3.4)

### 4.3.1 Grouping Nonlinearities

To begin, we must set up the global structure of the simulation. Here we take aim specifically at the fact that previous work does not necessarily *localize* nonadaptible elements of the reference circuit. This has the potential to implicate normal Wave Digital Filter building blocks into global iterative schemes, which we would like to avoid. To accomplish this we'll again return to the replacement graph technique of Fränken *et al.* [197, 198]. Rather than using replacement graphs to keep multiport linear elements in one block of the structure (their original intent), or using it to group nonadaptible linear elements together at the root of the tree (as we did in §4.3.3), we'll here use the replacement graph technique to group all of the *nonlinear* ports together at the root of the tree. Again, one single replacement graph is introduced for the entire collection of all nonlinear elements. This yields a global structure with all nonlinear elements grouped at the top of the tree, an  $\mathcal{R}$ -type topology which interfaces these nonlinear elements to the rest of the circuit, and a collection of one or more Wave Digital Filter trees below. Again the trees below may take any form and are handled with classical techniques.

As an example of how the method of Fränken *et al.* can be applied to derive the Wave Digital Filter structure, we consider one distortion stage from the Electro-Harmonix Big Muff Pi distortion pedal. Full details on the Wave Digital Filter simulation of this circuit are given in [231]. The Big Muff Pi circuit is shown in Figure 4.5a. To derive the Wave Digital Filter structure for this circuit, first a graph representing the circuit is formed (Figure 4.5b) using replacement graphs for the nonlinearities: an NPN transistor and a diode pair. In this graph, nodes correspond to circuit nodes and are each assigned a lowercase letter; nameless replacement graph nodes are indicated in gray. Graph edges correspond to ports in the circuit and are each assigned an Arabic numeral and nameless replacement graph edges are indicated in gray. To decompose this graph, we follow the procedure of Fränken *et al.* [198] to find split components (Figure 4.5c). This yields a Wave Digital Filter structure with two series adaptors, two parallel adaptors, an  $\mathcal{R}$ -type adaptor, linear one ports, and nonlinear devices grouped into a vector. From here a modified SPQR tree is formed (Figure 4.5d). A Wave Digital Filter adaptor structure follows by identity from this SPQR tree (Figure 4.5e). In this Wave Digital Filter structure everything is handled using classical techniques except the grouped nonlinearities (shaded in dark gray) and the  $\mathcal{R}$ -type adaptor (shaded in light gray). For those, the proposed method is used to solve them jointly. A rearranged version of Figure 4.5e which highlights the derived adaptor structure is shown in Figure 4.5f.

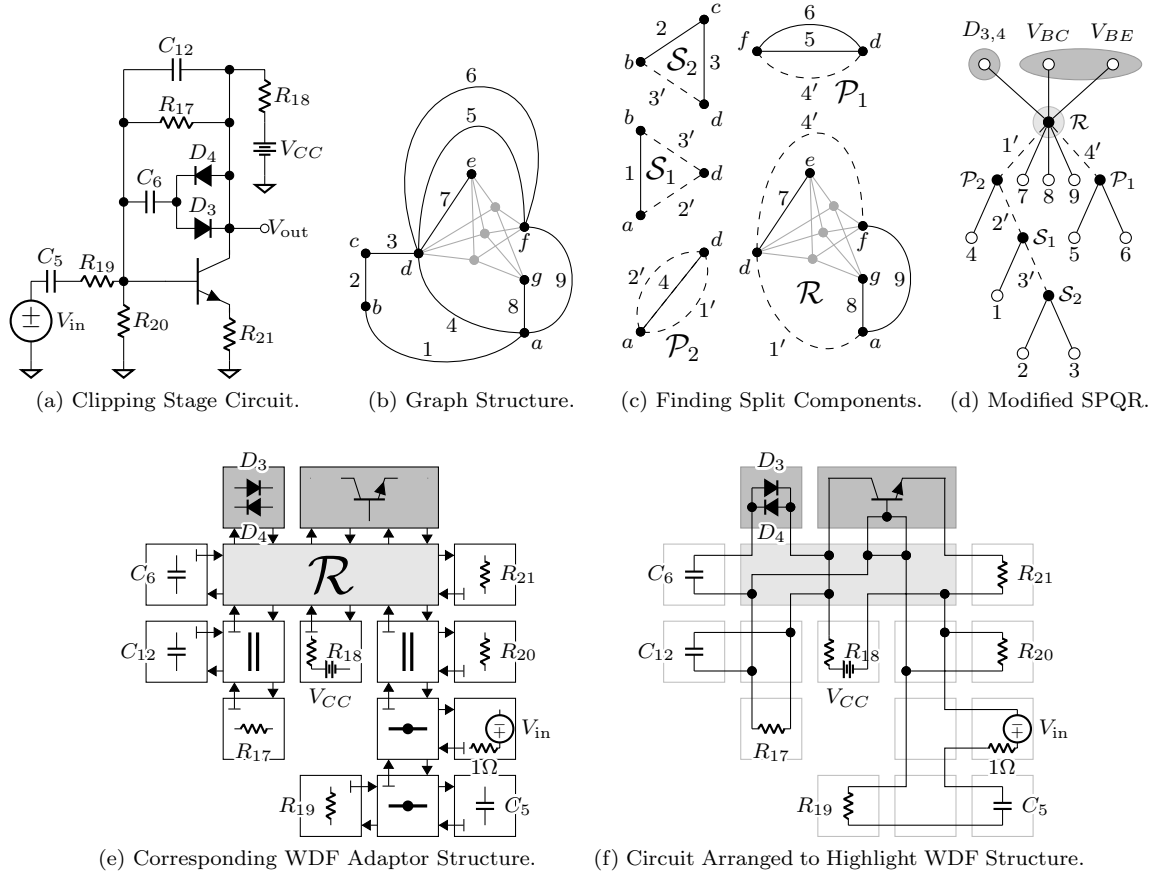


Figure 4.5: Deriving a WDF Adaptor Structure for the Big Muff Pi Clipping Stage.

### 4.3.2 Mathematical Structure

To set up the mathematics describing the root structure, we must look closely at what variables are used to describe the classical Wave Digital Filter trees, the  $\mathcal{R}$ -type topology, and the vector of nonlinear elements. The nonlinearities at the root of the tree are naturally described in the Kirchhoff domain. As we saw earlier in this Chapter, common nonlinear electrical devices used in audio circuits are described in the Kirchhoff domain by functions relating port voltages to port currents

$$\mathbf{i} = \mathbf{f}(\mathbf{v}). \quad (4.23)$$

In Chapter 2 we developed methods for finding the scattering matrix of  $\mathcal{R}$ -type topologies. So given our tool set they may be said to be naturally expressed in the wave domain by a scattering relationship

$$\mathbf{b} = \mathbf{S}\mathbf{a}. \quad (4.24)$$

Partitioning the ports of the  $\mathcal{R}$ -type adaptor into “internal” /  $i$  (facing the nonlinearities) and “external” /  $e$  (facing the classical trees below), this scattering relationship is represented by the equation

$$\begin{bmatrix} \mathbf{b}_i \\ \mathbf{b}_e \end{bmatrix} = \begin{bmatrix} \mathbf{S}_{11} & \mathbf{S}_{12} \\ \mathbf{S}_{21} & \mathbf{S}_{22} \end{bmatrix} \begin{bmatrix} \mathbf{a}_i \\ \mathbf{a}_e \end{bmatrix} \quad (4.25)$$

We’ll discuss how to populate this partitioned  $\mathbf{S}$  matrix at the end of this Section.

Now, our issue is that the Kirchhoff-domain nonlinearities take a vector of voltages  $\mathbf{v}_c$  as an input and produce a vector of currents  $\mathbf{i}_c$  as an output, while the ports facing the nonlinearities produce a vector of reflected wave variables  $\mathbf{b}_i$  as an output and expect a vector of incident wave variables  $\mathbf{a}_i$  as an input. Clearly these variables are not coherent. Luckily, we know that wave variables and Kirchhoff variables are just linear combinations of one another, so we can develop a matrix to allow these variables to interface. First consider a “converter” which receives a vector of wave variables  $\mathbf{a}_c$  and the vector of nonlinearity currents  $\mathbf{i}_c$  as inputs, and produces a vector of nonlinear port voltages  $\mathbf{v}_c$  and vector of reflected waves  $\mathbf{b}_c = \mathbf{a}_i$  as outputs. This linear relationship takes the form

$$\begin{bmatrix} \mathbf{v}_c \\ \mathbf{b}_c \end{bmatrix} = \begin{bmatrix} \mathbf{C}_{11} & \mathbf{C}_{12} \\ \mathbf{C}_{21} & \mathbf{C}_{22} \end{bmatrix} \begin{bmatrix} \mathbf{i}_c \\ \mathbf{a}_c \end{bmatrix} \quad (4.26)$$

In the block diagram of the algorithm, we’ll call this the “ $w-K$  converter” since it converts between wave and Kirchhoff variables [118]. We’ll discuss how to populate this partitioned  $\mathbf{C}$  matrix at the end of this Section.

The entire mathematical structure at the root is thus described by the system of equations<sup>2</sup>

$$\text{Kirchhoff nonlinearity} \quad \left\{ \begin{array}{l} \mathbf{i}_c = \mathbf{f}(\mathbf{v}_c) \end{array} \right. \quad (4.27)$$

$$\text{ } w-K \text{ converter} \quad \left\{ \begin{array}{l} \mathbf{v}_c = \mathbf{C}_{11}\mathbf{i}_c + \mathbf{C}_{12}\mathbf{a}_c \\ \mathbf{b}_c = \mathbf{C}_{21}\mathbf{i}_c + \mathbf{C}_{22}\mathbf{a}_c \end{array} \right. \quad (4.28)$$

$$\text{compatibility} \quad \left\{ \begin{array}{l} \mathbf{a}_c = \mathbf{b}_i \\ \mathbf{a}_i = \mathbf{b}_c \end{array} \right. \quad (4.30)$$

$$\text{scattering} \quad \left\{ \begin{array}{l} \mathbf{b}_i = \mathbf{S}_{11}\mathbf{a}_i + \mathbf{S}_{12}\mathbf{a}_e \\ \mathbf{b}_e = \mathbf{S}_{21}\mathbf{a}_i + \mathbf{S}_{22}\mathbf{a}_e \end{array} \right. \quad (4.32)$$

$$(4.33)$$

and is shown as a vector signal flow graph in Figure 4.6a.

We can immediately see some issue with this signal flow graph that would present this mathematical structure from being implemented directly. It contains numerous delay-free directed loops, two of which are emphasized on the Figure. Therefore, in this form, the structure is still noncomputable. To begin to solve this problem, we can perform some algebraic manipulations on the structure that

---

<sup>2</sup>Thank you to Maximilian Rest for catching a typographical error in [230].

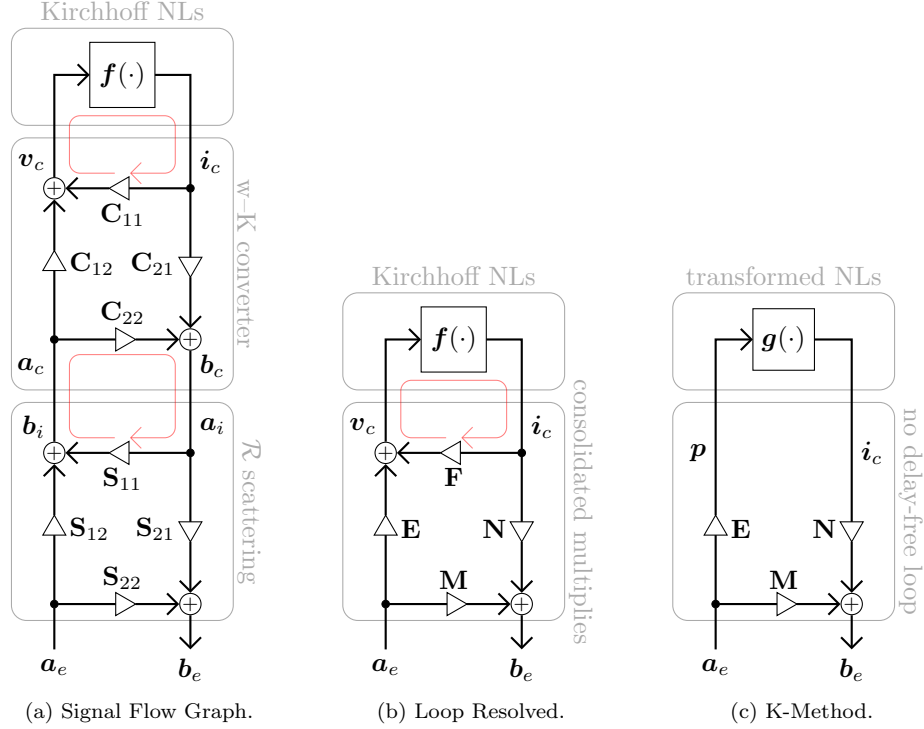


Figure 4.6: Proposed Method Signal Flow Graphs.  $\mathbf{a}_E$  is Supplied by and  $\mathbf{b}_E$  Delivered to Classical WDF Subtrees Below.

simplify the structure. First, we consider (4.28) and (4.33) in matrix form

$$\begin{bmatrix} \mathbf{v}_c \\ \mathbf{b}_e \end{bmatrix} = \begin{bmatrix} \mathbf{C}_{12} & \mathbf{0} \\ \mathbf{0} & \mathbf{S}_{21} \end{bmatrix} \begin{bmatrix} \mathbf{a}_c \\ \mathbf{a}_i \end{bmatrix} + \begin{bmatrix} \mathbf{C}_{11} & \mathbf{0} \\ \mathbf{0} & \mathbf{S}_{22} \end{bmatrix} \begin{bmatrix} \mathbf{i}_c \\ \mathbf{a}_e \end{bmatrix} \quad (4.34)$$

and (4.29)–(4.32) in matrix form (eliminating  $\mathbf{b}_i$  and  $\mathbf{b}_c$ )

$$\begin{bmatrix} \mathbf{I} & -\mathbf{S}_{11} \\ -\mathbf{C}_{22} & \mathbf{I} \end{bmatrix} \begin{bmatrix} \mathbf{a}_c \\ \mathbf{a}_i \end{bmatrix} = \begin{bmatrix} \mathbf{0} & \mathbf{S}_{12} \\ \mathbf{C}_{21} & \mathbf{0} \end{bmatrix} \begin{bmatrix} \mathbf{i}_c \\ \mathbf{a}_e \end{bmatrix}. \quad (4.35)$$

Solving (4.35) for the internal port variables  $\begin{bmatrix} \mathbf{a}_c^\top & \mathbf{a}_i^\top \end{bmatrix}^\top$  yields

$$\begin{bmatrix} \mathbf{a}_c \\ \mathbf{a}_i \end{bmatrix} = \begin{bmatrix} \mathbf{S}_{11}\mathbf{H}\mathbf{C}_{21} & \mathbf{S}_{12} + \mathbf{S}_{11}\mathbf{H}\mathbf{C}_{22}\mathbf{S}_{12} \\ \mathbf{H}\mathbf{C}_{21} & \mathbf{H}\mathbf{C}_{22}\mathbf{S}_{12} \end{bmatrix} \begin{bmatrix} \mathbf{i}_c \\ \mathbf{a}_e \end{bmatrix}, \quad (4.36)$$

where  $\mathbf{H} = (\mathbf{I} - \mathbf{C}_{22}\mathbf{S}_{11})^{-1}$ . Plugging (4.36) into (4.34) and recalling (4.27) yields a consolidated

version of (4.27)–(4.33)

$$\begin{cases} \mathbf{i}_c = f(\mathbf{v}_c) \\ \mathbf{v}_c = \mathbf{E}\mathbf{a}_e + \mathbf{F}\mathbf{i}_c \\ \mathbf{b}_e = \mathbf{M}\mathbf{a}_e + \mathbf{N}\mathbf{i}_c \end{cases} \quad (4.37)$$

with

$$\begin{cases} \mathbf{E} = \mathbf{C}_{12}(\mathbf{I} + \mathbf{S}_{11}\mathbf{H}\mathbf{C}_{22})\mathbf{S}_{12} \\ \mathbf{F} = \mathbf{C}_{12}\mathbf{S}_{11}\mathbf{H}\mathbf{C}_{21} + \mathbf{C}_{11} \\ \mathbf{M} = \mathbf{S}_{21}\mathbf{H}\mathbf{C}_{22}\mathbf{S}_{12} + \mathbf{S}_{22} \\ \mathbf{N} = \mathbf{S}_{21}\mathbf{H}\mathbf{C}_{21} \end{cases} \quad (4.38)$$

which is shown as a vector signal flow graph in Figure 4.6b.

In this form, the structure is still computable due to one remaining delay-free loop. However, this framework is now a standard mathematical form, basically a version of nonlinear state space with a length-0 state vector. So, we may use techniques that are known to resolve nonlinear state space systems to resolve this loop.

### 4.3.3 Resolving Implicit Relationships

So far, the development of this approach has exactly paralleled the development of the approach in §2.3 which allows Wave Digital Filter modeling of circuit involving multiple nonadaptable linear elements (e.g., open circuits, closed circuits, ideal sources, switches). When it comes to resolving the implicit loop remaining in that approach, the linearity of the nonadaptable elements involved means that only a matrix inverse is involved. However, now that we are considering the more complicated case of *nonlinear* nonadaptable elements, a more complicated solution is required. Here we'll consider two approaches to resolving the implicit loop, one based on table lookup and one based on Newton–Raphson iteration.<sup>3</sup>

#### Resolving with K Method

One approach to resolving the loop is called the K Method [55, 54], and was designed to resolve loops like this in nonlinear state space systems. The K Method reorganizes (4.37)–(4.38) into the form

$$\begin{cases} \mathbf{i}_c = (\mathbf{p}) \\ \mathbf{p} = \mathbf{E}\mathbf{a}_e \\ \mathbf{b}_e = \mathbf{M}\mathbf{a}_e + \mathbf{N}\mathbf{i}_c \end{cases} \quad (4.39)$$

---

<sup>3</sup>Other more exotic solutions may be possible, for instance using kernel regression [281], but they will not be discussed here.

again with

$$\begin{cases} \mathbf{E} = \mathbf{C}_{12}(\mathbf{I} + \mathbf{S}_{11}\mathbf{H}\mathbf{C}_{22})\mathbf{S}_{12} \\ \mathbf{M} = \mathbf{S}_{21}\mathbf{H}\mathbf{C}_{22}\mathbf{S}_{12} + \mathbf{S}_{22} \\ \mathbf{N} = \mathbf{S}_{21}\mathbf{H}\mathbf{C}_{21} \end{cases}. \quad (4.40)$$

Here the new nonlinear vector equation  $\mathbf{g}(\cdot)$  which maps  $\mathbf{g}(\cdot) : \mathbf{p} \rightarrow \mathbf{i}_c$  is related to the original Kirchhoff-domain nonlinear vector function  $\mathbf{f}(\cdot)$  which maps  $\mathbf{f}(\cdot) : \mathbf{v}_c \rightarrow \mathbf{i}_c$  according to the following transformation

$$\begin{bmatrix} \mathbf{p} \\ \mathbf{i}_c \end{bmatrix} = \begin{bmatrix} \mathbf{I} & -\mathbf{K} \\ \mathbf{0} & \mathbf{I} \end{bmatrix} \begin{bmatrix} \mathbf{v}_c \\ \mathbf{i}_c \end{bmatrix}. \quad (4.41)$$

In nonlinear state space systems in general, the matrix  $\mathbf{K}$  depends on the chosen discretization method [54] and the dynamics of the system. Since our system has no dynamics (we are dealing with dc nonlinearities only), we simply have  $\mathbf{K} = \mathbf{F}$  from (4.38). This system of equations is shown as a vector signal flow graph in Figure 4.6c. Since each entry in  $\mathbf{p}$  is formed by different linear combinations of voltages and currents, we can consider  $\mathbf{p}$  to be a pseudo-wave variable, albeit one without an immediate physical interpretation [123].

This transformation allows us to tabulate solutions to  $\mathbf{f}(\cdot)$ , which is explicit and easy to tabulate, and transform it to  $\mathbf{g}(\cdot)$ , a domain where it would be difficult to tabulate directly. Then table interpolation methods can be used on this tabulation. A limitation of this approach is that the tables can grow very unwieldy for more than two or three nonlinearities. Table lookup strategies can also be expensive in cases like this where the tabulation cannot be expected to be uniformly gridded.

### Resolving with Newton–Raphson Iteration

Another approach to resolving the loop is using Newton–Raphson iteration to resolve the loop. This approach was hinted at in [231] and formulated and studied in detail by Olsen *et al.* in [241]. Here we briefly recall the development in [241].

To form a zero-finding equation suitable for solution with Newton–Raphson iteration, we start by combining the first two equations of (4.37)

$$\mathbf{v}_c = \mathbf{E}\mathbf{a}_e + \mathbf{F}\mathbf{f}(\mathbf{v}_c). \quad (4.42)$$

This is rearranged to solve for zero, yielding a zero-finding equation  $\mathbf{h}(\mathbf{v}_c)$

$$\mathbf{h}(\mathbf{v}_c) = \mathbf{E}\mathbf{a}_e + \mathbf{F}\mathbf{f}(\mathbf{v}_c) - \mathbf{v}_c. \quad (4.43)$$

This zero-finding equation is used to solve for  $\mathbf{i}_c$  in the following way. First the value of  $\mathbf{a}_e$  produced by the Wave Digital Filter subtrees is plugged in to (4.43). Second, Newton–Raphson iteration is

used to find the value of  $\mathbf{v}_c$  which zeros  $\mathbf{h}(\mathbf{v}_c)$ . Third, this value of  $\mathbf{v}_c$  is plugged in to  $\mathbf{f}(\mathbf{v}_c)$ , finally yielding  $\mathbf{i}_c$ .

Newton–Raphson iteration is a standard numerical technique which forms successive approximations to a solution to the zero-finding equation using the Jacobian of the function. In our case, the iteration is done according to

$$\mathbf{v}_c^{(k+1)} = \mathbf{v}_c^{(k)} - \mathbf{J}\left(\mathbf{v}_c^{(k)}\right)^{-1} \mathbf{f}\left(\mathbf{v}_c^{(k)}\right) \quad (4.44)$$

where the superscripts in parentheses indicate iteration count and the operator  $\mathbf{J}(\cdot)$  indicates the Jacobian. The Jacobian is a matrix of partial derivatives of each function in the vector of functions with respect to each variable in the functions. This iteration continues until  $\mathbf{h}(\mathbf{v}_c)$  has converged sufficiently to zero. Details are given in any numerical methods textbook [166, 282].

To start the Newton–Raphson iteration, an initial guess  $\mathbf{v}_c^{(0)}$  is needed. An obvious choice of  $\mathbf{v}_c^{(0)}$  would be the value of  $\mathbf{v}_c$  which solved the system at the previous time step

$$\mathbf{v}_c^{(0)}(n) = \mathbf{v}_c(n-1) = \mathbf{E}\mathbf{a}_e(n-1) + \mathbf{F}\mathbf{f}(\mathbf{v}_c(n-1)). \quad (4.45)$$

Looking at the form of this equation, we can notice that the current value of the external incident waves  $\mathbf{a}_e(n)$  is also available. Taking this in to account, we get another option for an initial guess [241]

$$\mathbf{v}_c^{(0)}(n) = \mathbf{E}\mathbf{a}_e(n) + \mathbf{F}\mathbf{f}(\mathbf{v}_c(n-1)). \quad (4.46)$$

Experiments have shown that neither choice of initial guess is conclusively better than the other; the proper choice depends on the circuit in question. Therefore both should be tested to find which one minimizes iteration count for a given circuit [241].

#### 4.3.4 Deriving System Matrices

The final aspect of this approach is the formation of the system matrices  $\mathbf{S}$  and  $\mathbf{C}$ .

The scattering matrix  $\mathbf{S}$  is found exactly like any other  $\mathcal{R}$ -type adaptor, using the approach of §2.2. In fact it is slightly easier than normal since it does not need to be adapted—the K method, Newton–Raphson iteration, or whatever other approach is used to resolve the loop will take care of realizability. Because no attempt will be made towards traditional adaptation of the ports facing the nonlinearities, the port resistances of those ports can be arbitrary. In this work we always arbitrarily choose  $1\text{ k}\Omega$ .

The  $\mathbf{C}$  matrix is derived simply by rearranging the wave definitions used in the Wave Digital Filter with the standard Kirchhoff variables. We start with the parametric wave definition at the

ports of the nonlinearities

$$\mathbf{a}_c = \mathbf{R}_i^{\rho-1} \mathbf{v}_c + \mathbf{R}_i^\rho \mathbf{i}_c \quad (4.47)$$

$$\mathbf{b}_c = \mathbf{R}_i^{\rho-1} \mathbf{v}_c - \mathbf{R}_i^\rho \mathbf{i}_c, \quad (4.48)$$

where  $\mathbf{R}_i$  is a diagonal matrix of only the internal port resistances. This can be reorganized to match the structure of (4.26)

$$\mathbf{v}_c = -\mathbf{R}_i \mathbf{i}_c + \mathbf{R}_i^{1-\rho} \mathbf{a}_c \quad (4.49)$$

$$\mathbf{b}_c = -2\mathbf{R}_i^\rho \mathbf{i}_c + \mathbf{a}_c, \quad (4.50)$$

yielding the  $\mathbf{C}$  partitions

$$\mathbf{C} = \begin{bmatrix} \mathbf{C}_{11} & \mathbf{C}_{12} \\ \mathbf{C}_{21} & \mathbf{C}_{22} \end{bmatrix} = \begin{bmatrix} -\mathbf{R}_i & \mathbf{R}_i^{1-\rho} \\ -2\mathbf{R}_i^\rho & \mathbf{I} \end{bmatrix}. \quad (4.51)$$

## 4.4 Case Studies

In this Section, two case studies are given, demonstrating the application of the proposed method (§4.3) to circuits involving multiple nonlinearities. We'll start with a case study on the Envelope Generator from the TR-808 Bass Drum, which involves a diode and two NPN BJT transistors (§4.4.1). The second case study concerns the Nonlinear Bridged-T Resonator from the TR-808 Bass Drum, which involves one diode and one NPN BJT transistor. For each case study we'll walk through the steps required to derive the Wave Digital Filter structure and show experimental verification of the model compared to SPICE simulations, confirming the validity of the proposed approach.

### 4.4.1 Envelope Generator

In this first case study, we'll consider the Envelope Generator circuit from the Roland TR-808 Bass Drum circuit. The schematic of the Envelope Generator is shown in Figure 4.7a and the component values are shown in Table 4.1.

Some aspects of this reference circuit deserve special explanation, specifically how this subcircuit is separated from the rest of the circuit, the presence of capacitor  $C_0$ , and the changes to the value of  $R_{159}$ . The assumption that the input is an ideal voltage source  $v_{in}$  allows us to separate the input from the Pulse Shaper Circuit without any concern. The separation of the output from the Nonlinear Bridged-T Resonator is slightly more complicated and introduces a small amount of error. First we observe in a SPICE simulation that the Bridged-T resonator resonates around zero voltage at the “T” of the Bridged-T resonator, where  $R_{161}$  connects. We make the assumption that this “averages out” over time to simplify a ground connection, and in our simplified circuit we just connect  $R_{161}$  to ground. Second, we assume that the NPN BJT  $Q_{43}$  does not load down  $R_{159}$  at all, and connect

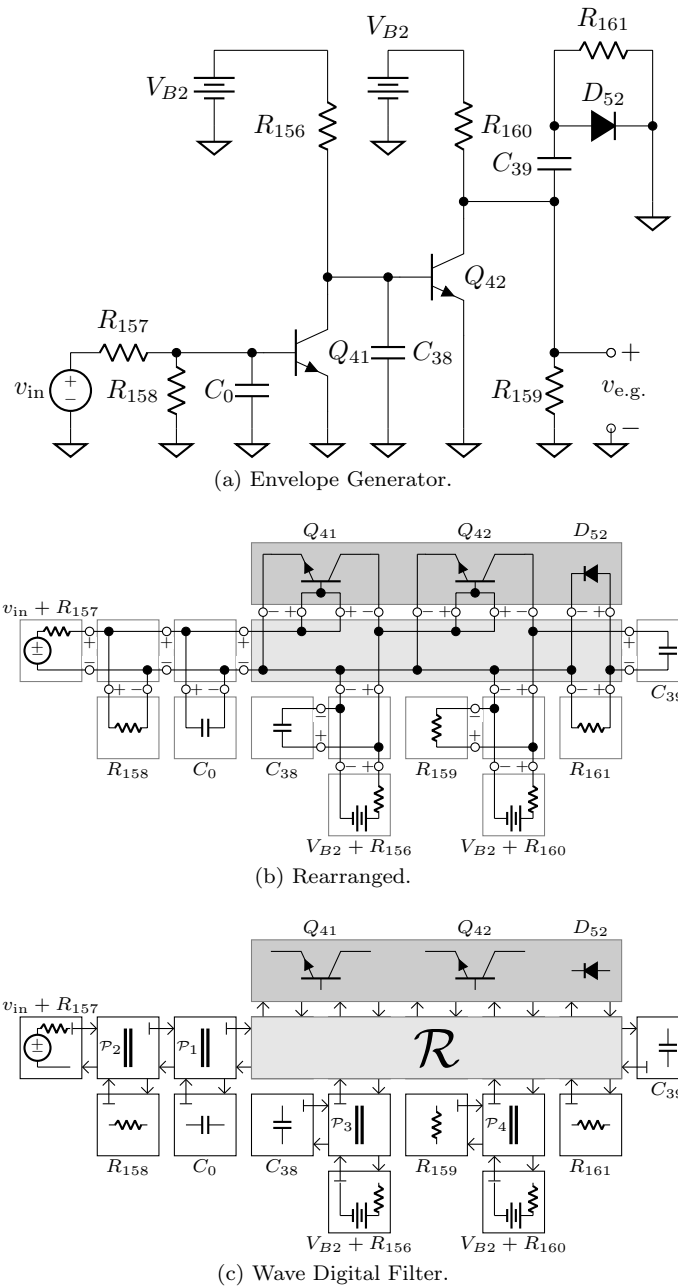


Figure 4.7: Envelope Generator Schematic, Rearranged to Highlight Topology, and Wave Digital Filter.

$R_{159}$  to ground as well. By hand we tune the value of  $R_{159}$  from  $100\text{ k}\Omega$  to  $106\text{ k}\Omega$  to ameliorate some of the error introduced by these assumptions. Finally, the capacitor  $C_0$  is added to the circuit to give some “memory” or “inertia” to the  $v_{BE}$  junction of  $Q_{41}$ . The reason this is necessary is that there is a dc path from the input to  $v_{BE}$  junction, and when there is a sharp edge of the input pulse  $v_{in}$ , the initial guesses for the Newton–Raphson solver become very poor. Luckily although adding this capacitor does help the solver, it does not significantly affect the dynamics of the circuit. We may also justify this addition somewhat from a physical perspective—semiconductor junctions often have some intrinsic capacitance (“Miller capacitance”) that is not accounted for by the Ebers–Moll model. This is also related to a technique used in SPICE modeling. In the SPICE context, a capacitor may be added in parallel to a controlling voltage of a nonlinearity and an inductor may be added in series to a controlling current of a nonlinearity as a convergence aid [146, p. 66].

Table 4.1: Envelope Generator Component Names and Values.

Component	Value	Note
$R_{156}$	$1\text{ M}\Omega$	
$R_{157}$	$8.2\text{ k}\Omega$	
$R_{158}$	$2.7\text{ k}\Omega$	
$R_{159}$	$106\text{ k}\Omega$	original value $100\text{ k}\Omega$
$R_{160}$	$22\text{ k}\Omega$	
$R_{161}$	$1\text{ M}\Omega$	
$C_0$	$6.8\text{ nF}$	added for stability
$C_{38}$	$0.1\text{ }\mu\text{F}$	
$C_{39}$	$0.033\text{ }\mu\text{F}$	
$V_{B2}$	$15\text{ V}$	
Transistors	2N3904	substitute for 2SC945(P)
$I_s$	$10\text{ fA}$	saturation current
$\beta_F$	300	forward current gain
$\beta_R$	4	reverse current gain
$V_T$	$25.85\text{ mV}$	thermal voltage
Diode	1N4148	substitute for IS2473
$I_s$	$2.52\text{ nA}$	saturation current
$V_T$	$25.85\text{ mV}$	thermal voltage

Forming a Wave Digital Filter simulation from this circuit may appear quite difficult, due to the presence of five nonlinear ports (two for each of the NPN BJTs and one diode) and the complicated topology. However, it can be handled in a straightforward and systematic fashion using the proposed technique. A rearranged version of this circuit that highlights its topology when grouping the nonlinearities is shown in Figure 4.7b and the Wave Digital Filter structure proper is shown 4.7c. The tree structure of the Wave Digital Filter is shown explicitly in Figure 4.8. In the Wave Digital Filter all of the standard adaptors and one-ports are handled with classical techniques, and the combination

of the  $\mathcal{R}$ -type adaptor and the five nonlinearities is handled using the proposed technique. The transistors are modeled using the Ebers–Moll model and the diode is modeled using the Shockley ideal diode model.

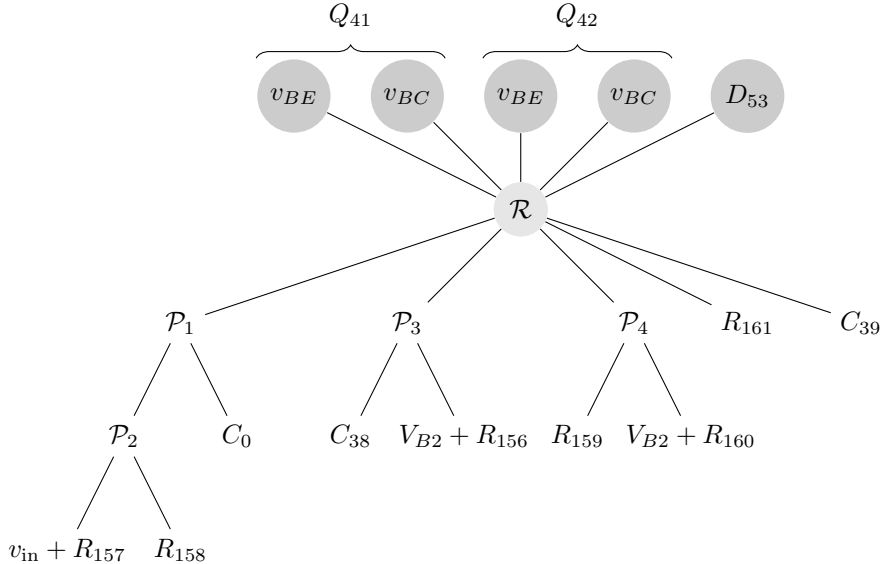


Figure 4.8: Envelope Generator Connection Tree.

The scattering matrix of the  $\mathcal{R}$ -type adaptor is found using the Modified Nodal Analysis method proposed in Chapter 2. The  $\mathcal{R}$ -type topology with Thévenin equivalents attached, as well as the port definitions of the nonlinearities, are shown in Figure 4.9.

To verify the model, we compare it against a SPICE simulation. Figure 4.10 shows the Envelope Generator's output voltage  $v_{e.g.}$  in response to a range of input pulses at different amplitudes  $\in [4.0, 6.5, 9.0, 11.5, 14.0]$ . The Wave Digital Filter simulation is run at a sampling rate of 44 100 Hz and the capacitors are discretized using the standard Bilinear Transform. For each pulse amplitude, there is good agreement between SPICE and the Wave Digital Filter. The worst errors happen right after the rising edge of the input pulse, but the rest of the envelope has a very good fit. It is also interesting to note that the envelope's shape and amplitude do not depend very much on the input pulse amplitude.

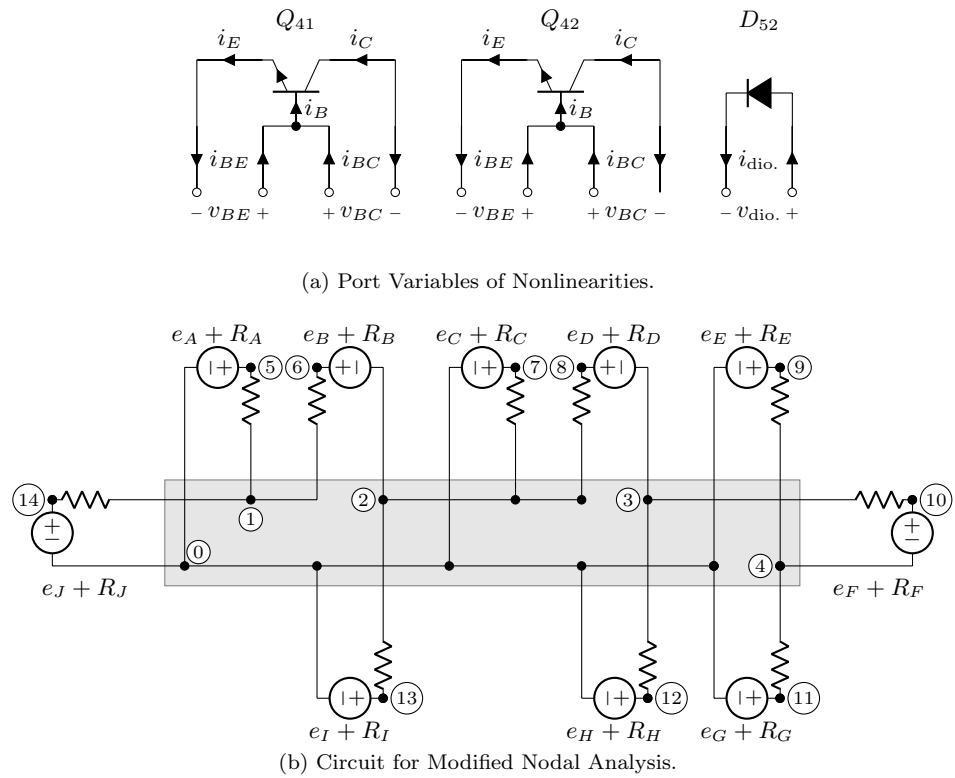


Figure 4.9: Definition of Port Variables of Nonlinearities and Circuit for Modified Nodal Analysis.

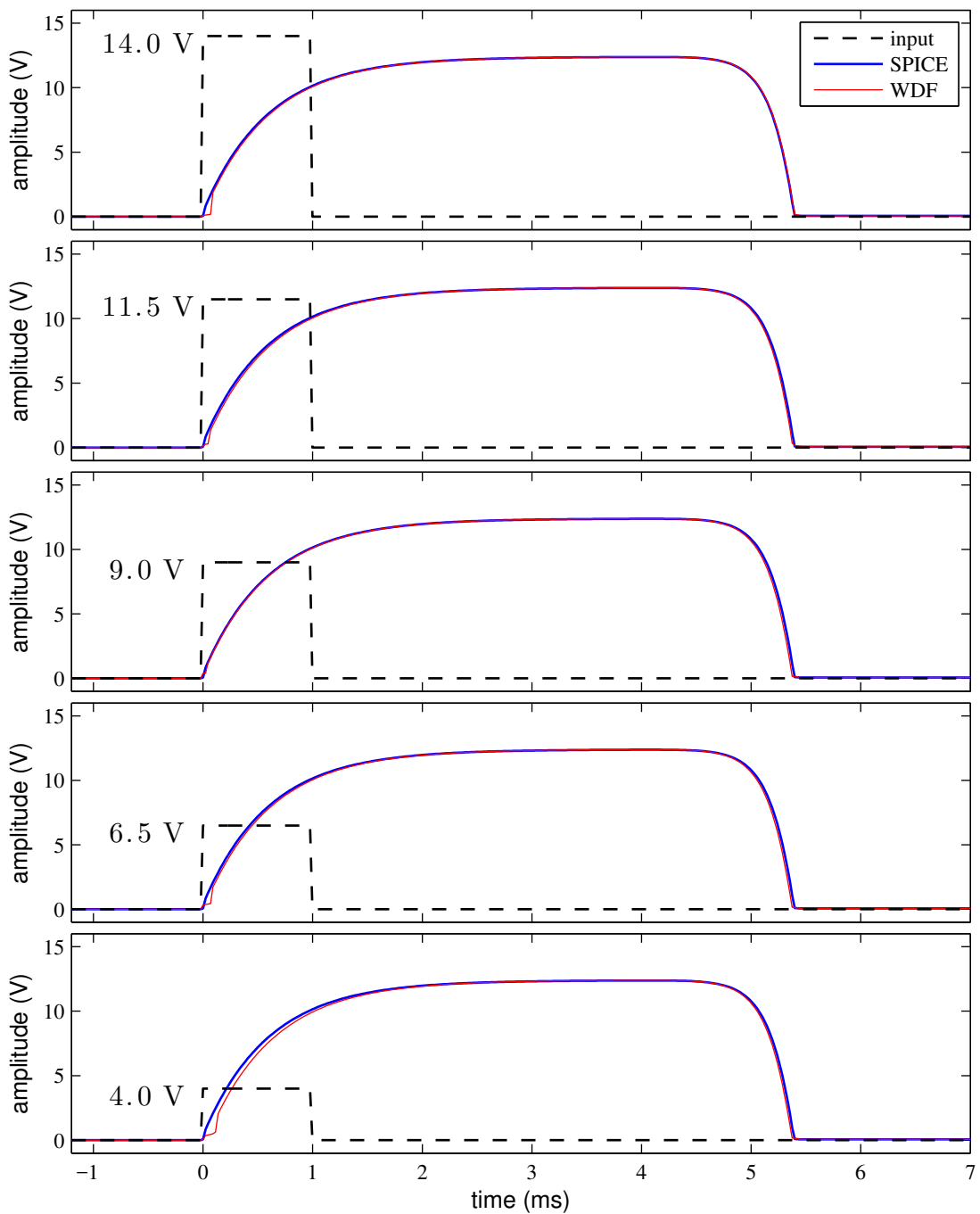


Figure 4.10: Time Domain Response of the Envelope Generator to Five Different Pulse Amplitudes  $\in [4.0, 6.5, 9.0, 11.5, 14.0]$ .

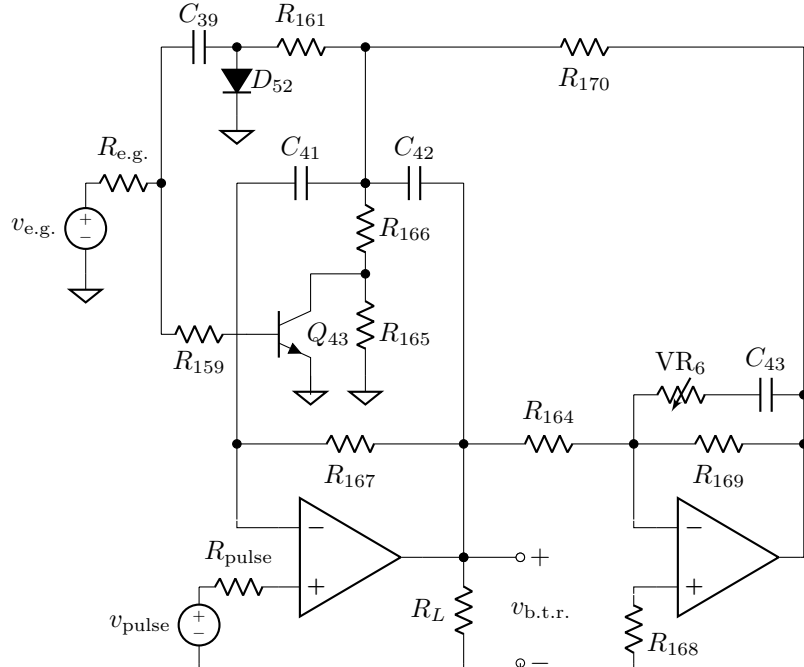
#### 4.4.2 Nonlinear Bridged-T Resonator With Feedback

In this second case study, we'll consider the Nonlinear Bridged-T Resonator circuit from the Roland TR-808 Bass Drum circuit. The schematic of the Nonlinear Bridged-T Resonator is shown in Figure 4.11a and the component values are shown in Table 4.2. We'll be modeling the operational amplifiers as ideal, replacing each one in the circuit with a nullor; this is shown in Figure 4.11b.

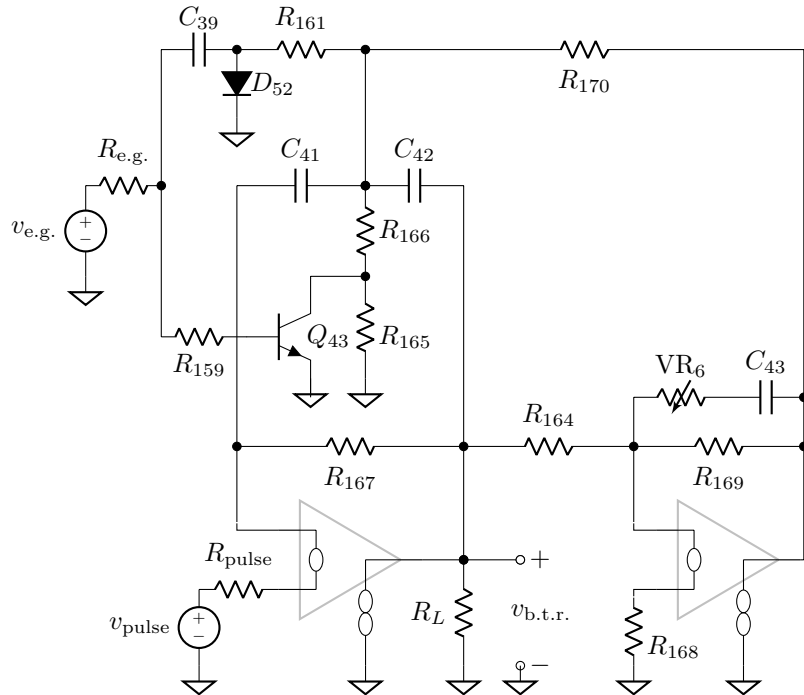
Some aspects of this reference circuit deserve special explanation, specifically the fictitious resistance  $R_{e.g.}$  and the resistor  $R_{pulse}$ . The small ( $1\Omega$ ) resistor  $R_{e.g.}$  is added to make the output  $v_{e.g.}$  from the Envelope Generator into a resistive voltage source and aid realizability. It can be justified physically somewhat as well, since the Envelope Generator will not act like a perfect source, but rather will be current-limited in some way.  $R_{pulse}$  is added for the same reason, to make  $v_{pulse}$  into an ideal source. However,  $R_{pulse}$  is not an approximation or simplification; it can be added through the circuit-theoretic equivalence that any impedance in series with a nullator is equivalent to just the nullator [145].

Table 4.2: Nonlinear Bridged-T Resonator Component Names and Values.

Component	Value	Note
$R_{159}$	$100\text{k}\Omega$	
$R_{161}$	$1\text{M}\Omega$	
$R_{164}$	$4.7\text{k}\Omega$	
$R_{165}$	$47\text{k}\Omega$	
$R_{166}$	$6.8\text{k}\Omega$	
$R_{167}$	$1\text{M}\Omega$	
$R_{168}$	$22\text{k}\Omega$	
$R_{169}$	$47\text{k}\Omega$	
$R_{170}$	$470\text{k}\Omega$	
$R_{load}$	$1\text{M}\Omega$	
$R_{e.g.}$	$1\Omega$	fictitious resistance
$R_{pulse}$	$1\text{k}\Omega$	added via nullator identity
VR <sub>6</sub>	$500\text{k}\Omega$	max value
$C_{39}$	$0.033\text{\mu F}$	
$C_{41}$	$0.015\text{\mu F}$	
$C_{42}$	$0.015\text{\mu F}$	
$C_{43}$	$33\text{\mu F}$	
Transistor	2N3904	substitute for 2SC945(P)
$I_s$	$10\text{fA}$	saturation current
$\beta_F$	300	forward current gain
$\beta_R$	4	reverse current gain
$V_T$	$25.85\text{mV}$	thermal voltage
Diode	1N4148	substitute for IS2473
$I_s$	$2.52\text{nA}$	saturation current
$V_T$	$25.85\text{mV}$	thermal voltage



(a) Nonlinear Bridged-T Resonator with Feedback.



(b) Altered Schematic for Simulation.

Figure 4.11: Nonlinear Bridged-T Resonator with Feedback Schematic and Nullor Realization.

Again, forming a Wave Digital Filter simulation of this circuit may appear quite difficult since there are three nonlinear ports (two for the NPN BJT and one diode) and a complicated topology. However, it can again be handled in a straightforward and systematic fashion using the proposed technique. A rearranged version of the circuit that highlights its topology when grouping the nonlinearities is shown in Figure 4.12a and the corresponding Wave Digital Filter structure is shown in Figure 4.12b. The tree structure of the Wave Digital Filter is shown explicitly in Figure 4.13. In the Wave Digital Filter all of the standard adaptors and linear one-ports are handled with classical techniques, and the combination of the  $\mathcal{R}$ -type adaptor and the three nonlinearities is handled using the proposed technique. The transistor is modeled using the Ebers–Moll model and the diode is modeled using the Shockley ideal diode model.

The scattering matrix of the  $\mathcal{R}$ -type adaptor is found using the Modified Nodal Analysis method proposed in Chapter 2. The  $\mathcal{R}$ -type topology with Thévenin equivalents attached, as well as the port definitions of the nonlinearities, are shown in Figure 4.14.

To verify this model, we compare it against a SPICE simulation. Figure 4.15 shows the Nonlinear Bridged-T Resonator's output voltage  $v_{b.t.r.}$  with six different settings of the decay knob  $d \in [0.01, 0.20, 0.40, 0.60, 0.80, 1.00]$ . The Wave Digital Filter simulation is run at 44100 Hz and the capacitors are discretized using the standard Bilinear Transform. For each decay knob setting, there is very good agreement between SPICE and the Wave Digital Filter. A zoom on the attack transient of each simulation is shown in Figure 4.16. Here the complex shape of the attack transient is quite visible. It is possible to identify the original edge of the input pulse, the small trailing edge of the pulse from the Pulse Shaper, a pitch shift during the attack (first 5 ms), and distortion of the decaying sinusoid after the attack due to leakage through  $Q_{43}$ . Notice that the Wave Digital Filter simulation matches very well even during this complex transient behavior.

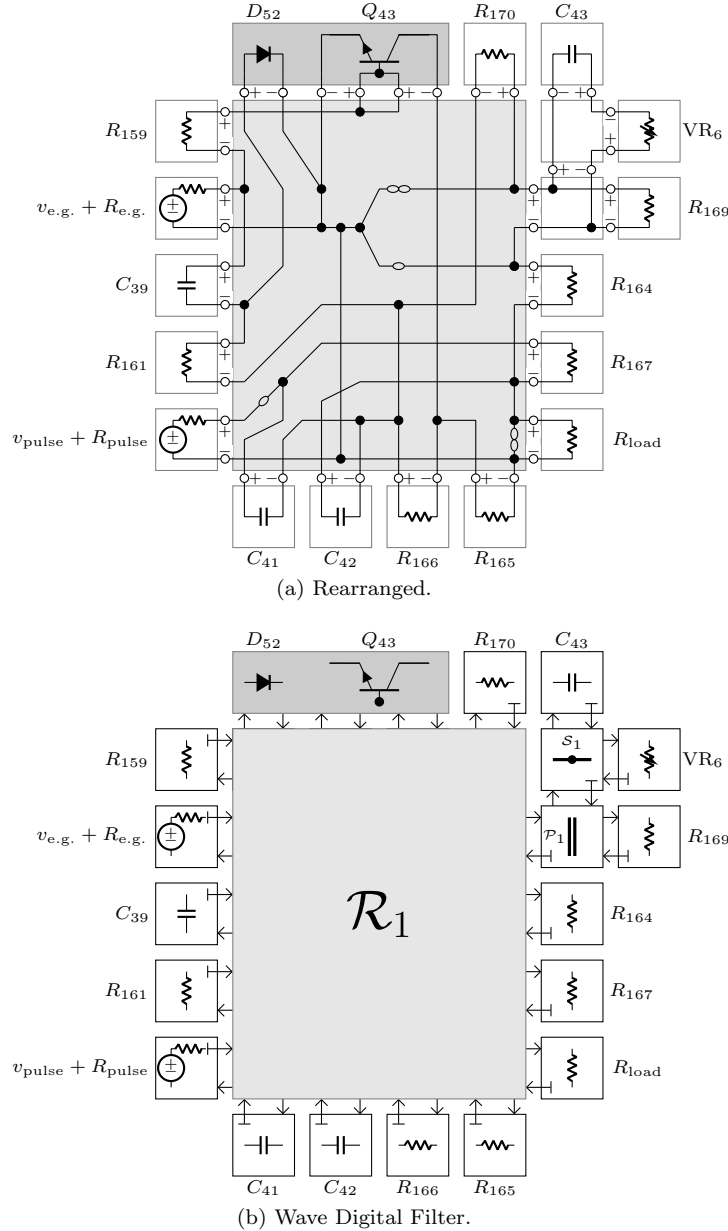


Figure 4.12: Nonlinear Bridged-T Resonator Rearranged to Highlight Topology, and Wave Digital Filter.

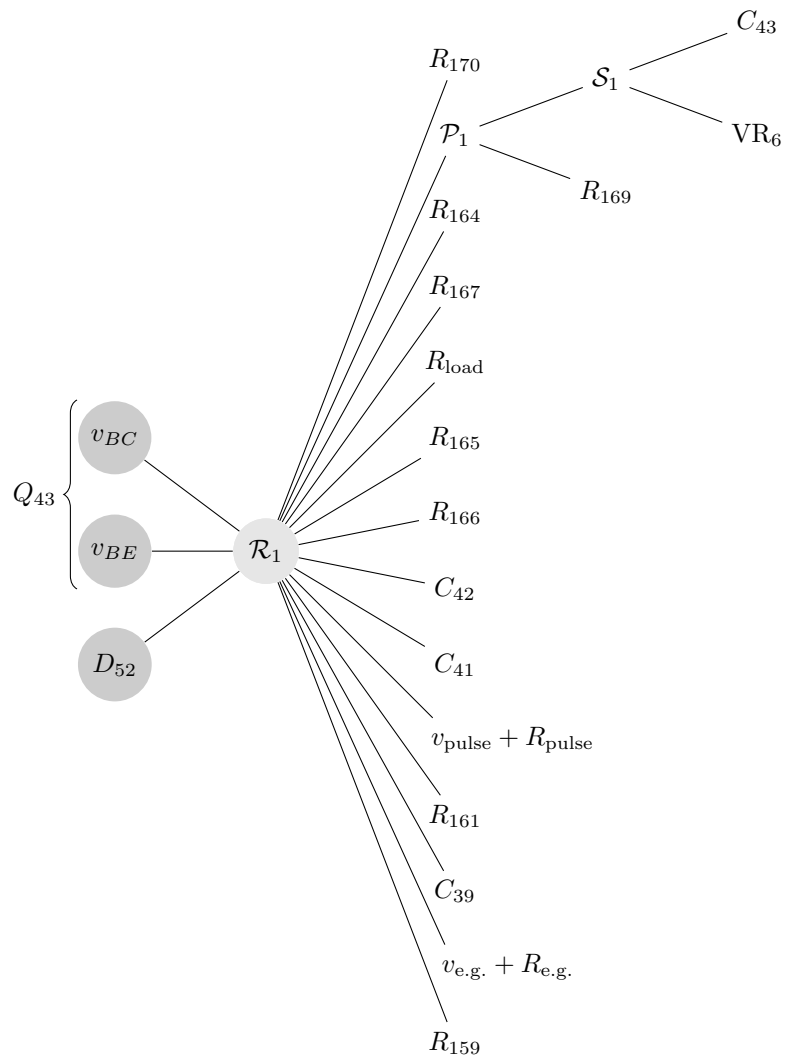
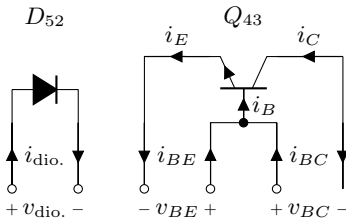
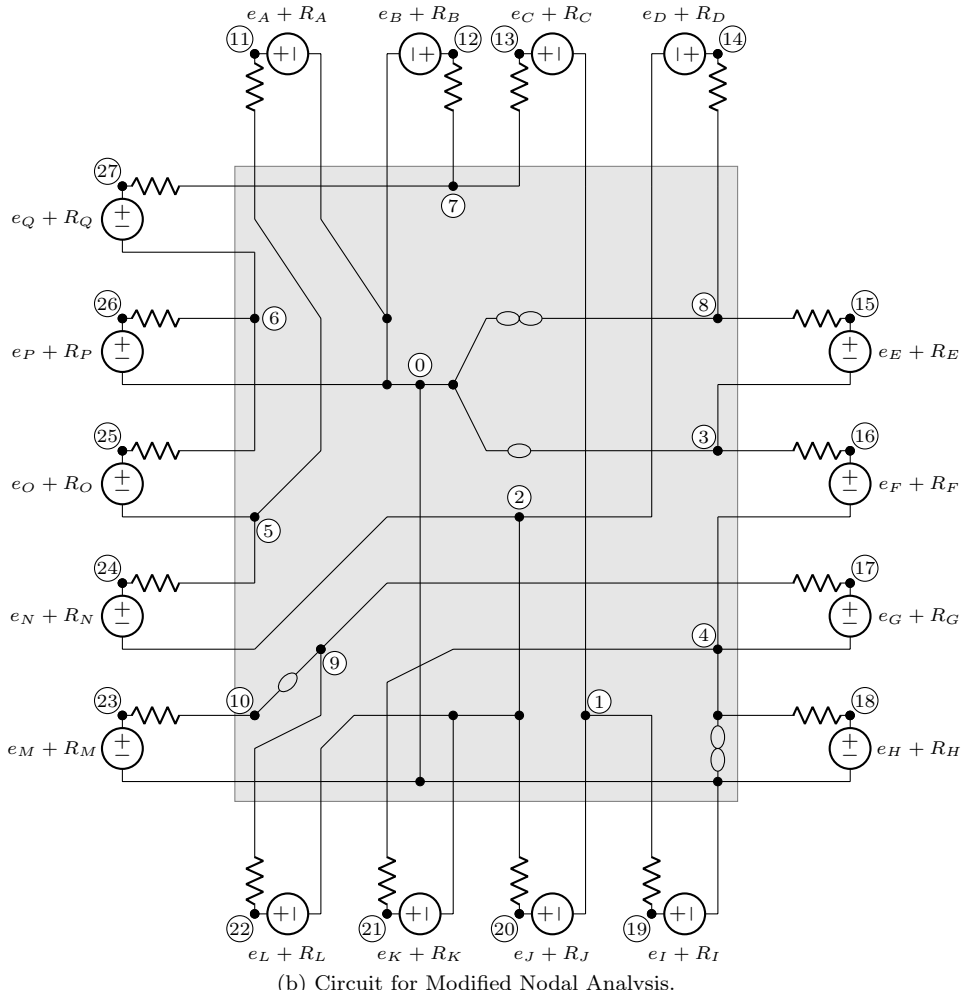


Figure 4.13: Nonlinear Bridged-T Resonator with Feedback Connection Tree.



(a) Port Variables of Nonlinearities.



(b) Circuit for Modified Nodal Analysis.

Figure 4.14: Definition of Port Variables of Nonlinearities and Circuit for Modified Nodal Analysis.

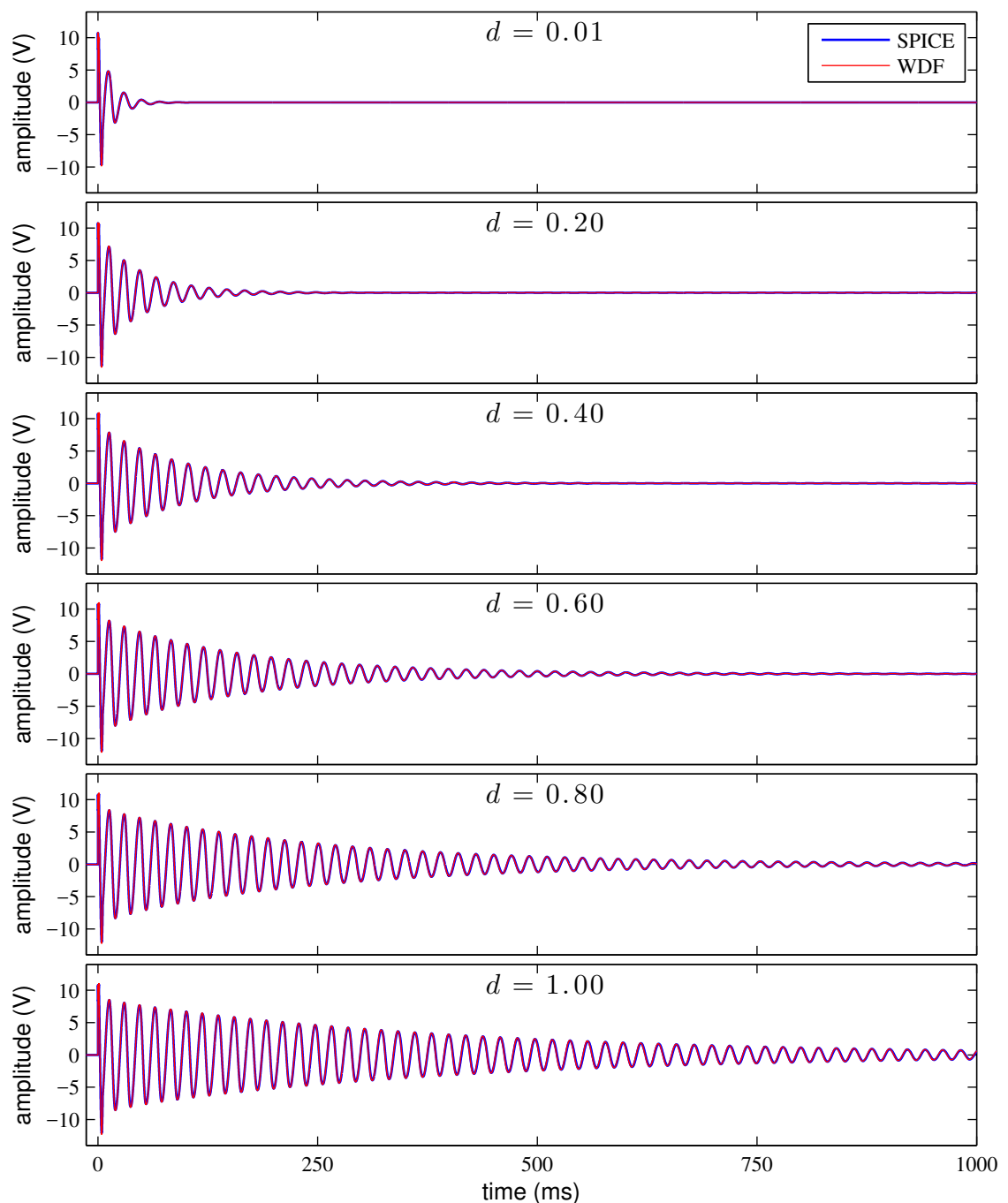


Figure 4.15: Time Domain Response of the Nonlinear Bridged-T Resonator at Six Different Decay Knob Settings  $d \in [0.01, 0.20, 0.40, 0.60, 0.80, 1.00]$ .

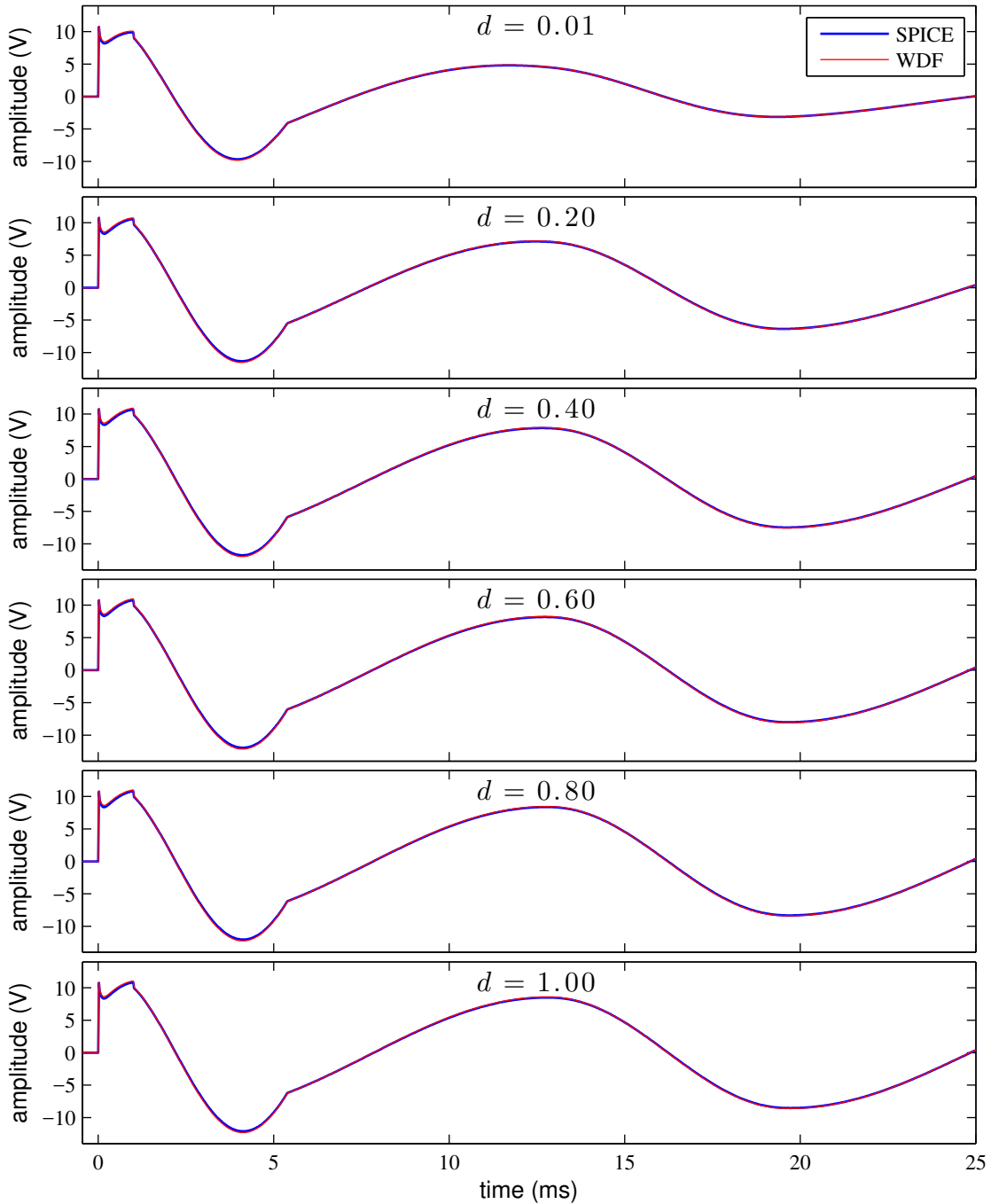


Figure 4.16: Time Domain Response of the Nonlinear Bridged-T Resonator at Six Different Decay Knob Settings  $d \in [0.01, 0.20, 0.40, 0.60, 0.80, 1.00]$ , Detail on Attack Transient.

## 4.5 Conclusion

In this Chapter, we've reviewed previous work on Wave Digital Filter modeling of circuits with more than one nonlinearity. We've proposed a technique that is more general than the techniques in the literature and avoids many of their pitfalls as well.

With this proposed technique, it is now theoretically possible to accommodate circuits including an arbitrary number of nonlinear circuit elements, including those that are very important in audio circuits like diodes, transistors, and triodes. Beyond the case studies we've shown on the TR-808 Bass Drum Envelope Generator and Nonlinear Bridged-T Resonator, this proposed method has enabled modeling of other nonlinear circuits including a transistor-based common emitter amplifiers [241] (Figure 4.17a), a triode-based common-cathode amplifier [243, 242] (Figure 4.17b), a distortion stage from the Big Muff Pi distortion pedal [230, 231] (Figure 4.17c), and a four-triode preamplifier stage from the Fender Bassman 5F6-A [270] (Figure 4.17d). The cathode amplifier includes Miller capacitances, which were recently handled as a special case in [262]. Here they are handled as a straightforward application of the generalized approach presented in this Chapter.

In the following Conclusion we'll put all of the building blocks of the TR-808 Bass Drum that we've developed in each Chapter together to form a complete simulation of the TR-808 Bass Drum circuit.

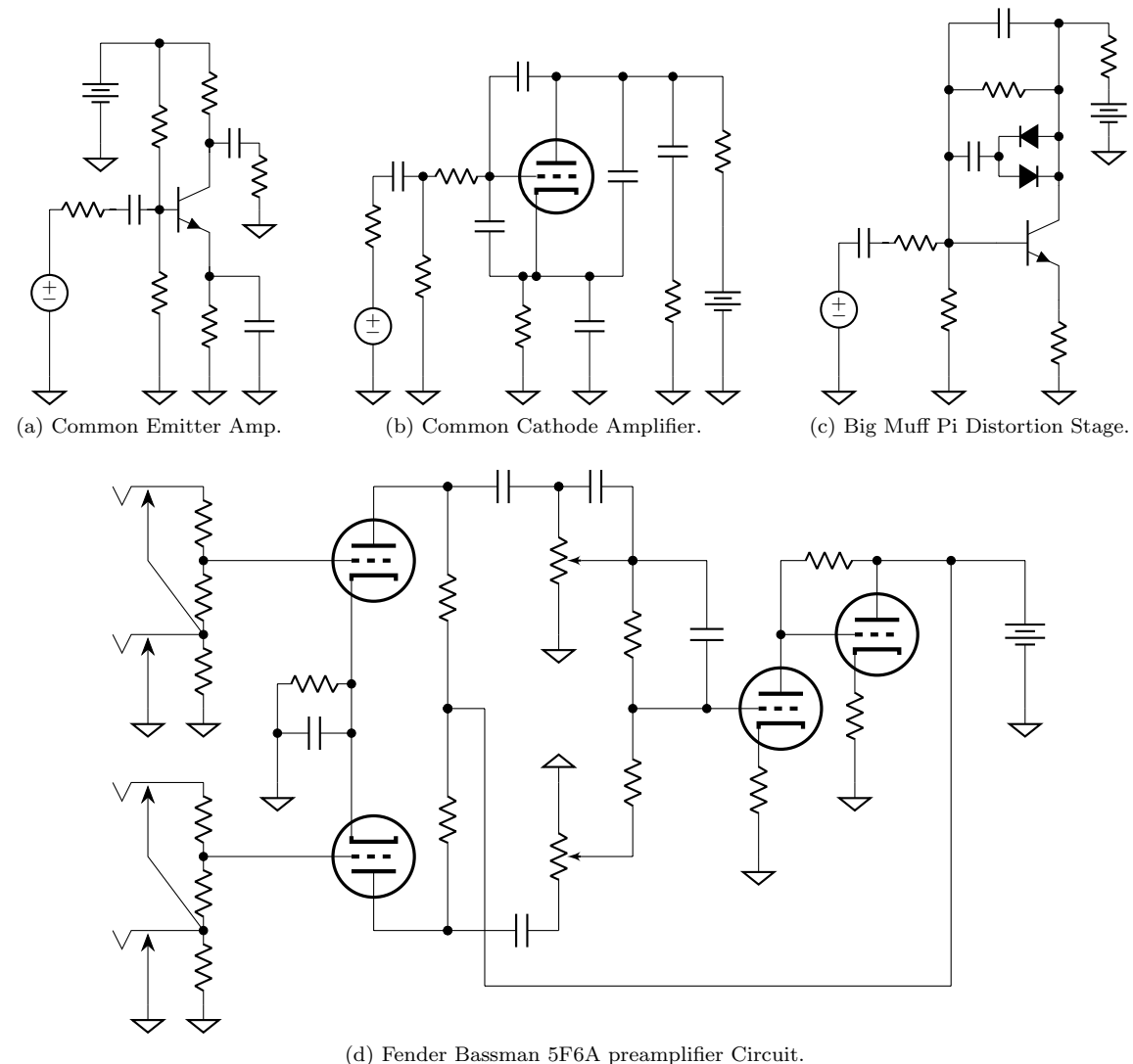


Figure 4.17: Circuits Which Have Been Modeled Using the Proposed Method.

# Conclusion

In the four Chapters of this dissertation, we've reviewed and extended the Wave Digital Filter approach to simulating electronic audio circuits. After all that, we've finally developed the Wave Digital Filter approach to a high enough degree of generality that it can be used to model complicated real-world audio circuitry. To conclude this work, we'll show and evaluate a Wave Digital Filter simulation of the entire TR-808 Bass Drum circuit, using the Wave Digital Filter simulations of the subcircuits that we developed to illustrate the principles developed in each Chapter: the Output Filter model from Chapter 1, the Pulse Shaper model from Chapter 3, the Envelope Generator model from Chapter 4, and the Nonlinear Bridged-T Resonator from Chapter 4. Following this demonstration, we'll review the contributions of each Chapter and close with some final comments.

## TR-808 Bass Drum Simulation

To demonstrate the accuracy of the Wave Digital Filter simulation, we'll examine simulations under a variety of tone and decay settings and pulse amplitudes, comparing them to reference SPICE simulations. At the same time this will give us the opportunity to see the precise effect of each of the TR-808 Bass Drum's controls and discuss some properties of the sound. For each of the reference simulations the maximum timestep of SPICE is set to  $1 / (16 \times 44100)$  seconds. For each of the Wave Digital Filter simulations, a sampling rate of  $44100 \times 8$  Hz is used. Despite the fact that the Wave Digital Filter simulation of each stage (Pulse Shaper, Envelope Generator, Nonlinear Bridged-T Resonator, and Output Filter) works well at 44100 Hz, the mild error in each stage accumulates when the simulations are combined and results in audible error in the simulation amplitude. This error is mainly related to the amplitude of the Bass Drum note. This effect is mitigated to an acceptable degree by oversampling. In these simulations, we also altered the input pulse slightly, from a perfect square-shaped pulse that is 1 ms wide, to one whose rising and falling edges are quickly ramped up and down respectively over  $4/44100$  s. This eases the simulation effort during the sharpest transients, and can be justified physically somewhat by the assumption that the chip on the TR-808 producing the pulses probably can't produce infinitely fast rise and fall times.

Recall that the behavior of the TR-808 Bass Drum is parameterized by the input pulse amplitude,

the decay control  $d$ , the tone control  $c$ , and the volume control  $l$ . To show the Wave Digital Filter model working under a range of conditions, we'll explore different combinations of these controls. First we'll study the effect of the tone control. Second, we'll study the effects of the input pulse amplitude. Third, we'll study the effect of the decay control. Finally, we'll discuss a unique effect resulting from quickly repeated notes.

## Tone Control Study

In Figure I, the Wave Digital Filter simulation is compared to a SPICE reference simulation for a family of tone control settings  $c \in [0.00, 0.50, 0.75, 0.90, 0.95, 0.99]$ . For each simulation the pulse amplitude is set to the normal unaccented amplitude, 4.0 V, and the decay control is set to  $d = 0.4$ . Here, and in every other simulation, the volume control is set to  $l = 0.99$ .

Here we can see some of the complex transient shapes that characterize the TR-808 Bass Drum. The beginning of each sound is driven by the large rising edge of the shaped pulse. One millisecond later, the smaller falling edge appears. During the first  $\approx 5.4$  ms, the Bridged-T Resonator has a higher frequency of oscillation, while the envelope generator is turned on. At  $\approx 5.4$  ms, the frequency of oscillation abruptly settles down to its base frequency.

The main effect of the tone control is to affect the shape of the transient during the first 6 ms of each note. Note that for  $c = 0.99$ , there are sharp edges visible from the input pulse and a visible corner around 5 ms. As the tone control is turned down these sharp edges diminish, until they are almost entirely smoothed out for  $c = 0.00$ .

For each of the six simulations, there is a good agreement between SPICE and the Wave Digital Filter simulation.

## Pulse Amplitude Study

In Figure II and Figure III (detail on transient), the Wave Digital Filter simulation is compared to a SPICE reference simulation for a family of input pulse amplitudes  $\in [4.0, 6.5, 9.0, 11.5, 14.0]$  V. Recall that the lowest amplitude, 4.0 V corresponds to an unaccented note; the higher amplitudes correspond to the range of controllable accent levels. For each simulation the decay control is set to  $d = 0.4$  and the tone control is set to  $c = 0.99$ . Here, and in every other simulation, the volume control is set to  $l = 0.99$ .

The main effect of the pulse amplitude is to change the amplitude of the Bass Drum. An important secondary effect is to alter several aspects of the timbre of the note. In Figure IV, each of the five simulations are shown overlaid, with their amplitude normalized by the corresponding pulse amplitude. It can be seen that as the pulse amplitude increases, the amplitude of the transient (first  $\approx 5$  ms) increases relative to the pulse amplitude. At the same time, as the pulse amplitude increases, the amplitude of the resonance (after  $\approx 5$  ms) decreases relative to the pulse amplitude. So, at low pulse amplitudes the resonance is more dominant and at high pulse amplitudes the transient

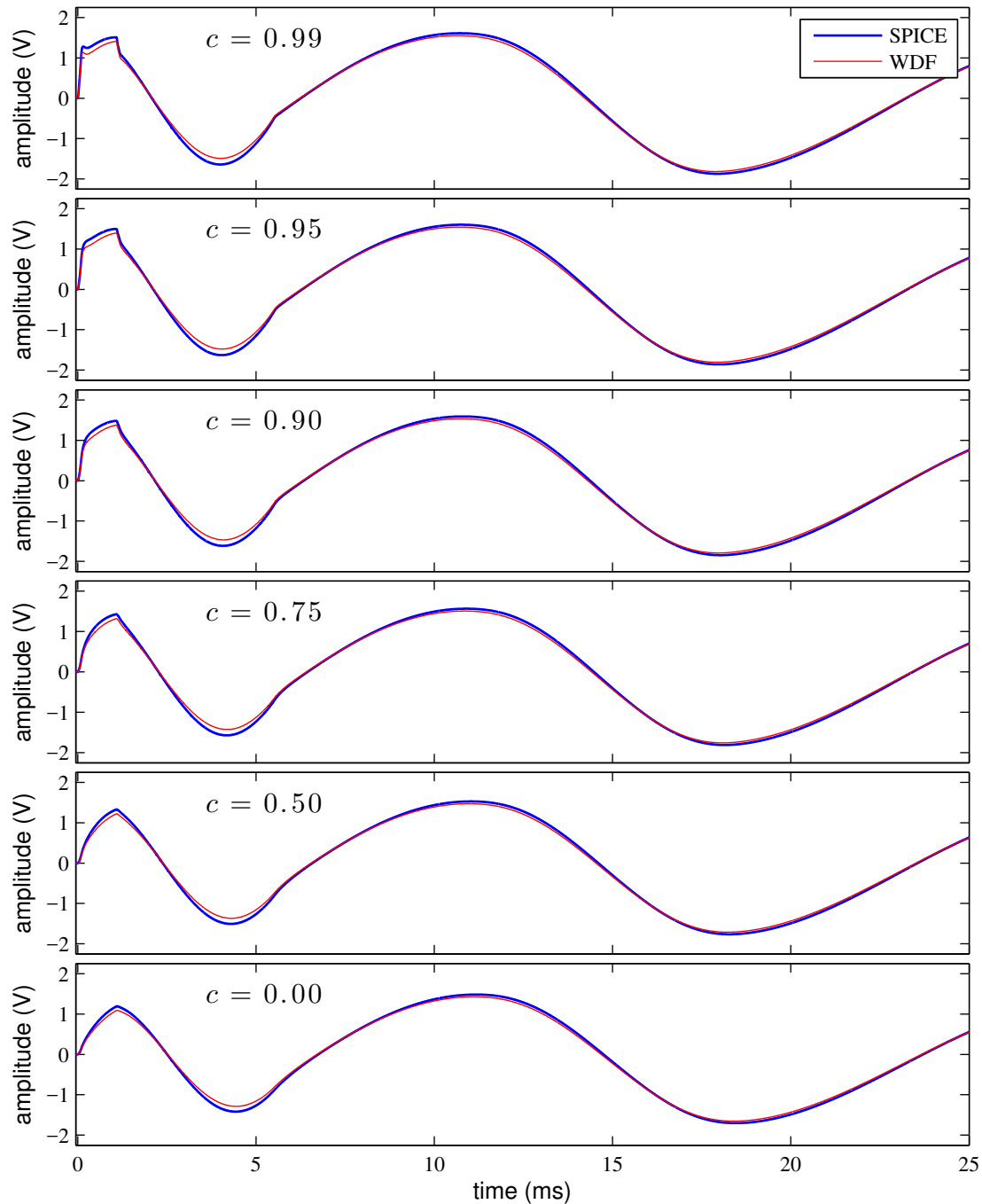


Figure I: Comparing Wave Digital Filter and SPICE for a Family of Tone Settings.

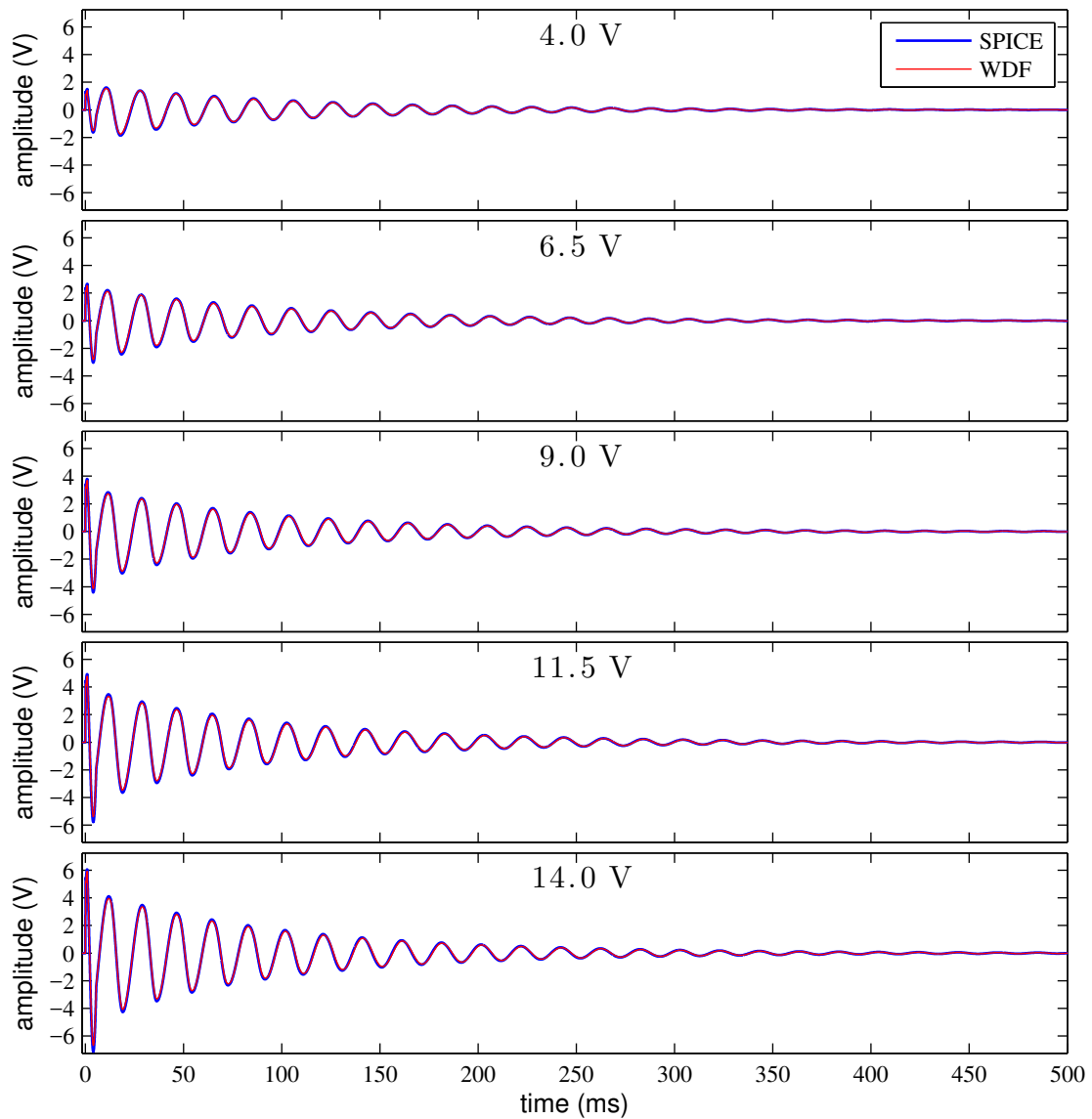


Figure II: Comparing Wave Digital Filter and SPICE for a Family of Input Pulse Amplitudes.

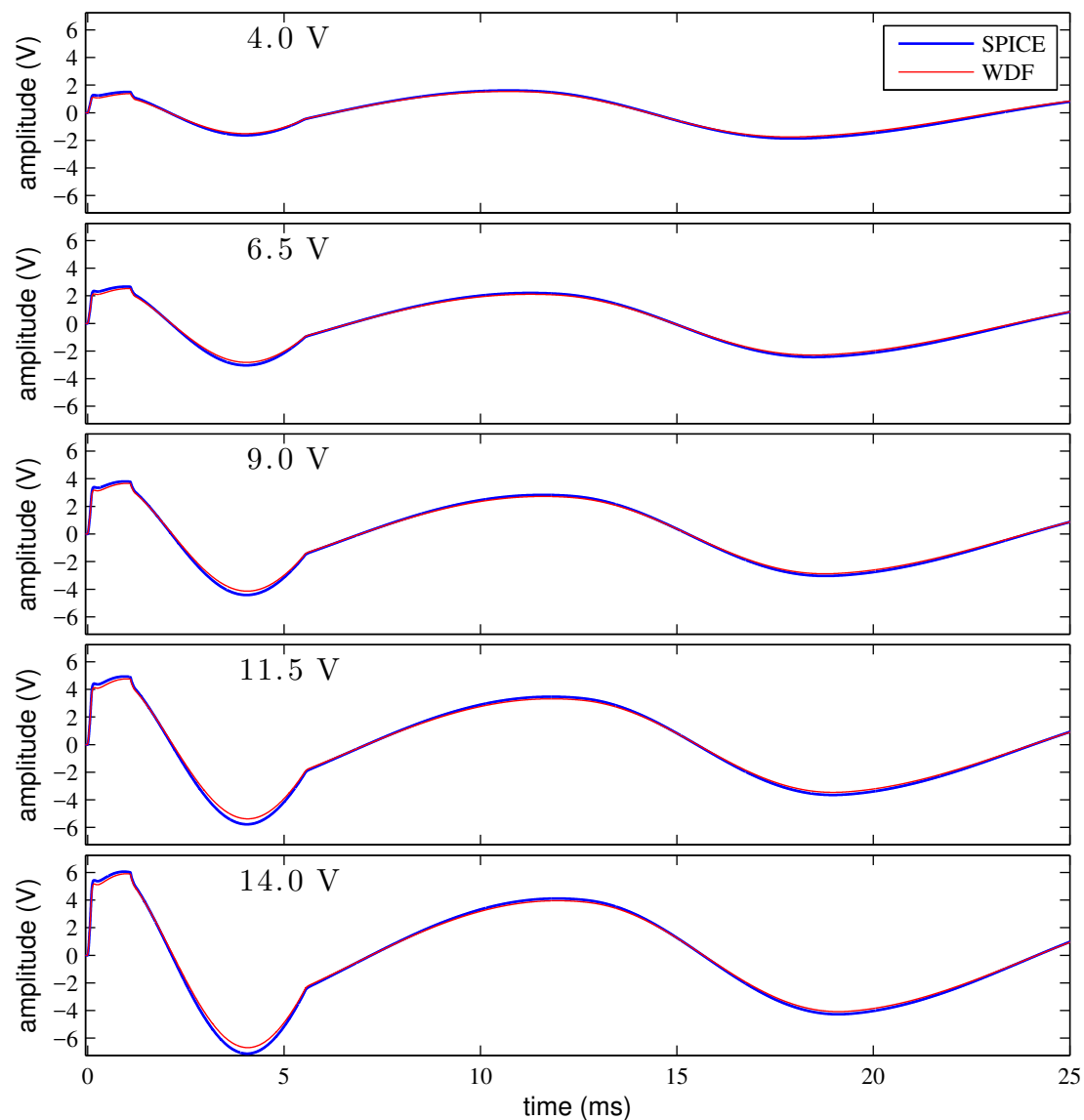


Figure III: Comparing Wave Digital Filter and SPICE for a Family of Input Pulse Amplitudes, Detail on Attack.

is more dominant. Another important timbral detail concerns the time evolution of the frequency of oscillation. Since the Bridged-T Resonator's frequency is linked to its state—the center frequency decreases as the amplitude decreases—notes with larger pulse amplitude have a longer and more pronounced pitch glide.

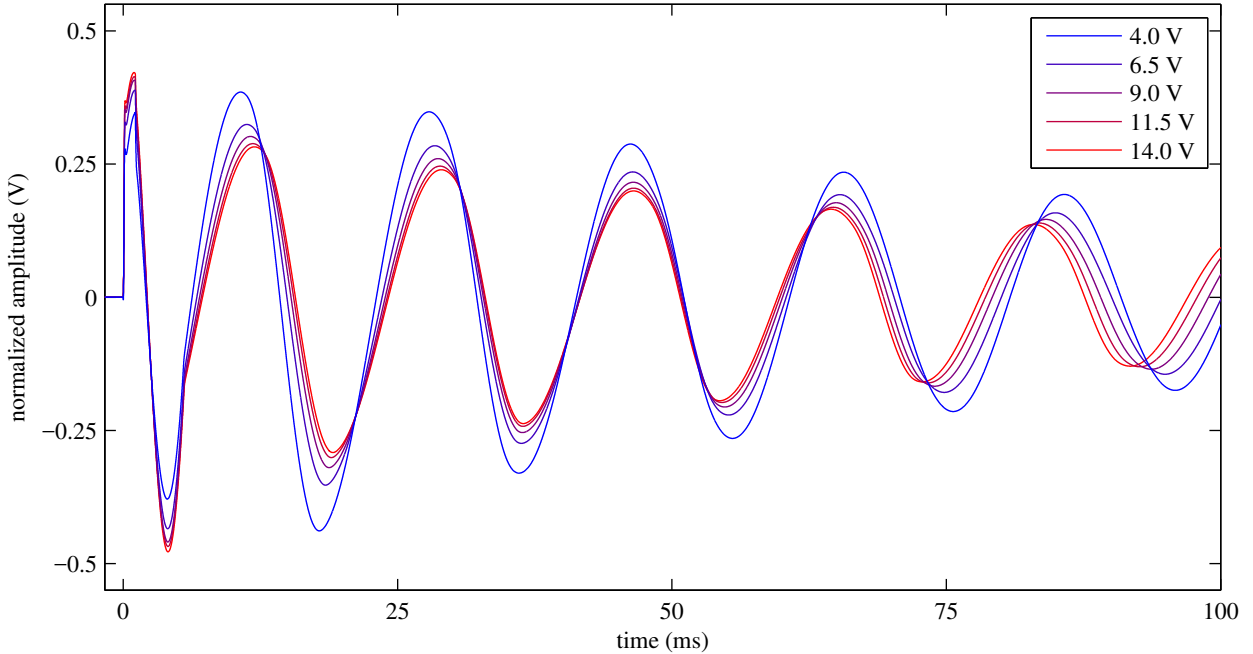


Figure IV: Normalizing Wave Digital Filter Simulations of Figure III by Pulse Amplitude.

For each of the five simulations, there is a good agreement between SPICE and the Wave Digital Filter simulation.

### Decay Control Study

In Figure V, the Wave Digital Filter simulation is compared to a SPICE reference simulation for a family of decay controls  $d \in [0.01, 0.20, 0.40, 0.60, 0.80, 1.00]$ . For each simulation the pulse amplitude is set to the normal unaccented amplitude, 4.0 V, and the tone control is set to  $c = 0.99$ . Here, and in every other simulation, the volume control is set to  $l = 0.99$ .

The main effect of the decay control is to change the decay length of the Bass Drum sound by varying the gain of the feedback amplifier composed of the op-amp,  $R_{164}$ ,  $R_{169}$ ,  $VR_6$ , and  $C_{43}$ . This is an important part of the Bass Drum's sound, which can be used to change the sound from a short click to a vaguely realistic kick drum sound, to a characteristic exaggerated long booming sound. The longest setting is commonly used as a bass sound in hip hop music. It can be seen that there is a roughly linear relationship between the decay control and the decay length.

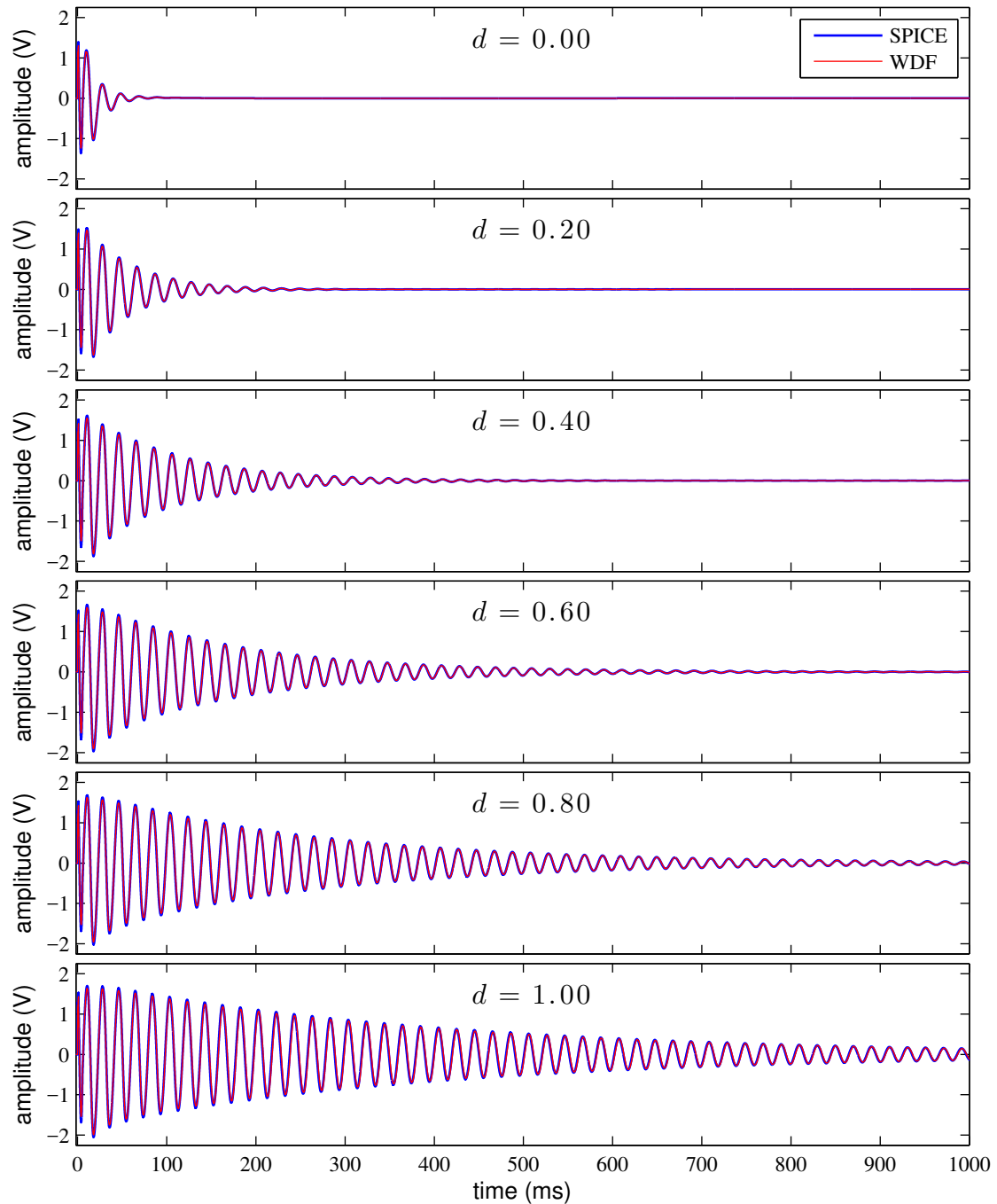


Figure V: Comparing Wave Digital Filter and SPICE for a Family of Decay Settings.

For each of the six simulations, there is a good agreement between SPICE and the Wave Digital Filter simulation.

## Variation Study

Part of the characteristic sound of analog audio circuits is due to a natural variation in their sound which would be difficult to capture using sampling. Figure VI shows a simulation where a new note is triggered every 250 ms. Each note has the same pulse amplitude, 14 V, and the Bass Drum is set with a decay setting of  $d = 1.00$ , a tone setting of  $c = 0.99$ , and a level setting of  $l = 0.99$ . The natural variation in amplitude that is visible in Figure VI is due to the interaction between the input signal and the state of the Bridged-T Resonator.

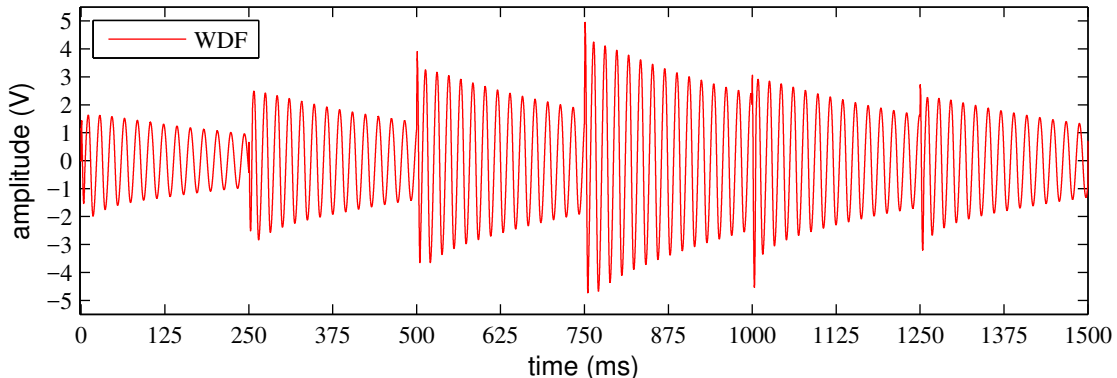


Figure VI: Demonstrating Amplitude and Timbre Variation on Repeated Notes.

Preserving this behavior is an emergent advantage of the physical modeling approach to Virtual Analog modeling. Nothing in our simulation strategies addresses this phenomenon directly and no specific provisions are made to try to emulate it, it is simply a desirable byproduct of simulating the physics of the circuitry effectively.

## Summary of Contributions

In this dissertation, techniques for discrete-time modeling analog audio circuitry using Wave Digital Filters were presented. The major contributions are a method for deriving the scattering matrices of  $\mathcal{R}$ -type adaptors which may include absorbed multiport linear elements (Chapter 2) and a method for handling multiple and multiport nonlinearities gathered at the root of a Wave Digital Filter tree (Chapter 4). Together, these two contributions raise the Wave Digital Filter formalism to a high degree of generality and render it suitable for Virtual Analog modeling of non-trivial audio circuitry. These advances were shown in action by creating a Wave Digital Filter simulation of the Bass

Drum circuit from a venerable analog drum machine, the Roland TR-808 Rhythm Composer. The Bass Drum can be broken into four sub-circuits—The Pulse Shaper, Envelope Generator, Nonlinear Bridged-T Resonator, and Output Filter—and each requires advances from this dissertation for accurate simulation.

What follows is a chapter-by-chapter review of the major and minor contributions of the dissertation.

## Chapter 1 Contributions

In Chapter 1, basic linear circuits containing linear one-ports, linear two-ports with *feedforward* connections, and standard series and parallel topological connections are considered. Here, the basic principles of Wave Digital Filters are reviewed, and classical Wave Digital Filter models of linear one-ports, two-ports, and three-ports were derived. Rules for realizing  $N$ -port series and parallel adaptors and circulators from three-port series and parallel adaptors and circulators are reviewed. Throughout, the focus is placed on dealing with the widest range of electronic circuit components and building blocks.

A contribution of the Chapter is a parametric wave definition which includes standard Wave Digital Filter voltage, power, and current waves as special cases—all of the Wave Digital Filter building blocks are derived using the parametric wave definition so that they will be valid no matter the type of waves preferred. A minor contribution of the Chapter is to derive Wave Digital Filter models of two-port devices which tend not to be reported in the literature, including voltage- and current-controlled voltage and current sources; ideal voltage, power, and current converters; active transformers and gyrators; and amplifier two-ports based on  $y$ -,  $z$ -,  $h$ -, and  $g$ -parameters. These derivations expand the range of circuits which can be modeled using the Wave Digital Filter approach. Another contribution of the Chapter is the application of alternative schemes to the Wave Digital Filter discretization of inductors and capacitors, including the well-known Warped Bilinear Transform [154], the  $\alpha$ -Transform, and the Möbius transform [155]. The Möbius transform discretization of the reactances yields new insights into constraints on Wave Digital Filter discretization, most notably the restriction that fully explicit methods such as Forward Euler cannot be used in the Wave Digital Filter context—this restriction arises not due to accuracy or stability concerns, but rather by construction.

The principles of classical linear Wave Digital Filters are used to make a Wave Digital Filter model of the Output Filter from the TR-808 Bass Drum. Part of this circuit is based around an NPN transistor emitter follower amplifier. Linearizing this amplifier gives us an opportunity to show the newly-derived Wave Digital Filter  $y$ -parameter models in action. The frequency domain behavior of the Wave Digital Filter model is shown to correspond exactly to a nonlinear SPICE simulation, except for the well-known frequency distortion of the Bilinear Transform, which is visible at high frequencies.

## Chapter 2 Contributions

In Chapter 2, more complex linear circuits containing linear two-ports in *feedback* arrangements and  $\mathcal{R}$ -type topologies (such as bridged connections) not decomposable into series and parallel connections are considered.

To begin, the method of Martens and Meerkötter, which enables Wave Digital Filter simulation of circuits containing  $\mathcal{R}$ -type topologies and reciprocal two-ports (specifically ideal transformers), is reviewed. This method cannot be used to simulate reference circuits containing non-reciprocal two-ports in feedback arrangement—these include voltage-controlled voltage sources, voltage-controlled current sources, current-controlled voltage sources, current-controlled current sources, and nullors. These elements are all essential parts of audio circuits based around operational amplifiers (which are modeled as ideal using nullors or as non-ideal using controlled sources) or ideal transistor amplifiers, or circuits based on the principles of amplifier feedback. For this reason, the restriction is a serious limitation for the modeling of audio circuitry.

The major contribution of this chapter is a Modified-Nodal-Analysis-based technique for deriving the scattering matrix and adaptation criteria for  $\mathcal{R}$ -type adaptors which may contain absorbed reciprocal and non-reciprocal two-port elements. Due to their importance for ideal operational amplifier modeling, special emphasis is given to the inclusion of nullors into the technique. This contribution sets up another contribution of the chapter—a method for handling multiple nonadaptable linear elements at the root of a Wave Digital Filter tree. This approach collects all linear nonadaptable elements into a vector and interfaces that vector to the rest of the circuit with an  $\mathcal{R}$ -type adaptor. The combination of the  $\mathcal{R}$ -type adaptor and vector of nonadaptable linear elements is resolved using a matrix inversion.

These topological advances are used to simulate a family of versions of the Bridged-T Resonator from the TR-808 Bass Drum circuit. These include a passive version, an active version based around an operational amplifier (ideal nullor-based model and limited-gain VCVS-based model), and a dual operational amplifier feedback version (ideal nullor-based model and limited-gain VCVS-based model). The frequency-domain behaviors of the Wave Digital Filter models are again shown to correspond exactly to SPICE simulations, again except for the well-known frequency distortion of the Bilinear Transform.

## Chapter 3 Contributions

In Chapter 3, circuits containing a single one-port nonlinearity (e.g., a diode) or a group of nonlinearities which can be consolidated into a single one-port nonlinearity (e.g., a diode clipper pair) are considered.

Starting with the work of Meerkötter and Scholz, techniques for handling one-port nonlinearities from the literature are reviewed. The simplest technique is to tabulate a family of solutions into a one-dimensional lookup table and use interpolation for solutions between tabulated points. This is

closely related to techniques based on piecewise linear models. For these approaches, the simplest approach is to tabulate in the  $v-i$  Kirchhoff domain (where constituent equations for standard elements like diodes are analytic). However, it is more convenient to control the final tabulation granularity by tabulating equations directly in the (typically implicit)  $a-b$  wave-domain, using an iterative solver. Single diodes can be solved *explicitly* in the wave domain using the Lambert  $\mathcal{W}$  function. In diode clipper circuits, reverse-biased diodes can be reasonably neglected so that the Lambert  $\mathcal{W}$  approach yields a good approximation. Standard nonlinearities (e.g., diodes) are described by a  $v-i$  relationship. Sometimes instantaneous  $v-q$  or  $\phi-i$  relationships are used to model nonlinear capacitors or inductors; techniques designed to accommodate nonlinear  $v-i$  relationships can be adapted to this task using a Wave Digital Filter version of the mutator from classical network theory.

The principles of handling reference circuits with a single one-port nonlinearity are used to make a Wave Digital Filter simulation of the Pulse Shaper from the TR-808 Bass Drum circuit. The unique nature of the Pulse Shaper's input signal requires the application of Möbius Transform techniques from Chapter 1 to the Pulse Shaper's capacitor discretization to ensure an accurate simulation. The time-domain behavior of this simulation is shown to have a good correspondence to SPICE simulations.

## Chapter 4 Contributions

In Chapter 4, circuits containing multiple nonlinearities alongside complicated topologies are considered.

First, techniques from the literature for handling multiple nonlinearites are reviewed. These include ad hoc models, simplified models which neglect all but the most significant nonlinear processes, extensions of the piecewise linear approach to the multiport case, techniques that aim at generality but are restricted to certain rare circuit topologies, and techniques based on global iteration of the Wave Digital Filter structure. Often, ad hoc unit delays have been introduced to ease realizability issues. None of these techniques succeed at localizing difficult aspects of the reference circuit to one part of the simulation, avoiding simplifications to the nonlinear equations, handling arbitrary circuit topologies, and keeping the dimensionality of the nonlinear problem contained.

To address these issues, Chapter 4 proposes the second major contribution of the dissertation, a method for handling multiple and multiport nonlinearities gathered at the root of a Wave Digital Filter tree. This can be considered an extension of the technique for handling multiple nonadaptable linear elements collected at the root of a Wave Digital Filter tree which was proposed in Chapter 2. However, since the nonadapatable elements in this case are nonlinear rather than linear, they cannot be solved with a matrix inverse. Rather, either table lookup or Newton–Raphson iteration is used to resolve the coupled nonlinear equations. In all these cases, the scattering behavior of the interface between the nonadaptable elements and the rest of the circuit is embodied by an  $\mathcal{R}$ -type scattering

matrix derived with the techniques from Chapter 2.

The advances relating to multiple and multiport nonlinear circuit elements are used to simulate the remaining two subcircuits from the TR-808 Bass Drum: the Envelope Generator and the full Nonlinear Bridged-T Resonator. The time-domain behavior of these simulations is shown to have a good correspondence to SPICE simulations, demonstrating the validity of the proposed method.

## Final Comments

The main contribution of this dissertation is turning a problem that usually required ad hoc treatment into a systematic problem setup with standard engineering solutions. We're far closer to a generalized Wave Digital Filter approach to Virtual Analog modeling of audio circuits than we were at the start of this dissertation. With the techniques introduced in Chapters 2 and 4, the Wave Digital Filter formalism is brought to a high degree of generality that is suitable for modeling most common audio circuits. For nonlinear audio circuits which stay substantially in a linear region of operation, it may be desirable to linearize the nonlinearities—the Wave Digital Filter models of  $y$ -,  $z$ -,  $h$ -, and  $g$ -parameter models introduced in Chapter 1 should be useful to this end. With these tools, we're able to set up the block diagram of a Wave Digital Filter from almost any audio reference circuit, and also derive a mathematical description of each block as well. At the same time, we've introduced refined techniques for handling standard electronic circuit elements. For example, in Chapter 1 we applied new discretization techniques to Wave Digital Filter capacitor and inductor modeling, adding new degrees of freedom to the Wave Digital Filter approach.

Although we have made significant strides towards realizing general audio circuits as Wave Digital Filters, quite a few matters remain for future work; here I'll mention a few. In our formulation, multiplication of a length- $N$  incident wave vector by an  $N$ -port  $\mathcal{R}$ -type scattering matrix requires  $N^2$  multiplications. This is simply the cost of a standard matrix–vector multiply, but for series and parallel adaptors there are well known techniques in the literature for realizing the scattering with fewer than  $N^2$  multiplications. In fact, it has been known since 1970 how to realize standard voltage-wave, three-port, series and parallel adaptors with a reflection-free port using only a single multiplication. The method of Martens and Meerkötter also achieves a lower bound which is below  $N^2$  for voltage-wave  $\mathcal{R}$ -type adaptors which do not include any non-reciprocal circuit elements. Their method is however restricted to work on reciprocal circuits. Future work should investigate ways of realizing  $\mathcal{R}$ -type connections that support non-reciprocal circuit elements (e.g., controlled sources, nullors) in a more efficient way.

We've introduced a technique for grouping nonlinearities at the root of a Wave Digital Filter tree and resolving the resulting implicit relationship using table lookup or Newton–Raphson iteration. Recent work by Holters and Zölzer [79] improves table-based methods in the context of Kirchhoff-domain state-space modeling; it should be possible to use this advance in the context of Wave

Digital Filter modeling to seed an initial guess for a Newton–Raphson solver. The Newton–Raphson approach to solving nonlinear equations is a standard mathematical tool. Framing the problem so it can be solved in that way links Wave Digital Filter modeling to a large engineering and mathematical literature. Although we've mentioned some refinements like backtracking, the potential for improving Wave Digital Filter modeling by choosing the most appropriate variation of Newton–Raphson solver or adapting Newton–Raphson solvers in a domain-specific way to Wave Digital Filter modeling is high.

We've used a Newton–Raphson solver or table lookup to resolve the implicit parts of this formulation. This is very similar to the approach used in Kirchhoff-domain state-space modeling. Although the work in this dissertation fits squarely into the Wave Digital Filter context, it points to a broader reconciliation between Kirchhoff-domain state-space modeling and Wave Digital Filters. Indeed although we've tried to elevate the Wave Digital Filter approach so that it may model any audio circuit, I do not wish to imply that it is superior computationally to state-space modeling in general. Still, the Wave Digital Filter approach has been shown to efficient in real-time implementation [243, 242]. To make a brief comment on the relative cost of each method, we consider non-time-varying circuits. Roughly, the cost of a Wave Digital Filter model grows linearly as circuit components or topological connections are added and bounds on the cost of a Kirchhoff-domain state-space model grows quadratically as reactive elements which hold state (capacitors and inductors) are added. The actual cost will depend on the sparsity of the state space matrices. This means that the Wave Digital Filter approach is more efficient for reference circuits involving many states, such as a Hammond organ vibrato/chorus circuit [154]. The state-space approach is more efficient for reference circuits involving few states. For example a ladder of a dozen resistive voltage dividers would end up as only a single multiplier in the state-space approach but would clearly involve two dozen multipliers in a voltage wave Wave Digital Filter. A non-computational advantage of the Wave Digital Filter remains however—the Wave Digital Filter approach would preserve the topology of the circuit and the voltage across / current through each electrical component in the circuit. Future work should look more closely at how the Wave Digital Filter and state-space approaches may be hybridized to simultaneously get the best of both worlds.

The most direct application of the Wave Digital Filter approach to Virtual Analog modeling is building digital models of existing audio circuits. This has important applications for preserving the sounds and musical traditions of the past and expanding access to rare and historical audio circuits. At the same time, the process may be run in reverse—Wave Digital Filter methods may be used as part of a computer-aided design process for creating new audio circuits. Wave Digital Filter modeling also has a great potential for modeling modded or circuit-bent instruments. Since Wave Digital Filter simulations are modular and derived directly from the reference circuit, it is easy to add, remove, or modify components (key operations of modding and circuit bending) in a systematic way. Perhaps the finest application of the techniques presented in this dissertation would

be the creation of digital models of circuit-bent instruments which can be used in the creation of new, interesting, useful, and even beautiful sounds.

## Appendix A

# Derivation of the Extended *y*-Parameter Model

This Appendix covers a topic related to the TR-808 Bass Drum Output Filter case study (§1.7). It details the derivation of an “extended” *y*-parameter model suitable for replacing the emitter follower and biasing voltage source  $V_{B2}$ . First, we will define an “extended” *y*-parameter model suitable for transient-mode simulations. Second, we’ll linearize the emitter-follower two-port around its operating point to solve for the extended *y* parameters in terms of the emitter follower constants and battery voltage. Third, we’ll solve for the dc solution of the entire circuit to find the correct operating point. Finally, we’ll put it all together to find the exact extended *y* parameters.

### A.1 Extended *y*-Parameter Model

A standard *y*-parameter model (§1.4.10) is intended to describe the small signal behavior of an amplifier. That is, it describes behavior around an operating point, not the dc bias itself. Since in Wave Digital Filter simulation we are interested primarily in transient-mode simulation of circuits, we must also preserve the dc signals that actually produce biases in the circuit. If there are no other nonlinear devices in the circuit and there is dc blocking on the output of the circuit, then it could be possible to model without the biases [6]. However, if there are any other nonlinearities in the circuit it is essential to model the bias correctly.

Recall the definition of a *y*-parameter model

$$\begin{bmatrix} i_1 \\ i_2 \end{bmatrix} = \begin{bmatrix} y_{11} & y_{12} \\ y_{21} & y_{22} \end{bmatrix} \begin{bmatrix} v_1 \\ v_2 \end{bmatrix}. \quad (\text{A.1})$$

To this definition we add dc terms to each of the port currents,  $I_1$  and  $I_2$ , creating the “extended”

*y*-parameter model

$$\begin{bmatrix} i_1 \\ i_2 \end{bmatrix} = \begin{bmatrix} y_{11} & y_{12} \\ y_{21} & y_{22} \end{bmatrix} \begin{bmatrix} v_1 \\ v_2 \end{bmatrix} + \begin{bmatrix} I_1 \\ I_2 \end{bmatrix}. \quad (\text{A.2})$$

The equivalent circuit that realizes the extended *y*-parameter model is shown in Figure A.1.

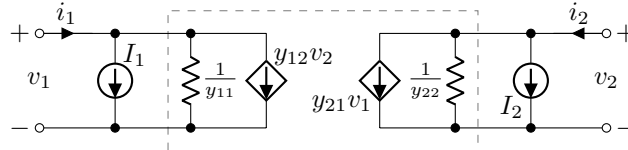


Figure A.1: Extended *y*-Parameter Equivalent Circuit.

If the dc current sources  $I_1$  and  $I_2$  can be associated with parallel resistances from the surrounding circuitry, then in a Wave Digital Filter the extended *y*-parameter model can be realized using standard parallel adaptors, standard resistive current sources, and the *y*-parameter two-port described in §1.4.10.

If the dc current sources  $I_1$  and  $I_2$  cannot be associated with parallel resistances from the surrounding circuitry, it may be inconvenient to implement as a Wave Digital Filter. The reason for this is that using the standard Wave Digital Filter approach, only a single nonadaptable element is allowed in the reference circuit. In Chapter 2 we will introduce a technique for handling multiple nonadaptable linear elements at the root of a Wave Digital Filter tree. But it is best to avoid those techniques if simpler ones are available. Here, it is possible to split the resistances  $1/y_{11}$  and  $1/y_{22}$  each into two parallel resistances with double the value.<sup>1</sup> In this way, part of the resistance can be associated with the *y*-parameter two port and part with the current source, and again the extended *y*-parameter model can be realized using standard parallel adaptors, standard resistive current sources, and the *y*-parameter two-port described in §1.4.10. This is illustrated in Figure A.2.

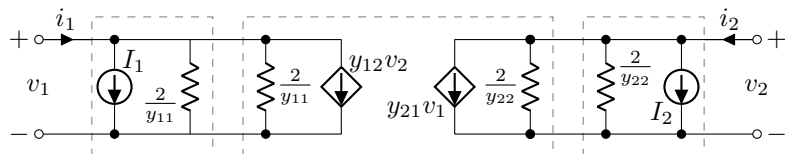


Figure A.2: Splitting Resistances on Extended *y*-Parameter Equivalent Circuit.

## A.2 Linearize Transistor

In the previous section we defined the extended *y*-parameter model, which is characterized by six parameters  $y_{11}$ ,  $y_{12}$ ,  $y_{21}$ ,  $y_{22}$ ,  $I_1$ , and  $I_2$ . To use it to describe an emitter follower two-port, we

<sup>1</sup>Any impedance  $z$  is equal to two impedances  $2z$  in parallel:  $z = \frac{1}{\frac{1}{2z} + \frac{1}{2z}}$ .

now must determine those six parameters in terms of the circuit components in the emitter follower two-port: the NPN transistor and the voltage source  $V_{B2}$ . This will be accomplished in two stages. First the emitter follower two-port will be replaced by a linear companion model. Second, we'll use linear algebra to solve for the  $y$ -parameter coefficients based on the two-port companion model.

Linear companion models [233, 146, 7] are used to replace a nonlinear device with an approximated version which is linearized around a particular operating point. As an example, consider the diode shown in Figure A.3a. Its  $v$ - $i$  characteristic, defined by the Shockley ideal diode model [246, 247]

$$i = f_{\text{Shockley}}(v) = I_s \left( e^{v/V_T} - 1 \right), \quad (\text{A.3})$$

is shown in Figure A.4a.

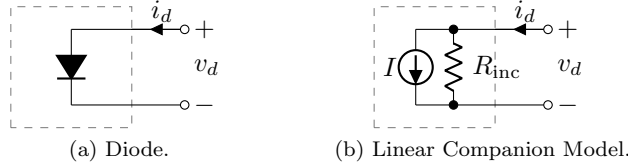


Figure A.3: Diode and Linear Companion Model.

To linearize the diode, we must find its incremental resistance  $R_{\text{inc}}$  and current offset  $I$  as a function of the operating point  $(v,i)$ . This companion model, which incidentally is just a resistive current source, is shown in Figure A.3b. The incremental conductance is found by differentiating the Shockley model (A.3) with respect to voltage

$$G_{\text{inc}} = \frac{df_{\text{Shockley}}(v)}{dv} = \frac{I_s}{V_T} e^{v/V_T}. \quad (\text{A.4})$$

The incremental resistance is the inverse of the incremental conductance

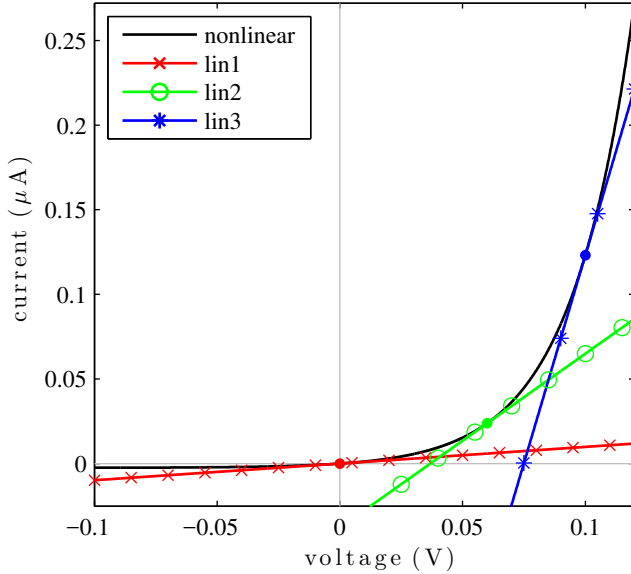
$$R_{\text{inc}} = \frac{1}{G_{\text{inc}}} = \frac{V_T}{I_s} e^{-v/V_T}. \quad (\text{A.5})$$

The current offset  $I$  accounts for the rest of the current which is not accounted for by the incremental resistance

$$I = f_{\text{Shockley}}(v) - vG_{\text{inc}} = I_s \left( e^{v/V_T} - 1 \right) - v \frac{V_T}{I_s} e^{-v/V_T}. \quad (\text{A.6})$$

Assuming an 1N914 diode with reverse bias saturation current  $I_s = 2.52 \text{ nA}$  and the standard room-temperature thermal voltage  $V_T = 25.85 \text{ mV}$ , Figure A.4a shows linearizations around three different operating points on a diode; tabulated properties of these linearizations are shown in Figure A.4b.

Now we can move on to linearizing the emitter-follower itself. We start with a suitable model

(a) Diode  $v$ - $i$  Characteristics and Example Linearizations.

name	operating point		linearized parameters		
	voltage	current	$G_{\text{inc}}$	$R_{\text{inc}}$	$I_{\text{op}}$
lin1	0 V	0 A	98.51 nS	10.15 MΩ	0 A
lin2	0.06 V	23.70 nA	1.028 μS	0.9724 MΩ	-37.92 nA
lin3	0.10 V	0.1231 μA	4.912 μS	0.2036 MΩ	-0.368 μA

(b) Example Linear Companion Model Parameters.

Figure A.4: Diode Linearization. Values rounded to four significant figures. Operating points marked with filled circles.

for the transistor's behavior. An NPN transistor, as shown in Figure A.5a, is described by the Ebers–Moll model [263].<sup>2</sup> The Ebers–Moll model gives the currents  $i_b$ ,  $i_c$ , and  $i_e$  as a function of the port voltages  $v_{be}$  and  $v_{bc}$  and is parameterized by the transistor parameters  $I_s$  (saturation current),  $\beta_F$  (forward current gain), and  $\beta_R$  (reverse current gain) as well as the thermal voltage  $V_T$ . Derived quantities  $\alpha_F = \beta_F/(1 + \beta_F)$  and  $\alpha_R = \beta_R/(1 + \beta_R)$  are also used to make the expressions more

<sup>2</sup>The Ebers–Moll model is complex enough to capture the essential behavior of the transistor at audio frequencies but neglects certain known effects, the simplest of which include terminal resistances and junction capacitances. These are included in a more complex model: the Gummel–Poon model [264].

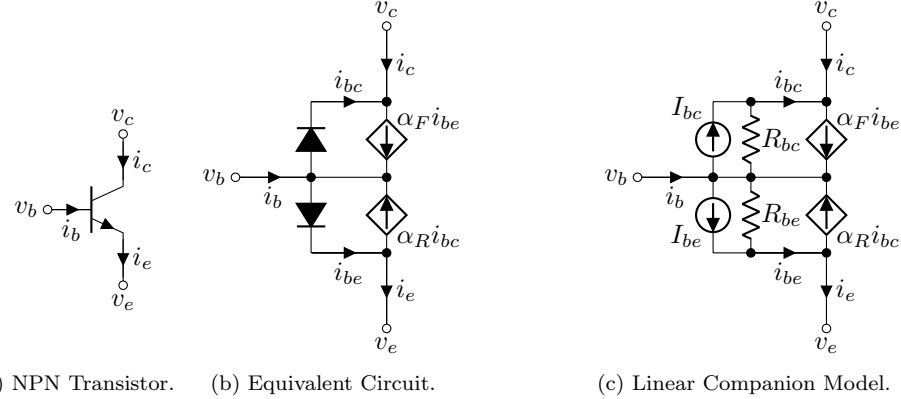


Figure A.5: NPN Transistor, Equivalent Circuit, and Linear Companion Model.

compact. The Ebers–Moll model is

$$i_e = \frac{I_s}{\alpha_F} \left( e^{v_{be}/V_T} - 1 \right) - I_s \left( e^{v_{bc}/V_T} - 1 \right) \quad (\text{A.7})$$

$$i_c = I_s \left( e^{v_{be}/V_T} - 1 \right) - \frac{I_s}{\alpha_R} \left( e^{v_{bc}/V_T} - 1 \right) \quad (\text{A.8})$$

$$i_b = \frac{I_s}{\beta_F} \left( e^{v_{be}/V_T} - 1 \right) + \frac{I_s}{\beta_R} \left( e^{v_{bc}/V_T} - 1 \right) . \quad (\text{A.9})$$

An equivalent circuit to the Ebers–Moll model can be formed by breaking these equations into diodes and controlled sources. This is shown in Figure A.5b. Going even further, we can linearize the diodes using the process described above, which yields the transistor linear companion model shown in Figure A.5c.

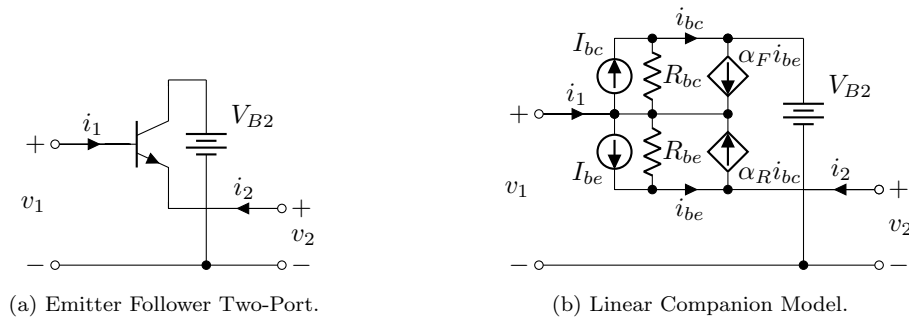


Figure A.6: Emitter-Follower Two-Port and Linearized Companion Model.

The emitter-follower two-port is shown in Figure A.6a. Plugging the transistor linear companion model we just developed yields the emitter-follower linear companion model two-port shown in

Figure A.6b. It may not look like it yet, but this two-port can be described completely by the extended  $y$ -parameter two-port. To accomplish that we must start with a mathematical description of the emitter-follower linear companion model.

We start by writing the two equations that satisfy Kirchhoff's Current Law at the positive terminal of port 1 and the positive terminal of port 2

$$i_1 = i_{be} + i_{bc} - \alpha_F i_{be} - \alpha_R i_{bc} \quad (\text{A.10})$$

$$i_2 = -i_{be} + \alpha_R i_{bc} \quad (\text{A.11})$$

which simplify to

$$i_1 = (1 - \alpha_F) i_{be} + (1 - \alpha_R) i_{bc} \quad (\text{A.12})$$

$$i_2 = (-1) i_{be} + (\alpha_R) i_{bc}. \quad (\text{A.13})$$

The expressions for the currents  $i_{be}$  and  $i_{bc}$  can be written in terms of the dc sources  $I_{be}$  and  $I_{bc}$ , the port voltages  $v_1$  and  $v_2$ , the incremental resistances  $R_{be}$  and  $R_{bc}$ , and the voltage source  $V_{B2}$

$$i_{be} = I_{be} + (v_1 - v_2) / R_{be} \quad (\text{A.14})$$

$$i_{bc} = I_{bc} + (v_1 - V_{B2}) / R_{bc}. \quad (\text{A.15})$$

Plugging (A.14)–(A.15) into (A.12)–(A.13) yields, in matrix form,

$$\begin{bmatrix} i_1 \\ i_2 \end{bmatrix} = \begin{bmatrix} 1 - \alpha_f & 1 - \alpha_R \\ -1 & \alpha_R \end{bmatrix} \begin{bmatrix} 1/R_{be} & -1/R_{be} \\ 1/R_{bc} & 0 \end{bmatrix} \begin{bmatrix} v_1 \\ v_2 \end{bmatrix} + \begin{bmatrix} 1 - \alpha_f & 1 - \alpha_R \\ -1 & \alpha_R \end{bmatrix} \begin{bmatrix} 1 & 0 & 0 \\ 0 & 1 & -1/R_{bc} \end{bmatrix} \begin{bmatrix} I_{be} \\ I_{bc} \\ V_{B2} \end{bmatrix}. \quad (\text{A.16})$$

Multiplying through yields

$$\begin{bmatrix} i_1 \\ i_2 \end{bmatrix} = \begin{bmatrix} \frac{1-\alpha_F}{R_{be}} + \frac{1-\alpha_R}{R_{bc}} & \frac{\alpha_F-1}{R_{be}} \\ -\frac{1}{R_{be}} + \frac{\alpha_R}{R_{bc}} & \frac{1}{R_{be}} \end{bmatrix} \begin{bmatrix} v_1 \\ v_2 \end{bmatrix} + \begin{bmatrix} (1 - \alpha_F) I_{be} + (1 - \alpha_R) \left( I_{bc} - \frac{V_{B2}}{R_{bc}} \right) \\ (-1) I_{be} + \left( -\frac{1}{R_{bc}} \right) \left( I_{bc} - \frac{V_{B2}}{R_{bc}} \right) \end{bmatrix}. \quad (\text{A.17})$$

This now gives the extended  $y$ -parameter terms (A.2) directly

$$y_{11} = \frac{1 - \alpha_F}{R_{be}} + \frac{1 - \alpha_R}{R_{bc}} \quad (\text{A.18})$$

$$y_{12} = \frac{\alpha_F - 1}{R_{be}} \quad (\text{A.19})$$

$$y_{21} = -\frac{1}{R_{be}} + \frac{\alpha_R}{R_{bc}} \quad (\text{A.20})$$

$$y_{22} = \frac{1}{R_{be}} \quad (\text{A.21})$$

$$I_1 = (1 - \alpha_F) I_{be} + (1 - \alpha_R) \left( I_{bc} - \frac{V_{B2}}{R_{bc}} \right) \quad (\text{A.22})$$

$$I_2 = (-1) I_{be} + \left( -\frac{1}{R_{bc}} \right) \left( I_{bc} - \frac{V_{B2}}{R_{bc}} \right). \quad (\text{A.23})$$

### A.3 DC Solution

Now that we've characterized the extended  $y$  parameters in terms of the emitter follower constants and the voltage source value, we must actually find the transistor linear companion model coefficients  $R_{be}$ ,  $R_{bc}$ ,  $I_{be}$ , and  $I_{bc}$ . To find these we first iteratively find a dc solution to the junction voltages of the transistor. Second, the linear companion model coefficients are defined in terms of the junction voltages.

Consider the circuit shown in Figure 1.54a under dc conditions. At steady-state, the capacitors all look like open circuits so only the reduced circuit shown in Figure A.7 remains. Looking at this circuit, we can write equations for the dc junction voltages  $V_{be} = V_b - V_e$  and  $V_{bc} = V_b - V_c$  in terms of the batteries  $V_{B2}$  and  $V_{-B2}$  and the resistors  $R_{173}$  and  $R_{176}$

$$V_{be} = -V_{-B2} - R_{176} I_b - R_{173} I_e \quad (\text{A.24})$$

$$V_{bc} = -V_{B2} - R_{176} I_b. \quad (\text{A.25})$$

Recall the Ebers–Moll model (A.7)–(A.9). Plugging (A.9) and (A.7) into (A.24)–(A.25) yields a system of two equations

$$V_{be} = -V_{-B2} - R_{176} \left( \frac{I_s}{\beta_F} \left( e^{\frac{V_{be}}{V_T}} - 1 \right) + \frac{I_s}{\beta_R} \left( e^{\frac{V_{bc}}{V_T}} - 1 \right) \right) - R_{173} \left( \frac{I_s}{\alpha_F} \left( e^{\frac{V_{be}}{V_T}} - 1 \right) - I_s \left( e^{\frac{V_{bc}}{V_T}} - 1 \right) \right) \quad (\text{A.26})$$

$$V_{bc} = -V_{B2} - R_{176} \left( \frac{I_s}{\beta_F} \left( e^{\frac{V_{be}}{V_T}} - 1 \right) + \frac{I_s}{\beta_R} \left( e^{\frac{V_{bc}}{V_T}} - 1 \right) \right). \quad (\text{A.27})$$

which simplifies to

$$V_{be} = -V_{-B2} + I_s \left( -\frac{R_{173}}{\alpha_F} - \frac{R_{176}}{\beta_F} \right) \left( e^{V_{be}/V_T} - 1 \right) + I_s \left( R_{173} - \frac{R_{176}}{\beta_R} \right) \left( e^{V_{bc}/V_T} - 1 \right) \quad (\text{A.28})$$

$$V_{bc} = -V_{B2} + I_s \left( -\frac{R_{176}}{\beta_F} \right) \left( e^{V_{be}/V_T} - 1 \right) + I_s \left( -\frac{R_{176}}{\beta_R} \right) \left( e^{V_{bc}/V_T} - 1 \right). \quad (\text{A.29})$$

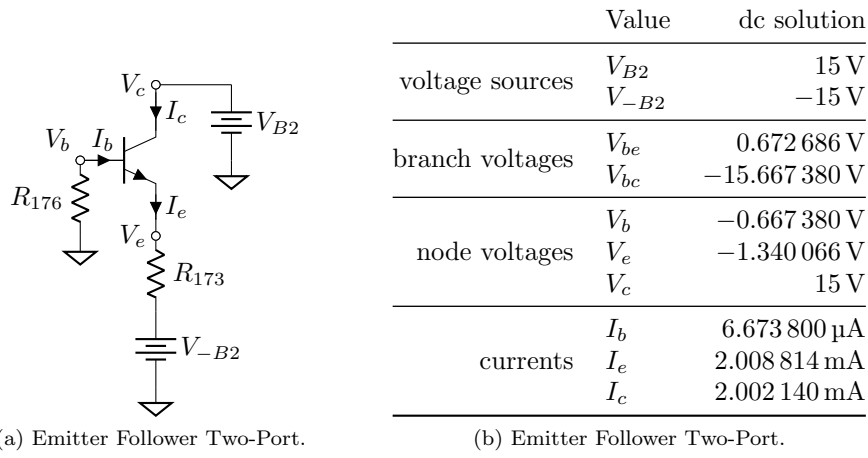


Figure A.7: TR-808 Bass Drum Output Filter at DC. Values Rounded to Six Decimal Places.

Nonlinear systems of equations like this are difficult or impossible to solve in closed form, so we will use Newton–Raphson iteration to solve for  $V_{be}$  and  $V_{ce}$ . This involves first rearranging (A.28)–(A.29) into a form suitable for “zero finding”

$$0 = -V_{be} - V_{-B2} + I_s \left( \frac{R_{173}}{\alpha_F} - \frac{R_{176}}{\beta_F} \right) \left( e^{V_{be}/V_T} - 1 \right) + I_s \left( -R_{173} - \frac{R_{176}}{\beta_R} \right) \left( e^{V_{bc}/V_T} - 1 \right) \quad (\text{A.30})$$

$$0 = -V_{bc} - V_{B2} + I_s \left( -\frac{R_{176}}{\beta_F} \right) \left( e^{V_{be}/V_T} - 1 \right) + I_s \left( -\frac{R_{176}}{\beta_R} \right) \left( e^{V_{bc}/V_T} - 1 \right), \quad (\text{A.31})$$

writing the zero-finding function  $H(\mathbf{v}) = \begin{bmatrix} h_1(V_{be}, V_{bc}) \\ h_2(V_{be}, V_{bc}) \end{bmatrix}$  in terms of the voltage vector  $\mathbf{v} = \begin{bmatrix} V_{be} & V_{bc} \end{bmatrix}^\top$

$$H(\mathbf{v}) = \begin{bmatrix} -V_{be} - V_{-B2} + I_s \left( \frac{R_{173}}{\alpha_F} - \frac{R_{176}}{\beta_F} \right) \left( e^{V_{be}/V_T} - 1 \right) + I_s \left( -R_{173} - \frac{R_{176}}{\beta_R} \right) \left( e^{V_{bc}/V_T} - 1 \right) \\ -V_{bc} - V_{B2} + I_s \left( -\frac{R_{176}}{\beta_F} \right) \left( e^{V_{be}/V_T} - 1 \right) + I_s \left( -\frac{R_{176}}{\beta_R} \right) \left( e^{V_{bc}/V_T} - 1 \right) \end{bmatrix}, \quad (\text{A.32})$$

choosing an initial guess  $\mathbf{v}^0$ , and successively choosing new guesses  $\mathbf{v}^{k+1}$  from the equation

$$\mathbf{v}^{k+1} = \mathbf{v}^k - \mathbf{J}(\mathbf{v}^k)^{-1} H(\mathbf{v}^k), \quad (\text{A.33})$$

where the superscripts indicate iteration count. Performing this update requires  $\mathbf{J} = \frac{dH}{d\mathbf{v}}$ , the Jacobian matrix (a matrix of partial derivatives). For our zero-finding function  $H(\mathbf{v})$  defined in (A.32),

Table A.1: Sequence of Newton Iterations to find DC Solution to TR-808 Bass Drum Output Filter. Voltages are truncated to the picovolt.

iteration	$V_{be}$	$V_{bc}$
0	0.6 V	-15 V
1	0.994 633 122 285 V	-15.652 383 401 925 V
2	0.968 783 221 024 V	-15.653 587 515 110 V
3	0.942 933 489 920 V	-15.654 791 620 327 V
4	0.917 084 222 191 V	-15.655 995 703 961 V
5	0.891 236 216 308 V	-15.657 199 728 830 V
6	0.865 391 646 388 V	-15.658 403 593 646 V
7	0.839 556 430 750 V	-15.659 607 022 734 V
8	0.813 746 669 043 V	-15.660 809 266 152 V
9	0.788 006 076 092 V	-15.662 008 287 624 V
10	0.762 452 751 708 V	-15.663 198 585 946 V
11	0.737 401 399 874 V	-15.664 365 501 907 V
12	0.713 659 807 469 V	-15.665 471 408 018 V
13	0.693 099 752 835 V	-15.666 429 115 054 V
14	0.678 979 807 360 V	-15.667 086 835 637 V
15	0.673 392 279 825 V	-15.667 347 108 020 V
16	0.672 695 127 654 V	-15.667 379 582 036 V
17	0.672 685 573 348 V	-15.667 380 027 085 V
18	0.672 685 571 585 V	-15.667 380 027 167 V
19	0.672 685 571 585 V	-15.667 380 027 167 V
20	0.672 685 571 585 V	-15.667 380 027 167 V

the Jacobian is given by

$$\mathbf{J} = \begin{bmatrix} \frac{\partial h_1}{\partial V_{be}} & \frac{\partial h_1}{\partial V_{bc}} \\ \frac{\partial h_2}{\partial V_{be}} & \frac{\partial h_2}{\partial V_{bc}} \end{bmatrix} = \begin{bmatrix} I_s \left( \frac{R_{173}}{\alpha_F V_T} - \frac{R_{176}}{\beta_F V_T} \right) e^{V_{be}/V_T} - 1 & I_s \left( -\frac{R_{173}}{V_T} - \frac{R_{176}}{\beta_R V_T} \right) e^{V_{bc}/V_T} \\ I_s \left( -\frac{R_{176}}{\beta_F V_T} \right) e^{V_{be}/V_T} & I_s \left( -\frac{R_{176}}{\beta_R V_T} \right) e^{V_{bc}/V_T} - 1 \end{bmatrix}. \quad (\text{A.34})$$

To choose a good initial guess, we'll use a little circuit design knowledge. In a properly-designed emitter follower, usually about one “diode drop” ( $\approx 0.6$  V) develops across base–emitter junctions. So, we'll choose  $V_{be}^0 = 0.6$  as our initial guess. We know the collector voltage is 15 V, and the base should end up biased *somewhere* between the two “rail” voltages  $V_{-B2} = -15$  V and  $V_{B2} = 15$  V. Lets just guess that  $V_b$  is exactly halfway between  $V_{-B2}$  and  $V_{B2}$ , at  $V_b = 0$  V, so that  $V_{bc}^0 = -15$  V.

The initial guess  $\mathbf{v}^0 = [V_{be}^0 \ V_{bc}^0]^\top = [0.6 \ -15]$  produces a sequence of increasingly refined estimates of the solution, which are shown in Table A.1. By iteration 18, the solver is already stable to the picovolt, and plugging the solution  $\mathbf{v} = [0.672685571585 \ -15.667380027167]^\top$  into  $H(\mathbf{v})$  indeed produces a solutions very close (within  $10^{-13}$ ) to zero. Since the Newton–Raphson solver has indeed very nearly zeroed the function, we can be confident that  $\mathbf{v}^{20}$  is a good solution to  $H(\mathbf{v})$ . The entire dc solution to this subcircuit is shown in Figure A.6b.

## A.4 Completed Model

Now we put it all together. Plugging the dc solution  $V_{be} = 0.672\,685\,571\,585$  V and  $V_{bc} = -15.667\,380\,027\,167$  V and known constant  $V_{B2}$ , the rest of the dc values are easily derived according to the following simple equivalences, branch voltage definitions, applications of Kirchhoff's Current Law, and the Ebers–Moll model of an NPN transistor:

$$V_e = V_{B2} \quad (\text{A.35})$$

$$V_b = V_e + V_{be} \quad (\text{A.36})$$

$$V_c = V_b - V_{bc} \quad (\text{A.37})$$

$$I_b = \frac{I_s}{\beta_F} \left( e^{v_{be}/V_T} - 1 \right) + \frac{I_s}{\beta_R} \left( e^{v_{bc}/V_T} - 1 \right) \quad (\text{A.38})$$

$$I_e = \frac{I_s}{\alpha_F} \left( e^{v_{be}/V_T} - 1 \right) - I_s \left( e^{v_{bc}/V_T} - 1 \right) \quad (\text{A.39})$$

$$I_c = I_e - I_b. \quad (\text{A.40})$$

Plugging  $V_{be}$  and  $V_{bc}$  into (A.4)–(A.6) yields the two incremental diode models. Plugging these values into (A.2) finally yields the extended  $y$ -parameter model. To use this in a Wave Digital Filter as in the case study, we transform these equation into the wave domain as in §1.4.10.

## Appendix B

# Derivation of the Output Filter Simplified Model

This Appendix covers a topic related to the TR-808 Bass Drum Output Filter case study (§1.7). It details the derivation of a simplified, physically-informed model which is compared to the more accurate Wave Digital Filter model in §1.7. This simplified model is inspired by the block diagram in the TR-808 Service Notes [135] and is similar to the approach taken in [2]. It is loosely inspired by the approach to modeling the distortion pedal volume and tone stage in [257].

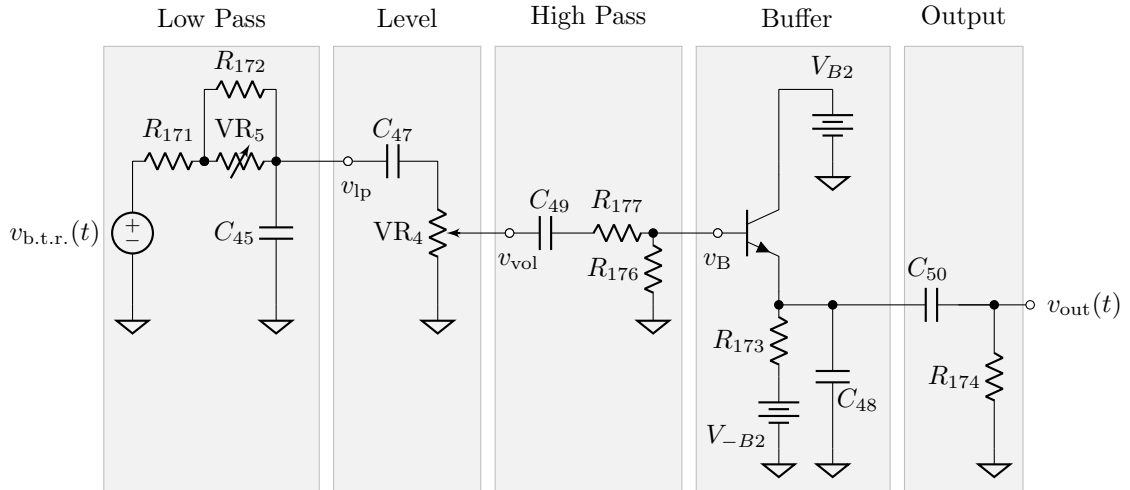


Figure B.1: TR-808 Bass Drum Tone, Level, and Output Buffer Simplified Model.

A breakdown of the TR-808 Output Filter (Figure 1.54a) into five stages is shown in Figure B.1. We make the assumptions of this breakdown explicit by forming an “equivalent” circuit using unity-gain voltage-controlled voltage sources between each stage, shown in Figure B.2.

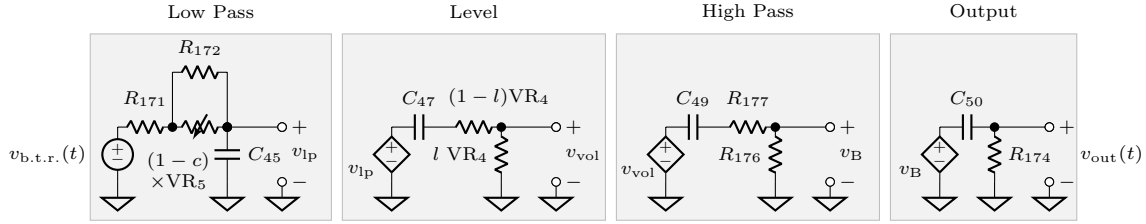


Figure B.2: TR-808 Bass Drum Tone, Level, and Output Buffer Equivalent Circuit.

By applying simple rules for voltage dividers and series/parallel impedance combinations, we find the continuous-time ( $s$ -plane) transfer function of each of the four stages. The buffer stage is assumed to simply act as a unity gain voltage amplifier.

The transfer function of the lowpass filter is

$$H_1(s) = \frac{V_{lp}(s)}{V_{in,tone}(s)} = \frac{1}{\left( \left( R_{171} + \frac{cR_{172}VR_5}{R_{172}+cVR_5} \right) C_{45} \right) s + 1}. \quad (\text{B.1})$$

The transfer function of the level stage is

$$H_2(s) = \frac{V_{vol}(s)}{V_{lp}(s)} = \frac{(lVR_4C_{47})s}{(VR_4C_{47})s + 1}. \quad (\text{B.2})$$

The transfer function of the high pass stage is

$$H_3(s) = \frac{V_B(s)}{V_{vol}(s)} = \frac{(R_{176}C_{49})s}{((R_{176} + R_{177})C_{49})s + 1} \quad (\text{B.3})$$

The transfer function of the output stage is

$$H_4(s) = \frac{V_{out}(s)}{V_B(s)} = \frac{(R_{174}C_{50})s}{(R_{174}C_{50})s + 1} \quad (\text{B.4})$$

The total transfer function is simply a cascade of the transfer functions of the four stages

$$H_{tone}(s) = \frac{V_{out,tone}(s)}{V_{in,tone}(s)} = H_1(s)H_2(s)H_3(s)H_4(s). \quad (\text{B.5})$$

We note that each stage is described by a first-order transfer function of the form

$$H(s) = \frac{\beta_1 s + \beta_0}{\alpha_1 s + \alpha_0}. \quad (\text{B.6})$$

These four transfer functions are summarized in Table B.1.

A standard approach to digitize continuous-time transfer functions like these four is to use the

Table B.1: Summary of Simplified Model Transfer Functions.

Stage	Name	Input	Output	$\beta_1$	$\beta_0$	$\alpha_1$	$\alpha_0$
Low Pass	$H_1(s)$	$V_{\text{in,tone}}(s)$	$V_{\text{lp}}(s)$	0	1	$\left(R_{171} + \frac{cR_{172}\text{VR}_5}{R_{172}+c\text{VR}_5}\right)C_{45}$	1
Level	$H_2(s)$	$V_{\text{lp}}(s)$	$V_{\text{vol}}(s)$	$l\text{VR}_4C_{47}$	0	$\text{VR}_4C_{47}$	1
High Pass	$H_3(s)$	$V_{\text{vol}}(s)$	$V_B(s)$	$R_{176}C_{49}$	0	$(R_{176} + R_{177})C_{49}$	1
Output	$H_4(s)$	$V_B(s)$	$V_{\text{out}}(s)$	$R_{174}C_{50}$	0	$R_{174}C_{50}$	1

bilinear Transform, a mapping from the  $s$  plane to the  $z$  plane according to the substitution [155, 97]

$$s \leftarrow \eta \frac{1 - z^{-1}}{1 + z^{-1}}, \quad \eta = 2/T. \quad (\text{B.7})$$

For a second order filter of the form (B.6) described by the parameters  $\beta_0$ ,  $\beta_1$ ,  $\alpha_0$ , and  $\alpha_1$ , the bilinear Transform yields a digital filter with a transfer function

$$\tilde{H}(z) = \frac{\tilde{\beta}_1 z^{-1} + \tilde{\beta}_0}{\tilde{\alpha}_1 z^{-1} + \tilde{\alpha}_0} \quad (\text{B.8})$$

where the digital filter parameters  $\tilde{\beta}_0$ ,  $\tilde{\beta}_1$ ,  $\tilde{\alpha}_0$ , and  $\tilde{\alpha}_1$  are given in terms of the continuous-time coefficients by

$$\begin{cases} \tilde{\beta}_1 &= \eta\beta_1 - \beta_0 \\ \tilde{\beta}_0 &= -\eta\beta_1 - \beta_0 \\ \tilde{\alpha}_1 &= \eta\alpha_1 - \alpha_0 \\ \tilde{\alpha}_0 &= -\eta\alpha_1 - \alpha_0 \end{cases}. \quad (\text{B.9})$$

Evaluating these transfer functions along the unit circle for families of different tone and volume parameters yields the magnitude responses shown in Figure B.3.

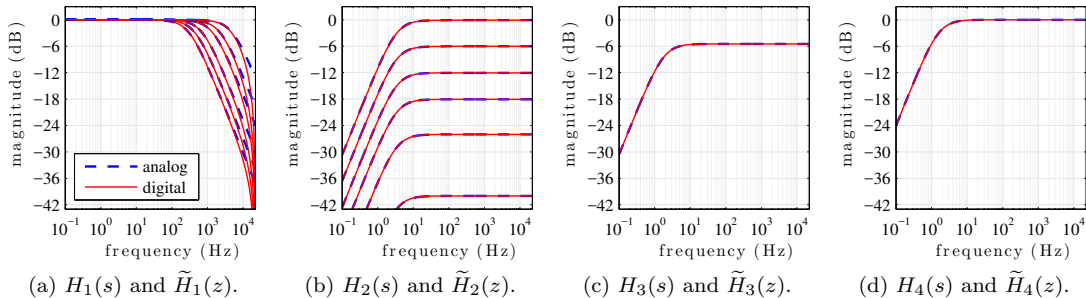


Figure B.3: Simplified TR-808 Bass Drum Tone, Level, and Output Buffer Magnitude Responses.



## Appendix C

# Tom/Conga equivalent Resistance Calculation

In this Appendix, we'll derive the linearization of a diode pair (§C), derive the transfer function of the Passive Bridged-T Filter (§C.1), and derive the transfer function of the Bridged-T Resonator (§C.2).

Our goal here is to linearize one branch of the Bridged-T Resonator that appears in the TR-808's Tom and Conga circuits so that it can be replaced with a single resistor  $R_1$  in a small-signal analysis and linear simulation. This analysis proceeds by linearizing the diode around dc, which yields a single resistor, and then calculating the equivalent resistance  $R_1$  as a function of the potentiometer value, knob setting, side branch resistance, and the linearized resistor.

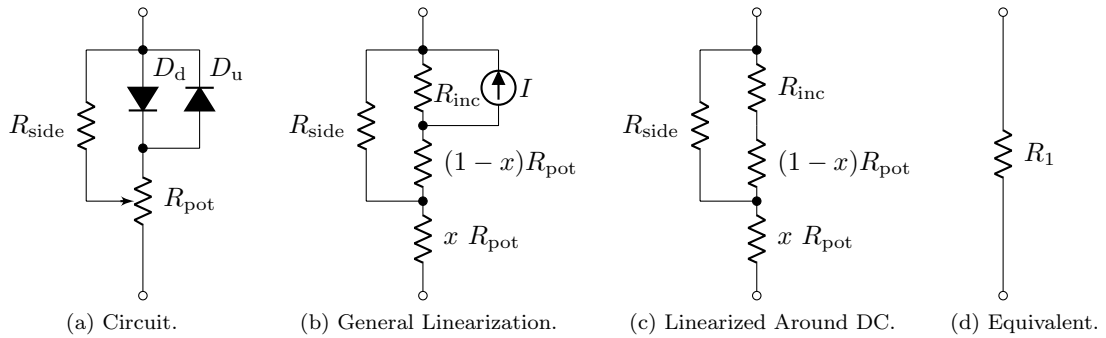


Figure C.1:  $R_1$  Branch, a General Linearization, a Linearization at DC, and Equivalent Resistance.

The  $v-i$  characteristic of the pair of identical diodes, each described by the Shockley ideal diode model, is

$$i = f_{\text{pair}}(v) = I_s \left( e^{v/V_T} - e^{-v/V_T} \right). \quad (\text{C.1})$$

To linearize this diode pair, we must find its incremental resistance  $R_{\text{inc}}$  and current offset  $I$  as a function of the operating point  $(v, i)$ . The incremental conductance is found by differentiating the Shockley model with respect to voltage

$$G_{\text{inc}} = \frac{df_{\text{pair}}(v)}{dv} = \frac{I_s}{V_T} \left( e^{v/V_T} + e^{-v/V_T} \right) = \frac{2I_s}{V_T} \cosh(v/V_T). \quad (\text{C.2})$$

The incremental resistance is the inverse of the incremental conductance

$$R_{\text{inc}} = \frac{1}{G_{\text{inc}}} = \frac{V_T}{2I_s} \operatorname{sech}(v/V_T). \quad (\text{C.3})$$

The current offset  $I$  accounts for the rest of the current which is not accounted for by the incremental resistance

$$I = f_{\text{pair}}(v) - vG_{\text{inc}} = I_s \left( e^{v/V_T} - e^{-v/V_T} \right) - v \frac{V_T}{2I_s} \operatorname{sech}(v/V_T). \quad (\text{C.4})$$

In particular, we are interested in linearizing the diode pair at dc. The voltage drop across the diode pair at dc is 0 V, so according to the preceding equations the linearized diode will have the following properties

$$G_{\text{inc}} = \frac{2I_s}{V_T} \quad (\text{C.5})$$

$$R_{\text{inc}} = \frac{V_T}{2I_s} \quad (\text{C.6})$$

$$I = 0. \quad (\text{C.7})$$

The current source has a value of 0 V, so it is equivalent to an open circuit. Therefore, in this specific case the diode's companion model is only a resistor, with no current source.

Now we can find the equivalent resistance of the entire branch. By inspection we can see that

$$R_1 = (1-x)R_{\text{pot}} + (R_{\text{side}} \parallel (R_{\text{inc}} + xR_{\text{pot}})) \quad (\text{C.8})$$

$$R_1 = (1-x)R_{\text{pot}} + \frac{1}{\frac{1}{R_{\text{side}}} + \frac{1}{xR_{\text{pot}}}} \quad (\text{C.9})$$

$$R_1 = (1-x)R_{\text{pot}} + \frac{(xR_{\text{pot}} + R_{\text{inc}}) R_{\text{side}}}{xR_{\text{pot}} + R_{\text{inc}} + R_{\text{side}}} \quad (\text{C.10})$$

$$R_1 = \frac{-R_{\text{pot}}^2 x^2 + (R_{\text{pot}}^2 - R_{\text{inc}} R_{\text{pot}}) x + R_{\text{inc}} R_{\text{pot}} + R_{\text{inc}} R_{\text{side}} + R_{\text{pot}} R_{\text{side}}}{R_{\text{pot}} x + R_{\text{inc}} + R_{\text{side}}}. \quad (\text{C.11})$$

The diodes in the TR-808 Tom/Conga voices are all 1S188FM (germanium diodes). In the absence of good information on the properties of these diodes, we'll just assume they are standard silicon diodes with  $I_s = 2.52 \text{ nA}$ . As always, we will assume room temperature and thus a thermal voltage of  $V_T = 25.85 \text{ mV}$ .

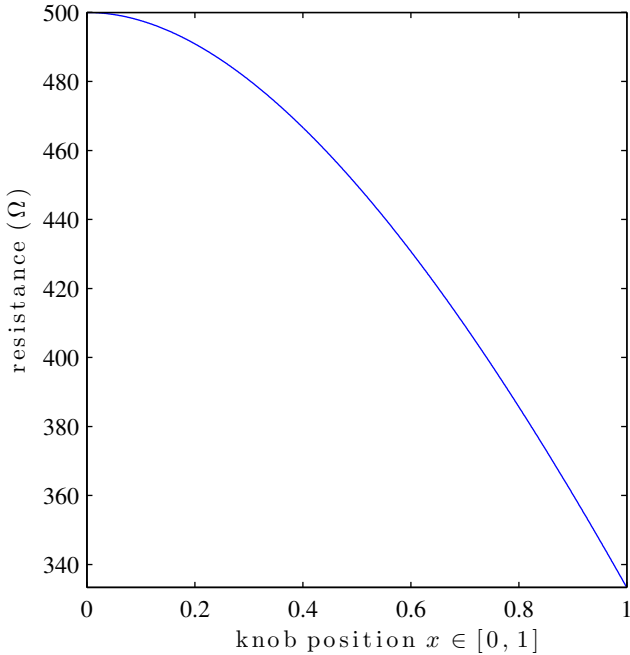
Figure C.2: Tom/Conga  $R_1$  Resistance as a Function of Knob Position  $x \in [0, 1]$ .

Table C.1: Bridged-T Resonator Values for Toms and Congas.

TR-808 Voice	$R_{pot}$		$R_{side}$		$G_{inc}$	$R_{inc}$	$R_1$
	Name	Value	Name	Value			
Low Tom/Conga	VR <sub>11</sub>	500 $\Omega$	$R_{231}$	1 k $\Omega$	0.194 971 nS	5.128 97 G $\Omega$	see (C.12)
Mid Tom/Conga	VR <sub>13</sub>	500 $\Omega$	$R_{260}$	1 k $\Omega$	0.194 971 nS	5.128 97 G $\Omega$	see (C.12)
High Tom/Conga	VR <sub>15</sub>	500 $\Omega$	$R_{287}$	1 k $\Omega$	0.194 971 nS	5.128 97 G $\Omega$	see (C.12)

All of the Tom and Conga  $R_1$  branches are described by the follow equation parameterized by the knob position  $x \in [0, 1]$

$$R_1 = \frac{-x^2 + x + 2}{x + 2} 500. \quad (\text{C.12})$$

A plot showing the relationship between knob position  $x$  and  $R_1$  is shown in Figure C.2 and a summary of the Toms and Congas linearizations is given in Table C.1.

## C.1 Derivation of Passive Bridged-T Filter Transfer Function

In this section of the appendix, we derive the transfer function of the Passive Bridged-T Filter.

To find the ontinuous-time frequency response of the Passive Bridged-T Filter, we can first write

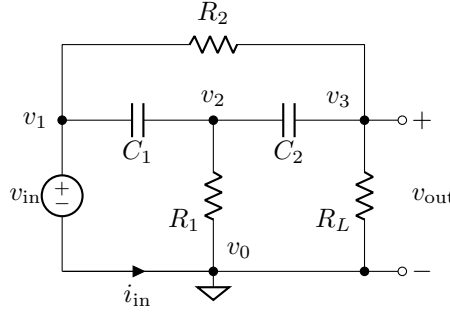


Figure C.3: Passive Bridged-T Filter with Nodes Labeled.

out the system of equations that describes its dynamics on the  $s$  plane. Labeling each node in the circuit as in Figure C.3 (taking the ground node as the datum node), we use standard stamp procedures [232, 52] to write a Modified Nodal Analysis matrix equation

$$\begin{bmatrix} G_2 + sC_1 & -sC_1 & -G_2 & 1 \\ -sC_1 & G_1 + s(C_1 + C_2) & -sC_2 & 0 \\ -G_2 & -sC_2 & G_2 + G_L + sC_2 & 0 \\ 1 & 0 & 0 & 0 \end{bmatrix} \begin{bmatrix} v_1 \\ v_2 \\ v_3 \\ i_{in} \end{bmatrix} = \begin{bmatrix} 0 \\ 0 \\ 0 \\ v_{in} \end{bmatrix}, \quad (\text{C.13})$$

recalling that conductances are the inverse of resistances:  $G_x = 1/R_x$ . By inverting the system matrix we can solve for the vector  $\begin{bmatrix} v_1 & v_2 & v_3 & i_{in} \end{bmatrix}^\top$  of node voltages and branch currents in terms of the vector  $\begin{bmatrix} 0 & 0 & 0 & v_{in} \end{bmatrix}^\top$  containing the input voltage

$$\begin{bmatrix} v_1 \\ v_2 \\ v_3 \\ i_{in} \end{bmatrix} = \begin{bmatrix} G_2 + sC_1 & -sC_1 & -G_2 & 1 \\ -sC_1 & G_1 + s(C_1 + C_2) & -sC_2 & 0 \\ -G_2 & -sC_2 & G_2 + G_L + sC_2 & 0 \\ 1 & 0 & 0 & 0 \end{bmatrix}^{-1} \begin{bmatrix} 0 \\ 0 \\ 0 \\ v_{in} \end{bmatrix}. \quad (\text{C.14})$$

We are interested in the output voltage  $v_{out}$  which happens to be identical to the node voltage  $v_3$ . Isolating the  $v_3$  row of the preceding matrix equation

$$v_{out} = \begin{bmatrix} 0 & 0 & 1 & 0 \end{bmatrix} \begin{bmatrix} 0 & 0 & 0 & 0 \\ 0 & \frac{1}{R_2} + sC_1 & -\frac{1}{R_2} & -sC_1 \\ 0 & -\frac{1}{R_2} & \frac{1}{R_2} + \frac{1}{R_L} + sC_2 & -sC_2 \\ 0 & -sC_1 & -sC_2 & \frac{1}{R_2} + sC_1 + sC_2 \\ 1 & 0 & 0 & 0 \\ 1 & -1 & 0 & 0 \end{bmatrix}^{-1} \begin{bmatrix} 0 \\ 0 \\ 0 \\ 0 \\ 1 \\ 0 \end{bmatrix} v_{in} \quad (\text{C.15})$$

and dividing through by  $v_{in}$  yields the continuous-time transfer function

$$H_{BT}(s) = \frac{V_{out}(s)}{V_{in}(s)} = \frac{(R_1 R_2 C_1 C_2) s^2 + (R_1 (C_1 + C_2)) s + 1}{(R_1 R_2 C_1 C_2) s^2 + \left(R_1 \left(1 + \frac{R_2}{R_L}\right) (C_1 + C_2) + R_2 C_2\right) s + \frac{R_2}{R_L} + 1}. \quad (\text{C.16})$$

## C.2 Derivation of Bridged-T Resonator Properties

In this section of the appendix, we derive the properties of the Bridged-T Resonator, shown in Figure C.4.

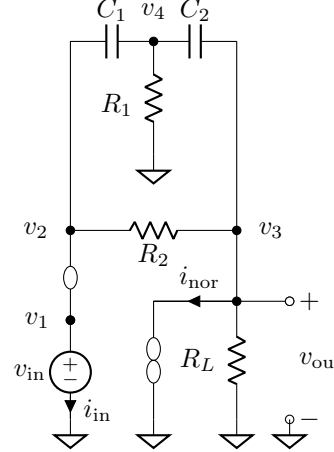


Figure C.4: Bridged-T Resonator Model (Ideal, Nullor-Based) with Nodes Labeled.

To find the continuous-time frequency response of the Bridged-T resonator, we can first write out the system of equations that describe its dynamics on the  $s$  plane. Labeling each node in the ideal nullor-based circuit model as in Figure C.4 (taking the ground node as the datum node), we use standard stamp procedures [232, 52] to write a Modified Nodal Analysis matrix equation

$$\begin{bmatrix} 0 & 0 & 0 & 0 & 1 & 0 \\ 0 & \frac{1}{R_2} + sC_1 & -\frac{1}{R_2} & -sC_1 & 0 & 0 \\ 0 & -\frac{1}{R_2} & \frac{1}{R_2} + \frac{1}{R_L} + sC_2 & -sC_2 & 0 & 1 \\ 0 & -sC_1 & -sC_2 & \frac{1}{R_2} + sC_1 + sC_2 & 0 & 0 \\ 1 & 0 & 0 & 0 & 0 & 0 \\ 1 & -1 & 0 & 0 & 0 & 0 \end{bmatrix} \begin{bmatrix} v_1 \\ v_2 \\ v_3 \\ v_4 \\ i_{in} \\ i_{nor} \end{bmatrix} = \begin{bmatrix} 0 \\ 0 \\ 0 \\ 0 \\ v_{in} \\ 0 \end{bmatrix}. \quad (\text{C.17})$$

By inverting the system matrix we can solve for the vector  $\begin{bmatrix} v_1 & v_2 & v_3 & v_4 & i_{in} & i_{nor} \end{bmatrix}^\top$  of node voltages and branch currents in terms of the vector  $\begin{bmatrix} 0 & 0 & 0 & 0 & v_{in} & 0 \end{bmatrix}^\top$  containing the input

voltage

$$\begin{bmatrix} v_1 \\ v_2 \\ v_3 \\ v_4 \\ i_{\text{in}} \\ i_{\text{nor}} \end{bmatrix} = \begin{bmatrix} 0 & 0 & 0 & 0 & 1 & 0 \\ 0 & \frac{1}{R_2} + sC_1 & -\frac{1}{R_2} & -sC_1 & 0 & 0 \\ 0 & -\frac{1}{R_2} & \frac{1}{R_2} + \frac{1}{R_L} + sC_2 & -sC_2 & 0 & 1 \\ 0 & -sC_1 & -sC_2 & \frac{1}{R_2} + sC_1 + sC_2 & 0 & 0 \\ 1 & 0 & 0 & 0 & 0 & 0 \\ 1 & -1 & 0 & 0 & 0 & 0 \end{bmatrix}^{-1} \begin{bmatrix} 0 \\ 0 \\ 0 \\ 0 \\ 0 \\ v_{\text{in}} \end{bmatrix}, \quad (\text{C.18})$$

We are interested in the output voltage  $v_{\text{out}}$  which happens to be identical to the node voltage  $v_3$ . Isolating the  $v_3$  row of the preceding matrix equation

$$v_{\text{out}} = \begin{bmatrix} 0 & 0 & 1 & 0 & 0 & 0 \end{bmatrix} \begin{bmatrix} 0 & 0 & 0 & 0 & 1 & 0 \\ 0 & \frac{1}{R_2} + sC_1 & -\frac{1}{R_2} & -sC_1 & 0 & 0 \\ 0 & -\frac{1}{R_2} & \frac{1}{R_2} + \frac{1}{R_L} + sC_2 & -sC_2 & 0 & 1 \\ 0 & -sC_1 & -sC_2 & \frac{1}{R_2} + sC_1 + sC_2 & 0 & 0 \\ 1 & 0 & 0 & 0 & 0 & 0 \\ 1 & -1 & 0 & 0 & 0 & 0 \end{bmatrix}^{-1} \begin{bmatrix} 0 \\ 0 \\ 0 \\ 0 \\ 0 \\ v_{\text{in}} \end{bmatrix} \quad (\text{C.19})$$

and dividing through by  $v_{\text{in}}$  yields the continuous-time transfer function

$$H_{\text{BTR}}(s) = \frac{V_{\text{out}}(s)}{V_{\text{in}}(s)} = \frac{(R_1 R_2 C_1 C_2) s^2 + (R_1 (C_1 + C_2) + R_2 C_1) s + 1}{(R_1 R_2 C_1 C_2) s^2 + (R_1 (C_1 + C_2)) s + 1}. \quad (\text{C.20})$$

Perhaps it will be surprising that the term  $R_L$  does not appear in the transfer function. This can be understood intuitively by the fact that any impedance in parallel with a norator is equivalent on a circuit-theoretic level to just the nullor [145]. In this case the parallel combination of  $R_L$  and the norator behaves equivalently to just the norator— $R_L$  does not affect the dynamics of this idealized version of the circuit. This is part of a larger class of equivalence theorems which are shown in Figure C.5; some of them are proved in [145, pp. 55–57].

This second-order transfer function (C.20) can be seen as an instance of the standard peaking filter second-order transfer function [283, pp. 124–126]

$$H_{\text{peak}} = \frac{\left(\frac{1}{\omega_c^2}\right) s^2 + \left(\frac{H_{\text{peak}}}{Q\omega_c}\right) s + 1}{\left(\frac{1}{\omega_c^2}\right) s^2 + \left(\frac{1}{Q\omega_c}\right) s + 1}, \quad (\text{C.21})$$

where  $\omega_c$  is the center frequency in radians/second,  $Q$  is the quality factor of the filter, and  $H_{\text{peak}}$  is the maximum of the magnitude response (at the center frequency).

By matching up  $s$  terms in the Bridged-T Resonator response (left) and the generic peaking filter

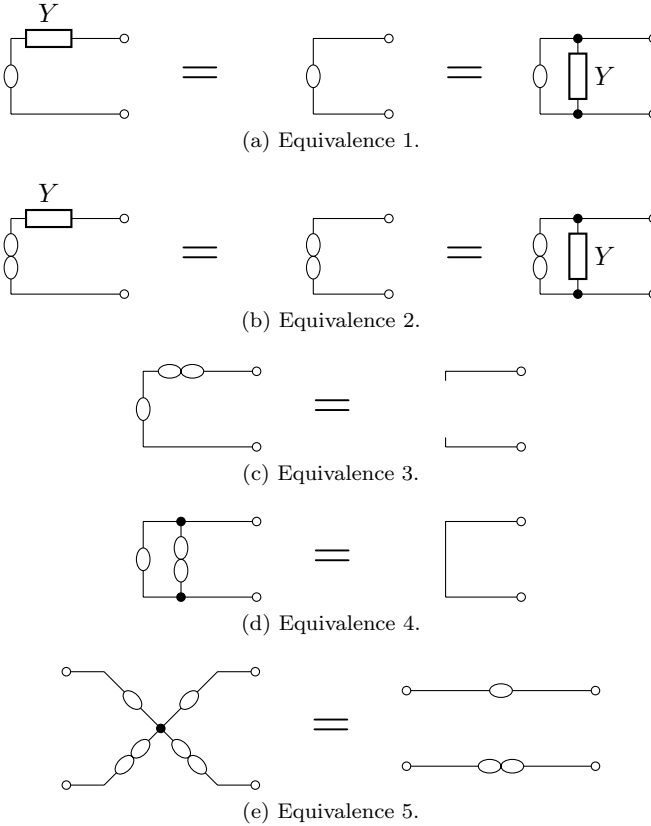


Figure C.5: Circuit-Theoretic Nullator and Norator Equivalences [145]. These equivalences show that a nullator in series or parallel with an impedance  $Y$  is equivalence to a nullator (Figure C.5a); a norator in series or parallel with an impedance  $Y$  is equivalent to a norator (Figure C.5b); a nullator and norator in series are equivalent to an open circuit (Figure C.5c); a nullator and norator in parallel are equivalent to a short circuit (Figure C.5d); and that a “star” connection of two nullors is equivalent to a single nullor (Figure C.5e).

response (right)

$$R_1 R_2 C_1 C_2 = \frac{1}{\omega_c^2} \quad (C.22)$$

$$R_1 (C_1 + C_2) + R_2 C_1 = \frac{H_{\text{peak}}}{Q \omega_c} \quad (C.23)$$

$$R_1 (C_1 + C_2) = \frac{1}{Q \omega_c}, \quad (C.24)$$

we can solve for the center frequency  $\omega_c$  by

$$\omega_c^2 = R_1 R_2 C_1 C_2 \rightarrow \omega_c = \sqrt{R_1 R_2 C_1 C_2},$$

the peak of the magnitude response  $H_{\text{peak}}$  by

$$H_{\text{peak}} = \frac{\frac{H_{\text{peak}}}{Q\omega_c}}{\frac{1}{Q\omega_c}} \longrightarrow H_{\text{peak}} = \frac{R_1(C_1 + C_2) + R_2C_1}{R_1(C_1 + C_2)}, \quad (\text{C.25})$$

and the quality factor  $Q$  by

$$Q = \frac{Q\omega_c}{\omega_c} = \frac{\sqrt{R_1R_2C_1C_2}}{R_1(C_1 + C_2)} = \frac{\sqrt{R_1R_2C_1C_2}}{(R_1C_1)^2 + (R_1C_2)^2} \longrightarrow Q = \frac{\sqrt{R_2/R_1}}{\sqrt{C_1/C_2} + \sqrt{C_2/C_1}}. \quad (\text{C.26})$$

To summarize, the three filter parameters  $\omega_c$ ,  $Q$ ,  $H_{\text{peak}}$  are given in terms of the circuit values  $R_1$ ,  $R_2$ ,  $C_1$ , and  $C_2$  by

$$\omega_c = \frac{1}{\sqrt{R_1R_2C_1C_2}} \quad (\text{C.27})$$

$$H_{\text{peak}} = \frac{R_1(C_1 + C_2) + R_2C_1}{R_1(C_1 + C_2)} = 1 + \frac{R_2C_1}{R_1(C_1 + C_2)} \quad (\text{C.28})$$

$$Q = \frac{\sqrt{R_2/R_1}}{\sqrt{C_1/C_2} + \sqrt{C_2/C_1}}. \quad (\text{C.29})$$

The center frequency in *Hertz* is given by

$$f_c = 2\pi\omega_c = \frac{1}{2\pi\sqrt{R_1R_2C_1C_2}}. \quad (\text{C.30})$$

We may also think about the continuous-time transfer function (C.20) in terms of its poles and zeros. In general a second-order transfer function<sup>1</sup> is written as

$$H(s) = \frac{n_2s^2 + n_1s + n_0}{d_2s^2 + d_1s + d_0} \quad (\text{C.31})$$

and in terms of its poles and zeros as

$$H(s) = \frac{(s - z_0)(s - z_1)}{(s - p_0)(s - p_1)}. \quad (\text{C.32})$$

The relationship between  $n_1$ ,  $n_2$ ,  $d_1$ ,  $d_2$  and  $z_0$ ,  $z_1$ ,  $p_0$ ,  $p_1$  is found by solving the numerator and denominator polynomials

$$N(s) = n_2s^2 + n_1s + n_0 = 0 \quad (\text{C.33})$$

$$D(s) = d_2s^2 + d_1s + d_0 = 0 \quad (\text{C.34})$$

---

<sup>1</sup>We use the convention that numerator terms are given with  $n.$  and denominator terms by  $d.$  rather than the more common convention to use  $b.$  and  $a.,$  due to the potential for confusion with incident and reflected waves in Wave Digital Filter notation.

using the quadratic formula. Solving the numerator and denominator polynomials, we find

$$z_0 = \frac{-n_1 + \sqrt{n_1^2 - 4n_2 n_0}}{2n_2} , \quad z_1 = \frac{-n_1 - \sqrt{n_1^2 - 4n_2 n_0}}{2n_2} \quad (\text{C.35})$$

$$p_0 = \frac{-d_1 + \sqrt{d_1^2 - 4d_2 d_0}}{2d_2} , \quad p_1 = \frac{-d_1 - \sqrt{d_1^2 - 4d_2 d_0}}{2d_2} . \quad (\text{C.36})$$

Plugging in the  $n$  and  $d$  terms from the Bridged-T Resonator transfer function C.20, we get

$$z_0 = \frac{-(R_1(C_1 + C_2) + R_2 C_1) + \sqrt{(R_1(C_1 + C_2) + R_2 C_1)^2 - 4R_1 R_2 C_1 C_2}}{2R_1 R_2 C_1 C_2} \quad (\text{C.37})$$

$$z_1 = \frac{-(R_1(C_1 + C_2) + R_2 C_1) - \sqrt{(R_1(C_1 + C_2) + R_2 C_1)^2 - 4R_1 R_2 C_1 C_2}}{2R_1 R_2 C_1 C_2} \quad (\text{C.38})$$

$$p_0 = \frac{-(R_1(C_1 + C_2)) + \sqrt{(R_1(C_1 + C_2))^2 - 4R_1 R_2 C_1 C_2}}{2R_1 R_2 C_1 C_2} \quad (\text{C.39})$$

$$p_1 = \frac{-(R_1(C_1 + C_2)) - \sqrt{(R_1(C_1 + C_2))^2 - 4R_1 R_2 C_1 C_2}}{2R_1 R_2 C_1 C_2} . \quad (\text{C.40})$$



# Bibliography

- [1] Qubais Reed Ghazala, *Circuit-bending: build your own alien instruments*, ser. Extreme Tech. Wiley, New York, 2005.
- [2] Kurt James Werner, Jonathan S. Abel, and Julius O. Smith, “A physically-informed, circuit-bendable, digital model of the Roland TR-808 bass drum circuit,” in *Proceedings of the 17th International Conference on Digital Audio Effects (DAFx-14)*, Erlangen, Germany, September 1–5 2014, pp. 159–166.
- [3] ——, “The TR-808 cymbal: a physically-informed, circuit-bendable, digital model,” in *Proceedings of the Joint Session of the International Computer Music Conference (ICMC) and the Sound and Music Computing Conference (SMC)*, vol. 40/11, Athens, Greece, September 14–20 2014, pp. 1453–1460.
- [4] ——, “More cowbell: a physically-informed, circuit-bendable, digital model of the TR-808 cowbell,” in *Proceedings of the 137th Convention of the Audio Engineering Society (AES)*, vol. 137, Los Angeles, CA, October 9–12 2014, convention paper #9207.
- [5] Alfred Fettweis, “Wave digital filters: Theory and practice,” *Proceedings of the IEEE*, vol. 74, no. 2, pp. 270–327, 1986.
- [6] Giovanni De Sanctis and Augusto Sarti, “Virtual analog modeling in the wave-digital domain,” *IEEE Transactions on Audio, Speech, and Language Processing*, vol. 18, no. 4, pp. 715–727, May 2010.
- [7] David Te-Mao Yeh, “Digital implementation of musical distortion circuits by analysis and simulation,” Ph.D. Dissertation, Stanford University, Stanford, CA, 2009.
- [8] Vesa Välimäki, Federico Fontana, Julius O. Smith, and Udo Zölzer, “Introduction to the special issue on virtual analog audio effects and musical instruments,” *IEEE Transactions on Audio, Speech, and Language Processing*, vol. 18, no. 4, pp. 713–714, May 2010.
- [9] Jussi Pekonen and Vesa Välimäki, “The brief history of virtual analog synthesis,” in *Proceedings of the Forum Acusticum*, Aalborg, Denmark, June 27 – July 1 2011, pp. 461–466.

- [10] Vesa Välimäki, Stefan Bilbao, Julius O. Smith, Jonathan S. Abel, Jyri Pakarinen, and David Berners, *Virtual Analog Effects*, 2nd ed. John Wiley & Sons, 2011, ch. 12, pp. 473–522, appears in [284].
- [11] Federico Avanzini and Sergio Canazza, *Virtual analogue instrument: an approach to active preservation of the Studio di Fonologia Musicale*, 2012, pp. 89–108, appears in [285].
- [12] Julius O. Smith, “Physical modeling synthesis update,” *Computer Music Journal*, vol. 20, pp. 44–56, 1996.
- [13] Eric Barbour, “The cool sound of tubes,” *IEEE Spectrum*, vol. 35, no. 8, pp. 24–35, August 1998, also available as [14].
- [14] ——. (1999, January 4) The cool sound of tubes. IEEE Spectrum. [Online]. Available: <http://spectrum.ieee.org/consumer-electronics/audiovideo/the-cool-sound-of-tubes>
- [15] Felix Eichas, Marco Fink, and Udo Zölzer, “Feature design for the classification of audio effect units by input/output measurements,” in *Proceedings of the 18th International Conference on Digital Audio Effects (DAFx-15)*, Trondheim, Norway, November 30 – December 3 2015, pp. 27–33.
- [16] Thomas Hélie, “On the use of Volterra series for real-time simulations of weakly nonlinear analog audio devices: Application to the Moog ladder filter,” in *Proceedings of the 9th International Conference on Digital Audio Effects (DAFx-06)*, vol. 9, Montréal, Canada, September 18–20 2006, pp. 7–12.
- [17] ——, “Volterra series and state transformation for real-time simulations of audio circuits including saturations: Application to the Moog ladder filter,” *IEEE Transactions on Audio, Speech, and Language Processing*, vol. 18, no. 4, pp. 747–759, 2010.
- [18] François Georges Germain, “A nonlinear analysis framework for electronic synthesizer circuits,” Master’s Thesis, McGill University, Montréal, Canada, October 2011.
- [19] François G. Germain, Jonathan S. Abel, Philippe Depalle, and Marcelo M. Wanderley, “Uniform noise sequencers for nonlinear system identification,” in *Proceedings of the 15th International Conference on Digital Audio Effects (DAFx-12)*, York, United Kingdom, September 17–21 2012.
- [20] Felix Eichas, Stephan Möller, and Udo Zölzer, “Block-oriented modeling of distortion audio effects using iterative minimization,” in *Proceedings of the 18th International Conference on Digital Audio Effects (DAFx-15)*, Trondheim, Norway, November 30 – December 3 2015, pp. 243–248.

- [21] Felix Eichas and Udo Zölzer, “Black-box modeling of distortion circuits with block-oriented models,” in *Proceedings of the 19th International Conference on Digital Audio Effects (DAFx-2016)*, Brno, Czech Republic, September 5–9 2016.
- [22] ——, “Modeling of an optocoupler-based audio dynamic range control circuit,” in *Proceedings of the SPIE, Novel Optical Systems Design and Optimization XIX*, vol. 99480Y, San Diego, California, August 29–31 2016.
- [23] Jyri Pakarinen and David Te-Mao Yeh, “A review of digital techniques for modeling vacuum-tube guitar amplifiers,” *Computer Music Journal*, vol. 33, no. 2, pp. 85–100, 2009.
- [24] Kristjan Dempwolf, Martin Holters, Stephan Möller, and Udo Zölzer, “The influence of small variations in a simplified guitar amplifier model,” in *Proceedings of the 12th International Conference on Digital Audio Effects (DAFx-09)*, Como, Italy, September 1–4 2009.
- [25] David Te-Mao Yeh, Balázs Bank, and Matti Karjalainen, “Nonlinear modeling of a guitar loudspeaker cabinet,” in *Proceedings of the 11th International Conference on Digital Audio Effects (DAFx-08)*, Espoo, Finland, September 1–4 2008, pp. 89–96.
- [26] Tim Stilson and Julius Smith, “Alias-free digital synthesis of classic analog waveforms,” in *Proceedings of the International Computer Music Conference (ICMC)*, Hong Kong, 1996, pp. 332–335.
- [27] Amar Chaudhary, “Band-limited simulation of analog synthesizer modules by additive synthesis,” in *Proceedings of the 105th Convention of the Audio Engineering Society (AES)*, vol. 105, San Francisco, CA, September 26–29 1998, convention paper #4779.
- [28] Vesa Välimäki, “Discrete-time synthesis of the sawtooth waveform with reduced aliasing,” *IEEE Signal Processing Letters*, vol. 12, no. 3, pp. 214–217, March 2005.
- [29] Timothy Scott Stilson, “Efficiently-variable non-oversampled algorithms in virtual-analog music synthesis—a root-locus perspective,” Ph.D. Dissertation, Stanford University, Stanford, California, 2006.
- [30] Vesa Välimäki and Antti Huovilainen, “Oscillator and filter algorithms for virtual analog synthesis,” *Computer Music Journal*, vol. 30, no. 2, pp. 19–31, Summer 2006.
- [31] ——, “Antialiasing oscillators in subtractive synthesis,” *IEEE Signal Processing Magazine*, pp. 116–125, March 2007.
- [32] Juhan Nam, Vesa Välimäki, Jonathan S. Abel, and Julius O. Smith, “Alias-free virtual analog oscillators using a feedback delay loop,” in *Proceedings of the International Conference on Digital Audio Effects (DAFx-09)*, Como, Italy, September 1–4 2009.

- [33] Juhan Nam, Vesa Välimäki, Antti Huovilainen, Jonathan S. Abel, and Julius O. Smith, “Efficient anti-aliasing oscillator algorithms using low-order fractional delay filters,” *IEEE Transactions on Audio, Speech, and Language Processing*, vol. 18, no. 4, pp. 773–785, May 2010.
- [34] Vesa Välimäki, Juhan Nam, Julius O. Smith, and Jonathan S. Abel, “Alias-suppressed oscillators based on differentiated polynomial waveforms,” *IEEE Transactions on Audio, Speech, and Language Processing*, vol. 18, no. 4, pp. 786–798, May 2010.
- [35] Jussi Pekonen, Juhan Nam, Julius O. Smith, Jonathan S. Abel, and Vesa Välimäki, “On minimizing the look-up table size in quasibandlimited classical waveform oscillators,” in *Proceedings of the 13th International Conference on Digital Audio Effects (DAFx-10)*, Graz, Austria, September 6–10 2010.
- [36] Jari Kleimola and Vesa Välimäki, “Reducing aliasing from synthetic audio signals using polynomial transition regions,” *IEEE Signal Processing Letters*, vol. 19, no. 2, pp. 67–70, February 2012.
- [37] Vesa Välimäki, Jussi Pekonen, and Juhan Nam, “Perceptually informed synthesis of bandlimited classical waveforms using integrated polynomial interpolation,” *Journal of the Acoustical Society of America (JASA)*, vol. 131, no. 1, pp. 974–986, January 2012.
- [38] Jussi Pekonen, Juhan Nam, Julius O. Smith, and Vesa Välimäki, “Optimized polynomial spline basis function design for quasi-bandlimited classical waveform synthesis,” *IEEE Signal Processing Letters*, vol. 19, no. 3, pp. 159–162, March 2012.
- [39] Fabián Esqueda, Vesa Välimäki, and Stefan Bilbao, “Aliasing reduction in soft-clipping algorithms,” in *Proceedings of the 23rd European Signal Processing Conference (EUSIPCO)*, Nice, France, August 31 – September 4 2015, pp. 2059–2063.
- [40] ——, “Antialiased soft clipping using an integrated bandlimited ramp,” in *Proceedings of the 24th European Signal Processing Conference (EUSIPCO)*, Budapest, Hungary, August 29 – September 2 2016, pp. 1043–1047.
- [41] ——, “Rounding corners with BLAMP,” in *Proceedings of the 19th International Conference on Digital Audio Effects (DAFx-16)*, Brno, Czech Republic, September 5–9 2016, pp. 121–128.
- [42] A. H. Gray, Jr. and John D. Markel, “Digital lattice and ladder filter synthesis,” *IEEE Transactions on Audio and Electroacoustics*, vol. 21, no. 6, pp. 491–500, December 1973, reprinted in [286].
- [43] Augustine H. Gray, Jr. and John D. Markel, “A normalized digital filter structure,” *IEEE Transactions on Acoustics, Speech, and Signal Processing*, vol. 23, no. 3, pp. 268–277, June 1975.

- [44] Dana Massie, "Coefficient interpolation for the Max Mathews phasor filter," in *Proceedings of the 133th Convention of the Audio Engineering Society (AES)*, San Francisco, CA, October 26–29 2012, convention paper #8698.
- [45] Aaron Wishnick, "Time-varying filters for musical applications," in *Proceedings of the 17th International Conference on Digital Audio Effects (DAFx-14)*, Erlangen, Germany, September 1–5 2014, pp. 69–76.
- [46] David Te-Mao Yeh, John Nolting, and Julius O. Smith, "Physical and behavioral circuit modeling of the SP-12 sampler," in *Proceedings of the International Computer Music Conference (ICMC)*, Copenhagen, Denmark, August 30 2007. [Online]. Available: [https://ccrma.stanford.edu/~dtyeh/papers/yeh07\\_icmc\\_sp12.pdf](https://ccrma.stanford.edu/~dtyeh/papers/yeh07_icmc_sp12.pdf)
- [47] David Te-Mao Yeh and Julius O Smith, "Discretization of the '59 Fender Bassman tone stack," in *Proceedings of the 9th International Conference on Digital Audio Effects (DAFx-06)*, Montréal, Canada, September 18–20 2006, pp. 1–5.
- [48] Chet Gney and Kurt James Werner, "Digitizing the Ibanez Weeping Demon wah pedal," in *Proceedings of the 18th International Conference on Digital Audio Effects (DAFx-15)*, Trondheim, Norway, November 30 – December 3 2015, pp. 257–264.
- [49] Samuel J. Mason, "Feedback theory—further properties of signal flow graphs," *Proceedings of the IRE*, vol. 44, no. 7, pp. 920–926, July 1956.
- [50] ———, "Topological analysis of linear nonreciprocal networks," *Proceedings of the IRE*, vol. 45, no. 6, pp. 829–838, 1957.
- [51] Martin Krämer, "Design of a cmos sample-and-hold amplifier for a high precision front-end circuit using an extended  $g_m/i_{ds}$  method," Master's Thesis, Technische Universität, Kaiserslautern, Kaiserslautern, Germany, May 4 2009.
- [52] Jiri Vlach and Kishore Singhal, *Computer methods for circuit analysis and design*. New York: Van Nostrand Reinhold Company, 1983.
- [53] Ph. Depalle and S. Tassart, "State space sound synthesis and a state space synthesizer builder," in *Proceedings of the International Computer Music Conference*, Banff, Canada, 1995, pp. 88–95.
- [54] Gianpaolo Borin, Giovanni De Poli, and Davide Rocchesso, "Elimination of delay-free loops in discrete-time models of nonlinear acoustic systems," *IEEE Transactions on Speech and Audio Processing*, vol. 8, no. 5, pp. 597–605, September 2000.

- [55] ——, “Elimination of delay-free loops in discrete-time models of nonlinear acoustic systems,” in *Proceedings of the IEEE Workshop on Applications of Signal Processing to Audio and Acoustics (WASPAA)*, Mohonk, NY, October 19–22 1997.
- [56] Julius O. Smith, “Efficient simulation of the reed-bore and bow-string mechanisms,” in *Proceedings of the International Computer Music Conference (ICMC)*, The Hague, The Netherlands, 1986, pp. 275–280.
- [57] David Te-Mao Yeh, Jonathan S. Abel, and Julius O. Smith, “Automated physical modeling of nonlinear audio circuits for real-time audio effects—part I: Theoretical development,” *IEEE Transactions on Audio, Speech, and Language Processing*, vol. 18, no. 4, pp. 728–737, 2010.
- [58] David Te-Mao Yeh, “Automated physical modeling of nonlinear audio circuits for real-time audio effects—part II: BJT and vacuum tube examples,” *IEEE Transactions on Audio, Speech, and Language Processing*, vol. 20, no. 4, pp. 1207–1216, 2012.
- [59] David Te-Mao Yeh and Julius O. Smith, “Simulating guitar distortion circuits using wave digital and nonlinear state-space formulations,” in *Proceedings of the 11th International Conference on Digital Audio Effects (DAFx-08)*, Espoo, Finland, September 1–4 2008, pp. 19–26.
- [60] David T. Yeh, Jonathan S. Abel, Andrei Vladimirescu, and Julius O. Smith, “Numerical methods for simulation of guitar distortion circuits,” *Computer Music Journal*, vol. 32, no. 2, pp. 23–42, 2008.
- [61] Jaromír Mačák, “Real-time digital simulation of guitar amplifiers as audio effects,” Ph.D. Dissertation, Brno University of Technology, Brno, Czech Republic, 2012.
- [62] Piero Rivera Benois, “Simulation framework for analog audio circuits based on nodal DK method,” Master’s Thesis, Helmut Schmidt Universität, Hamburg, Germany, December 2013.
- [63] Kristjan Dempwolff, Martin Holters, and Udo Zölzer, “Discretization of parametric analog circuits for real-time simulations,” in *Proceedings of the 13th International Conference on Digital Audio Effects (DAFx-10)*, Granz, Austria, September 6–10 2010.
- [64] Gene F. Franklin, J. David Powell, and Michael L. Workman, *Digital Control of Dynamic Systems*, 3rd ed. Menlo Park, CA: Addison-Wesley, 1998.
- [65] Jyri Pakarinen, Vesa Välimäki, Federico Fontana, Victor Lazzarini, and Jonathan S. Abel, “Recent advances in real-time musical effects, synthesis, and virtual analog models,” *EURASIP Journal on Advances in Signal Processing*, 2011, article ID 940784.
- [66] Oliver Kröning, Kristjan Dempwolff, and Udo Zölzer, “Analysis and simulation of an analog guitar compressor,” in *Proceedings of the 14th International Conference on Digital Audio Effects (DAFx-11)*, Paris, France, September 19–23 2011, pp. 205–208.

- [67] Henrique António Magalhães Martins Antão, “Modelação física do compressor audio UREI 1176LN,” Master’s thesis, Universidade de Aveiro, Aveiro, Portugal, February 2014.
- [68] Martin Holters and Udo Zölzer, “Physical modelling of a wah-wah effect pedal as a case study for application of the nodal DK method to circuits with variable parts,” in *Proceedings of the International Conference on Digital Audio Effects (DAFx-11)*, Paris, France, September 19–23 2011, pp. 31–35.
- [69] Jaromir Macák, Jiri Schimmel, and Martin Holters, “Simulation of Fender type guitar preamp using approximation and state-space model,” in *Proceedings of the 15th International Conference on Digital Audio Effects (DAFx-12)*, York, UK, September 17–21 2012, pp. 153–158.
- [70] Kristjan Dempwolf and Udo Zölzer, “A physically-motivated triode model for circuit simulations,” in *Proceedings of the International Conference on Digital Audio Effects (DAFx-11)*, vol. 11, Paris, France, September 19–23 2011, pp. 257–264.
- [71] Felix Eichas, Marco Fink, Martin Holters, and Udo Zölzer, “Physical modeling of the MXR Phase 90 guitar effect pedal,” in *Proceedings of the 17th International Conference on Digital Audio Effects (DAFx-14)*, Erlangen, Germany, September 1–5 2014.
- [72] Jaromír Mačák, “Simulation of analog flanger effect using BBD circuit,” in *Proceedings of the 19th International Conference on Digital Audio Effects (DAFx-16)*, Brno, Czech Republic, September 5–9 2016, pp. 99–102.
- [73] Martin Holters, Kristjan Dempwolf, and Udo Zölzer, “A digital emulation of the Boss SD-1 Super Overdrive pedal based on physical modeling,” in *Proceedings of the 131st Convention of the Audio Engineering Society (AES)*, New York, NY, October 20–23 2011, convention paper #8506.
- [74] Ben Holmes and Maarten van Walstijn, “Improving the robustness of the iterative solver in state-space modelling of guitar distortion circuitry,” in *Proceedings of the 18th International Conference on Digital Audio Effects (DAFx-15)*, Trondheim, Norway, November 30 – December 3 2015, pp. 49–56.
- [75] ——, “Physical model parameter optimisation for calibrated emulation of the Dallas Range-master tremble booster guitar pedal,” in *Proceedings of the 19th International Conference on Digital Audio Effects (DAFx-16)*, Brno, Czech Republic, September 5–9 2016, pp. 47–54.
- [76] Martin Holters and Udo Zölzer, “A generalized method for the derivation of non-linear state-space models from circuit schematics,” in *Proceedings of the 23rd European Signal processing Conference (EUSIPCO)*, Nice, France, August 31 – September 4 2015, pp. 1073–1077.

- [77] ——, “Circuit simulation with inductors and tratransform based on the Jiles–Atherton model of magnetization,” in *Proceedings of the 19th International Conference on Digital Audio Effects (DAFx-16)*, Brno, Czech Republic, September 5–9 2016, pp. 55–60.
- [78] Jaromir Macak, “Nonlinear transformer simulation for real-time digital audio signal processing,” in *IEEE International Conference on Telecommunications and Signal Processing (TSP)*, vol. 34, August 18–20 2011, pp. 495–499.
- [79] Martin Holters and Udo Zölzer, “A k-d tree based solution cache for the non-linear equation of circuit simulations,” in *Proceedings of the 24th European Signal Processing Conference*, Budapest, Hungary, August 29 – September 2 2016, pp. 1028–1032.
- [80] Antoine Falaize and Thomas Hélie, “Guaranteed-passive simulation of an electro-mechanical piano: a port-Hamiltonian approach,” in *Proceedings of the 18th International Conference on Digital Audio Effects (DAFx-15)*, Trondheim, Norway, November 30 – December 3 2015, pp. 57–64.
- [81] Nicholas Lopes, Thomas Hélie, and Antoine Falaize, “Explicit second-order accurate method for the passive guaranteed simulation of port-Hamiltonian system,” *IFAC-PapersOnLine*, vol. 48, no. 13, pp. 223–228, 2015.
- [82] Antoine Falaize-Skrzek and Thomas Hélie, “Simulation of an analog circuit of a wah pedal: a port-Hamiltonian approach,” in *Proceedings of the 135th Convention of the Audio Engineering Society*, New York, NY, October 17–20 2013, convention paper #8981.
- [83] Antoine Falaize, Nicholas Lopes, Denis Matignon, and Bernhard Maschke, “Energy-balanced models for acoustic and audio systems: a port-Hamiltonian approach,” in *Proceedings of the Unfold Mechanics for Sounds and Music Colloquium*, Paris, France, September 11–12 2014.
- [84] Antoine Falaize and Thomas Hélie, “Passive simulation of electrodynamic loudspeaker for guitar amplifiers: a port-Hamiltonian approach,” in *Proceedings of the International Symposium on Musical Acoustics (ISMA)*, Le Mans, France, July 7–12 2014.
- [85] Antoine Falaize, Nicolas Papazoglou, Thomas Hélie, and Nicholas Lopes, “Compensation of loudspeaker’s nonlinearities based on flatness and port-Hamiltonian approach,” in *Proceedings of the 22ème Congrès Français de Méchanique*, Lyon, France, August 24–28 2015.
- [86] Antoine Falaize and Thomas Hélie, “Passive guaranteed simulation of analog audio circuits: A port-Hamiltonian approach,” *Applied Sciences*, vol. 6, no. 10, 2016, article #273.
- [87] Alfred Fettweis, “Some principles of designing digital filters imitating classical filter structures,” *IEEE Transactions on Circuit Theory*, vol. 18, no. 2, pp. 314–316, 1971.

- [88] ——, “Digital filters structures related to classical filter networks,” *Archiv fur Elektronik und Übertragungstechnik (AEÜ, International Journal Of Electronics And Communications)*, vol. 25, pp. 79–89, 1971, reprinted in [286].
- [89] Vitold Belevitch, *Classical Network Theory*. San Francisco, CA: Holden-Day, 1968.
- [90] I. Haritantis, A. G. Constantinides, and T. Deliyannis, “Wave active filters,” *Proceedings of the IEEE*, vol. 123, no. 7, pp. 676–682, July 1976.
- [91] Alfred Fettweis and Klaus Meerkötter, “On adaptors for wave digital filters,” *IEEE Transactions on Acoustics, Speech and Signal Processing*, vol. 23, no. 6, pp. 516–525, December 1975.
- [92] Alfred Fettweis, “Pseudo-passivity, sensitivity, and stability of wave digital filters,” *IEEE Transactions on Circuit Theory*, vol. 19, no. 6, pp. 668–673, November 1972, reprinted in [286].
- [93] Stefan Bilbao, “Wave and scattering methods for the numerical solution of partial differential equations,” Ph.D. Dissertation, Stanford University, Stanford, CA, May 2001, also available as [287].
- [94] ——, *Wave and Scattering Methods for Numerical Simulation*. New York: John Wiley and Sons, Ltd, July 2004.
- [95] Julius O. Smith III, “Waveguide filter tutorial,” in *Proceedings of the International Computer Music Conference (ICMC)*, Champaign-Urbana, IL, August 23–26 1987, pp. 9–16.
- [96] ——, “Physical modeling using digital waveguides,” *Computer Music Journal*, vol. 16, no. 4, 1992.
- [97] Julius O. Smith, *Physical Audio Signal Processing for Virtual Musical Instruments and Audio Effects*, 2010, online book. [Online]. Available: <https://ccrma.stanford.edu/~jos/pasp/>
- [98] Giovanni De Sanctis, “Una nuova metodologia per l’implementazione automatica di strutture ad onda numerica orientata alla modellazione ad oggetti di interazioni acustiche,” Master’s thesis, Politecnico di Milano, Milan, Italy, 2002.
- [99] Stefan Petrausch, “Block based physical modeling,” Ph.D. Dissertation, Friedrich-Alexander-Universität Erlangen–Nürnberg, Erlangen, Germany, 2006.
- [100] Rudolf Rabenstein, Stefan Petrausch, Augusto Sarti, Giovanni De Sanctis, Cumhur Erkut, and Matti Karjalainen, “Block-based physical modeling for digital sound synthesis,” *IEEE Signal Processing Magazine*, pp. 42–54, March 2007.

- [101] Rudolf Rabenstein and Stefan Petrausch, “Block-based physical modeling with applications in musical acoustics,” *International Journal of Applied Mathematics and Computer Science*, vol. 18, no. 3, pp. 295–305, 2008.
- [102] Matti Karjalainen, “Efficient realization of wave digital components for physical modeling and sound synthesis,” *IEEE Transactions on Audio, Speech, and Language Processing*, vol. 16, no. 5, pp. 947–956, July 2008.
- [103] Rafael C. D. Paiva and Vesa Välimäki, “The Helmholtz resonator tree,” in *Proceedings of the 15th International Conference on Digital Audio Effects (DAFx-12)*, York, UK, September 17–21 2012.
- [104] Harry F. Olson, *Dynamical Analogies*. New York, NY: D. Van Nostrand Company, 1943.
- [105] Malcolm C. Smith, “Synthesis of mechanical networks: The inerter,” *IEEE Transactions on Automatic Control*, vol. 47, no. 10, pp. 1648–1662, October 2002.
- [106] M. Darrieus, “Les modèles mécaniques en électrotechnique leur application aux problèmes de stabilité,” *Bulletin de la Societe Francais des Electriciens*, vol. 96, pp. 794–819, August 1929.
- [107] W. Hähnle, “Die Darstellung elektromechanischer Gebilde durch rein elektrische Schaltbilder,” *Wissenschaftliche Veröffentlichungen aus dem Siemens-Konzern*, vol. 11, pp. 1–23, 1932.
- [108] F. A. Firestone, “A new analogy between mechanical and electrical systems,” *Journal of the Acoustical Society of America (JASA)*, vol. 4, pp. 249–267, January 1933.
- [109] Stefan D Bilbao, Julien Bensa, Richard Kronland-Martinet, and Julius O. Smith III, “The wave digital piano hammer,” *Journal of the Acoustical Society of America (JASA)*, vol. 112, no. 5, p. 2239, 2002.
- [110] Scott A. Van Duyne, John R. Pierce, and Julius O. Smith III, “Traveling wave implementation of a lossless mode-coupling filter and the wave digital hammer,” in *Proceedings of the International Computer Music Conference (ICMC)*, Århus, Denmark, 1994, pp. 411–418.
- [111] Federico Pedersini, Augusto Sarti, and Stefano Tubaro, “Block-wise physical model synthesis for musical acoustics,” *Electronics Letters*, vol. 35, no. 17, pp. 1418–1419, August 19 1999.
- [112] Vesa Välimäki, Jyri Pakarinen, Cumhur Erkut, and Matti Karjalainen, “Discrete-time modelling of musical instruments,” *Reports on Progress in Physics*, vol. 69, pp. 1–78, 2006.
- [113] Stefan Bilbao, Julien Bensa, and Richard Kronland-Martinet, “The wave digital reed: A passive formulation,” in *Proceedings of the 6th International Conference on Digital Audio Effects (DAFx-03)*, London, UK, September 8–11 2003, pp. 225–230.

- [114] Maarten van Walstijn, "Wave-based simulation of wind instrument resonators," *IEEE Signal Processing Magazine*, vol. 24, no. 2, pp. 21–31, March 2007.
- [115] Maarten van Walstijn and Gary P. Scavonne, "The wave digital tonetone model," in *Proceedings of the International Computer Music Conference (ICMC)*, Berlin, Germany, 2000, pp. 465–468.
- [116] Maarten van Walstijn, "Discrete-time modelling of brass and woodwind instruments with application to musical sound synthesis," Ph.D. Dissertation, University of Edinburgh, Edinburgh, UK, 2002.
- [117] Maarten van Walstijn and Murray Campbell, "Discrete-time modeling of woodwind instrument bores using wave variables," *Journal of the Acoustical Society of America (JASA)*, vol. 113, no. 1, pp. 575–585, January 2003.
- [118] Matti Karjalainen, Jyri Pakarinen, Cumhur Erkut, Paulo A. A. Esquef, and Vesa Välimäki, "Recent advances in physical modeling with k- and w-techniques," in *Proceedings of the 7th International Conference on Digital Audio Effects (DAFx-04)*, Naples, Italy, October 5–8 2004, pp. 107–112.
- [119] Matti Karjalainen, Tuomas Paatero, Jyri Pakarinen, and Vesa Välimäki, "Special digital filters for audio reproduction," in *Proceedings of the 32nd International Conference of the Audio Engineering Society (AES)*, Hillerød, Denmark, September 21–23 2007.
- [120] Stefan Petrausch and Rudolf Rabenstein, "Interconnection of state space structures and wave digital filters," *IEEE Transactions on Circuits and Systems II: Express Briefs*, vol. 52, no. 2, pp. 90–93, February 2005.
- [121] S. S. Lawson and A. G. Constantinides, "A method for deriving digital filter structures from classical filter networks," in *Proceedings of the IEEE International Symposium on Circuits and Systems (ISCAS)*, Newton, MA, April 21–23 1975, pp. 170–173.
- [122] M. N. S. Swamy and K. S. Thyagarajan, "A new type of wave digital filter," *Journal of the Franklin Institute*, vol. 300, no. 1, pp. 41–58, July 1975.
- [123] Stuart S. Lawson, "On a generalization of the wave digital filter concept," *International Journal of Circuit Theory and Applications*, vol. 6, no. 2, pp. 107–120, 1978.
- [124] Stuart Lawson and Ahmand Mirzai, *Wave Digital Filters*. New York, NY: Ellis Horwood, 1990.
- [125] Nobuo Nagai, Ed., *Linear Circuits, Systems and Signal Processing*. New York: Marcel Dekker, 1990.

- [126] Paulo Diniz, Eduardo da Silva, and Sergio Netto, *Digital Signal Processing: System analysis and design*. Cambridge, United Kingdom: Cambridge University Press, 2002.
- [127] Axel Sedlmeyer and Alfred Fettweis, “Digital filter with true ladder configuration,” *Circuit Theory and Applications*, vol. 1, pp. 5–10, 1973, reprinted in [286].
- [128] Alfred Fettweis, H. Levin, and A. Sedlmeyer, “Wave digital lattice filters,” *Circuit Theory and Applications*, vol. 2, pp. 203–211, 1974.
- [129] M. E. Van Valkenburg, *Introduction to Modern Network Synthesis*. New York, NY: John Wiley & Sons, 1960.
- [130] Dietrich Fränken, Klaus Meerkötter, and Joachim Waßmuth, “Passive parametric modeling of dynamic loudspeakers,” *IEEE Transactions on Speech and Audio Processing*, vol. 9, no. 8, pp. 885–891, November 2001.
- [131] John Eargle, *Loudspeaker Handbook*, 2nd ed. Springer Science+Business Media, 2003.
- [132] Augusto Sarti and Giovanni De Sanctis, “Systematic methods for the implementation of non-linear wave-digital structures,” *IEEE Transactions on Circuits and Systems I: Regular Papers*, vol. 56, no. 2, pp. 460–472, February 2009.
- [133] OV Valle, “What is Analog Circuit Behavior (ACB)?” Online, February 14 2014. [Online]. Available: <http://www.rolandus.com/blog/2014/02/14/analog-circuit-behavior-acb/>
- [134] Greg Rule, *Electro shock!: groundbreakers of synth music*. Hal Leonard, 1999.
- [135] Roland Corporation, “TR-808 service notes,” Tech. Rep., June 1981.
- [136] Thomas D. Rossing, *The Science of Sound*, 2nd ed. Reading, MA: Addison-Wesley, 1990.
- [137] Harvey Fletcher and Irvin G. Bassett, “Some experiments with the bass drum,” *Journal of the Acoustical Society of America (JASA)*, vol. 64, no. 6, pp. 1570–1576, December 1978.
- [138] Alfred Fettweis, “Realizability of digital filter networks,” *Archiv fur Elektronik und Übertragungstechnik (AEÜ, International Journal Of Electronics And Communications)*, vol. 30, pp. 90–96, February 1976.
- [139] ——, “Digital circuits and systems,” *IEEE Transactions on Circuits and Systems*, vol. 31, no. 1, pp. 31–48, January 1984.
- [140] Giovanni De Sanctis, Augusto Sarti, and Stefano Tubaro, “Automatic synthesis strategies for object-based dynamical physical models in musical acoustics,” in *Proceedings of the 6th International Conference on Digital Audio Effects (DAFx-03)*, London, UK, September 8–11 2003.

- [141] Kurt James Werner, Julius O. Smith III, and Jonathan S. Abel, “Wave digital filter adaptors for arbitrary topologies and multiport linear elements,” in *Proceedings of the 18th International Conference on Digital Audio Effects (DAFx-15)*, Trondheim, Norway, November 30 – December 3 2015, pp. 379–386.
- [142] Gernot Kubin, “Wave digital filters: Voltage, current, or power waves?” in *IEEE International Conference on Acoustics, Speech, and Signal Processing (ICASSP)*, vol. 10, Tampa, Florida, April 1985, pp. 69–72.
- [143] Julius O. Smith, “Music applications of digital waveguides,” CCRMA, Stanford University, Stanford, California, CCRMA Technical Report STAN-M-39, May 29 1987, includes [288], [56].
- [144] Chikkannan Eswaran and Alfred Fettweis, “Realization of generalized wave digital filters using adaptors,” *Archiv fur Elektronik und Übertragungstechnik (AEÜ, International Journal Of Electronics And Communications)*, vol. 32, no. 7, pp. 285–295, July 1978.
- [145] Leonard T. Bruton, *RC-Active Circuits*. Englewood Cliffs, New Jersey: Prentice-Hall Inc, 1980.
- [146] Andrei Vladimirescu, *The SPICE Book*. New York, NY: John Wiley & Sons, 1994.
- [147] Herbert J. Carlin, “Singular network elements,” *IEEE Transactions on Circuit Theory*, vol. 11, no. 1, pp. 67–72, March 1964.
- [148] Sanjit Kumar Mitra, *Analysis and Synthesis of Linear Active Networks*. New York: John Wiley & Sons, 1969.
- [149] Arnold Tustin, “A method of analysing the behavior of linear systems in terms of time series,” *Journal of the Institution of Electrical Engineers*, vol. 94, no. 1, pp. 130–142, May 1947.
- [150] Dietrich Fränken and Karlheinz Ochs, “Numerical stability properties of passive Runge-Kutta methods,” in *Proceedings of the IEEE International Symposium on Circuits and Systems (ISCAS)*, vol. 3, Sydney, Australia, May 6–9 2001, pp. 473–476.
- [151] ——, “Synthesis and design of passive Runge-Kutta methods,” *International Journal of Electronics and Communications (AEÜ)*, vol. 55, no. 6, pp. 417–425, 2001.
- [152] ——, “Automatic step-size control in wave digital simulation using passive numerical integration methods,” *International Journal of Electronics and Communications (AEÜ)*, vol. 58, pp. 391–401, 2004.
- [153] Germund G. Dahlquist, “A special stability problem for linear multistep methods,” *BIT Numerical Mathematics*, vol. 3, no. 1, pp. 27–43, March 1963.

- [154] Kurt James Werner, William Ross Dunkel, and François G. Germain, “A computational model of the Hammond organ vibrato/chorus using wave digital filters,” in *Proceedings of the 19th International Conference on Digital Audio Effects (DAFx-16)*, Brno, Czech Republic, September 5–9 2016, pp. 271–278.
- [155] François G. Germain and Kurt J. Werner, “Design principles for lumped model discretisation using Möbius transforms,” in *Proceedings of the 18th International Conference of Digital Audio Effects (DAFx-15)*, Trondheim, Norway, November 30 – December 3 2015, pp. 371–378.
- [156] Mohamad Adnan Al-Alaoui, “Novel digital integrator and differentiator,” *Electronics Letters*, vol. 29, no. 4, pp. 376–378, February 1993.
- [157] Tomislav B. Šekara and Milić R. Stojić, “Application of the  $\alpha$ -approximation for discretization of analogue systems,” *Facta Universitatis (Niš), Ser.: Elec. Energ.*, vol. 18, no. 3, pp. 571–586, December 2005.
- [158] Mohamad Adnan Al-Alaoui, “Al-Alaoui operator and the  $\alpha$ -approximation for discretization of analog systems,” *Facta Universitatis (Niš), Ser.: Elec. Energ.*, vol. 19, no. 1, pp. 143–146, April 2006.
- [159] Zeev Nehari, *Conformal Mapping*. Dover Publications, 2011.
- [160] Georg Hetmanczyk and Karlheinz Ochs, “Wave digital simulation of Burgers’ equation using Gear’s method,” in *Proceedings of the 51st Midwest Symposium on Circuits and Systems (MWSCAS)*, Knoxville, Tennessee, August 10–13 2008, pp. 161–164.
- [161] Bengt Lindberg, “On smoothing and extrapolation for the trapezoidal rule,” *BIT Numerical Mathematics*, vol. 11, no. 1, pp. 29–52, March 1971.
- [162] Wenzhong Gao, Eugene Solodovnik, Roger Dougal, and A. P. Sakis Meliopoulos, “Elimination of numerical oscillations in power system dynamic simulation,” in *Eighteenth Annual IEEE Applied Power Electronics Conference and Exposition 2003 (APEC ’03)*, vol. 2, 2003, pp. 790–794.
- [163] Soo-Chang Pei and Hong-Jie Hsu, “Fractional bilinear transform for analog-to-digital conversion,” *IEEE Transactions on Signal Processing*, vol. 56, no. 5, pp. 2122–2127, May 2008.
- [164] Richa Barsainya and Tarun Kumar Rawat, “Novel wave digital equivalents of passive elements,” in *Proceedings of the IEEE India Conference (INDICON)*, New Delhi, India, December 17–20 2015.
- [165] Richa Barsainya, Tarun Kumar Rawat, and Rachit Mahendra, “A new realization of wave digital filters using GIC and fractional bilinear transform,” *Engineering Science and Technology, an International Journal*, vol. 19, pp. 429–437, 2016.

- [166] C. William Gear, *Numerical Initial Value Problems in Ordinary Differential Equations*. Englewood Cliffs, NJ: Prentice-Hall, 1971.
- [167] Thomas Felderhoff, "Simulation of nonlinear circuits with period doubling and chaotic behavior by wave digital filter principles," *IEEE Transactions on Circuits and Systems—I: Fundamental Theory and Applications*, vol. 41, no. 7, pp. 485–491, July 1994.
- [168] Georg Hetmanczyk and Karlheinz Ochs, "Initialinitial of linear multistep methods in multidimensional wave digital models," in *Proceedings of the 52nd IEEE International Midwest Symposium on Circuits and Systems (WMWSCAS)*, Cancun, Mexico, August 2–5 2009, pp. 786–789.
- [169] A. Antoniou and M. G. Rezk, "Digital-filter synthesis using concept of generalised-immittance convertor," *IEE Journal on Electronic Circuits and Systems*, vol. 1, no. 6, pp. 207–216, November 1977.
- [170] C. Eswaran. and V. Ganapathy, "On the stability of digital filters designed using the concept of generalized-immittance convertor," *IEEE Transactions on Circuits and Systems*, vol. 28, no. 7, pp. 745–747, July 1981.
- [171] C. Eswaran, V. Ganapathy, and A. Antoniou, "On the sensitivity of GIC-based wave digital filters," *IEEE Transactions on Circuits and Systems*, vol. 29, no. 9, pp. 639–642, September 1982.
- [172] Alfred Fettweis, "Reciprocity, inter-reciprocity, and transposition in wave digital filters," *International Journal of Circuit Theory and Applications*, vol. 1, no. 4, pp. 323–337, December 1973.
- [173] Stefano D'Angelo and Vesa Välimäki, "Wave-digital polarity and current inverters and their application to virtual analog audio processing," in *IEEE International Conference on Acoustics, Speech and Signal Processing (ICASSP)*, Kyoto, Japan, March 25–30 2012, pp. 469–472.
- [174] Matti Karjalainen and Jyri Pakarinen, "Wave digital simulation of a vacuum-tube amplifier," in *IEEE International Conference on Acoustics, Speech and Signal Processing (ICASSP)*, 2006, pp. 153–156.
- [175] Jyri Pakarinen and Matti Karjalainen, "Enhanced wave digital triode model for real-time tube amplifier emulation," *IEEE Transactions on Audio, Speech, and Language Processing*, vol. 18, no. 4, pp. 738–746, May 2010.
- [176] Stefano D'Angelo, Jyri Pakarinen, and Vesa Välimäki, "New family of wave-digital triode models," *IEEE Transactions on Audio, Speech, and Language Processing*, vol. 21, no. 2, pp. 313–321, February 2013.

- [177] Willis W. Harman and Dean W. Lytle, *Electrical and Mechanical Networks: An Introduction to their Analysis*. New York: McGraw-Hill, 1962.
- [178] Phillip Bello, “Extension of Brune’s energy function approach to the study of LLF networks,” *IRE Transactions on Circuit Theory*, vol. 7, no. 3, pp. 270–280, September 1960.
- [179] Kurt James Werner, W. Ross Dunkel, Maximilian Rest, Michael Jørgen Olsen, and Julius O. Smith III, “Wave digital filter modeling of circuits with operational amplifiers,” in *Proceedings of the 24th European Signal Processing Conference (EUSIPCO)*, Budapest, Hungary, August 29 – September 2 2016, pp. 1033–1037.
- [180] Masamitu Kawakami, “Some fundamental considerations on active four-terminal linear networks,” *IRE Transactions on Circuit Theory*, vol. 5, no. 2, pp. 115–121, June 1958.
- [181] Vatché Vorperian, *Fast Analytical Techniques for Electrical and Electronic Circuits*. Cambridge: Cambridge University Press, 2004.
- [182] Jean-Pierre Thiran, “On unit element structures for wave digital filters,” *IEEE Transactions on Circuits and Systems*, vol. 24, no. 1, pp. 20–28, January 1977.
- [183] T. Yanagisawa and K. Kawashima, “Active gyrator,” *Electronics Letters*, vol. 3, no. 3, pp. 105–107, March 1967.
- [184] Thomas Felderhoff, “A new wave description for nonlinear elements,” in *IEEE International Symposium on Circuits and Systems (ISCAS)*, vol. 3, Atlanta, GA, May 12–15 1996, pp. 221–224.
- [185] Augusto Sarti and Giovanni De Poli, “Toward nonlinear wave digital filters,” *IEEE Transactions on Signal Processing*, vol. 47, no. 6, pp. 1654–1668, June 1999.
- [186] Augusto Sarti and Giovanni De Poli, “Generalized adaptors with memory for nonlinear wave digital structures,” in *Proceedings of the European Signal Processing Conference (EUSIPCO)*, vol. 3, Trieste, Italy, September 10–13 1996, pp. 1941–1944.
- [187] Augusto Sarti and Giovanni De Sanctis, “Memory extraction from dynamic scattering junctions in wave digital structures,” *IEEE Signal Processing Letters*, vol. 13, no. 12, pp. 729–732, December 2006.
- [188] B. D. H. Tellegen, “La recherche pour una série complète d’éléments de circuit idéaux non-linéaires,” *Recdconti del Seminario Matematico e Fisico di Milano*, vol. 25, no. 1, pp. 134–144, 1955.
- [189] Johan Huijsing, *Operational Amplifiers: Theory and Design*, 2nd ed. Springer, 2011.

- [190] B. R. Myers, “Nullor model of the transistor,” *Proceedings of the IEEE*, vol. 53, no. 7, pp. 758–759, July 1965.
- [191] G. Martinelli, “On the nullor,” *Proceedings of the IEEE*, vol. 53, no. 3, p. 332, March 1965.
- [192] Pragati Kumar and Raj Senani, “Bibliography on nullors and their applications in circuit analysis, synthesis and design,” *Analog Integrated Circuits and Signal Processing*, vol. 33, pp. 65–76, 2002.
- [193] Adel S. Sedra and Kenneth C. Smith, *Microelectronic Circuits*, 5th ed., ser. The Oxford Series in Electrical and Computer Engineering. New York: Oxford University Press, 2004.
- [194] Lars Wanhammar, Baharak Soltanian, Kenny Johansson, and Oscar Gustafsson, “Synthesis of circulator-tree wave digital filters,” in *Proceedings of the 5th International Symposium on Image and Signal Processing and Analysis (ISPA)*, Istanbul, Turkey, September 27–29 2007, pp. 206–211.
- [195] Lars Wanhammar, Baharak Soltanian, Oscar Gustafsson, and Kenny Johansson, “Synthesis of bandpass circulator-tree wave digital filters,” in *IEEE International Conference on Electronics, Circuits and Systems (ICECS)*, St. Julian’s, Malta, August 31 – September 3 2008, pp. 834–837.
- [196] Bhunesh Kumar and Naeem Ahmad, “Studies on circulator-tree wave digital filters,” Master’s Thesis, Linköpings universitet institute of technology, Linköping, Sweden, 2009.
- [197] Dietrich Fränken, Jörg Ochs, and Karlheinz Ochs, “Generation of wave digital structures for connection networks containing ideal transformers,” in *Proceedings of the International Symposium on Circuits and Systems (ISCAS ’03)*, vol. 3, May 25–28 2003, pp. 240–243.
- [198] ——, “Generation of wave digital structures for networks containing multiport elements,” *IEEE Transactions on Circuits and Systems I: Regular Papers*, vol. 52, no. 3, pp. 586–596, March 2005.
- [199] Paul Horowitz and Winfield Hill, *The Art of Electronics*, 2nd ed. Cambridge, UK: Cambridge University Press, 1980.
- [200] G. O. Martens and Klaus Meerkötter, “On N-port adaptors for wave digital filters with application to a bridged-tee filter,” in *Proceedings of the IEEE International Symposium on Circuits and Systems (ISCAS)*, Munich, Germany, April 1976, pp. 514–517.
- [201] Klaus Meerkötter and Dietrich Fränken, “Digital realization of connection networks by voltage-wave two-port adaptors,” *Archiv fur Elektronik und Übertragungstechnik (AEÜ, International Journal Of Electronics And Communications)*, vol. 50, no. 6, pp. 362–367, 1996.

- [202] Huynh Huu Lê, "Wave digital adaptos for Brune, Darlington C and D, and twin-T sections," Ph.D. Dissertation, University of Manitoba, Winnipeg, Canada, August 1977.
- [203] G. O. Martens and H. H. Lê, "Wave digital adaptors for reciprocal second-order sections," *IEEE Transactions on Circuits and Systems*, vol. 25, no. 12, pp. 1077–1083, December 1978.
- [204] Mark R. Jarmasz, "Design of canonic wave digital filters which suppress all zero-input parasitic oscillations," Masters thesis, University of Manitoba, Winnipeg, Canada, 1983.
- [205] Masatoshi Suzuki, Nobuhiro Miki, and Nobuo Nagai, "New wave digital filters for basic reactance sections," *IEEE Transactions on Circuits and Systems*, vol. 32, no. 4, pp. 337–348, April 1985.
- [206] M. R. Jarmasz and G. O. Martens, "Design of canonic wave digital filters using Brune and matched 4-port adaptors," *IEEE Transactions on Circuits and Systems*, vol. 34, no. 5, pp. 480–495, May 1987.
- [207] Mark R. Jarmasz, "A simplified synthesis of lossless two-port wave digital and analog filters," Ph.D. Dissertation, University of Manitoba, Winnipeg, Canada, February 1990.
- [208] Masakiyo Suzuki and Nobuo Nagai, *Wave Digital Filter Synthesized With The Darlington Procedure of Classical Circuit Theory*. Marcel Dekker, 1990, ch. 11, pp. 311–342, appears in [125].
- [209] R. Nouta, "The Jaumann structure in wave-digital filters," *Circuit Theory and Applications*, vol. 2, pp. 163–174, 1974.
- [210] M. H. Fahmy, "Digital realization of C and D-type sections," *Circuit Theory and Applications*, vol. 3, pp. 395–402, 1975.
- [211] Keio Electronic Laboratory Corporation, "Korg Mini Pops 120 service manual," Tech. Rep., 1976.
- [212] Rafael C. D. Paiva, Stefano D'Angelo, Jyri Pakarinen, and Vesa Välimäki, "Emulation of operational amplifiers and diodes in audio distortion circuits," *IEEE Transactions on Circuits and Systems II: Express Briefs*, vol. 59, no. 10, pp. 688–692, October 2012.
- [213] Bruce Carter and Thomas R. Brown, "Handbook of operational amplifier applications," Texas Instruments, Dallas, TX, Application Report SBOA092A, October 2001.
- [214] J. Alvin Connelly and Pyung Choi, *Macromodeling with SPICE*. Englewood Cliffs, NJ: Prentice-Hall, 1992.

- [215] Barry M. Cohn, Donald O. Pederson, and James E. Solomon, “Macromodeling of operational amplifiers,” in *Proceedings of the IEEE International Solid-State Circuits Conference (ISSCC)*, February 13–15 1974, pp. 42–43.
- [216] Graeme R. Boyle, Barry M. Cohn, Donald O. Pederson, and James E. Solomon, “Macromodeling of integrated circuit operational amplifiers,” *IEEE Journal of Solid-State Circuits*, vol. 9, no. 6, pp. 353–364, December 1974.
- [217] Roy Pines Sallen and Edwin L. Key, “A practical method of designing RC active filters,” *IRE Transactions on Circuit Theory*, vol. 2, no. 1, pp. 74–85, March 1955.
- [218] James Karki, “Analysis of the Sallen–Key architecture,” Texas Instruments, Dallas, TX, Application Report SLOA024B, July 1999, rev. September 2002.
- [219] Bruce Carter, “More filter design on a budget,” Texas Instruments, Dallas, TX, Application Report SLOa096, December 2001.
- [220] Lawrence P. Huelsman, Ed., *Active Filters: Lumped, Distributed, Integrated, Digital, and Parameteric*. McGraw–Hill, 1970.
- [221] T. Deliyannis, “High-Q factor circuit with reduced sensitivity,” *Electronics Letters*, vol. 4, no. 26, pp. 577–579, December 27 1968.
- [222] T. Deliyannis, Yichuang Sun, and J. K. Fidler, *Continuous-Time Active Filter Design*. CRC Press, 1999.
- [223] Joseph J. Friend, Cliff A. Harris, and Dan Hilberman, “STAR: An active biquadratic filter section,” *IEEE Transactions on Circuits and Systems*, vol. 22, no. 2, pp. 115–121, February 1975.
- [224] Tim Schwerdtfeger and Anton Kummert, “A multidimensional signal processing approach to wave digital filters with topology-related delay-free loops,” in *IEEE International Conference on Acoustics, Speech and Signal Processing (ICASSP)*, Florence, Italy, May 4–9 2014, pp. 389–393.
- [225] ——, “A multidimensional approach to wave digital filters with multiple nonlinearities,” in *Proceedings of the 22nd European Signal Processing Conference (EUSIPCO)*, Lisbon, Portugal, September 1–5 2014, pp. 2405–2409.
- [226] Timothy Schwerdtfeger and Anton Kummert, “Newton’s method for modularity-preserving multidimensional wave digital filters,” in *Proceedings of the IEEE International Workshop on Multidimensional Systems (nDS)*, Vila Real, Portugal, September 7–9 2015.

- [227] Tim Schwerdtfeger, Krzysztof Galkowski, and Anton Kummert, “Stabilization of a class of active ladder circuits based on a wave repetitive process approach by means of multidimensional wave digital filters,” in *Proceedings of the 8th International Workshop on Multidimensional Systems*, Erlangen, Germany, September 9–11 2013, pp. 1–6.
- [228] Alberto Bernardini and Augusto Sarti, “Dynamic adaptation of instantaneous nonlinear bipoles in wave digital networks,” in *Proceedings of the 24th European Signal Processing Conference (EUSIPCO)*, Budapest, Hungary, August 29 – September 2 2016, pp. 1038–1042.
- [229] David Te-Mao Yeh, “Tutorial on wave digital filters,” January 25 2008. [Online]. Available: <https://ccrma.stanford.edu/~dtyeh/papers/wdftutorial.pdf>
- [230] Kurt James Werner, Vaibhav Nangia, Julius O. Smith III, and Jonathan S. Abel, “A general and explicit formulation for wave digital filters with multiple/multiport nonlinearities and complicated topologies,” in *Proceedings of the IEEE Workshop on Applications of Signal Processing to Audio and Acoustics (WASPAA)*, New Paltz, NY, Octobter 18–21 2015.
- [231] ——, “Resolving wave digital filters with multiple/multiport nonlinearities,” in *Proceedings of the 18th International Conference on Digital Audio Effects (DAFx-15)*, Trondheim, Norway, November 30 – December 3 2015, pp. 387–394.
- [232] Chung-Wen Ho, Albert E. Ruehli, and Pierce A. Prennan, “The modified nodal approach to network analysis,” *IEEE Transactions on Circuits and Systems*, vol. 22, no. 6, pp. 504–509, June 1975.
- [233] William J. McCalla, *Fundamentals of Computer-Aided Circuit Simulation*. Boston, MA: Kluwer Academic Publishers, 1988.
- [234] Sundaram Seshu and Myril B. Reed, *Linear graphs and electrical networks*. Reading, Massachusetts: Addison–Wesley, 1961.
- [235] Tim Stilson and Julius O. Smith, “Analyzing the Moog VCF with considerations for digital implementation,” in *Proceedings of the International Computer Music Conference (ICMC)*, Hong Kong, 1996, pp. 398–401.
- [236] Rafael Cauduro Dias de Paiva, Jyri Pakarinen, Vesa Välimäki, and Miikka Tikander, “Real-time audio transformer emulation for virtual tube amplifiers,” *EURASIP Journal on Advances in Signal Processing*, 2011, article ID 347645.
- [237] Peter G. Sulzer, “A note on a bridged-T network,” *Proceedings of the IRE*, vol. 39, no. 7, pp. 819–821, 1951.
- [238] ——, “Wide-range RC oscillator,” *Electronics*, vol. 23, pp. 88–89, September 1950.

- [239] Robert-Eric Gaskell, "Modeling the nonlinear behavior of operational amplifiers," in *Proceedings of the 137th Convention of the Audio Engineering Society (AES)*, Los Angeles, CA, October 9–12 2014, convention paper #9206.
- [240] Kurt James Werner, Vaibhav Nangia, Alberto Bernardini, Julius O. Smith III, and Augusto Sarti, "An improved and generalized diode clipper model for wave digital filters," in *Proceedings of the 139th Convention of the Audio Engineering Society (AES)*, New York, NY, October 29 – November 1 2015, convention paper #9360.
- [241] Michael Jørgen Olsen, Kurt James Werner, and Julius O. Smith III, "Resolving grouped nonlinearities in wave digital filters using iterative techniques," in *Proceedings of the 19th International Conference on Digital Audio Effects (DAFx-16)*, Brno, Czech Republic, September 5–9 2016, pp. 279–286.
- [242] Maximilian Rest, "A modular realtime wave digital filter framework with support for arbitrary topologies and multiple/multiport nonlinearities," Master's Thesis, Technische Universität Berlin, Berlin, Germany, June 2016.
- [243] Maximilian Rest, W. Ross Dunkel, Kurt James Werner, and Julius O. Smith, "RT-WDF—a modular wave digital filter library with support for arbitrary topologies and multiple nonlinearities," in *Proceedings of the 19th International Conference on Digital Audio Effects (DAFx-16)*, Brno, Czech Republic, September 5–9 2016, pp. 287–294.
- [244] Federico Pedersini, Augusto Sarti, and Stefano Tubaro, "Object-based sound synthesis for virtual environments using musical acoustics," *IEEE Signal Processing Magazine*, vol. 17, no. 6, pp. 37–51, November 2000.
- [245] Matti Karjalainen, "BlockCompiler: Efficient simulation of acoustic and audio systems," in *Proceedings of the 114th Convention of the Audio Engineering Society (AES)*, Amsterdam, The Netherlands, March 22–25 2003, convention paper #5756.
- [246] W. Shockley, "The theory of  $p-n$  junctions in semiconductors and  $p-n$  junction transistors," *The Bell System Technical Journal*, vol. 28, no. 3, pp. 435–489, July 1949.
- [247] S. M. Sze, *Physics of semiconductor devices*, 2nd ed. New York: John Wiley & Sons, 1981.
- [248] Klaus Meerkötter and Reinhard Scholz, "Digital simulation of nonlinear circuits by wave digital filter principles," in *IEEE International Symposium on Circuits and Systems (ISCAS)*, vol. 1, Portland, OR, May 8–11 1989, pp. 720–723.
- [249] Leon O. Chua and Sung Mo Kang, "Section-wise piecewise-linear functions: Canonical representations, properties, and applications," *Proceedings of the IEEE*, vol. 65, no. 6, pp. 915–929, June 1977.

- [250] T. Matsumoto, “A chaotic attractor from Chua’s circuit,” *IEEE Transactions on Circuits and Systems*, vol. 31, no. 2, pp. 1055–1058, December 1984.
- [251] Leon O. Chua, “Memristor—the missing circuit elements,” *IEEE Transactions on Circuit Theory*, vol. 18, pp. 507–519, September 1971.
- [252] Julius O. Smith, “Elimination of limit cycles and overflow oscillations in time-varying lattice and ladder digital filters,” in *Proceedings of the IEEE Conference on Circuits and Systems*, San Jose, CA, May 1986, pp. 197–209, also available as [289].
- [253] Kurt James Werner and Smith III Julius O, “An energetic interpretation of nonlinear wave digital filter lookup table error,” in *Proceedings of the IEEE International Symposium on Signals, Circuits and Systems (ISSCS)*, Iași, Romania, July 9–10 2015.
- [254] Julian Parker and Stephano D’Angelo, “A digital model of the Buchla Lowpass Gate,” in *Proceedings of the 16th International Conference on Digital Audio Effects (DAFx-13)*, Maynooth, Ireland, September 2–5 2013.
- [255] R. M. Corless, G. H. Gonnet, D. E. G. Hare, D. J. Jeffrey, and D. E. Knuth, “On the Lambert W function,” *Advances in Computational Mathematics*, vol. 5, no. 1, pp. 329–359, 1996.
- [256] T. P. Dence, “A brief look into the Lambert W function,” *Applied Mathematics*, vol. 4, pp. 887–892, 2013.
- [257] David T. Yeh, Jonathan S. Abel, and Julius O. Smith, “Simplified, physically-informed models of distortion and overdrive guitar effects pedals,” in *Proceedings of the International Conference on Digital Audio Effects (DAFx-07)*, Bordeaux, France, September 2007, pp. 189–196.
- [258] David Te-Mao Yeh, Jonathan Abel, and Julius O Smith, “Simulation of the diode limiter in guitar distortion circuits by numerical solution of ordinary differential equations,” in *Proceedings of the International Conference on Digital Audio Effects (DAFx-10)*, Bordeaux, France, September 10–15 2007, pp. 197–204.
- [259] David Te-Mao Yeh, Jonathan S. Abel, Andrei Vladimirescu, and Julius O. Smith, “Numerical methods for simulation of guitar distortion circuits,” *Computer Music Journal*, vol. 32, no. 2, pp. 23–42, Summer 2008.
- [260] Jaromir Macak and Jiri Schimmel, “Nonlinear circuit simulation using time-variant filter,” in *Proceedings of the 12th International Conference on Digital Audio Effects (DAFx-09)*, Como, Italy, September 1–4 2009.
- [261] Rafael Cauduro Dias de Paiva, “Circuit modeling studies related to guitars and audio processing,” Ph.D. Dissertation, Aalto University, Espoo, Finland, September 2013.

- [262] Alberto Bernardini, Kurt James Werner, Augusto Sarti, and Julius Orion Smith III, “Modeling nonlinear wave digital elements using the Lambert function,” *IEEE Transactions on Circuits and Systems—I: Regular Papers*, vol. 63, no. 8, pp. 1231–1242, August 2016.
- [263] J. J. Ebers and John L. Moll, “Large-signal behavior of junction transistors,” *Proceedings of the IRE*, vol. 42, pp. 1761–1772, December 1954.
- [264] H. K. Gummell and H. C. Poon, “An integral charge control model of bipolar transistors,” *Bell System Technical Journal*, vol. 49, pp. 827–852, May–June 1970.
- [265] Harold Shichman and David A. Hodges, “Modeling and simulation of insulated-gate field-effect transistor switching circuits,” *IEEE Journal of Solid-State Circuits*, vol. 3, no. 3, pp. 285–289, September 1968.
- [266] Walter Sjursen, “Improved SPICE model for triode vacuum tubes,” *Journal of the Audio Engineering Society (JAES)*, vol. 45, no. 12, pp. 1082–1088, December 1997.
- [267] Francesco Santagata, Augusto Sarti, and Stefano Tubaro, “Non-linear digital implementation of a parametric analog tube ground cathode amplifier,” in *Proceedings of the 10th International Conference on Digital Audio Effects (DAFx-07)*, Bordeaux, France, September 10–15 2007, pp. 169–172.
- [268] Norman Koren, “Improved SPICE model for triode vacuum tubes,” *Glass Audio*, vol. 8, no. 5, pp. 18–27, 1996.
- [269] G. C. Cardarilli, Marco Re, and Leonardo Di Carlo, “Improved large-signal model for vacuum triodes,” in *Proceedings of the IEEE International Symposium on Circuits and Systems (ISCAS)*, Taipei, Taiwan, May 24–27 2009, pp. 3006–3009.
- [270] W. Ross Dunkel, Maximilian Rest, Kurt James Werner, Michael Jørgen Olsen, and Julius O. Smith III, “The Fender Bassman 5F6-A family of preamplifier circuits—a wave digital filter case study,” in *Proceedings of the 19th International Conference on Digital Audio Effects (DAFx-16)*, Brno, Czech Republic, September 5–9 2016, pp. 263–270.
- [271] Klaus Meerkötter and Thomas Felderhoff, “Simulation of nonlinear transmission lines by wave digital filter principles,” in *Proceedings of the IEEE International Symposium on Circuits and Systems (ISCAS)*, vol. 2, San Diego, CA, May 1992, pp. 875–878.
- [272] Peter Raffensperger, “Toward a wave digital filter model of the Fairchild 670 limiter,” in *Proceedings of the 15th International Conference on Digital Audio Effects (DAFx-12)*, York, UK, September 17–21 2012.

- [273] Jyri Pakarinen, Miikka Tikander, and Matti Karjalainen, “Wave digital modeling of the output chain of a vacuum-tube amplifier,” in *Proceedings of the 12th International Conference on Digital Audio Effects (DAFx-09)*, Como, Italy, September 1–4 2009, pp. 55–59.
- [274] Marco Fink and Rudolf Rabenstein, “A Csound opcode for a triode stage of a vacuum tube amplifier,” in *Proceedings of the 14th International Conference on Digital Audio Effects (DAFx-11)*, Paris, France, September 19–23 2011, pp. 365–370.
- [275] Julian Parker, “A simple digital model of the diode-based ring-modulator,” in *Proceedings of the 14th International Conference on Digital Audio Effects (DAFx-11)*, Paris, France, September 19–23 2011, pp. 163–166.
- [276] Stefan Petrausch and Rudolf Rabenstein, “Wave digital filters with multiple nonlinearities,” in *Proceedings of the 12th European Signal Processing Conference (EUSIPCO)*, Vienna, Austria, September 6–10 2004, pp. 77–80.
- [277] Alberto Bernardini, Kurt James Werner, Augusto Sarti, and Julius O. Smith, “Modeling a class of multi-port nonlinearities in wave digital structures,” in *Proceedings of the European Signal Processing Conference (EUSIPCO)*, Nice, France, August 31 – September 4 2015.
- [278] Alfred Fiedler and Horst Grotstollen, “Simulation of power electronic circuits with principles used in wave digital filters,” in *Conference Record of the IEEE Industry Application Conference (IAC)*, Orlando, Florida, October 8–12 1995, pp. 2438–2443.
- [279] ——, “Simulation of power electronic circuits with principles used in wave digital filters,” *IEEE Transactions on Industry Applications*, vol. 33, no. 1, pp. 49–57, January/February 1997.
- [280] Alberto Bernardini, Kurt James Werner, Augusto Sarti, and Julius O. Smith III, “Multi-port nonlinearities in wave digital structures,” in *Proceedings of the IEEE International Symposium on Signals, Circuits, and Systems (ISSCS)*, Iași, Romania, July 9–10 2015.
- [281] Daniel J. Gillespie and Daniel P. W. Ellis, “Modeling nonlinear circuits with linearized dynamical models via kernel regression.” in *Proceedings of the IEEE Workshop on Applications of Signal Processing to Audio and Acoustics (WASPAA)*, New Paltz, NY, October 20–23 2013, pp. 1–4.
- [282] Parviz Moin, *Fundamentals of Engineering Numerical Analysis*. Cambridge University Press, 2010.
- [283] Udo Zölzer, *Digital audio signal processing*, 2nd ed. West Sussex, United Kingdom: John Wiley & Sons, 2008.
- [284] Udo Zölzer, Ed., *DAFX: Digital Audio Effects*, 2nd ed. John Wiley & Sons, 2011.

- [285] M. Novati and J. Dack, Eds., *The Studio di Fonologia—A Musical Journey.* Milan, Italy: Hal Leonard, June 2012.
- [286] Digital Signal Processing Committee, IEEE Acoustics, Speech, and Signal Processing Society, *Selected Papers in Digital Signal Processing, II*, ser. Selected Reprint Series. New York, NY: IEEE Press, 1976.
- [287] Stefan Damian Bilbao, “Wave and scattering methods for the numerical integration of partial differential equations,” CCRMA, Stanford University, Stanford, CA, CCRMA Technical Report STAN-M-108, May 2001. [Online]. Available: <https://ccrma.stanford.edu/files/papers/stanm108.pdf>
- [288] Julius O. Smith, “A new approach to digital reverberation using closed waveguide networks,” in *Proceedings of the International Computer Music Conference (ICMC)*, Burnaby, B.C., Canada, August 22 1985, pp. 47–53, also available as [290].
- [289] ——, “Elimination of limit cycles and overflow oscillations in time-varying lattice and ladder digital filters,” CCRMA, Stanford University, Stanford, California, CCRMA Technical Report STAN-M-35, 1986.
- [290] ——, “A new approach to digital reverberation using closed waveguide networks,” CCRMA, Stanford University, Stanford, California, CCRMA Technical Report STAN-M-31, 1985.